DOCTORAL THESIS

Design of Acetylcholinesterase Reactivators and Poly(ADP-ribose) Polymerase Inhibitors Based on Hydroxamic Acids and Oximes

Denys Bondar

TALLINNA TEHNIKAÜLIKOOL
TALLINN UNIVERSITY OF TECHNOLOGY
TALLINN 2023

TALLINN UNIVERSITY OF TECHNOLOGY
DOCTORAL THESIS
73/2023

Design of Acetylcholinesterase Reactivators and Poly(ADP-ribose) Polymerase Inhibitors Based on Hydroxamic Acids and Oximes

DENYS BONDAR

TAL TECH PRESS

TALLINN UNIVERSITY OF TECHNOLOGY
School of Science
Department of Chemistry and Biotechnology
This dissertation was accepted for the defence of the degree of Doctor of Philosophy in Chemistry on 17/11/2023

Supervisor: Dr. Yevgen Karpichev
School of Science
Tallinn University of Technology
Tallinn, Estonia

Opponents: Olga Tšubrik, PhD
OÜ Alminnovo (member of the board)
Tartu, Estonia

Prof. Jean-Manuel Raimundo
Interdisciplinary Center of Nanoscience of Marseille
Aix-Marseille University
Marseille, France

Defence of the thesis: 22/12/2023, Tallinn

Declaration:
Hereby I declare that this doctoral thesis, my original investigation and achievement, submitted for the doctoral degree at Tallinn University of Technology has not been submitted for doctoral or equivalent academic degree.

Denys Bondar

---
signature

European Union
European Regional
Development Fund

Investing
in your future

Copyright: Denys Bondar, 2023
ISSN 2585-6898 (publication)
ISBN 978-9916-80-089-8 (publication)
Printed by Koopia Niini & Rauam

TALLINNA TEHNIKAÜLIKOOL
DOKTORITÖÖ
73/2023

Hüdroksaamhapetel ja oksiimidel põhinevate atsetüülkoliinesteraasi reaktivaatorite ja polü(ADP-riboos)polümeraasi inhibiitorite disain

DENYS BONDAR

TAL TECH
KIRJASTUS

Contents

List of Publications 6
Author's Contribution to the Publications 6
Author's Other Publications and Conference Presentations 7
Introduction 8
Abbreviations 9
Compound Codes 11
1 Literature Overview 13
1.1 Hydroxylamine and its derivatives as α-nucleophiles 14
1.2 Oximes as derivatives of hydroxylamine 15
1.2.1 Oximes: preparation, properties, and applications 18
1.2.2 Oximes as AChE reactivators 21
1.2.3 Oximes reactivators of OP-inhibited AChE in the CNS 25
1.3 Hydroxamic acids as derivatives of hydroxylamine 27
1.3.1 Hydroxamic acids: preparation, properties, and applications 29
1.3.2 Hydroxamic acids as AChE reactivators 31
1.3.3 Hydroxamic acids as antitumor agents 33
1.4 Oxazolopyrimidines as a versatile scaffold for drug design 36
1.5 Carbon nanoparticles as platforms for drug delivery 39
2 Goals of the Present Work 41
3 Results and Discussion
3.1 Nanodiamond carrier for oxime delivery (Unpublished results) 42
3.2 Design of arylhydroxamic acids as an AChE reactivator (Publication II) 48
3.3 Design of PARP inhibitors based on cyclic arylhydroxamic acids (Publication III) 55
3.4 Design of Oxazolopyrimidines as VEGFR2 inhibitors (Publication I) 61
4 Conclusions 65
References 66
Acknowledgements 86
Abstract 87
Lühikokkuvõte 88
Appendix 1 89
Appendix 2 105
Appendix 3 121
Curriculum vitae 149
Elulookirjeldus 150

List of Publications

This thesis was prepared based on the following publications by the author:

I Velihina, Ye.; Scattolin, Th.; **Bondar, D**.; Pil'o, S.; Obernikhina, N.; Kachkovskyi, O.; Semenyuta, I.; Caligiuri, I.; Rizzolio, F.; Brovarets, V.; Karpichev, Y.; Nolan S. P. Synthesis, *in silico* and *in vitro* Evaluation of Novel Oxazolopyrimidines as Promising Anticancer Agents. *Helv. Chim. Acta*, **2020**, 103 (12), #e2000169.

II **Bondar, D**.; Kapitanov, I. V.; Pulkrabkova, L.; Soukup, O.; Jun, D.; Botelho, F. D.; França, T. C. C.; Kuča, K.; Karpichev, Y. N-substituted arylhydroxamic acids as acetylcholinesterase reactivators. *Chem.-Biol. Interact.*, **2022**, 110078.

III **Bondar, D**.; Bragina, O.; Lee, J. Y.; Semenyuta, I.; Järving, I.; Brovarets, V.; Wipf, P.; Bahar, I.; Karpichev, Y. Hydroxamic Acids as PARP-1 Inhibitors: Molecular Design and Anticancer Activity of Novel Phenanthridinones, *Helv. Chim. Acta,* **2023**, #e202300133.

Author's Contribution to the Publications

Contribution to the papers in this thesis are:

I The author carried out synthetic experiments, prepared final compounds for characterization and biological studies. The author contributed to the final manuscript preparation and compilation of supporting material.

II The author planned synthesis and carried out the chemical experiments. The author participated in biological studies and complied the supporting information (characterization of intermediates and reaction products). The author played a major role in the final manuscript preparation.

III The author planned and carried out the synthesis. The author participated in biological studies and played a major role in the final manuscript preparation and complied the supporting information (characterization of intermediates and reaction products).

Author's Other Publications and Conference Presentations

Other Publications:

I Bolkvadze, V.; **Bondar, D**.; Vaher, M.; Halling, E.; Gorbatsova, J.; Mazina-Šinkar, J. The influence of organic solvents on phenylethylamines in capillary zone electrophoresis. *J. Chromatogr. A*, **2022**, 1675.

II Vasiliev, G.; Kubo, A.-L.; Vija, H.; Kahru, A.; **Bondar, D**.; Karpichev, Y.; Bondarenko, O. Synergistic antibacterial effect of copper and silver nanoparticles and their mechanism of action. *Sci. Rep.*, **2023**, 9202.

Oral Presentations:

I Designing N-Substituted Arylhydroxamic Acids as Catalytic Acetylcholinesterase Reactivators. *GSFMT conference 2020*, Tallinn, Estonia, 4-5.2.**2020**

II Oxime-Functionalized Nanodiamonds as a Platform for Treatment of Organophosphate Poisoning. *2020 Virtual MRS Spring Meeting & Exhibit*, Boston, 27.11-4.12.**2020**.

III Oxime-Functionalized Nanodiamonds as A Platform for Treatment of Organophosphate Poisoning. *European Advanced Materials Congress*, Stockholm, Sweden, 22-27.08.**2021**.

IV Nanodiamonds for targeted drug delivery, Invited speaker, Nanodiamonds for targeted drug delivery. Invited speaker, *V International Conference "Pharmacology and Pharmaceutical Technology"*, Kyiv, Ukraine, 26.11.**2021**.

V Drug coating design of nanodiamonds for targeted delivery. *5th International Symposium on Nanoparticles, Nanomaterials, and Applications 2022*, Caparica, Portugal, 24-27.01.**2022**

Poster Presentations:

I Designing N-substituted arylhydroxamic acids as catalytic acetylcholinesterase reactivators, *10th International Conference of Chemistry Toulouse-Kiev*, Toulouse, France, 2-4.06.**2019**.

II Scaffold hopping approach for designing new 7-piperazin- and 7-(1,4-diazepan)-substituted [1,3]oxazolo[5,4-d]pyrimidines as prospective anticancer agents, *10th International Conference of Chemistry Toulouse-Kiev*, Toulouse, France, 2-4.06.**2019**.

III Oxime-Functionalized Nanodiamonds as a Platform for Treatment of Organophosphate Poisoning, *2020 Virtual MRS Spring Meeting & Exhibit*, Boston, 27.11-4.12.**2020**.

IV Nanodiamonds as a Platform for Biomedical Application. *GSFMT Scientific Conference 2021*, Tartu, Estonia, 14-15.06.**2021**.

V Functional antimicrobial surfaces with Cu(II) polyoxotungstates, *5th International Symposium on Nanoparticles, Nanomaterials, and Applications 2022*, Caparica, Portugal, 24-27.01.**2022**

Introduction

Organic chemistry encompasses the exploration of structural arrangements, synthetic techniques, and chemical transformations within a wide range of carbon compounds. These compounds span from small organic molecules to substantial biomolecules such as nucleic acids, enzymes and polysaccharides. Given the pivotal role of organic reactions in biological processes, a profound understanding of organic chemistry stands as a cornerstone of the life sciences. Dating back to 1897, when German chemists at Bayer AG pioneered the synthesis of aspirin, the inaugural synthetic drug, organic synthesis has been a pivotal element in the field of medicinal chemistry, which forms one of the fundamental pillars of modern science.

In confronting contemporary healthcare challenges, there exists an acute need for the cost-effective and environmentally benign production of new organic compounds that exhibit advanced pharmacological potency. This endeavour aims to yield therapeutically superior drug candidates, specifically tailored to combat life-threatening conditions such as cancer and organophosphate poisoning.

This demands a synthetic strategy that combines diverse structural functionalities and heterocyclic scaffolds via various contemporary organic chemistry methodologies. The imperative of embracing agile, adaptable, and sustainable green chemistry techniques cannot be overestimated. The design of novel pharmacophores serves not only to expedite drug development but also to enrich our comprehension of reaction mechanisms. Furthermore, it fosters the discovery of new reactions and advanced scaffolds, propelling the continual expansion of our knowledge and the potential for groundbreaking advancements in the field.

This doctoral thesis is focused on a rational drug design that resulted in α-nucleophiles that exhibit therapeutic potential and practical utility as prospective pharmaceutical agents. Specifically, this thesis advances the chemical strategy for drug design based on two classes of α-nucleophiles, oximes and hydroxamic acids, to enhance their therapeutic efficacy while reducing cytotoxicity.

Structure optimization of arylhydroxamic acids as reactivators of acetylcholinesterase (AChE) inhibited by organophosphorus toxicants was investigated (Publication II). The *N*-(benzyloxy)- and *N*-(hydroxy)phenanthridinones were studied as the first hydroxamic acids – inhibitors of poly(ADP-ribose)polymerase (PARP), a promising target for antitumor agents (Publication III). The versatile oxazolopyrimidine scaffold in drug design was further expanded through the synthesis of isomeric oxazolo[4,5-*d*]pyrimidines and oxazolo[5,4-*d*]pyrimidines, exhibiting potent anticancer activity via targeting VEGFR2. (Publication I). The nanodiamond-based nanocarrier for delivery of quaternary oximes, reactivators of the OP-inhibited human AChE, was developed. In addition to the above-mentioned publications, the results of this work have been presented at international conferences in Estonia, Sweden, and Portugal.

Abbreviations

Ac	Acetate
ACh	Acetylcholine
AChE	Acetylcholinesterase
aq	Aqueous
BChE	Butylcholinesterase
Boc	*tert*-Butoxycarbonyl
CAS	Catalytic active site
CWA	Chemical warfare agent
Ch	Choline
CNP	Carbon nanoparticle
CNS	Central nervous system
DCM	Dichloromethane
DFP	Diisopropyl fluorophosphate
DSC	Differential scanning calorimetry
DMF	Dimethylformamide
DNA	Deoxyribonucleic acid
TJ	Tight junction
EtOH	Ethanol
*h*AChE	*Homo sapiens* acetylcholinesterase
HAT	Histone acetyltransferase
HDAC	Histone deacetylases
IC_{50}	Half-maximal inhibitory concentration
IR	Infrared
log P	Logarithm of the partition coefficient
MD	Molecular docking
MeCN	Acetonitrile
MeOH	Methanol
MMP	Matrix metalloproteinase
NMR	Nuclear magnetic resonance
NPA	*p*-nitrophenylacetate
NPDEP	*p*-nitrophenyl ether of diethylphosphoric acid
NPDEPS	*p*-nitrophenyl ether of diethylphosphonic acid
NPTS	*p*-nitrophenyl ether of toluene sulfonic acid
OP	Organophosphorus
PAMPA	Parallel Artificial Membrane Permeability Assay
PARP	Poly (ADP-ribose) polymerase
Pd/C	Palladium on charcoal
PEG	Polyethylene glycol
PI	Propidium iodide

pK_a	Logarithm of the acid dissociation constant
PNS	Peripheral nervous system
QSAR	Quantitative structure-activity relationship
SAR	Structure-activity relationship
SAHA	Salicylhydroxamic acid
SPECT	Solid-state photon emission computed tomography
t-Bu	*tert*-butyl
TEA	Triethylamine
TFA	Trifluoroacetic acid
THF	Tetrahydrofuran
TLC	Thin-layer chromatography
VEGF	Vascular endothelial growth factor

Compound Codes

Entry	Compound	Code			
		Thesis	Paper I	Paper II	Paper III
1	Benzhydroxamic acid	**1a**		**1a**	
2	*N*-Methylbenzhydroxamic acid	**1b**		**1b**	
3	*N*-Butylbenzlhydroxamic acid	**1c**		**1c**	
4	*N*-Phenylbenzhydroxamic acid	**1d**		**1d**	
5	3-Methoxybenzhydroxamic acid	**2a**		**2a**	
6	*N*-Methyl-3-methoxybenzhydroxamic acid	**2b**		**2b**	
7	*N*-Butyl-3-methoxybenzhydroxamic acid	**2c**		**2c**	
8	*N*-Phenyl-3-methoxybenzhydroxamic acid	**2d**		**2d**	
9	4-Methoxybenzhydroxamic acid	**3a**		**3a**	
10	*N*-Methyl-4-methoxybenzhydroxamic acid	**3b**		**3b**	
11	*N*-Butyl-4-methoxybenzhydroxamic acid	**3c**		**3c**	
12	*N*-Phenyl-4-methoxybenzhydroxamic acid	**3d**		**3d**	
13	2-Hydroxybenzohydroxamic acid	**4a**		**4a**	
14	*N*-Methyl-2-hydroxybenzhydroxamic acid	**4b**		**4b**	
15	*N*-Butyl-2-hydroxybenzhydroxamic acid	**4c**		**4c**	
16	*N*-Phenyl-2-hydroxybenzhydroxamic acid	**4d**		**4d**	
17	*N*-(Benzyloxy)benzamide	**5a**			**1a**
18	5-(Benzyloxy)phenanthridin-6(5H)-one	**5b**			**2a**
19	10-Methoxy-5-(benzyloxy)phenanthridin-6(5H)-one	**5c**			**2b**
20	10-Methoxy-2-nitro-5-(benzyloxy)phenanthridin-6(5H)-one	**5d**			**2c**
21	9-Methoxy-5-(benzyloxy)phenanthridin-6(5H)-one	**5e**			**2d**
22	7-Hydroxy-5-(benzyloxy)phenanthridin-6(5H)-one	**5f**			**2e**
23	2-(Dimethylamino)-*N*-(5-(benzyloxy)-6-oxo-5,6-dihydrophenanthridin-3-yl)acetamide	**5g**			**4e**
24	2-(Dimethylamino)-*N*-(5-hydroxy-6-oxo-5,6-dihydrophenanthridin-3-yl)acetamide	**5h**			**4f**
25	2-(Dimethylamino)-*N*-(5-(benzyloxy)-6-oxo-5,6-dihydrophenanthridin-2-yl)acetamide	**5i**			**4g**
26	2-(Dimethylamino)-*N*-(5-hydroxy-6-oxo-5,6-dihydrophenanthridin-2-yl)acetamide	**5j**			**4h**
27	2-Nitro-5-(benzyloxy)phenanthridin-6(5H)-one	**5r**			**2j**
28	2-Amino-5-(benzyloxy)phenanthridin-6(5H)-one	**5s**			**3b**
29	2-aryl-4-(dichloromethylidene)-1,3-oxazol-5(4H)-one	**6a**	**1**		
30	Phenylamidine hydrochloride	**6b**	**2a**		
31	4-Chlorobenzamidine hydrochloride	**6c**	**2b**		
32	1-Phenyl-1H-imidazol-5(4H)-one	**6d**	**3a**		

33	4-Chloro-1H-imidazol-5(4H)-one	**6e**	**3b**		
34	Oxazolo[4,5-*d*]pyrimidine	**6f**	**6**		
35	5-Phenyl-2-phenyloxazolo[4,5-*d*]pyrimidin-7(6H)-one	**6g**	**4a**		
36	5-(4-Chlorophenyl)-2-phenyloxazolo[4,5-*d*]pyrimidin-7(6H)-one	**6h**	**4b**		
37	5-Phenyl-7-chloro-2-phenyloxazolo[4,5-*d*]pyrimidine	**6i**	**5a**		
38	5-(4-Chlorophenyl)-7-chloro-2-phenyloxazolo[4,5-*d*]pyrimidine	**6j**	**5b**		
39	tert-Butyl 4-(5-(4-phenylphenyl)-2-phenyloxazolo[4,5-*d]*pyrimidin-7-yl)piperazine-1-carboxylate	**6k**	**7a**		
40	tert-Butyl 4-(5-(4-(4-clorobenzene) phenyl)-2-phenyloxazolo[4,5-*d*]pyrimidin-7-yl)piperazine-1-carboxylate	**6l**	**7b**		
41	4-(5-(4-phenylphenyl)-2-phenyl oxazolo[4,5-*d*]pyrimidin-7-yl-piperazin-1-ium trifluoroacetate	**6m**	**8a**		
42	4-[5-(4-(4-methoxycarbonylphenyl)phenyl)-2-phenyloxazolo [4,5-*d*]pyrimidin-7-yl-piperazin-1-ium trifluoroacetates	**6n**	**8b**		
43	4-[5-(4-(4-chlorophenyl)phenyl)-2-phenyloxazolo[4,5-*d*]pyrimidin-7-yl-piperazin-1-ium trifluoroacetates	**6o**	**8c**		
44	Phenylboronic acid	**6p**	**9a**		
45	4-Carboxymethoxyphenylboronic acid	**6q**	**9b**		
46	2,5-Diphenyl-7-phenyloxazolo[4,5-*d*]pyrimidine	**6r**	**10a**		
47	2,5-Diphenyl-7-(4-methoxycarbonylphenyl)oxazolo[4,5-*d*]pyrimidine	**6s**	**10b**		
48	Benzoyl bromide	**6t**	**11**		
49	Oxazolo[3,4-*d*][1,3]oxazine	**6u**	**12**		
50	Oxazolo[5,4-*d*]pyrimidin-7-one	**6v**	**13**		
51	2,5-Diphenyl-7-chlorooxazolo[5,4-*d*]pyrimidine	**6w**	**14**		
52	7-Phenyl-oxazolo[5,4-*d*]pyrimidine	**6x**	**15a**		
53	7-(4-Methoxycarbonylphenyl)oxazolo[5,4-d]pyrimidine	**6y**	**15b**		

1 Literature Overview

The α-effect, characterized by an unusually high nucleophilicity due to an adjacent lone pair of electrons to the reactive center, was first reported in 1947.[1] Only 15 years later Edwards and Pearson introduced this term to the organic chemistry after a careful consideration of experimental data and factors behind reactivity of such reactants.[2] For the first time such substrates, later named α-nucleophiles, were recognized as a separate class amongst nucleophilic agents.[1]

In essence, α-effect nucleophiles experience positive deviation from the Bronsted relationship for "normal" nucleophiles, demonstrating higher nucleophilic reactivity than it is anticipated from the Brønsted plot. Prominent examples of α-nucleophiles include hypochlorite, hydroperoxide anions, hydroxylamine, and its derivatives (oximate, hydroxamate, amidoximate ions) among others.[3, 4]

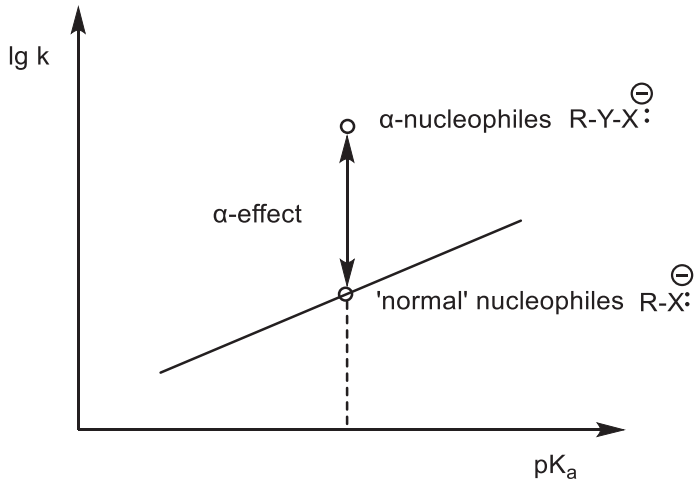

***Figure 1**. Enhanced reactivity of α-nucleophiles presented as positive deviation (teal arrow) from the Brønsted plot built for the 'normal' nucleophiles.*

The extent of the α-effect can be measured in two ways: 1) as the ratio of the rate constants $k_{\alpha\text{-nuc}}/k_{nuc}$; or 2) as the difference between lg $k_{\alpha\text{-nuc}}$– lg k_{nuc} ($k_{\alpha\text{-nuc}}$ and k_{nuc} are, respectively, rate constants characterizing the reactivity of an α-nucleophile and a 'normal' one) at $pK_a^{\alpha\text{-nuc}} \approx pK_a^{nuc}$. Typically, using the Brønsted model the values for reactivity of such typical α-nucleophiles, as ClO^- and HOO^- ions, rise upwards by 2–3 logarithmic units.[4, 5] The nature of the α-effect is the main topic of scientific interest,[2, 6] with possible application in the development of efficient treatments against hazardous chemicals (pesticides, CWAs, esters of sulfuric acid).

Extensive studies on the unusually high reactivity of α-nucleophiles showed an interplay of factors.[7] Nowadays, it is assumed that phenomena leads to 1) nucleophile ground state destabilization due to electron pair repulsion;[8] 2) stabilization of the transition state;[9] 3) high thermodynamic stability of the products;[6, 10] and 4) enhanced solvation effects.[11, 12] The extent of the α-effect is controlled by several factors: 1) nature of solvent;[4, 11] 2) the basicity sensitivity of standard anionic nucleophiles (β_{nuc});[13, 14] 3) electrophile hybridization. [11, 15]

The solvent has a profound impact.[11, 12] It was shown that in nucleophilic substitutions of *p*-nitrophenyl acetate and related esters, the extent of the α-effect is determined by the solvent mixture.[11] Notably, while the presence of the α-effect in the gas phase was initially debated, recent research reaffirms its role in both solution and gas.[16]

The value of β_{nuc}[10, 17] and the reactant pK_b[12, 18] also affect the extent of the α-effect. It is insignificant or even absent in chemical reactions involving highly basic α-nucleophiles[12, 19] or with low values of β_{nuc}.[12, 14]

The hybridization of the electrophilic center is crucial in the extent of α-effect. Thus, for reactions at the sp^3-hybridized carbon atom, the elevation is generally negligible.[11] In contrast, sp^2-carbon's reactivity with α-nucleophiles increase by 50–100 times.[11] At *sp*-hybridized electrophilic center the surge is even higher. As a result, in equimolar mixture of ethanol and water hydroperoxide anion is 10^4 times more reactive with the *sp*-carbon atom of benzonitriles.[20]

Understanding the unique reactivity of α-nucleophiles provided insights into reaction kinetics and allowed their use as innovative treatments against toxicants.[21, 22]

1.1 Hydroxylamine and its derivatives as α-nucleophiles

Hydroxylamines, or alkoxyamines, are the class of organic compounds originating from hydroxylamine (NH_2OH). Their classification, based on substitution at nitrogen and oxygen atoms, includes mono-, di-, or tri-substituted types. Notably, oximes and hydroxamic acids can be regarded as further extension of organic derivatives of NH_2OH, sharing a common α-core (NOH group) (***Figure 2***).

Wilhem Clemens Lossen first synthesized hydroxylamine in 1865.[23] Hydroxylamines are weakly basic (pK_a = 5.9 in water)[4] and mostly exist in protonated forms in physiologically relevant medium. They have a low energy of inversion (~62.76 kJ/mol)[24, 25] at nitrogen and rapidly rotate along O–N bond. As a result, tri-substituted hydroxylamines imitate both enantiomers of chiral ethers and alkanes reducing synthetic and structural uncertainty due caused by the presence of stereogenic center.

These derivatives (*N*-alkyl substituted hydroxylamines, oximes and hydroxamic acids) are used as detoxifying agents against certain environmental toxins, especially, esters of sulfuric acid and OP compounds.[26, 27]

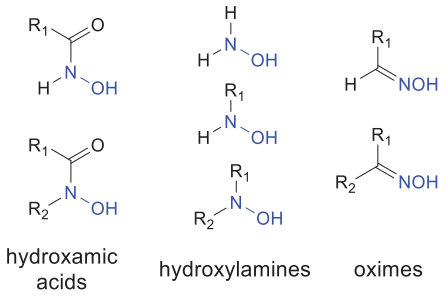

***Figure 2**. Structural relationship between hydroxylamine and its derivatives.*

Central to hydroxylamines' reactivity is the neighbouring oxygen atom to the nitrogen, both possessing lone electron pairs. This unique composition results in the α-effect, making them supernucleophilic compared to analogues of similar basicity.[28] This common *N*-OH motif defines hydroxylamines, oximes, and hydroxamates as α-nucleophiles.[26]

Depending on conditions, these ambident nucleophiles can target electrophiles either through their oxygen or nitrogen atoms.[27, 29]

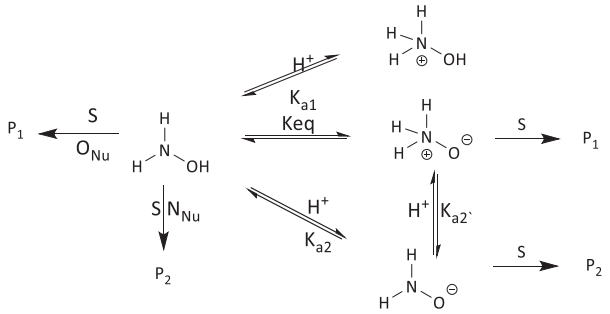

***Scheme 1**. Proton transfer equilibria and nucleophilic species of hydroxylamine in aqueous medium, S – electrophilic substrate; P_1, P_2 – products of the reaction.*

In aqueous media, hydroxylamine and its *N*-alkyl derivatives often exist in an equilibrium, as a positively charged $^{+}NH_3OH$, and as potential nucleophilic species NH_2OH, $^{+}NH_3O^{-}$, NH_2O^{-}. However, it was postulated, that in reactions with acetyl halides and esters of carboxylic, phosphoric and phosphate acids, hydroxylamine reacts as a neutral species.[30] However, if we consider the description of the α-effect in details,[1, 2] the anionic form of hydroxylamine fulfils all the needed criteria: 1) a nucleophilic center is a negatively charged atom (oxygen); 2) absence of substituents at the nucleophilic center that sterically lock the attack on the electrophile; 3) the nucleophile contains a group capable to stabilize the transition state. Finally, there is an electronegative nitrogen with a lone pair of electrons in the α-position to the reaction center in the hydroxylamine, which destabilizes the ground state of the reagent and stabilizes the transition state of the nucleophilic substitution reaction. Kinetic studies confirmed the elevated reactivity of hydroxylamine anion in the substitution of the acyl group in basic solution.[18]

This was consolidated by investigations into reactions of bis-(2,4-dinitrophenyl)-phosphate,[26, 27] 2,4-dinitrophenyl diethyl phosphate with anionic forms of hydroxylamine, *N*-methyl and *N*,*N*-dimethyl derivative, that acted as classical α-nucleophiles.[31]

The kinetic behavior of the uncharged hydroxylamine in substitution of acyl groups is even more surprising. The values of reactivity exhibited by NH_2OH in reactions with NPDEP, NPDEPS, NPTS and NPA in the corresponding graphs are significantly higher not only for the standard reaction series ($\Delta = \lg k_2^{NH2OH} - \lg k_2^{nucl}$. ≈ 9.0 (NPA), Δ ≈ 6.0 (NPTS), Δ ≈ 6.0 (NPDEP), Δ ≈ 6.1 (NPDEPS)), but also for the Brønsted-type correlation for α-nucleophiles (Δ ≈ 3.4 (NPA), Δ ≈ 1.6 (NPTS), Δ ≈ 1.6 (NPDEP).[18] Obviously, the neutral species of hydroxylamine shows an abnormally high reactivity even among inorganic α-nucleophiles and reacts with the studied substrates as a typical α-nucleophile with c $pK_a \approx 1 - 5$. If we examine the extent of the α-effect of the neutral specie by the ratio and consider that the basicity of the oxygen in NH_2OH is like oxygen in H_2O, then the differences in basicity are ~16 orders of magnitude, and the α-effect for NH_2OH is one of the most important among inorganic α-nucleophiles.

The hydroxylamine scaffold remains largely underused in medicinal chemistry, despite possible enlargement of libraries of drug candidates without making complex chiral centers. Notable instances include natural antibiotics Esperamicin A1[32, 33] and

Calichemicin [34] exhibiting anticancer activity, the biomolecule SB-219383[35], a selective inhibitor of bacterial tyrosyl tRNA synthase.

Due to the supposed weakness and polarity of N-O bond hydroxylamine moiety is avoided as inherently fragile.[36, 37] As expected, there are a few examples of their application. Amongst them are the di- and trimeric hydroxylamine-based mimetics of β-(1→3)-glucans[24] and a selective inhibitor of human sialidase NEU3.[38] Unfortunately, hydroxylamines with unsubstituted -OH or -NH groups, especially *N*-arylhydroxylamines, are intermediates in metabolism of amines and further converted into electrophiles *via* acylation or sulfation.[39, 40] Then these metabolites bind to DNA, causing numerous gene mutations. However, the tri-substituted ones evade this pathway due to absence of free -NH or OH groups, ensuring reduced carcinogenic potential and diminished false-positive outcomes in biochemical assays.[39] Furthermore, heteroatom–heteroatom moiety such as N-O and N-N bonds, as well as other electrophilic moieties, are fairly common in approved drugs.[37] Thus, avoiding hydroxylamine scaffold in drug development due to expected false screening and lability of N-O bond leads to decrease of prodrugs and their quality.[37, 41]

1.2 Oximes as derivatives of hydroxylamine

Oximes are derivatives of hydroxylamine represented by the general structure $R_1R_2C{=}NOH$, wherein R_1 represents an organic substituent and R_2 is either hydrogen or another organic substituent, characterizing aldoximes or ketoximes, respectively.

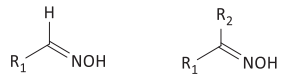

Aldoxime Ketoxime

***Figure 3**. Structural derivatives of oximes.*

Schiff pioneered the condensation of primary amines with carbonyl compound in 1864,[42] and this reaction was extensively studied afterwhile.[43] The term 'oxime', which is coined from words oxygen and imide, was introduced in the 19th century, after synthesis of methylglyoxime by Victor Meyer and Alois Janny.[44]

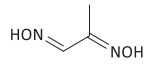

Methylglyoxime

***Figure 4**. Methylglyoxime prepared in 1882.*

The 'defining' structural fragment in oximes is >C=N−OH, and in solution they exist as equilibria of two forms: *syn*-(*Z*) and *anti*-(*E*) isomer. Numerous studies found that *syn*-form is the most stable. This was supported by the DSC experiment in which the *anti*-isomer was heated and melted to yield the *syn*-one.[45] Thus, except for aromatic aldoximes, most aldoximes prefer the *syn*-form,[46] but ketoximes are synthesized as a mixture of *syn*- and *anti*- isomers that could be separated.[47, 48] Although the oxime in its *anti*-form coexist with the *syn*-oxime, it is a minor species.[45, 49] These diastereomers have different physicochemical properties and biological activity.[50, 51] Researchers used

ab initio and density functional theory (DFT) approaches to investigate the molecular structure and conformational stability of *anti*- and *syn*-isomer of certain aliphatic aldoximes.[52]

Tautomerism in oximes is possible, and three main tautomeric forms (***Figure 5***), oximes, nitrone, and nitroso compounds, were found.[49, 53] Other cyclic isomers are possible depending on the structure.[53] These tautomers may have different biological activity,[49] although it was not reported in the literature. The oxime–nitrone isomerization was the first to be detected.[54] Despite that both the nitrone and nitroso tautomers are less stable than the oxime form,[55] the nitrone is more reactive than the oxime, notably in cyclo- and nucleophilic addition to unsaturated electrophiles.[56, 57] The presence of an electron-donating group in oxime reduces the energy gap between oxime and its nitrone form and stabilizes the latter, enabling cycloaddition to proceed more easily. [56] At higher pH, however, the oxime is more reactive than nitrone.[58]

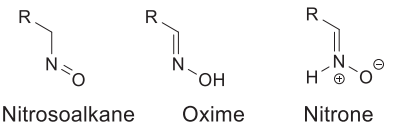

Figure 5*. Tautomers of oximes.*

The mechanism of the oxime–nitrone tautomerism was studied extensively (***Scheme 2***). Recent theoretical calculations by Lopez *et al.* propose this isomerization as a bimolecular reaction *via* two oximes or two nitrones.[57] Previously, the oxime–nitrone tautomerism was attributed to a thermal 1,2-hydrogen shift coupled with solvation effects.[45, 59]

Oximes possess amphoteric properties, owing to the moderately acidic hydroxy group and the somewhat basic nitrogen atom. Most oximes dissolve in aqueous sodium hydroxide, forming a sodium salt. [60] They can be regenerated to starting form upon the addition of a weak acid, such as acetic acid.

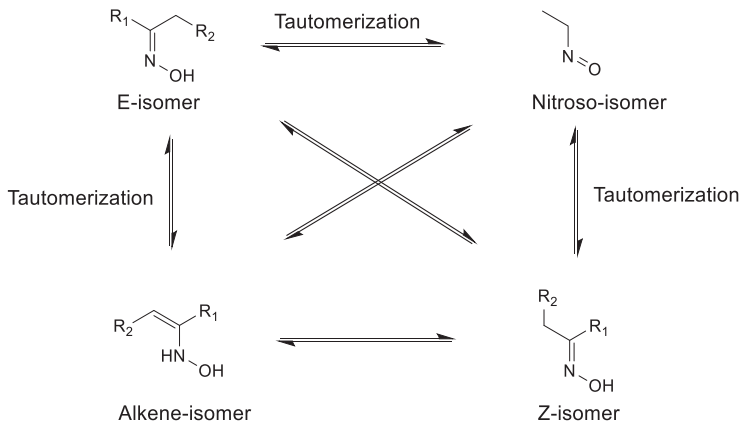

Scheme 2*. Isomerism in oximes.*

1.2.1 Oximes: preparation, properties, and applications

Oxime and its derivatives are key intermediates in organic synthesis.[61] Comprehensive reviews covered their application in the synthesis of amines, amides, aldehydes/ketones, nitroalkanes, hydroxylamines, hydroxylamine *O*-ethers, 1,3-heteroazoles, and many other compounds.[62, 63] The classical synthesis of oximes involves the reaction of aldehydes or ketones with hydroxylamine hydrochloride in the presence of a base (***Scheme 3***), but many improvements were made, ranging from refluxing reactants in alcohols to greener, cheaper, solvent-free methods with short reaction times.[64, 65] For this reaction, many catalysts could be used, such as silica gel in the presence of a base[66] or microwave irradiation.[67] The reaction in ethanol is aided by ultrasound irradiation using Na_2SO_4 as a dehydrating agent.[68] Other techniques include Al_2O_3 driven transformations,[69] ZnO/CH_3COCl,[70] TiO_2/SO_4^{-2}[71], and Bi_2O_3-catalyzed reactions,[72] potentially combined with microwave irradiation[73] or grinding.[74]

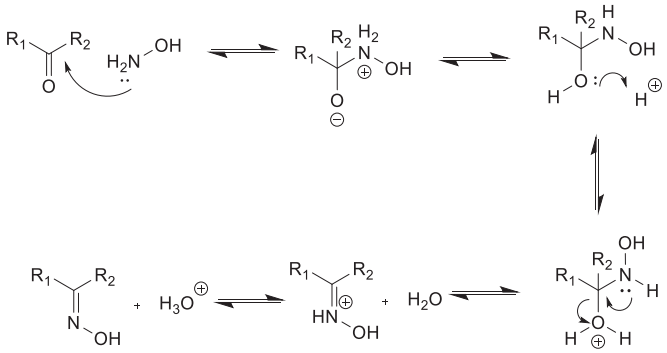

Scheme 3. *Formation of oximes by reaction of hydroxylamine with a ketone.*

The resulting oximes are stable and usually crystalline, making oximation an efficient approach for characterizing and purifying carbonyl compounds. Crude aldehydes and ketones could be isolated by converting them into oximes, followed by recrystallization and hydrolysis by diluted sulfuric acid.

Also, oximes are prepared by mild reduction of nitro compounds. Carbon monoxide (CO) reacts with copper salt solutions to form cuprous CO complexes, potent reducing agents.[75] In 1972 Knifton reported that Copper salt solutions in amine solvents are effective catalysts for the selective reduction of nitroalkanes to their oximes.[76]

In 1987 a paper was published by Barton and co-workers on reduction of aliphatic nitro compounds into oximes under homogenous conditions using CS_2 in the presence of an excess of triethylamine.[77] The method is particularly well suited for reducing allylic nitro derivatives. The choice of base is critical in the reaction success. A mixture of oxime and nitrile was obtained by using a stronger base. Potassium carbonate is a more suitable and effective reagent for promoting base-catalysed reactions under solid–liquid phase transfer catalysis conditions (***Scheme 4, a***).[78]

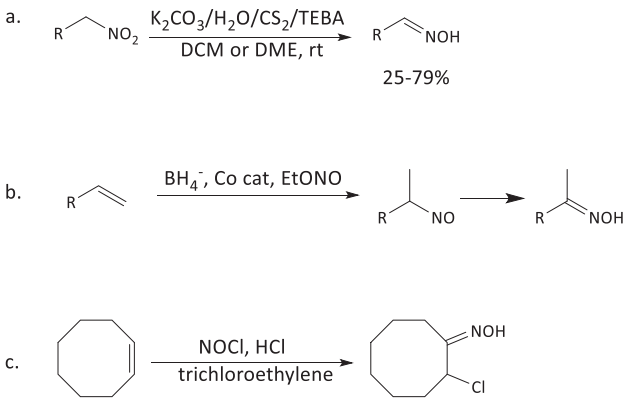

Scheme 4*. Synthesis of oximes by a) reduction of aliphatic nitroalkanes; b) nitrosation of alkenes; c) treatment of alkenes with NOCl.*

The chemistry of nitro compounds is crucial for such well-known reactions, like Henry and Nef,[79] an important synthetic methodology allowing interconversion of nitro and other functional groups. Bu_3SnH, $Se/NaBH_4$, CS_2, or $SnCl_2$ (frequently in combination with thiophenol) are the most often used techniques for converting primary nitroalkanes to oximes.[80]

The synthesis of nitrogen-containing molecules such as amino acids and heterocycles can benefit from using olefins as the starting material. Okamoto and colleagues found that use of bis(dimethylglyoximato)cobalt(II) complex to catalyze the reduction–nitrosation of styrenes with ethyl nitrite and tetrahydroborate anion gives the acetophenone oximes[81] (***Scheme 4, b***). Another pathway is treatment of alkenes with NOCl that yields α-chloro oximes (***Scheme 4, c***).[82]

Fileti and Ponzio reported more than a century ago that 1,2-diketones could be synthesized by treating methylene ketones with sodium nitrite in aqueous HCl. This method, however, has only been used for a few water-soluble substrates.[83]

In 2004 Rüedi and colleagues reported a simple oximation process that allows for the selective synthesis of 1,2-dione monoximes and/or their hydrolyzed 1,2-diketone derivatives using the necessary amount of *in situ* formed nitrosyl chloride and corresponding ketones (***Scheme 5***).[84] This reaction is a valuable method in organic synthesis because of its versatility and high efficiency, as well as due to synthetic importance of 1,2-dicarbonyl compounds. Furthermore, the reaction can be carried out on a preparative extent without product loss, making this process suitable for industrial use.

In medicinal chemistry the resulting hydroxy-imine derivatives are well-known for their antibacterial, anti-fungal, anti-inflammatory, antioxidant, and anti-cancer properties.[85, 86] Due to their unique effectiveness positively charged oximes became acknowledged as best available antidotes to OP compounds.

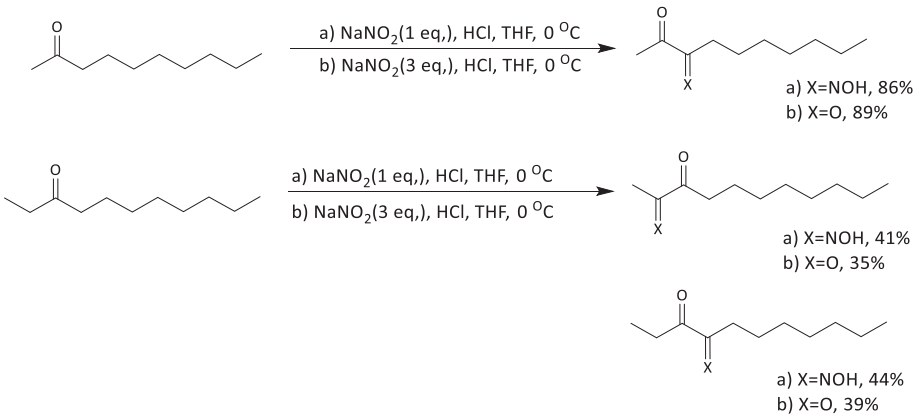

Scheme 5. *Synthesis of 1,2-dione monoximes andr 1,2-diketones.*

The first OP pesticide, tetraethyl pyrophosphate, was developed in the mid-1800s but they widely used in agriculture only after World War II. These compounds are very toxic, and OP poisoning symptoms include nausea, vomiting, diarrhoea, muscular tremors, and confusion, and can result in death from minutes to days, depending on toxicity.[87] In 1955 Wilson and Ginsburg from Columbia University reported that hydroxylamine derivatives, in particular oximes, may reverse cholinesterase inhibition caused by OP compounds, and can be used as efficient antidotes.[88] Three years later Grob and his group expanded this discovery, showing that a novel oxime, pyridine-2-aldoxime (Pralidoxime) added to atropine, can reverse the neuromuscular block caused by OP poisoning, and reactivate AChE.[89] This ability to restore work of the AChE made the oxime scaffold the starting point for further optimization of antidotes.[90]

Since the discovery of Pralidoxime against OP poisoning, several research groups developed a variety of bioactive compounds with oxime moieties hoping to make more effective medicines. However, Pralidoxime remains the only FDA-approved antidote for the treatment of OP poisoning until now.

Oxime-based cephalosporins are utilized as antimicrobial agents in addition to being used as OP antidotes.[91] Penicillin and cephalosporin antibiotics are the most used antibacterial drugs against infections among β-lactams.[92] Hundreds of unique cephalosporins were developed since the discovery of cephalosporin C in the 1950s.[93] Cephalosporin C is hydrolysed chemically or enzymatically to 7-aminocephalosporanic acid, which is a critical step in the production of various cephalosporin derivatives.[94] Cefuroxime, ceftizoxime, cefpodoxime, and cefmenoxime are FDA-approved oximes that can be used to treat a variety of bacterial illnesses (***Figure 7***).

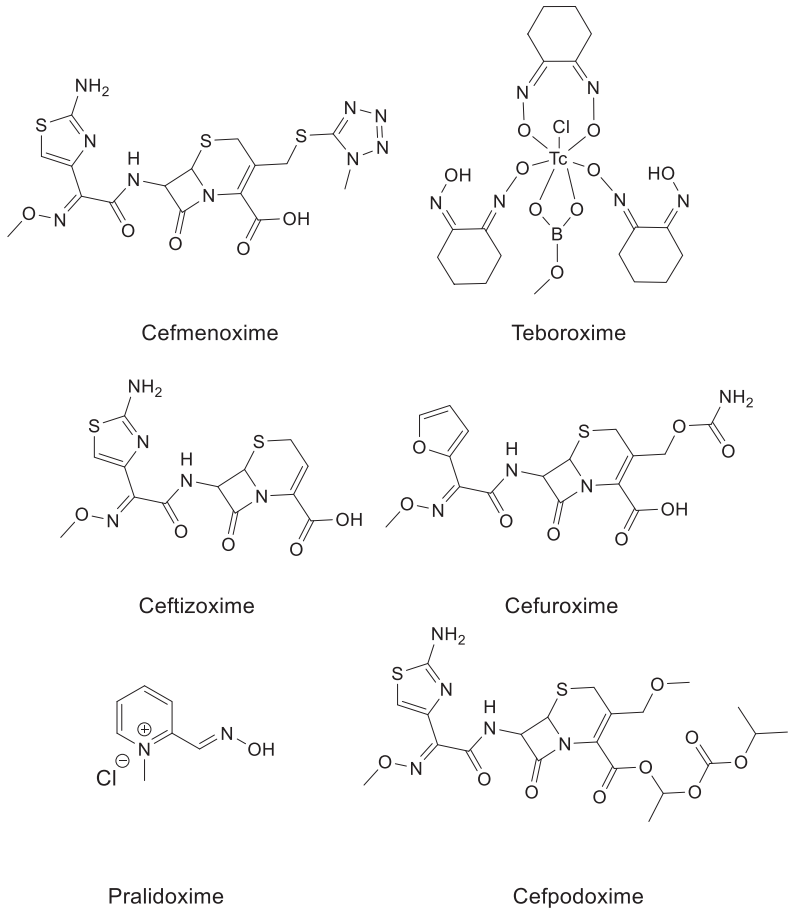

***Figure 7**. Oximes, approved by FDA for medical use.*

Teboroxime, also known as Tc-99m-teboroxime, is an uncharged lipophilic formulation made from methylboronic acid, tin (II) chloride, and technetium dioxime complexes (BATOs).[95, 96] Since the FDA approval in 1991, it was used as a myocardial perfusion imaging agent.[97, 98] Tc-99m-teboroxime was then withdrawn from market due to its fast metabolism, which prevented high-quality pictures.[99] However, some countries reintroduced it to the market for SPECT. Its pharmacokinetics and distribution in connection to coronary artery disease and ischemia were studied.[100, 101] This oxime is the active component of Cardiotec drug,[102] approved to treat high blood pressure by the FDA.

1.2.2 Oximes as AChE reactivators

The CWAs[103] are represented by nerve agents, such as G-type or V-type gases, which inhibit acetylcholinesterase, or blister agents, such as chloroalkyl sulfides (HD, Mustard gas), that attack soft tissue (***Figure 8***). These substances are of great concern in the war against terrorism, and rogue regimes potentially could use them on the battlefield or in the act of terrorism, as any chemical factory producing OP pesticides able to make them. The Project Coast in South Africa during apartheid (paraoxon),[104] the death of Kim Jong

Nam in 2017 (VX),[105, 106] and the Salisbury poisoning with 'Novichok' toxin[107] are notable examples of use OP as tools of for assassinations, as well as attempted killing of a Russian dissident in August 2020.[108] Despite the efforts to limit misuse and mishandle of toxic OP pesticides, their toxicity results in about 220,000 fatalities annually.[109]

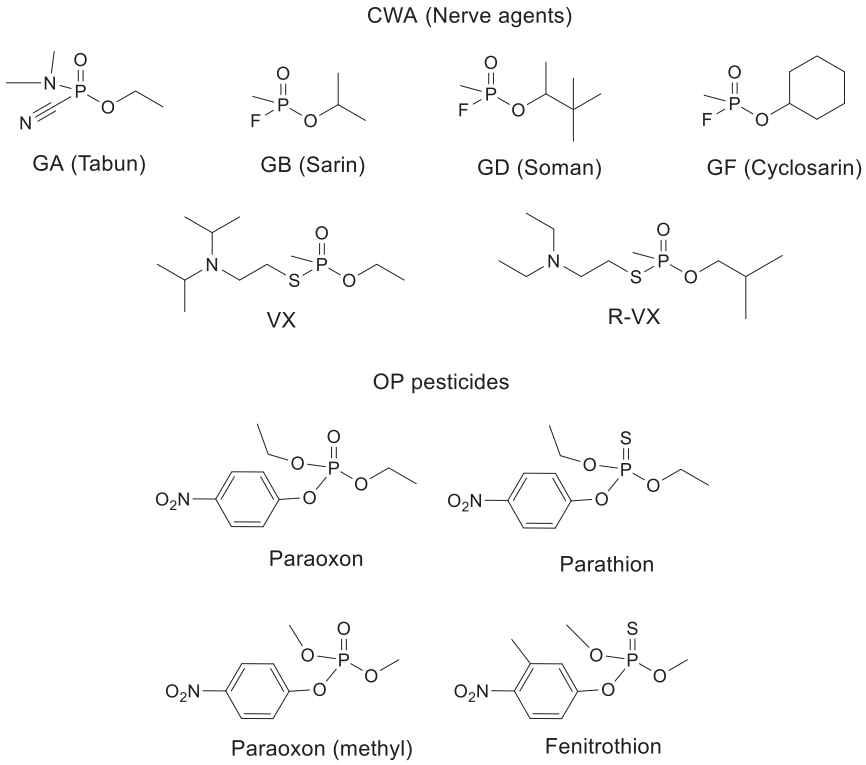

***Figure 8**. Examples of toxic organophosphorus compounds.*

Methylphosphonothioate VX has the highest toxicity of all the CWAs with LD_{50}=8 μg/kg intravenously and of 28 μg/kg per-cutaneous, rabbit.[110] VX absorbed through the skin has a median human mortality dosage of 0.14 μg/kg. Due to its low volatility and Henry's law constants, VX is the most lasting organophosphorus agent. Furthermore, due to its low solubility in water and the presence of stable P–S bond, this molecule is highly resistant to aqueous hydrolysis. When VX hydrolysis occurs under neutral conditions, the reaction is very selective and yields relatively harmless phosphonic acid (***Scheme 6***, Path A), but in presence of base, Path B is possible, producing extremely poisonous phosphothioate.[110]

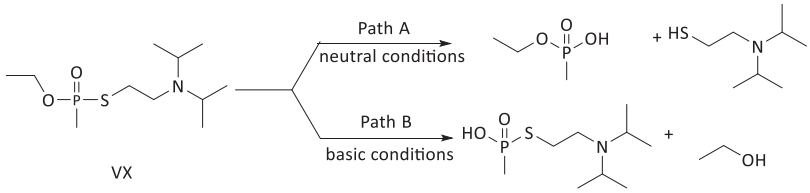

***Scheme 6**. Chemical transformation of VX in the environment.*

Although the Great powers agreed[111] to stop using these weapons and destroy their stockpiles, their critical components are simple to produce, despite international regulations on raw materials. Due of their lethality, they are the most likely weapons of choice for terrorists, and even moderately skilful organic chemists can prepare them.[112] In 1995, the fanatical group Aum Shinrikyo attacked victims in the Tokyo subway with sarin.[113] Sarin delivered by rockets was used at least twice in the 2013 and 2017 chemical attacks on civilians in Syria.[114]

The OP compounds inhibit AChE, an enzyme, which regulates the amount of neurotransmitter acetylcholine in organism (***Scheme 7***). Under normal conditions the catalytic triad of serine–histidine–glutamate in the active site of AChE catalyzes the hydrolysis of neuromediator. There are two stages in the mechanism: the 1st step – the serine residue attacks acetylcholine, making a tetrahedral intermediate that collapses to the acetyl-AChE and releases choline; the 2nd one – a water molecule, activated by the nearby histidine, attacks the conjugate, making a second tetrahedral intermediate that finally breaks yielding serine and acetic acid This mechanism exhibits exceptional efficiency as the enzyme cleaves over 10^4 molecules of the mediator per second.[115]

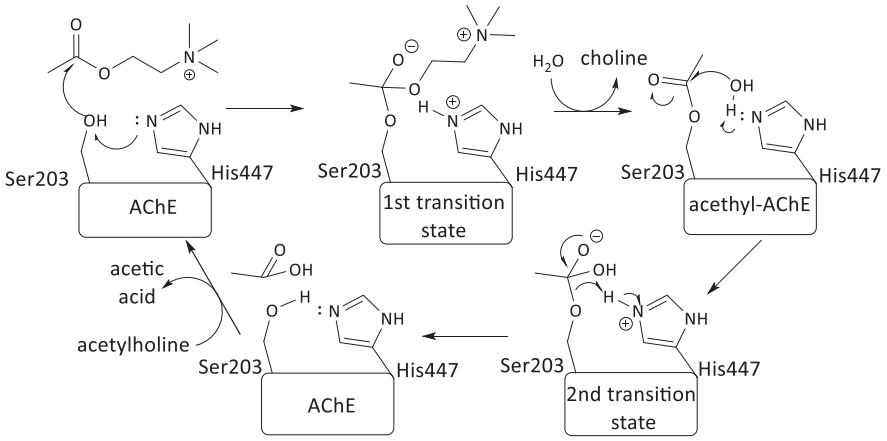

Scheme 7*. Hydrolysis of acetylcholine by AChE.*

Toxic OP chemicals, such as CWAs and pesticides, covalently bind to serine esterases (AChE and BChE) blocking them. The mechanism of AChE inhibition by OPs is like the first step of hydrolysis. Being phosphorylating agents, these compounds react with a serine hydroxyl group in the active site of AChE.[116] The nucleophilic serine attacks the phosphorus atom once the OP reaches the bottom of the active site gorge, generating a bipyramidal transition state, which is followed by the leaving group's departure and the production of the phosphorylated serine (***Scheme 8***).[117] The phosphorylated adduct is a remarkable mimic of the early stage of hydrolysis. The catalytic histidine, on the other hand, cannot activate H_2O molecule in the 2nd step because it is either pushed into a non-productive conformation (e.g., VX and tabun conjugates) or is isolated from water (e.g., soman conjugate).[116] As a result, the spontaneous hydrolysis of phosphorylated enzyme is very slow, ranging from hours for dimethyl phosphoryl conjugates to days for V-agent conjugates with AChE.

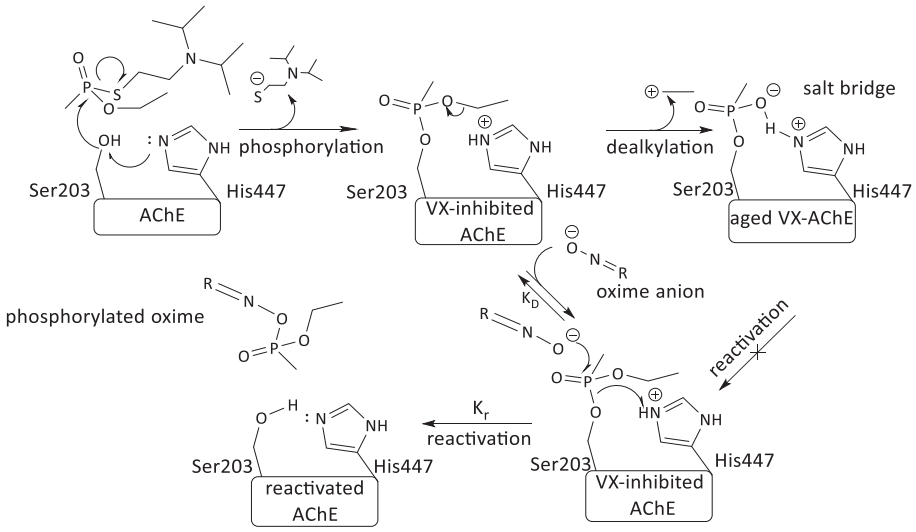

***Scheme 8**. Reactivation of VX-inhibited AChE.*

The conjugate's spontaneous hydrolysis competes with a time-dependent intramolecular reaction that results in an 'aged' form of the conjugate. The dealkylation of the alkoxy group present on the phosphorus atom in AChE conjugates results in the formation of a phosphonate adduct. Soman ages in 2–4 minutes, sarin in 5 hours, tabun in 46 hours, and VX in 48 hours. The phosphonic oxyanion that results from a salt bridge with the protonated triad histidine, stabilizing the conjugate. Furthermore, any negatively charged nucleophile is prevented from accessing the phosphorus atom by the phosphonic oxyanion. As a result, 'aged' conjugates are not cleaved. This causes acetylcholine to build up at neuron synapses, causing neurological and respiratory failure, and eventually death in minutes.

The effects of antidotes are based on the chemical re-activation of the OP-inhibited AChE.[118] The better reactivation capacity can be expected from a potential reactivator with higher nucleophilicity. Since the discovery of pralidoxime[88] researchers have been working on effective antidotes for OP poisoning, and quaternary pyridine oximes [119] are the 'lead' structures for acetylcholinesterase reactivators(***Figure 9***).[120] The antidotes fit via their quaternary, positively charged pyridinium scaffold into the choline pocket of the enzyme active site, while the nucleophilic attack by the oxime group through the oxygen atom at the phosphorous of the OP conjugate restores AChE activity.[121] This produces an OP-oxime intermediate, whose rapid decomposition into secondary compounds is critical for reactivation capacity. Once the oxime antidote cleaves the OP toxicants, AChE is irreversibly reactivated, and hydrolysis of acetylcholine is restored.

Anticholinergic medications (ideally atropine) and 'true' reactivators of AChE are generally combined in the standard treatment of OP poisoning. Anticholinergic drugs block acetylcholine's actions at nicotinic and muscarinic receptor sites, whereas oximes reactivate AChE inhibited by OP compounds.

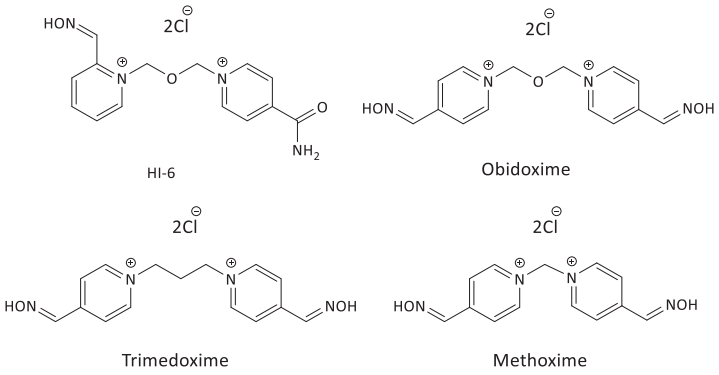

Figure 9. *Examples of quaternary oximes – reactivators of OP-inhibited AChE.*

The advantages of oximes in treating OP poisoning are still discussed[117] since the efforts to improve reactivation efficacy by enhancement of oxime structure yielded limited success[122–124] The pyridinium cation prevents the uptake of OP antidotes into the CNS, which results, for example, in the numerous studies of tertiary oximes as an alternative to the quaternary reactivators.[125]

1.2.3 Oximes reactivators of OP-inhibited AChE in the CNS

The blood–brain barrier (BBB) consists of the endothelial cells that form cerebral micro vessels.[126] Its main role is to maintain a tightly controlled microenvironment for reliable neuronal signaling and to divide the brain extracellular fluid from the circulating blood.[127] The BBB is almost impenetrable to viruses, bacteria, proteins, and polar compounds thanks to tight junctions (TJ) between endothelial cells and low levels of pinocytic activity (***Figure 10***).[128] The BBB acts as a 'physical barrier' because complex tight junctions between adjacent endothelial cells force most molecular traffic to take a transcellular route. The presence of specific transport pathways on the luminal and abluminal membranes regulates transcellular traffic, providing a selective 'transport barrier', and a combination of intracellular and extracellular enzymes allows the BBB to serve as a 'metabolic barrier'. The BBB facilitates the entry of required nutrients into the brain, and effluxes potentially harmful compounds. It separates the vesicles of neurotransmitters and neuroactive agents that act centrally and peripherally, and it regulates the ionic microenvironment of neurons. The small OP compounds (CWAs, pesticides) can freely diffuse through the BBB and inactivate AChE in CNS.[128]

The primary concern about improvements of OP antidotes remains the need to secure better entry of AChE reactivators to CNS, possibly by using delivery system to transport the 'true' reactivator (quaternary oxime, in particular) across the BBB.[129, 130]

Although many potent drugs based on pyridinium scaffold[131] were previously developed and are still used as antidotes in treatment of OP poisoning, they cannot easily enter the CNS to fully restore activity of inhibited AChE. Only a few experimental studies indicate that oximes can gain access to brain to a certain degree, reaching <<10% of their plasma levels.[132] As a result, oximes can reactivate AChE at peripheral nervous system but not in CNS. As a result, they offer little or no protection against the neuronal effects of OP poisoning, amongst them epileptic attacks, concussions, cognitive and mental state changes. This problem led to the creation of oxime-based drugs, which can pass through the BBB and undo the effects of OP on AChE in the CNS.

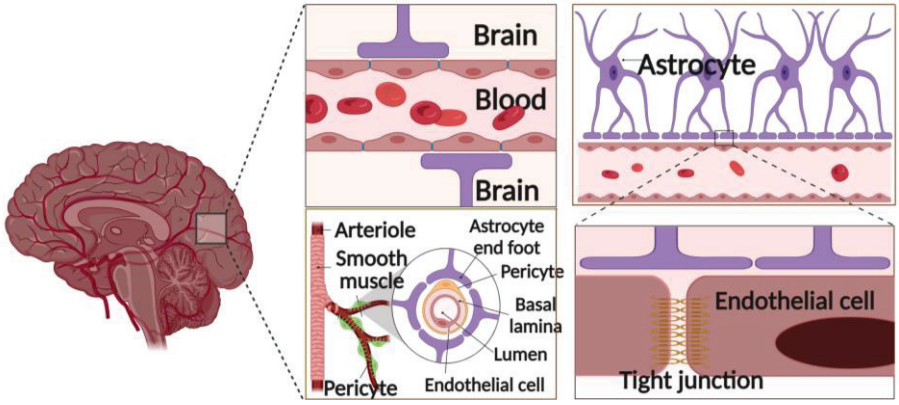

***Figure 10**. Structure of the Blood Brain barrier. Created with BioRender.com.*

Studies of non-quaternary AChE reactivators to enable them crossing the BBB have received attention recently.[133] These uncharged reactivators, which are capable of diffusing across the BBB and reactivating AChE within CNS, are considered as a novel method to increase BBB permeability. It was reported that the neutral oximes monoisonitrosoacetone (MINA) and diacetylmonoxime (DAM) (***Figure 11***), which contain aldo- or ketoxime moiety as a reactivating function, cross the BBB, but experimental *in vitro* reactivation potency toward OP-inhibited AChE is much lower than that of Pralidoxime and other quaternary oximes.[134, 135] In 2009 the investigation to compare the capacity of the tertiary oximes MINA and DAM to reactivate inhibited AChE with several quaternary oximes, showed reactivation AChE in the brain, reduced symptoms of poisoning, and improved survival.[135] During the last decade, there was a renewed interest in ability of MINA to cross the BBB and reactivate inhibited AChE in the CNS.[134] *In vivo* experiment with guinea pig had shown that MINA is able to restore the activity of AChE in the brain up to one third.[136] However, this treatment has serious limitations due to high toxicity of metabolites. Therefore, it remains a very challenging issue to find a scaffold providing as high efficiency towards inhibited AChE as quaternary oximes along with effective BBB permeability. Some examples include conjugates of salicylaldoximes inspired by a structure of donepezil[118] and sugar–oxime conjugates.[137]

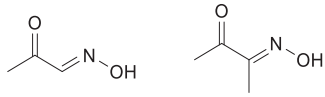

MINA DAM

***Figure 11**. Ternary oximes able to cross BBB.*

Three main factors limit this type of reactivators: (1) they can hardly penetrate the BBB to restore brain AChE due to their positive charge; (2) their reactivation capacities for AChE depends on the OP inhibitor; (3) restoring 'aged' AChE is difficult by oxime antidotes. New and effective uncharged reactivators for crossing the BBB were developed[125]. However, more investigation is required to find a broad-spectrum reactivator suitable for the entire range of OPs. There are currently no truly versatile antidotes among the pyridinium oximes.[138] Combining two or more oximes with

complementing actions would be a temporary solution to this problem,[113] for example, using Obidoxime and HI-6 combined.[139] Further studies are required for 'aged' AChE because there is no treatment available to restore activity of the enzyme. Future progress in this area will enhance protection of civilians against toxic OP compounds widely used both in pest control and agriculture.[103, 111]

1.3 Hydroxamic acids as derivatives of hydroxylamine

Hydroxamic acids are the organic α-nucleophiles having a general formula $R_1CON(OH)R_2$; where a carbonyl group is attached to the NOH scaffold, so formally they can be regarded as hydroxylamine in which one proton at nitrogen is replaced by acyl group. On the other hand, hydroxamic acids could be considered as *N*-hydroxy amides, but are highly reactive contrary to ordinary amides, which are more stable.[140]

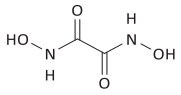

***Figure 12**. The first hydroxamic acid synthesized by Lossen.*

This new class of organic compounds was discovered by the German chemist, Wilhelm Clemens Lossen, who synthesized oxalyl hydroxamic acid in 1869.[23] They are chemically and metabolically quite reactive.[141] In basic solution hydroxamic acids are unstable and rapidly undergo rearrangement *via* isocyanate intermediate (***Scheme 9***), discovered by Lossen in 1872.

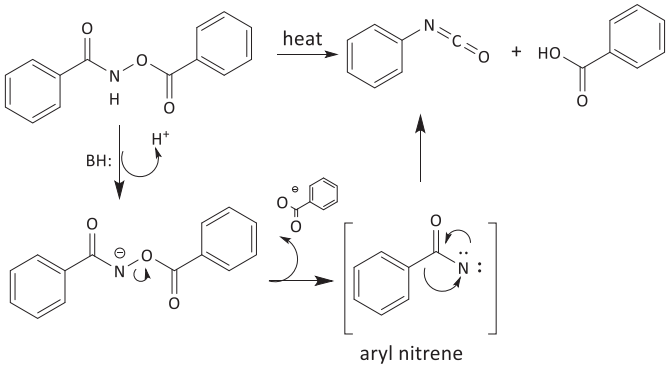

***Scheme 9**. Mechanism of Lossen rearrangement.*

Hydroxamic acids are common and frequently used reactants in synthesis, possibly due to their clear correlation to the parent hydroxylamine and carboxylic acids, both structurally and synthetically. In fact, hydroxamic acids are the oximes of carboxylic acids, as shown in their tautomeric *iminol* form, RC(OH)=NOH, which predominates in basic media[142] and, is structurally similar to ketoximes. It is commonly accepted that for hydroxamic acids, the *N-hydroxyamide*/*keto* form, rather than the *hydroximic* form (***Scheme 10, a***), predominates in acidic media, often required for coloured complexes to form.[143, 144]

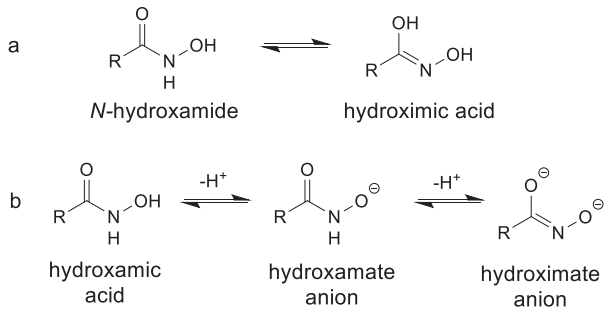

***Scheme 10**. Tautomerism (a) and acid-base properties (b) of hydroxamic acids.*

Hydroxamic acids are diprotic, because in DMSO the proton from the NH group is primarily removed, while in water the hydroxyl group of HAs with pK_a range from 8.5 to 9.5 reacts afterwhile. Due to the stability of the hydroxamate anion, these acids are readily soluble in alkaline solutions. The acidity of hydroxamic acids is increased by electron withdrawing group (EWG) substituents, and the pK_a is decreased when an alkyl or aryl group replaces the proton NH (***Figure 13***). The hydroximate dianion is formed by the second deprotonation, which takes place only under harsh conditions and happens outside the pH range typical for physiological conditions (***Figure 13***).[145]

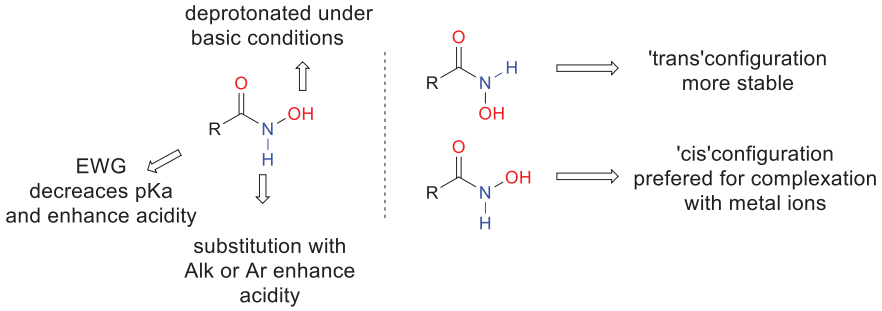

***Figure 13**. Influence of substituents on acid-base properties of hydroxamic acids.*

These acids can chelate metal ions like Fe(III) and Zn (II). They adopt a *cis* configuration during complexation, enabling a greater interaction with the cation.[146] The acids form bidentate *O,O*' complexes with transition metals, which attain bright colours to solutions. Due to the great stability of the formed complexes and existence of *siderophores* in nature storing Fe(III) inside cells, hydroxamates have a strong affinity towards Fe(III).[147] The stoichiometry and structure of metal hydroxamate complexes in solution are generally unknown. The graphic representation of interaction of hydroxamic acids with metal cations is shown in ***Scheme 11***.

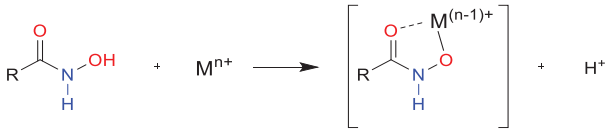

***Scheme 11**. Complexation of hydroxamic acids with metal ions.*

1.3.1 Hydroxamic acids: preparation, properties, and applications

Numerous methods have been developed to insert hydroxamic acid functionality. The typical approach is direct coupling of carboxylic acids or esters with hydroxylamines (or substituted hydroxylamines) to form unsubstituted hydroxamic acids. Hydroxamic acids can be easily prepared by *N*-acylation of hydroxylamine or nucleophilic substitution of esters, these two methods have been recently reviewed.[148] Using protected hydroxylamine or activated carboxylic acids in the presence of base, hydroxylamine can be acylated to produce *N*-alkylhydroxylamine,[148] *O*-alkylhydroxylamine [148, 149] or *O*-polymer supported hydroxylamine[150] By treating esters with hydroxylamine (or protected hydroxylamine) under basic conditions, it is possible to achieve nucleophilic substitution of esters.[149] These approaches have also been explored in a solid phase, by applying various *N*- or *O*-polymer-supported hydroxylamines.[148, 150]

Synthesis of other compounds, like *N*-substituted hydroxamic acids, is more challenging, and special procedures are required to obtain these derivatives. There are three possible synthetic routes (***Figure 14***). The first strategy involves alkylation of nitrogen in the corresponding hydroxamic acid precursor (Path A). *N*-substituted hydroxylamine and activated carboxylic acid are used in the second pathway (Path B). The third route involves *N*-oxidation of amides (Path C)

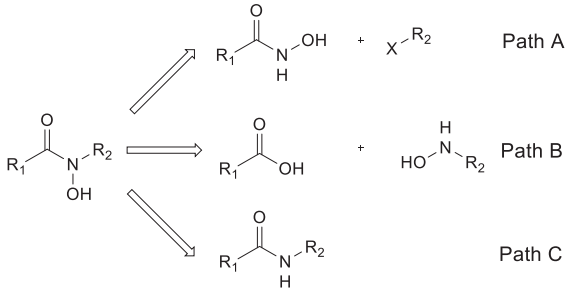

Figure 14*. Synthetic methodologies to obtain N-substituted hydroxamic acids.*

Therapeutic action of hydroxamic acids could be attributed to three factors according to mechanism of action. The first therapeutic effect is due to chelating ability towards metals, namely iron. If there is an excess of ferrous ions in human body, then an increased amount of reactive oxygen species (ROS) are produced via the Fenton and Haber-Weiss mechanisms, making it poisonous.[151] These ROS cause vascular permeability, DNA deterioration, protein and lipid brakes, degradation of cell membranes, tissue damage and total destruction.[152, 153] Finally, iron overaccumulation results in fatal damage to the liver or heart.

A special medical therapy is needed to protect internal organs from an excess of iron because humans tend to accumulate iron and extract it very slowly. Chelation therapy, which uses hydroxamic chelating agents to create complexes with the iron, is the standard course of treatment. Then, it will be easier to eliminate through the biliary or urinary tracts.[154] The preferred compound today is feroxamine B (***Figure 15***). This hydroxamate compound can complex metal ions other than iron,[155] making them useful for treating metal poisoning from actinides, plutonium, or aluminium.[156, 157] Complexation of hydroxamic ligands with metals results in antioxidant,[158] antibacterial,[159] and metal detoxification properties.[154]

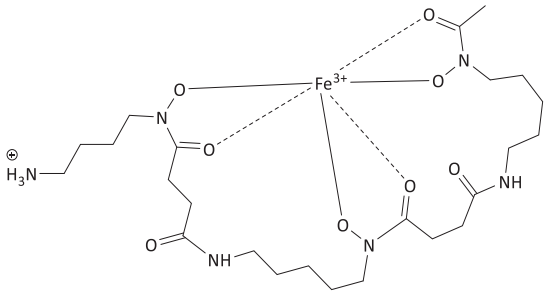

***Figure 15**. Feroxamine B, complex of deforoxamine B with iron(III) cation.*

The second type of action is defined by ability to arrest function of metalloproteases,[160] resulting in a variety of therapeutic actions, including antifungal,[161] anticancer,[162, 163] anti-inflammatory,[164] and anti-scaring,[165] antiviral,[166, 167] neurodegenerative,[168] osteoarthritis-preventing,[169, 170] and antidiabetic ones.[171] Any matrix metalloproteinases (MMPs), for example HDAC and various carbonic anhydrases could be inhibited by suitable hydroxamic acids. As the result, extracellular matrix proteins, such as collagen, elastin, gelatine, matrix glycoproteins, and proteoglycans, are degraded resulting in tissue restructuring.[172]

These enzymes are important in mitosis and growth of tumour cell.[173] MMPs are thought to represent the early stages of the metastatic process, which indicates the importance of cancer evolution. MMP inhibitors are intriguing molecules because they control the malignancy of cancer and reduce invasiveness.[163] More specifically, water, which is connected to the zinc (II) ion of the active site, causes MMPs to cleave amide bonds of peptides.[174] Derivatives of hydroxamic acid can chelate the zinc ion, displacing the water and inactivating the enzyme. Maramistat, a broad-spectrum inhibitor that operates at the nanomolar level, exhibits this method of action (***Figure 16***).[175] Hydroxamic acids may also possess antihypertensive action by deactivating the angiotensin converting enzyme (Vasopeptidase), which regulates blood pressure.[176, 177]

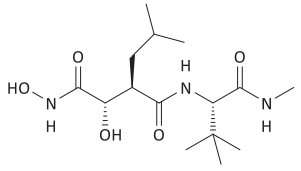

***Figure 16**. Maramistat, a MMP inhibitor.*

Finally, derivatives of hydroxamic acid could produce nitric oxides, which results in hypotensive effects.[178, 179] Nitric oxide, a molecule capable of regulating a wide range of physiological functions, including regulation of the cardiovascular system,[178] is produced by hydroxamic acids[180] and their *N*-substituted derivatives.[181] This could explain their vasodilator properties,[179] and as a result, their potential importance in the development of hypotensive drugs.

The key issue in use of hydroxamic acid function is their toxicity. In fact, because of their interactions with DNA, compounds containing the hydroxamic acid moiety exhibit *in vitro* mutagenicity.[182] Possible explanations are the the Lossen rearrangement into highly reactive isocyanate and intramolecular nucleophilic 1,2-shift. The study of acetyl-CoA activity in bacteria demonstrated the physiological activation of hydroxamic

acids into their corresponding *O*-acetyl derivatives. The formation of an unsaturated complex containing an anionic acetohydroxamate, water, and acetyl nitrene should also cause the dehydration of hydroxamic acids when Zn(II) is present, followed by nitrene rearrangement into the isocyanate.[183]

1.3.2 Hydroxamic acids as AChE reactivators

Ever since the discovery of Tabun in 1936 considerable efforts were made to develop antidotes to treat acute OP-poisoning.[184, 185] The idea of reactivation of inhibited AChE was proposed by Wilson in 1951,[186] when he reported that treatment of OP-inhibited enzyme with concentrated solutions of hydroxylamine for several days restored up to 90% of its initial catalytic activity. Later he reported[187] that hydroxamic acids are even better antidotes and could reactivate 96% of the DFP-inhibited AChE in 24 h, which is more than 4 times higher reactivation potency shown by hydroxylamine (***Table 1***).

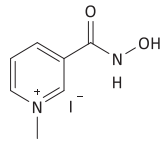

Figure 17*. The charged derivative of nicotine hydroxamic acid, used by I.G. Wilson as an antidote.*

Until now there is no consistent correlation of antidotes' structure with reactivation capacity because the efficacy of reactivator is defined by the structure of OP inhibitor.[188] Also the groups attached to phosphorus due to steric and electronic effects have a defining role in the vulnerability of inhibitor to nucleophilic attack, rate of aging, etc.[88] The first design of reactivators was based on the idea that a properly constructed nucleophile capable of breaking the P-O bond, thereby unblocking the serine hydroxyl. Amongst prepared and tested agents in the early 1950s, two groups of supernucleophiles, hydroxamic acids and oximes, were recognized as the most promising. The pH dependence of the reactivation indicated that the effective nucleophile is deprotonated hydroxamate, which attacked the phosphoryl group bound to AChE.[189] At physiological pH, a hydroxamic acid would be ionized: its proton could be accepted by the imidazolium ring at the catalytic triad.

Table 1*. The reactivation of DFP-inhibited AChE, adopted and changed from Ref.218.*

Compound	Concn. (M)	% Reactivation 1h	3h	6h
Phenyl glyoxime	0.01	50	64	67
Diacetylmonoxime	0.01	32	58	64
Monoisonitrosoacetone	0.01	15	40	56
Glyoxime	0.01	1	2	3
Diacetyl monoxime	0.01	0	0	0
Acetoxime	0.01	0	0	0
Picolinhydroxamic acid	0.05	44	56	-
Nicotinhydroxamic acid	0.01	2	6	11
Nicotynhydroxamic acid methiodide	0.01	3	8	15
SAHA	0.01	2	11	17

Inhibitor: 10^{-6} M DFP

Following the pioneering works of Wilson, in the 1950s several attempts were made to develop a potent reactivator of inhibited AChE trying a series of non-charged tertiary aliphatic oximes and hydroxamic acids for this role. Their separate application and, especially, combination with anticonvulsant atropine had increased the LD_{50} doses of sarin in *in vivo* experiments and restored catalytic activity of the inhibited enzyme.[190–193] Due to their uncharged and lyophilic nature, they were able easily to cross the BBB, into the CNS.[194] However, the discovery of quaternary pyridinium oximes (obidoxime, Pralidoxime) as highly potent reactivators of human inhibited AChE stopped any further studies of hydroxamic acids further in general and to reactivate AChE in the CNS specifically.[136]

It should be noted that approved combination of quaternary oximes with anticholinergic antidotes considerably reduce the signs and symptoms of OP poisoning, but cannot destroy OP inhibitors, making it impossible to lower their concentration in the blood and tissues.[116] As a result, a reactivated AChE could be again inhibited by blood-circulating OP compounds, so recurrent administration of antidotes and constant medical care, such as breathing ventilation, are needed when toxic symptoms first arise during severe OP intoxication.[195] In a case of real chemical attack, such constant medical attention and treatment of victims as well as of their physical injuries will place a significant pressure on the medical staff. The contamination of soil by persistent OP poisons and their efficient destruction also remains a challenge.[196]

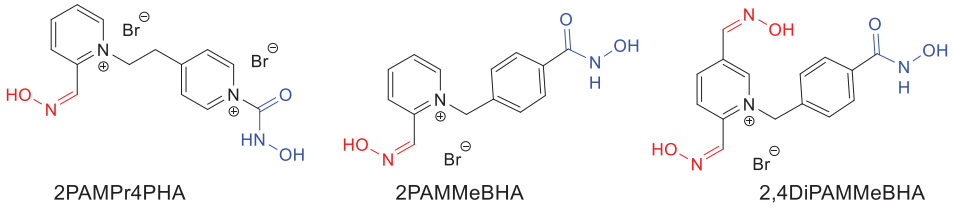

***Figure 18**. Structure of hybrid oxime-hydroxamate antidotes.*

To be used in therapy one needs to develop a highly reactive nucleophile for the OP-inhibited AChE, limiting any side reaction and ensuring efficiency at low concentration to minimize immunologic responses in organism, while able to destroy free OP inhibitors in plasma. In 2016 to satisfy these conditions Amitai's research group developed a bifunctional oxime-hydroxamate drug (***Figure 18***): the hybrid design consists of hydroxamate OP degrading moiety linked to oxime functionality, that directly reactivates OP-inhibited AChE, and produces a therapeutic agent capable of protection and reactivation simultaneously (***Table 2***).[197]

***Table 2**. The reactivation of OP-inhibited AChE, adopted and changed from Ref.197.*

Compound	% Reactivation after		
	Sarin	Cyclosarin	VX
2PAMPr4PHA	70	70	55
2PAMMeBHA	60	60	56
2DiPAMMeBHA	69	60	71
2PAM	90	65	94

Reactivator concentration 0.05 mM with Sarin and Cyclosarin-AChE and 0.375 mM with VX-AChE, 50 mM phosphate pH=7.4, 0.03% BSA, 37 °C

Screening of 155,000 small molecules resulted in selections of 33 nucleophiles chosen as dual OP-ChE reactivators and OP inhibitor detoxifiers,[198] including benzamidoxime, benzaldoxime, a non-quaternary pyridine amidoxime, and several arylhydroxamic acids (***Figure 19***). The reported VX-inhibited BChE reactivation rates were slower with mono-quaternary pyridinium oximes and faster with known bis-quaternary reactivators, providing insight into the design of novel therapeutics and decontamination agents against CWAs.

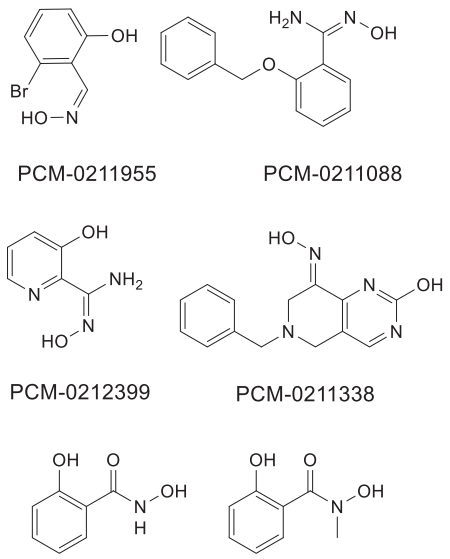

Figure 19*. Structures of uncharged antidotes of VX-inhibited BChE and studied arylhydroxamic acids.*

1.3.3 Hydroxamic acids as antitumor agents

Numerous compounds with the hydroxamic acid moiety were synthesized to develop more potent anticancer agents.[199, 200] Several hydroxamic acids exhibit antitumor activity acting as enzyme inhibitors. Mostly they are aimed to suppress HDAC and other MMP, known to play key roles in the cancer cell mitosis.

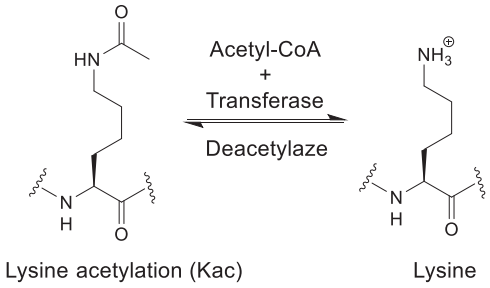

Scheme 12*. Action of HDAC on deacetylation of lysine residues in histones.*

The activity of histone acetyltransferase (HAT) and HDAC, are pivotal in the regulation of gene expression through their action on the lysine (often marked as 'K') residues of histone proteins, among other substrates, is amongst key mechanisms in gene control.

Histone acetylation is abnormally high during cancer growth (***Scheme 12***). Meanwhile, reciprocal increased histone deacetylation silence tumor suppressor genes, preventing their antitumor activity. This genetic malfunction emerged as a crucial target in cancer therapy. Many human tumors contain inactive histone deacetylated tumor-suppressor genes,[201, 202] and studies proved that inactivation of HDAC causes cancer cell lines to differentiate, undergo apoptosis, and limit their gene expression. Also, HDAC inhibitors have relatively low toxicity towards normal cells and stop mostly only cancer cells from proliferating and surviving.

The first HDAC inhibitor to receive FDA approval for the treatment of cutaneous T cell lymphoma was hydroxamate Vorinostat (suberoylanilide hydroxamic acid) in 2006. Since then, numerous HDAC inhibitors of different structures were developed. In phase I trials, Vorinostat proved effective against solid tumors and hematologic malignancies when administered intravenously or orally.[203] In refractory advanced patients with CTCL, including big cell transformation and Sézary syndrome, Vorinostat 400 mg/day was safe and efficacious with an overall response rate of 24-30 % in phase II of clinical trials.[203]

MMPs, on the other hand, are proteolytic endopeptidases that require zinc and are crucial for the insertion and modification of extracellular structures. They have been connected to the development and metastasis of cancer.[204] MMP inhibitors control the proliferation and malignancy of cancer cells. Three imidazole side chains from histidine residues coordinate the zinc ion in these enzymes, and water serves as the fourth ligand. Inhibitors of hydroxamic acid often swap out the water molecule.[205] There are two separate generations of MMP-acting inhibitors. Hydroxamic acid peptidomimetics, such as Batimastat, which imitate naturally occurring MMP substrates by having a peptide backbone with a hydroxamate moiety, are examples of the 1st-generation MMP inhibitors.

The 2nd generation MMP inhibitors are non-peptidic and more selective, possibly because their design is based on study of the MMP active site using NMR and X-ray crystallography.[205] One of them, Prinomastat (AG-3340), was designed by using a protein drug design tool and likewise contains the hydroxamate functionality. This drug inhibits MMP-2, -9, -3, and -13 with an IC_{50} of less than 0.13 ng/ml.[206]

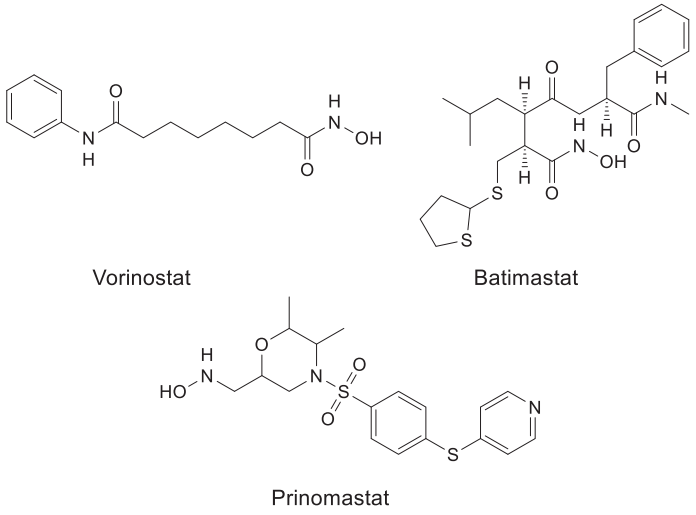

Figure 19*. Structures of HDAC inhibitors based on hydroxamic moiety.*

The poly (ADP-ribose) polymerase (PARP) enzyme is one of the promising molecular targets for the development of antitumor drugs, involved in numerous cellular processes, ranging from DNA repair to cell death.[207] The early examples of PARP inhibitors commonly known as the 1st generation ones (***Figure 20***) were developed in the 1980s based on observations that nicotinamide, a second product of the PARP-catalyzed reaction, causes moderate inhibition of the poly ADP-ribosylation. Later, in the 1990s, even more efficient the 2nd generation of PARP inhibitors was discovered containing quinazoline scaffold. This newer entity includes isoquinolines, quinazoline diones, phthalazinones, and phenanthridines and was characterized by high anti-cancer potency combined with remarkable selective action towards cancer cells in the presence of healthy ones.[208]

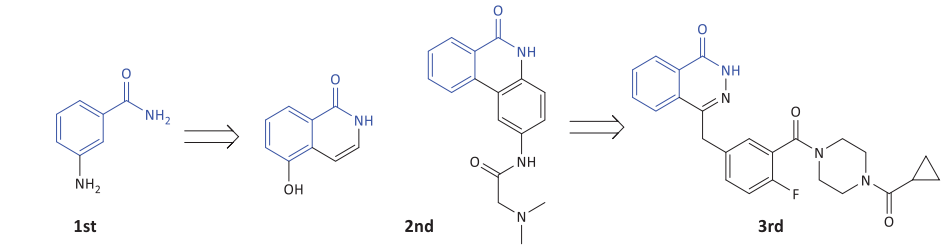

Figure 20*. Consequential development of PARP inhibitors of the first, second and third generation.*

Currently, the 3rd PARP inhibitors are being developed, many of which are undergoing Phase II clinical trials. In December 2014, the European Medicines Agency (EMA) in the EU and the FDA in United Stated approved Olaparib (***Figure 20***) for use as a single anticancer agent allowing the first PARP inhibitor of latest generation for everyday medical use.[209]

Such a huge interest in PARP enzymes as a molecular target resulted in an exponential rise of published papers on PARP inhibitors since 1990 (***Figure 21***) with remarkable focus on target-specific design of the new antitumor agents and higher efficacy.[210] Another milestone was reached in 2005 after several PARP inhibitors were approved as an anti-cancer drug by FDA.[211]

Currently the design and synthesis of new potent PARP inhibitors focus on prodrugs containing phenantridinone scaffold. This class of nitrogen heterocyclic compounds is essential and has a broad application in medicinal chemistry.[212] Phenanthridinone is an important scaffold and occurs widely in alkaloids and biologically active compounds.[213, 214] While many classical reactions were used to obtain phenanthridinone moiety, the development of more efficient and less expensive synthetic pathways continues to be of a great interest in modern synthetic chemistry. [215–217]

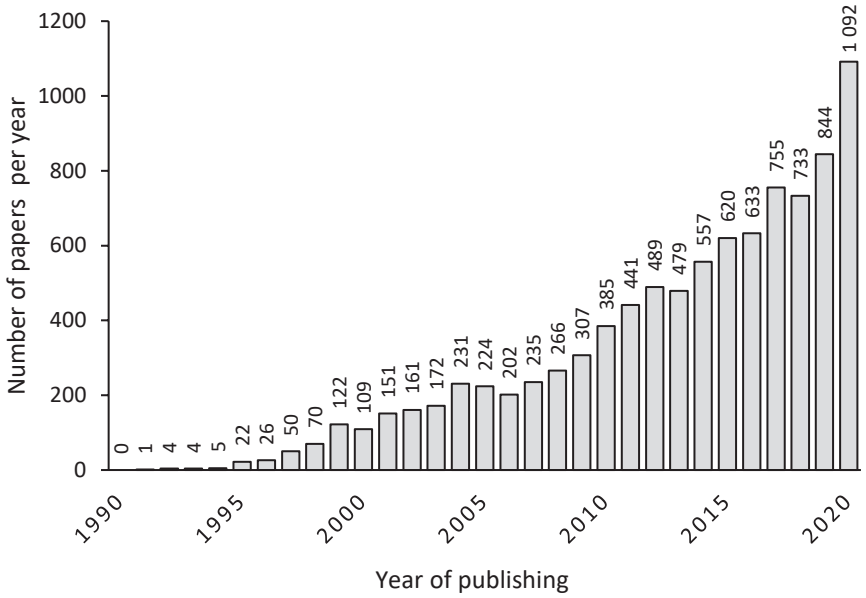

***Figure 21**. Bibliometric data on peer-reviewed documents published on PARP inhibitors according to the Clarivate Analytics Web of Science (WoS) database for years 1990-2020; the inquiry was made in November 2021*.

Recently an attempt was made to develop derivatives of Olaparib bearing aliphatic hydroxamic acid moiety as dual PARP and HDAC inhibitors.[218] The studied compounds demonstrated antiproliferative activities in selected human cancer cells and were more active then Olaparib and SAHA in some of the tested malignant cell lines.

1.4 Oxazolopyrimidines as a versatile scaffold for drug design

The oxazolopyrimidine moiety provides a flexible platform for the development of bioactive compounds targeting a variety of enzymes or receptors, such as adenosine kinase inhibitors,[219, 220] uncharged antagonists of cannabinoid receptor 2,[221] inhibitors of fatty acid amide hydrolase,[222] agonists of endothelial differentiation gene-1 receptor,[223] and antagonists of purinergic G protein-coupled receptors (***Figure 22***).[224] Thus, there is no doubt about the importance of and widespread interest in pharmacophore structure in biological and pharmacological research.

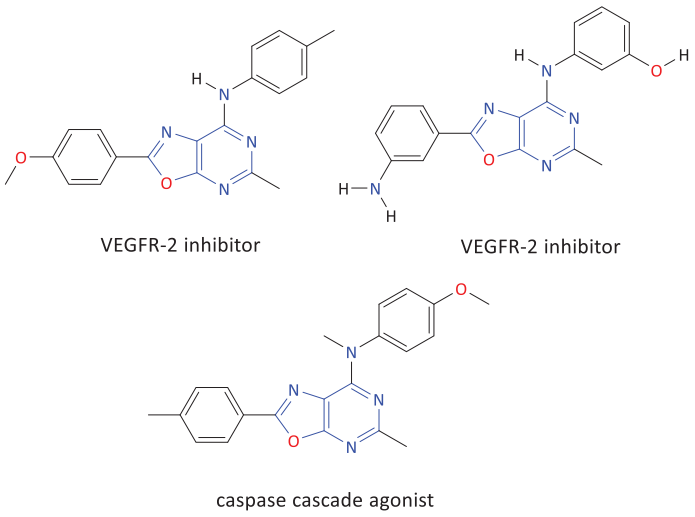

***Figure 22**. Structures of anticancer agents based on oxazolo[5,4-d]pyrimidines scaffold.*

Various diseases with uncontrolled cellular proliferation are included in the category of cancer. There is plenty of preclinical and clinical data suggesting angiogenesis plays a role in tumor growth. Several cancer types, including breast, colon, lung, bladder, renal carcinoma, and lung cancer, have shown utility of anti-angiogenic therapy. Notably, vascular endothelial growth factor (VEGF) is essential for the survival of several types of cancer. Inhibiting intracellular tyrosine kinase receptors and blocking angiogenic factors like VEGF and its receptors are the two main tactics used in anti-angiogenic therapy.[225]

The VEGF is a signalling enzyme made up from six glycoproteins: VEGF-A, -B, -C, -D, -E, and placenta growth factor.[226] Angiogenesis is mediated by VEGF through various tyrosine kinase domain receptors. VEGFR1 (Flt-1) plays a crucial role in developmental angiogenesis, monocyte migration, recruitment of endothelial cell progenitors, and induction of growth factors from liver sinusoidal endothelial cells.[227, 228] VEGFR2 (KDR/Flk-1) primarily regulates VEGF-A-induced angiogenesis, influencing microvascular permeability, endothelial cell survival, and proliferation.[227, 229]

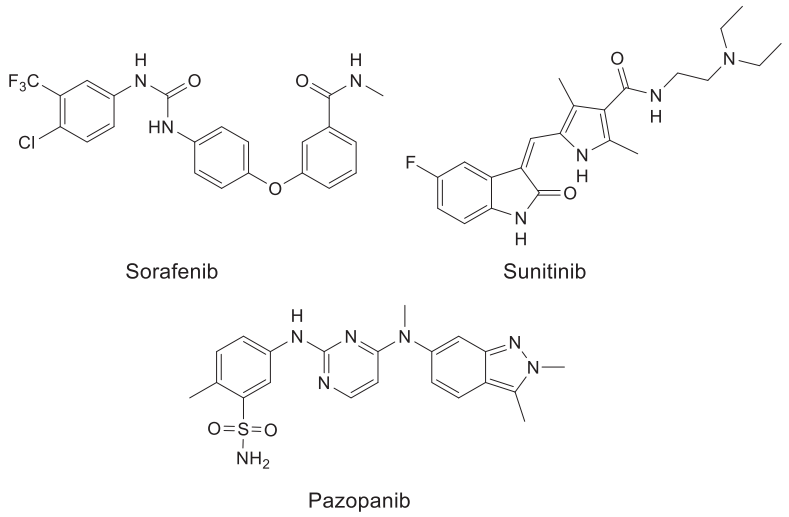

Figure 23*. Structures of small-molecule anti-VEGFR cancer drugs.*

VEGFR3 controls expression in embryonic vasculature and later becomes connected to lymphatic endothelial cells.[230] Diverse binding modes between the VEGF family members and their respective receptors contributed to the study of its interaction. Notably, three major classes of VEGF-targeting agents were developed: monoclonal antibodies (e.g., bevacizumab), VEGF decoy receptors (e.g., aflibercept), and small molecule tyrosine kinase inhibitors (e.g., sorafenib, sunitinib, pazopanib) (***Figure 23***).[225] Additionally, among the tyrosine kinase inhibitors, several bicyclic *N*-containing heterocycles act as ATP purine ring mimics, binding to the enzyme's hinge region *via* hydrogen bonds.[231, 232] Thus, oxazolo[*5,4-d*]pyrimidines are potential antimetabolites similarly to known purine antagonist drugs, such as mercaptopurine, thioguanine, azathioprine (***Figure 24***).

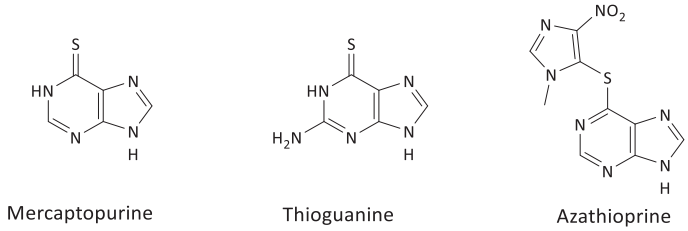

Figure 24*. Structures of purine antagonists used as antitumor drugs.*

Oxazolo[*5,4-d*]pyrimidines, which are 9-oxapurine analogs of nucleobases, have previously shown strong suppression of VEGFR2.[233, 234] As a result, synthesis and modification of anticancer agents based on the oxazolopyrimidine scaffold are of a great interest.[235] Recently, action of 7-piperazine- and 7-diazepan-substituted [1,3]oxazolo[*4,5-d*]pyrimidines *in vitro* against several cancer cell lines was studied. At submicromolar and micromolar concentrations, these compounds inhibited growth, were cytostatic and cytotoxic.[236]

1.5 Carbon nanoparticles as platforms for drug delivery

Drug delivery is the key issue for distribution of drugs in body, to increase their release into targeted tissue and enhance the selectivity of drug actions while reducing the adverse effects of their use.[205, 237, 238] Nanochemistry is set to transform drug development due to the new innovative and exciting possibilities.[239] A large potential for versatile and multipurposed applications makes use of nanoparticles for drug delivery particularly attractive. Possible ways are design of drug delivery platforms, contrast agents for imaging, etc.[240–242] The CNPs are promising for treatment of neurological diseases due to permeability over the BBB.[238] Expected that CNPs will be used as platforms in future cancer therapy.[243] Nanoparticles are emerging as fascinating structures for multi-modal therapy to enhance drug efficiency.[244] In this regard, carbon-based nanoparticles are among the top candidates for the construction of multifunctional drug delivery platforms.[245, 246]

CNPs are generally categorized as carbon nanotubes, graphene, mesoporous carbon, nanodiamonds, and fullerenes based on their structure and composition.[247] These materials demonstrated enhanced drug-loading, biocompatibility, and low toxicity due to their superior optical activity and large absorption surface area.[248] Detailed studies were done on design of biocompatible scaffolds and nanomedicines using functionalized CNPs.[249] Particularly CNPs chemically modified by functional groups, drugs, or polymers were useful for biomedical applications.[250] However, CNPs also interact with the physiological medium in the human body, for example, plasma proteins in the blood and cellular enzymes upon crossing the cancer cell membrane. As a result, the nanopowder is rapidly excreted from the bloodstream by the kidneys, ending up in an incomplete drug release at the targeted tissues. The circulation time of anti-cancer drugs in blood, their permeability pathways into cancer, and controlled release inside can be achieved by changing the type of coating, which greatly affects the overall properties of nanocarrier.

Since their discovery in 1960s nanodiamonds attracted a lot of interest due to their unique properties.[251] The nanoparticles have a dualistic nature of a nanoparticle (nanosize, large surface area, high adsorption capacity, biocompatibility) and of a diamond (high Young's modulus, fluorescence, chemical inert core).[247] The NDs revealed the lowest cytotoxicity among the CNPs in *in vitro* comparative studies, included carbon nanotubes (CNT) and graphene oxide (GO)(***Figure 25***).[252]

The properties of nanodiamonds are defined by the way of their production. The primary one is detonation synthesis by an explosion inside a closed chamber followed by air oxidation or ozone treatment. Only carboxylic groups are present on the surface of the detonated nanoparticle. The presence of one type of functionality on its surface enables fine control over surface chemistry and further chemical modifications using classic synthetic methods.[253] Controlled drug release inside cells and improved ND delivery into the targeted tissues are both made possible by surface modification.[250] Setyawati exploited surface tuning of NDs by several methods in 2016 causing a vascular barrier to become more porous, which increased the transport of anti-cancer drugs.[254]

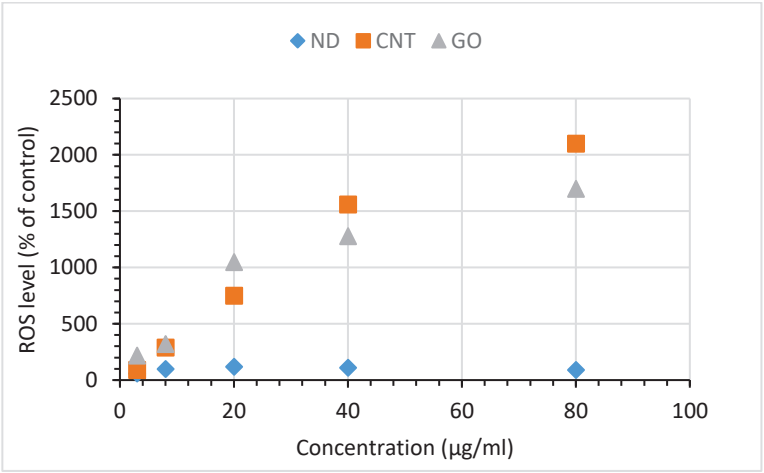

***Figure 25**. Production of ROS in HeLa cells after incubation by carbon nanoparticle for 24h. Adopted and changed from Ref.252*.

In 2010, a report that demonstrated improved doxorubicin administration into the targeted cells by coating on the Nanodiamonds surface was published. [255] In 2018 nanodiamonds were used as a platform for delivering anti-HIV drugs into the CNS.[256] In a mouse model, researchers demonstrated systematic *in vivo* brain administration of NDs loaded with human serum albumin.[257] Nanodiamonds are the prospective platform for biomedical applications and drug delivery systems because of their exceptional characteristics.[258]

2 Goals of the Present Work

The present study primarily focused on the systematic design and development of two well-known classes of α-nucleophiles for biomedical applications. Two critical enzymes: acetylcholinesterase (AChE) and poly(ADP-ribose) polymerase (PARP) were targeted. The inhibition of AChE, an enzyme responsible for modulating acetylcholine levels, can lead to neurodegenerative damage, while the suppression of PARP, pivotal in cancer proliferation and its suppression results in tumour apoptosis.

In the course of this work, methods of organic chemistry were used to synthesize bioactive compounds based on an α-nucleophile scaffold, achieving robustness and employing inexpensive and available chemical reagents to lower production cost of candidate molecule.

This study includes development of library of compounds with optimized physicochemical properties to overcome known drawbacks of traditional drugs and enhance their therapeutic efficacy.

The specific goals of this work are the following:

- Development of nanodiamonds as a platform for drug delivery of quaternary oximes into CNS for reactivation of OP-inhibited AChE.
- Rational design of *N*-substituted aryl hydroxamic acids as potential AChE reactivators with optimized balance between nucleophilicity, lipophilicity, and reactivation capacity.
- Synthesis and QSAR study of cyclic aryl hydroxamic acids, *N*-(benzyloxy)- and *N*-(hydroxy)phenanthridinones targeting PARP1 enzyme, a promising target for antitumor treatment.
- Preparation and QSAR study of oxazolo[4,5-*d*]pyrimidines and oxazolo[5,4-*d*]pyrimidines as potential VEGFR inhibitors.

3 Results and Discussion

3.1 Nanodiamond carrier for oxime delivery (Unpublished results)

In literature sections **1.2.1** and **1.2.2**, it was shown that currently available antidotes contain charged mono- or bis-pyridinium scaffold and, thus, have low permeability across the blood-brain barrier to restore activity of the inhibited AChE in the CNS. The BBB prevents more than 98 % of molecules from passing through, making it difficult to develop antidotes that will diffuse through the BBB and have a high reactivation capacity for blocked AChE as quaternary oximes. The properties of CNT discussed in section **1.4** clearly indicated their applicability for targeted drug delivery to enhance therapy. Amongst them, nanodiamonds, due to their unique interplay of a nanoparticle (nanosize, a big loading area, biocompatibility) and a diamond (inert core, physical stability) found a wide use in drug delivery. In this study, the detonated nanodiamonds after oxidative treatment to produce carboxylic functional groups (**ND-COOH**) were applied to prepare ND-based carriers and transport quaternary pyridinium oximes as AChE reactivators over the BBB model and reactivate OP-inhibited enzyme.



***Figure 26**. Structure of designed oxime antidotes based on ND carrier.*

As a result, 3 bioactive compounds **ND-A1**, **ND-A2**, and **ND-A3** were designed and prepared (***Figure 26***). They had a biocompatible linker and a covalently attached 4-hydroximinopyridinium moiety as an antidote – reactivator of OP-inhibited AChE. The pharmacophore and the **ND-COOH** were connected via the short-chain polyethylene glycol. When 4-oximinopyridine was grafted to the linker, quaternary oximes, 4-hydroximinopyridinium salts, were formed on the surface of the nanoparticles (***Scheme 13***). The resulting materials were characterised by analytical methods such as FTIR, ssNMR, and DLS.

Fourier transform infrared (FTIR) spectroscopy shows that **ND-COOH** revealed the presence of a limited number of functional groups (***Figure 27***). The carboxyl functional groups on the surface of the nanodiamonds were identified by characteristic absorbance of O-H stretching at 3420 cm^{-1} and bond bending noted at 1628 cm^{-1}. Additionally, the C=O bond stretch absorbance was clearly observed at 1775 cm^{-1}. The broad absorbance bands were detected in the 'fingerprint region' (1000–1500 cm^{-1}) and can be attributed to overlapping peaks. Specifically, peaks corresponding to absorbance by C–O–C bond stretch, O–H deformational vibrations, epoxy C–O bond stretches, and C–C bond stretches formed during the oxidative purification of **ND-COOH**.

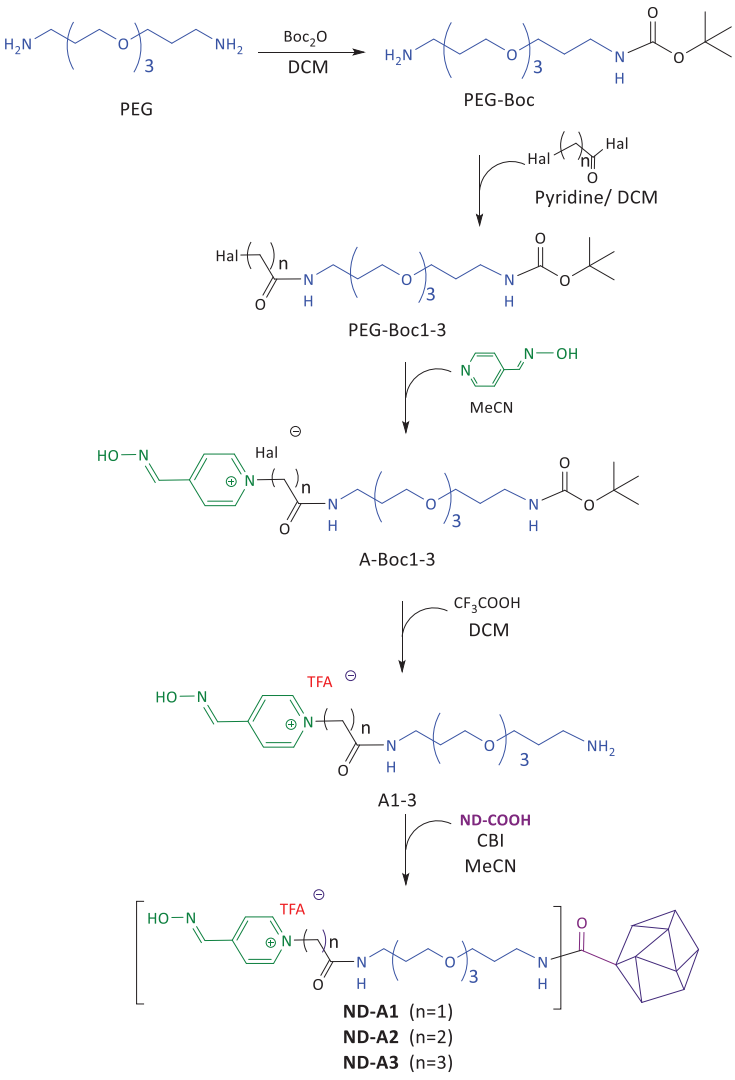

***Scheme 13**. Synthesis of 4-hydroximinopyridinium group grafting on the ND carrier.*

Infrared spectra of the final products **ND-A1-A3** confirmed the introduction of novel functional groups onto the nanodiamond surface. The previously observed broad absorbance line of the O-H bond stretches disappeared. At the same time, a characteristic absorbance of the amide C(O)-N-H bond stretches emerged near 3120 cm^{-1}. Also, a shift in the C=O bond stretch absorption to approximately 1670 cm^{-1} was observed. Noteworthy is the strong absorbance of the C-H bond stretching near 2500 cm^{-1}, the C=N bond around 1650 cm^{-1}, and the aromatic C=C bonds between 1600 and 1500 cm^{-1} present in **ND-A1-A3**. Moreover, a more complex region of the spectrum, spanning 1000–1500 cm^{-1}, was revealed. This region was assumed to be a combination of various vibrational absorptions: the C–O–C bond stretches, N–H deformational vibrations, aromatic C-C deformations, C–C bond stretches, amide C–N bond stretches, and C–N–H deformational bands (***Figure 27***).

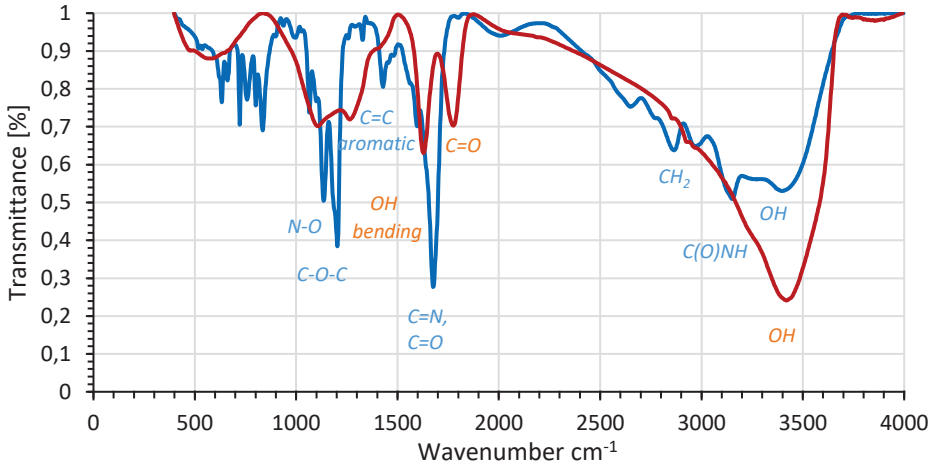

***Figure 27**. FTIR spectra of ND-COOH (red) and ND-A2 (blue).*

The ^{13}C MAS NMR spectrum of **ND-COOH** shows a broad signal with a chemical shift at δ = 38.0 ppm and a line width Δν = 12 ppm showing that the ND-COOH consists of a vast diamond core built up of sp^3-hybridized carbon partially covered by a graphitic-like layer of amorphous sp^2 carbons (***Figure 28a***). The narrower line with peak at 52.8 ppm and a line width Δν = 9 ppm are attributed to the carbons from the partially disordered sp^3 shell with dangling bonds terminated by small number of sp^2 carbon of carboxy group.

Due to the oxidative method of purification of detonation nanodiamonds a majority of surface are sp^3-hybridized atoms. The spectrum contains a broad peak with a chemical shift at 73.8 ppm and a line width Δν = 7 ppm is attributed to C-O-H groups, the secondary shoulders at 85.6 and 98.1 ppm could be attributed to the C-O-C-O-C-OH and O-C-OH carbons.

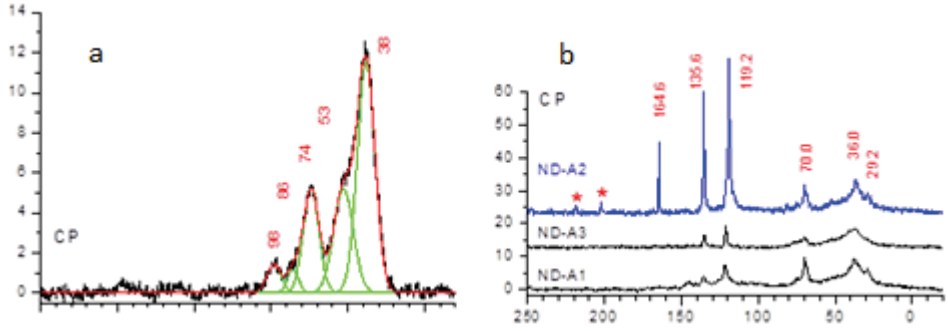

***Figure 28**. ^{13}C MAS NMR of **ND-COOH** (a) and **ND-A1-A3** (b).*

The ssNMR spectra of the NDs reveal significant difference after surface modification (***Figure 28b***). First, in the NMR spectrum of **ND-A1** a new narrow peak of sp^3 carbons appeared with a chemical shift δ =29.2 ppm and a line width Δν = 5 ppm which could be attributed to sp^3 carbon from polyethylene glycol chain present in the oxime reactivator. At the same time, the broad peak of core sp^3 carbons was unchanged and still present

with a chemical shift at a δ = 37.6 ppm and a line width Δν = 10 ppm, thus, proving that our chemical modifications did not change the inner structure of the nanodiamonds and occurred only on the surface. The narrow peak at 69.9 ppm shows that some C-O-H groups were still present on the surface of **ND-A1** after modification, but it had a smaller width than the one from starting material, showing that there were fewer of these groups after. On the one hand, it could be explained that during modification the surface hydroxy groups could be easily substituted by the amine-containing reactivator, but the low resolution of ^{13}C MAS spectrum of **ND-A1** complicated the analysis. Absence of secondary shoulders of the surface C-O-C-O-C-OH and O-C-OH bonds could be correlated to their higher reactivity under the reaction conditions. The narrow peak with a chemical shift at δ= 121.5 ppm and a line width Δν = 5 ppm was attributed to trifluoroacetate, present as a negative counterion to the synthesized positively charged oxime. The broad peak at δ= 135.7 ppm and a line width Δν = 5 ppm was attributed to the aromatic sp^2 carbons of the pyridine moiety of the synthesized reactivator, which covalently bounded to the surface. The broad peak with a chemical shift at a δ= 145.1 ppm and a line width Δν= 3 ppm was attributed to the aromatic sp^2 carbons connected to the positively charged nitrogen of the carbaldoxime moiety due to his combining negative mesomeric and inductive effect shifts their signal up field. Unfortunately, the signals of carbonyl atoms of the reactivator were not observed due to the low intensity of carbonyl peaks in ^{13}C NMR and low signal-to-noise ratio in the spectrum of **ND-A1**.

The colloidal stability and size distribution of studied nanodiamonds and in polar solvent were studied using DLS using ZetaSizer Nano S with a He-Ne laser to measure the hydrodynamic diameter and particle size distribution of the nanodiamond aggregates. The suspension of **ND-COOH** in MilliQ water comprised two distinct populations of the aggregate, a minor population exhibited a hydrodynamic diameter of ca. 15 nm, while a more dominant fraction presented with a hydrodynamic diameter exceeding 100 nm. When suspended in PBS, the **ND-COOH** exhibited a tendency for forming larger aggregates, revealing sole fraction with hydrodynamic diameter of 395 nm. The enhanced aggregation in PBS can likely be attributed to the salting-out effect, a phenomenon frequently present in electrolyte solutions. Further study of **ND-A1** in PBS indicated enlarged aggregation with a hydrodynamic diameter of 530 nm. Meanwhile, **ND-A2** possessed dual populations with diameters measuring 165 nm and 615 nm, respectively; **ND-A3** reveals the size of ca. 460 nm with higher polydispersity. These findings underscore that the grafting of organic functionalities onto the **ND-COOH** surface visibly increased tendencies to aggregation when the nanoparticles are dispersed in solution.

The mammalian cell toxicity was studied by MTT cytotoxicity assay, when the viability of MDCK cells after treatment with **ND-A1** was evaluated to have IC_{50} values >500 μg/ml. It supports the general point of view that NDs are non-toxic to a variety of cell types, but they remain persistent, as most carbon nanoparticles[259]. The structure of a 'corona' on the carbon-based nanomaterial is essential, and if organic materials on the carbon nanoobjects are composed of the fragments that are fully degraded, no exposure takes place. To address this question, the functional fragment composed of 4-pyridiniumoxime linked to PEG-diamine was studied in aerobic biodegradation by means of modified closed bottle test (CBT OECD 301D),[260, 261] which allows measuring BOD without opening the flasks, thereby reducing the number of parallels required for each compound and increasing test throughput. The biological oxygen consumption was measured with an optode oxygen sensor system using oxygen sensor spots. The ultimate biodegradation (mineralization) is achieved when the test compound is totally utilized by the inoculum

microorganisms resulting in the production of carbon dioxide, water, and minerals[262]. In the CBT, it is used to operate the term 'readily biodegradable' for those chemicals which have passed CBT showing 60% of or more, assuming these compounds to biodegrade rapidly and completely in aquatic environments under aerobic conditions. The compounds demonstrating biodegradation of 20% to 60% are called inherently biodegradable. The studied oxime does not pass the CBT reaching less than 20%, i.e., it is not readily biodegradable but may reach 20% of biodegradation if the time of experiment is extended or a higher-tier OECD simulation tests applied. Therefore, the **ND-A1** is non-toxic to mammalian cells and not readily biodegradable in the environment.

To assess the capacity of the synthesized **ND-A1-A3** to cross the cellular barriers there were chosen MDCK and HUVEC assays, two of the predominant *in vitro* models for studying the BBB.[263]

The ability of **ND-COOH** and **ND-A1** to diffuse over the MDCK's cell membrane from the donor compartment into the acceptor compartment in the double-well experiment was measured by UV-VIS spectrometry at different incubation times and assessed quantitatively as apparent permeability, P_{app} [264](***Table 3***). In this model, compounds showing P_{app} >3×10^{-6} cm/s have high potential to enter the CNS, and compounds with P_{ap} <1×10^{-6} cm/s have very low chances to penetrate the BBB.[265] The starting ND material**,** **ND-COOH** were dispersed with quaternary oximes - antidotes Pralidoxime (***Figure 7***) and HI-6 (***Figure 9***) in OptiMEM serum media. UV-Vis spectroscopy and fluorometric analysis revealed no detectable presence of **ND-COOH** in the acceptor compartment and there was no evidence that the monolayer was disturbed by nanoparticles.

Table 3*. Apparent permeability of* ***ND-A1*** *and selected small molecular drugs across the MDCK cell membrane.*

Compound	BBB Penetration Estimation P_{app} ± SEM (× 10^{-6} cm s^{-1})	CNS (+/-)
ND-COOH (100 µg/ml) + Pralidoxime	0.00 ± 0.00	**CNS -**
ND-COOH (100 µg/ml) + HI-6	0.00 ± 0.00	**CNS -**
ND-A1 10 µg/ml	14.55 ± 1.10	**CNS +**
ND-A1 100 µg/ml	4.68 ± 2.46	**CNS +/-**
Donepezil	26.80 ± 2.70	**CNS +**
Testosteron	30.16 ± 3.99	**CNS +**
7-methoxytacrine	17.19 ± 3.56	**CNS +**
Sulfasalazin	0.96 ± 1.06	**CNS -**
Cefuroxime	0.00 ± 0.00	**CNS -**
Obidoxime	1.00 ± 0.33	**CNS -**
	expressed as P_{app} ± SEM	

At the same time, **ND-A1** demonstrates ability to diffuse from the donor compartment through the MDCK cell membrane. The **ND-A1** at a lower concentration (10 µg/mL in suspension) showed remarkably better permeability than in a higher concentration (100 µg/mL), which is assumed to be related to an increased aggregation of NDs at higher concentrations or to their accumulation inside the cells. A preliminary assessment of the intracellular quantity revealed that cells accumulated roughly 13% (for 10 µg/ml) and

30% (for 100 μg/ml) of the overall concentration of **ND-A1**. The P_{app} value for **ND-A1** is evaluated to come across the BBB with the permeability similar to 7-methoxytacrine, a drug for treatment of Alzheimer's disease[266] and only about twice lower compared to the drugs known to be capable of easily crossing the BBB – hormone testosterone and donepezil, reversible cholinesterase inhibitor. The Obidoxime, established antidote – reactivator of OP-inhibited AChE demonstrates extremely low permeability.

The reactivation potency of oximes **ND-A1 – A3** were assessed on human recombinant AChE inhibited by V-agents Sarin (GB) and VX, and by OP pesticide paraoxon (POX) (***Table 4***).[131, 267] The AChE activity was determined spectrophotometrically using a modified approach described by Ellman.[268] The **ND-A1 – A3** demonstrated relatively low reactivation capacity compared to Obidoxime but exceed it in the apparent permeability across the BBB model. The reactivation efficiency is not concentration-dependent: increase in concentration from 10 μg/ml to 100 μg/ml changed reactivation capacity of the conjugates insignificantly or slightly reduced it.

Table 4*. Reactivation capacity of* ***ND-A1 – A3*** *towards AChE inhibited by OP*

Oxime	% Reactivation after Sarin		VX		POX	
	100 μg/ml (% ± SD)	10 μg/ml (% ± SD)	100 μg/ml (% ± SD)	10 μg/ml (% ± SD)	100 μg/ml (% ± SD)	10 μg/ml (% ± SD)
Obidoxime	30.88± 0.34	12.29± 0.21	35.36± 0.79	14.91± 0.31	57.79± 1.14	21.69± 0.22
ND-A1	0.88 ± 0.35	0.58 ± 0.04	0.80 ± 0.00	0.70 ± 0.70	1.93 ± 0.92	1.93 ± 0.34
ND-A2	1.11 ± 0.41	1.17 ± 0.01	0.54 ± 0.47	0.71 ± 0.05	1.53 ± 0.38	2.48 ± 1.14
ND-A3	0.56 ± 1.74	1.13 ± 0.52	1.10 ± 0.45	0.82 ± 0.01	1.89 ± 0.44	0.95 ± 0.02

Following cell lysis in the MDCK experiment, the intracellular accumulation of **ND-A1** in the MDCK monolayer was assessed. The ability of **ND-COOH** and **ND-A1** to facilitate transport of the antidotes across BBB was studied in the experiments on uptake and internalization using MDCK and HUVEC cell lines. HUVEC cells were grown on gelatin-coated coverslips until the confluent layer was reached and treated with an astrocyte medium mixed 50:50 with endothelial cell growth medium for 24 h to form uniform layer of cells. **ND-A1** successfully penetrated HUVEC and MDCK cells after 1 h at the lowest concentration of 10 μg/ml. The HUVEC cells were visualized using Imaris software and rotated to illustrate the intracellular **ND-A1** particles by using section and 3D view (***Figure 25***) and fluorescent antibodies. The difference between the TJs of control and cells treated with NDs is obvious. Longer incubation periods with NDs disrupt the TJs considerably and the TJs' integrity depends on the concentration of NDs. NDs showed the formation of large aggregates upon entering the cell irrespective of their initial concentration. However, the cytoskeleton of HUVEC seemed intact even at 24 h treatment with the highest concentration.

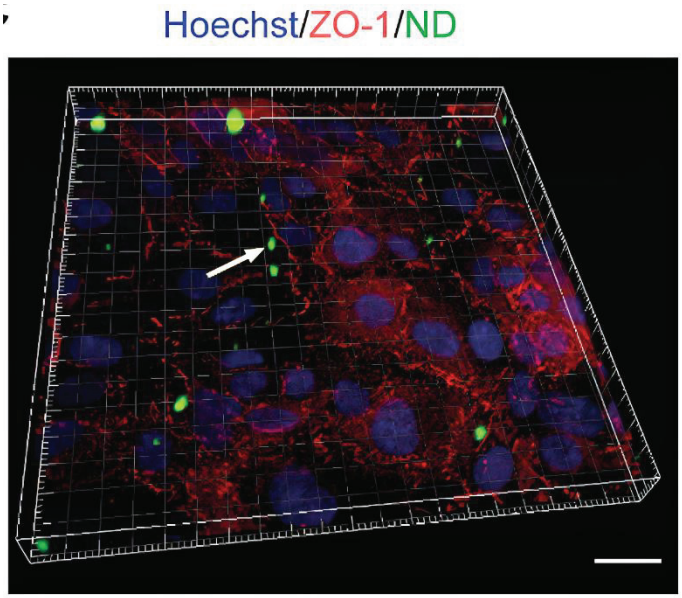

***Figure 29**. Confocal microscopy analysis of HUVEC after 1 h of ND-A1 at concentration of exposure using 3D Imaris image analysis.*

Nanodiamonds have emerged as a viable drug delivery system for crossing the BBB into the CNS, as shown by *in vitro* studies using the MDCK and HUVEC assays. The **ND-A1**, **ND-A3** and **ND-A3** demonstrated ability to restore human inhibited AChE, but the reactivation capacity towards human inhibited AChE is not strictly dose-dependent. Enhanced therapeutic efficiency may be achieved through structural optimization of the antidote and advanced synthetic techniques for improved surface modification. Our findings prove the potential of detonated NDs as an innovative platform to deliver therapeutic drugs to the targeted tissues.

3.2 Design of arylhydroxamic acids as AChE reactivators (Publication II)

As was shown in section **1.3.2**, more efforts are needed to develop a flexible antidote that can be used to address damage to both the peripheral and central nervous systems to effectively treat acute OP poisoning.

Finding a right balance of properties, such as hydrophobicity, BBB score, toxicity, biodegradability, reactivation capacity, is criteria for choosing the most promising antidotes. As a starting point, hydrophobicity (log $P_{o/w}$) of possible hydroxamic reactivators was calculated by three open access cheminformatics tools: a) www.chemicalize.com; b) www.molinspiration.com; c) www.vcclab.org and evaluated in relation to the BBB score predicted by www.cbligand.org.

According to the calculations, the solubility in water of *N*-substituted hydroxamic acids decreases as the chain length increases. Alkyl substituents longer than hexyl are too hydrophobic and may bind to the BBB rather than facilitate transportation over the barrier. Butyl chain would be ideal, according to our calculations, as it exhibits more noteworthy hydrophobic qualities than unsubstituted analogs and *N*-methyl derivatives, but does not reach the “plateau” in the graph of BBB score vs log P. The behaviour of *N*-phenyl derivative differs from the *N*-alkyl ones, which may be related to influence of

its aromatic ring. It was assumed that *N*-butyl hydroxamic acids will be leading structures able to reactivate the blocked AChE with improved permeability across the BBB and stability against Lossen rearrangement.

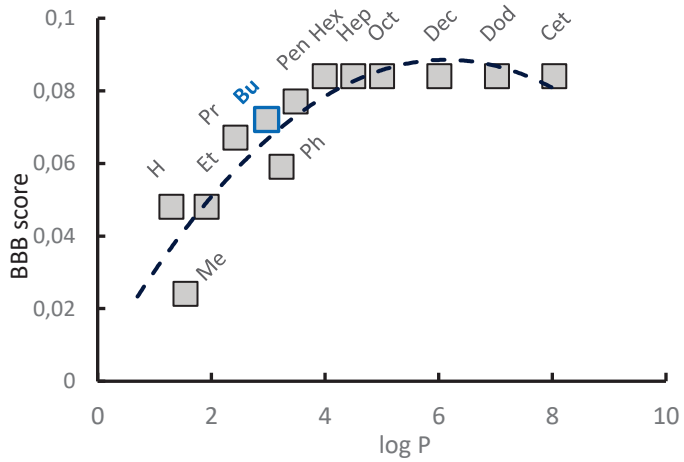

***Figure 30**. Correlation between BBB score (www.cbligand.org) vs partitioning coefficient octanol – water log P (www.molinspiration.com) calculated for N-substituted salycilhydroxamic acids. Adopted and changed from Publication II.*

The structures of four *N*-butyl hydroxamic acids were chosen for molecular docking calculations to select the candidates with the best optimized properties. The Salicylhydroxamic acids **4a**-**c** were chosen as prospective examples to explore changes of properties in the series H–Me–*n*–Bu–Ph, were the *ortho*–hydroxyl group adjacent to the reactive centre could assist in intramolecular reactivation reactions.

Protonation states of the *N*-butyl arylhydroxamic acids **1c**, **2c**, **3c** and **4c** and salicylhydroxamic acid **4a** at pH 7.4 were modelled, using the Chemicalize site. Docking results showed that most of the molecules were neutral with few single charged anions formed by deprotonation (***Table 5***).

The docking energy calculations, ligand-protein interaction energies were analyzed to understand binding modes and molecular reactivation factors (***Table 6***). Specific parameters, the interatomic distances between the nucleophile of the ligand and the P atom (d_{NP}), the angle formed by these two atoms and Ser203 oxygen atom (θ_{NPO}), the residues interacting with the ligand through hydrogen bonds (E_{Hbond}), and the interaction energy values (E_{inter}) were crucial for determining successful nucleophilic attacks. The compounds showcased negative binding energy values, indicating stabilization within the HssAChE-OP complexes. Notably, protonation states did not significantly alter poses for a molecule. Docking results of *N*-butylhydroxamic acids demonstrated the best E_{Hbond} / E_{inter} ratio, particularly the **4c**. The study also highlighted the role of acidity dissociation constants (pK_a) in hydroxamic acids, pointing out their significance in deprotonation under physiological conditions.

***Table 5**. The protonation states of prepared acids. Adopted and changed from Publication II.*

Compound	Protonation state	Distribution at pH=7.4
1c	HA	87.24%
	A^-	12.76%
2c	HA	86.37%
	A^-	13.63%
3c	HA	88.28%
	A^-	11.72%
4a	HA	78.04%
	A^-	18.26%
4b	HA	78.01%
	A^-	18.91%
4c	HA	76.67%
	A^-	18.72%
4d	HA	62.97%
	A^-	27.09%

The studied compounds showed negative binding energy values in all models, indicating effective stabilization of the ligands within the HssAChE-OP complexes. Despite varying protonation states, no significant pose variations were observed for any molecule. ***Table 6*** contain data on the neutral species, being the predominant form for all ligands. *N*-butyl salicylhydroxamic acid **4c** outperform the *N*-phenyl derivative in terms of E_{Hbond}. Among the *N*-butyl derivatives, **4c** emerged as the most promising candidate. Varying from *N*-butyl to *N*-phenyl does not markedly change reactivation potential but does intensify compound toxicity. The binding of *N*-butyl salicylhydroxamic acid **4c** to AChE was stronger than that of *N*-phenyl derivative (***Figure 31***) and its computed pose in the CAS allowed attack on the inhibited AChE.

***Table 6**. Docking energies of designed acids with HssAChE inhibited by GB. Adopted and changed from Publication II.*

Compound	d_{NucP} (Å)	θ_{NucPO} (°)	E_{Hbond} (kcal/mol)	E_{inter} (kcal/mol)
1c	6.22	151.96	-5.00	-95.97
2c	4.69	149.70	-6.38	-96.72
3c	4.52	155.42	-6.40	-101.36
4a	6.18	148.35	-8.84	-76.22
4b	5.54	145.90	-12.57	-75.92
4c	5.67	151.95	-7.96	-99.49
4d	5.31	143.10	-5.00	-100.11

Although compounds **4a** and **4b** exhibited the lowest interactions in the CAS of HssAchE complexes, their nucleophile-to-phosphorus distances were relatively minimal. Combined with stable hydrogen bond interactions, these factors suggest that **4a** and **4b** might also possess strong HssAchE reactivation properties. Notably, reduced nucleophile-to-phosphorus distances enhance the likelihood of nucleophilic attacks on the phosphorus atom, facilitating the removal of nerve agents.

Key residues facilitating ligand stabilization in HssAChE-GB via hydrogen bonding include Tyr124, Ser125, Tyr133, and Tyr337. In HssAChE-VX, significant hydrogen-bonding residues are Tyr124, Phe295, and Arg296, while in HssAChE-PON, they are Tyr124, Trp286, and Arg296.

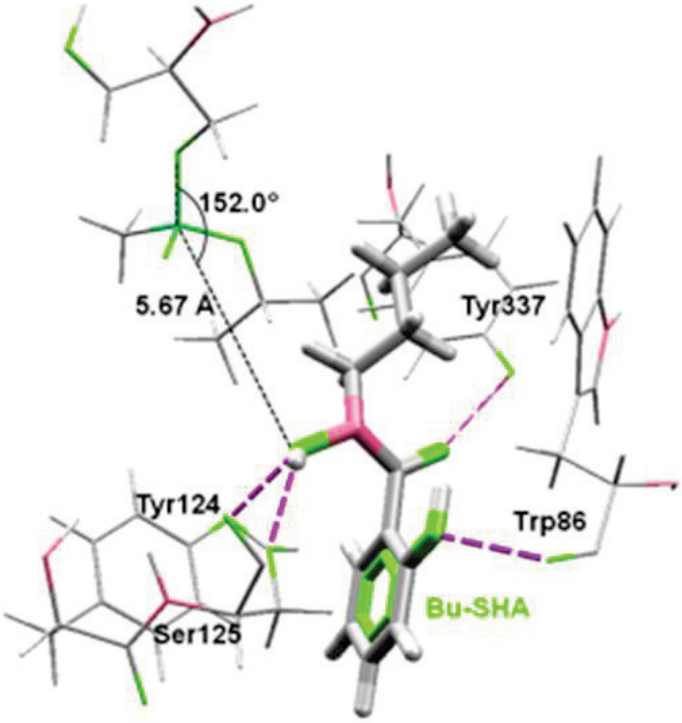

***Figure 31**. Molecular docking of **4c** in CAS of AChE. Adopted and changed from Publication II.*

As a result, a series of benzhydroxamic **1a**, 3-methoxybenzhydroxamic **2a**, 4-methoxybenzhydroxamic **3a**, and salicylic hydroxamic acids **4a** were prepared and converted into corresponding *N*-H (**a**), *N*-methyl (**b**), *N*-butyl (**c**), and *N*-phenyl (**d**) derivatives according to the ***Scheme 14***. The substances were purified and crystallized to obtain pure compounds, characterized by melting points, HRMS, ^{1}H and ^{13}C NMR spectroscopy, FTIR.

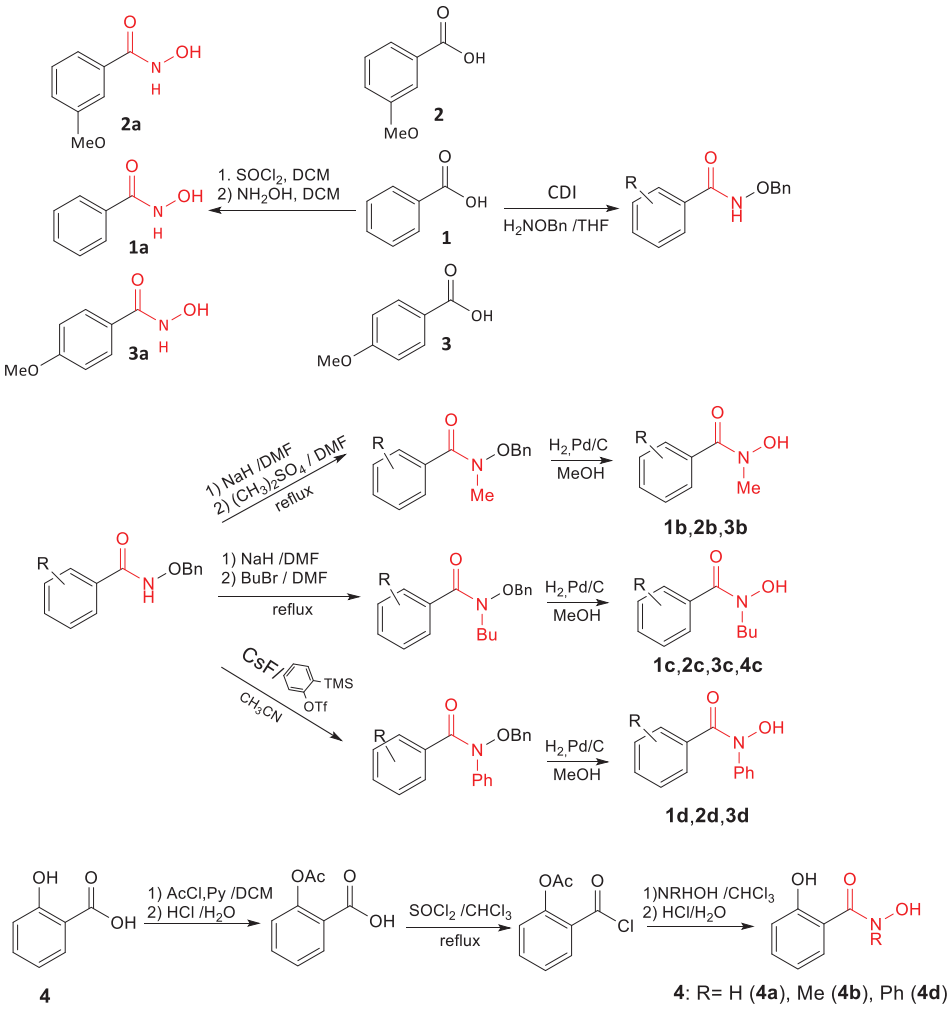

***Scheme 14**. Synthesis of hydroxamic acids. Adopted and changed from Publication II.*

The experimental study of passive transport prediction across the BBB was done using the PAMPA assay[269] for a series of *N*-butyl derivatives (**1c**, **2c**, **3c**, **4c**) and salicylhydroxamic acids (**4a-d**) with varying substituents at the nitrogen (***Table 7***). All compounds exhibited a high predicted BBB permeation. Specifically, the *N*-butyl derivatives showed a permeation order of **3c** < **1c** < **2c** < **4c**, highlighting the salicylhydroxamic derivative as the most promising candidate for BBB penetration. For the salicylhydroxamic acids **4a-d**, there was negligible difference between the Pe values for *N*-H **4a** and *N*-methyl derivatives **4b**, but the *N*-phenyl salicylhydroxamic acid **4d** showed a significant enhancement, with the order being **4a** ≈ **4b** < **4d** < **4c**. Compound **4c**, an N-butyl derivative of salicylhydroxamic acid, emerged as the most promising in terms of BBB permeability among all the compounds evaluated.

***Table 7**. BBB penetration predictions for compounds based on PAMPA assay. Adopted and changed from Publication II.*

Compound	P_e (×10^{-6} cm s^{-1}) ± SEM	n	CNS Prediction	Tendency
4a	5.64 ± 0.87	3	**CNS (+)**	Acceptable
4b	5.58 ± 0.81	3	**CNS (+)**	Acceptable
4d	12.63 ± 1.71	2	**CNS (+)**	Good
4c	29.03 ± 0.95	2	**CNS (+)**	High
2c	23.75 ± 1.38	2	**CNS (+)**	High
1c	11.69 ± 2.15	2	**CNS (+)**	Good
3c	7.06 ± 2.94	2	**CNS (+)**	Acceptable

n = number of measurements;

CNS + (high BBB permeation predicted): P_e (×10^{-6} cm s^{-1}) > 4.0[269]

The ability of the designed hydroxamic acids to restore activity of human AChE inhibited by GB, VX, and paraoxon was tested (***Figure 32***). The prepared compounds exhibited moderate reactivation potency in all cases. The *N*-methyl derivatives were always more active than *N*-H compounds. Noticeable, the *N*-butyl substituted acids demonstrated relatively increased reactivation capacity, particularly towards VX. The *N*-butyl salicylhydroxamic acid **4c** exhibited most promising activity amongst other *N*-butyl derivatives.

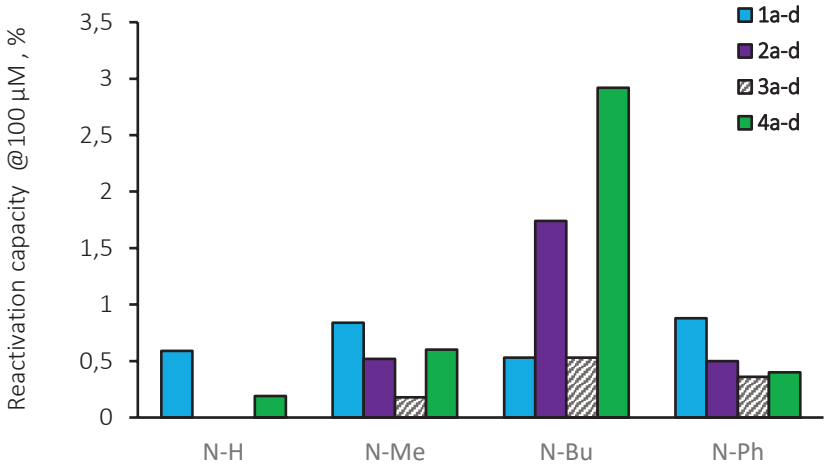

***Figure 32**. Reactivation potency towards VX-inhibited AChE of studied hydroxamic acids. Adopted and changed from Publication II.*

A striking difference was observed between the activities of *N*-butyl and *N*-phenyl derivatives. The cytotoxicity of the studied compounds was assessed using Chinese hamster ovary (CHO-K1) cells. It was found that the introduction of the *N*-methyl group generally led to a decrease in toxicity, particularly when replacing an *N*-H. This trend was consistent until the introduction of more hydrophobic substituents, such as extending from *N*-methyl to *N*-butyl, which increased toxicity. However, it was noted that *N*-butyl derivatives were typically less toxic than their *N*-phenyl analogs, except for *N*-butyl

salicylhydroxamic acid **4c**. When considering the combined data, the preference for *N*-butyl substituted hydroxamic acids (**1c**, **2c**, **3c**, **4c**) over other derivatives became evident, leading to their selection for biodegradation studies.

The arylhydroxamic acids are known to undergo biodegradation, especially in the presence of glucose or a combination of glucose and peptone.[4] Acyclic hydroxamic acids generate reactive intermediates with potential biological implications, including DNA interactions.[166] Later studies revealed that salicylhydroxamic acid biotransformation in liver tissues is influenced by its metal ion chelation ability. [156] For assessing biodegradability, the Closed Bottle test (CBT) was used on *N*-butyl substituted hydroxamic acids.[270] Of the four *N*-butyl derivatives tested, only benzhydroxamic acid derivative **1c** pass the test on readily biodegradability (***Table 8***). The introduction of the butyl substituent to other aryl hydroxamic acids affected their biodegradability, with 3-methoxy **2c** and 4-methoxy **3c** derivatives nearing the 20% threshold, marking them as inherently biodegradable. On the other hand, salicylhydroxamic acid **4c**, which did not reach the 20% threshold, was classified as non-biodegradable within the experimental timeframe. Despite this, **4c** exhibited higher persistence and toxicity compared to other *N*-butyl derivatives.

Table 8. *Biodegradability of N-butyl hydroxamic acids **1c, 2c, 3c, 4c**. Adopted and changed from Publication II.*

Structures	D% 28 days	D% 33 days
1c	70	73
2c	25	27
3c	26	28
4c	13	14
D% - biodegradation percentage		

A series of arylhydroxamic acids with varying nitrogen substituents was synthesized and their hydrophobicity, BBB score, and potential to bind the active site of human AChE inhibited by OP compounds were assessed. Increased hydrophobicity coined predicted BBB permeability. Notably, as the nitrogen substituent was enlarged from to *N*-butyl or *N*-hexyl, permeability peaked, a finding confirmed by the in vitro PAMPA test which highlighted **4c** as having superior permeability. Molecular docking revealed that *N*-butyl derivatives met reactivator configuration requirements, with *N*-butyl salicylhydroxamic acid **4c** exhibiting a pronounced E_{Hbond}. While all compounds showed moderate reactivation capacities, the **4c** stood out, whereas *N*-phenyl compounds exhibited higher toxicity. Interestingly, *N*-methyl derivatives were less toxic than their *N*-H counterparts. Of all compounds, *N*-butyl derivatives, particularly *N*-butylsalicylhydroxamic acid **4c**, showcased the best balance of properties. However, **4c** has the lowest biodegradability. These insights help the development of improved antidotes against OP poisoning.

3.3 Design of PARP inhibitors based on cyclic arylhydroxamic acids (Publication III)

The hydroxamic moiety found wide application in design of anticancer drugs aimed at suppression of HDAC enzymes but were not used to disrupt normal work of PARP protein, another important target for antitumor therapy. The literature data in section **1.3.3** demonstrated that latest developments in anticancer treatment highlighted the different biological and pharmacological properties of hydroxamic acids that led to their application in medicine. The hydroxamic acids are the class of α-nucleophiles with a strong potential for antitumor activity.

The hydroxamate moiety is the key structural element in many highly potent and selective inhibitors of a variety of metal-dependent enzymes, including HDAC. However, it exhibits relatively low stability *in vivo*, which could be avoided by appropriate drug design. Among the possible methods, direct acylation of the suitable N-O derivative, direct oxidation of the matching amide, and N-substitution of hydroxamic acids allowed the synthesis of new biologically active molecules. It was reported that hydroxamic acids were combined with additional pharmacophore groups in one molecule to create medicines that simultaneously target PARP and HDAC. Although the intended multidrug activity was seen and both PARP and HDAC were inhibited, substantial non-selective cytotoxicity reduced the total effectiveness.

The fact that hydroxamic acids are binding to metal ions inside the cell is a drawback. In fact, it is known that the *N*-hydroxy metabolites generate reactive species that causes negative side effects. However, the *N*-OH species' reactivity typically occurs when the nitrogen atom is not included in a cyclic structure and does not significantly arise for the bioactive heterocycles containing endocyclic *N*-OH (*N*-OR) groups. To the best of our knowledge, there have been no comprehensive studies of *N*-O substituted phenanthridinones as possible PARP inhibitors due to inherited toxicity as N-hydroxy derivatives of benzamide and aryl hydroxamic acid and their O-substituted derivatives.

We chose to use *N*-(benzyloxy)benzamides as starting compounds to produce novel phenanthridinones based on our prior experience with hydroxamic acids as an effective reactivator of the inhibited AChE. Using *N*-(benzyloxy)benzamide **5a** as a substrate, double excess of iodobenzene as an arylating agent under catalysis by $PdCl_2$ (10 mol%) and silver nitrate as an oxidant in 1 mL of glacial acetic acid in an argon atmosphere the reaction was carried out (***Scheme 15***). The system was then degassed three to four times by a vacuum pump and flushed with argon. The required product **5b** was obtained in a 36% yield after 24 hours of refluxing the resultant suspension under argon flow.

To enhance reaction efficiency, several parameters were evaluated, including the type of catalyst, its amount, oxidants, solvents, the temperature of the reaction, and the duration.

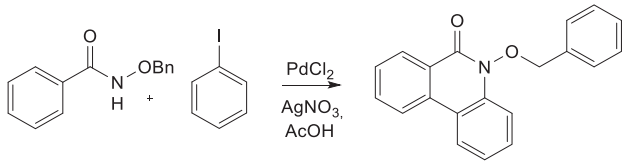

5a **5b** (36%)

Scheme 15*. Initial reaction parameters to obtain phenanthridinone scaffold* ***5a*** *(0.2 mmol), iodobenzene (2.0 equiv.), catalyst (10 mol %), 1 mL AcOH, reflux 24 h.*

A range of catalysts were explored, with a focus not just on the rare and pricey metals but also on commonly available *d*-metals. Among all tested, palladium acetate was identified as the most effective (***Table 9***). In contrast, cobalt acetate exhibited no activity, even when its proportion was increased to 20%. A Pyridine-based catalyst, initially seemed promising, led to the complete consumption of the starting material, *N*-(benzyloxy)benzamide **5a**, via the Lossen rearrangement, attributed to the basic nature of its organic ligand. Interestingly, despite palladium chloride containing a higher percentage of Pd compared to palladium acetate, it was found to be less effective.

Table 9*. Optimization of the catalyst. Adopted and changed from Publication III.*

Cat	Oxidant	Solvent	Yield*
$PdCl_2$	$AgNO_3$	AcOH	36
$Pd(PPh_3)$	$AgNO_3$	AcOH	53
$Pd_2(dba)_3$	$AgNO_3$	AcOH	34
$Pd(OAc)_2$	$AgNO_3$	AcOH	62
$Co(OAc)_2$	$AgNO_3$	AcOH	00
$Cl\text{-}Co(dmH)_2Py$	$AgNO_3$	AcOH	-

Reaction conditions: ***5a*** (0.2 mmol), iodobenzene (2.0 equiv.), catalyst (10 mol %) with 1 mL solvent in 24 h; * detected conversion by NMR

After that, different oxidants were tried to increase the yield of the desired product, and silver oxide proved to be the best one. Usage of double excess of that oxidant gave the best result under used reaction conditions. The starting acetic acid was more efficient as a solvent, while the formic and propionic considerably lowered the reaction yield (***Table 10***).

Table 10*. Optimization of the oxidant and its loading, solvent. Adopted and changed from Publication III.*

Cat	Oxidant	Solvent	Yield*
$Pd(OAc)_2$	$AgNO_3$	AcOH	62
$Pd(OAc)_2$	$Na_2S_2O_8$	AcOH	53
$Pd(OAc)_2$	PIDA	AcOH	34
$Pd(OAc)_2$	$FeCl_3$	AcOH	14
$Pd(OAc)_2$	Ag_2O	AcOH	87
$Pd(OAc)_2$	Ag_2O (1.5 eq.)	AcOH	67
$Pd(OAc)_2$	Ag_2O (2.5 eq.)	AcOH	78
$Pd(OAc)_2$	Ag_2O	HCO2H	47
$Pd(OAc)_2$	Ag_2O	$CH_3CH_2CO_2H$	63

Reaction conditions: *N*-(benzyloxy)benzamide (0.2 mmol), iodobenzene (2.0 eq.), catalyst (10 mol %) with 1 mL solvent in 24 h;* detected conversion by NMR

To optimize the synthesis conditions, various parameters including catalyst loading, reaction temperature, and synthesis time were examined (***Table 11***). It was observed that the absence of the catalyst resulted in no yield. A catalyst loading of 2.5 %mol provided a yield of 51%, which further increased to 82% upon using 5 %mol of the catalyst at 120°C for 24 hours. However, increasing the catalyst loading to 10 %mol only

slightly improved the yield to 87%.The reaction's sensitivity to temperature was also evident. At an optimal catalyst loading of 5 %mol, decreasing the temperature to 100°C slashed the yield to 43% and further reducing it to 80°C completely halted the reaction. Time played a major role. With 5 %mol of the catalyst at 120°C, halving the reaction time to 12 hours resulted in a decreased yield of 34%. Extending the reaction time to 48 hours provided a yield of 77%, but a further extension to 72 hours slightly reduced the yield to 72%. These results underscore the importance of the optimization of the reaction with best conditions involve using a catalyst loading of 5-10 %mol at 120°C for 24 hours.

***Table 11**. Optimization of the catalyst loading, time and temperature of the reaction. Adopted and changed from Publication III.*

Cat	Temperature	Time	Yield*
10 %mol	120 °C	24 h	87
0 %mol	120 °C	24 h	00
2.5 %mol	120 °C	24 h	51
5 %mol	120 °C	24 h	82
5 %mol	100 °C	24 h	43
5 %mol	80 °C	24 h	00
5 %mol	120 °C	12 h	34
5 %mol	120 °C	48 h	77
5 %mol	120 °C	72 h	72

Reaction conditions: **5a** (0.2 mmol), 2 (2.0 equiv.); * detected conversion by NMR

The developed synthetic pathway was explored using the optimized reaction parameters with systematic examination of the substrates scope. All studied substrates offered average to good yields. For *N*-(benzyloxy)benzamide **5a**, the effects of electron-donating and electron-withdrawing groups were investigated. It was discovered that the corresponding products **5c-f** were produced in good yields from the *N*-(benzyloxy)benzamides with electron-donating groups (such as -OH, -OMe) (***Table 12***).

***Table 12**. Structure of prepared N-(benzyloxy)phenantridinones. Adopted and changed from Publication III.*

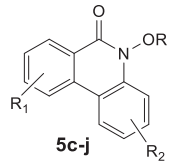

5c-j

Compound	R	R_1	R_2
5c	Bn	5-MeO	H
5d	Bn	5-MeO	3-O_2N
5e	Bn	6-MeO	H
5f	Bn	8-HO	H
5g	Bn	H	2-$NHC(O)CH_2NMe_2$
5h	H	H	2-$NHC(O)CH_2NMe_2$
5i	Bn	H	3-$NHC(O)CH_2NMe_2$
5j	H	H	3-$NHC(O)CH_2NMe_2$

Based on previously published data[271] we assume that palladium-catalysed dual C-H and N-H activation results in the cascade synthesis of the targeted phenanthridinones (***Scheme 16***). The suggested reaction mechanism involves C-H/N-H activation, when two new C-C/C-N bonds are formed and four existing bonds are simultaneously broken. The coordination of the Pd (II) species to the nitrogen atom in the first step of the catalytic cycle. This results in the formation of the five-membered palladacycle intermediate I, due to the electrophilic displacement of ortho-hydrogen in the phenyl moiety. Oxidative addition of aryl iodide results in Pd(IV) intermediate II that turns into *ortho*-arylated Pd(II) complex IV as a result of reductive elimination of Pd(II). Ligand exchange produces the *ortho*-arylated product and regenerates Pd(II) intermediate VI, which is oxidized by silver oxide to produce Pd(IV) complex V which, in turn, produces seven-membered Pd (IV) palladacycle VI. The latter is converted into the final product through reductive elimination of Pd(II). The isolation of the intermediate product of two ortho-arylations supports these two steps.

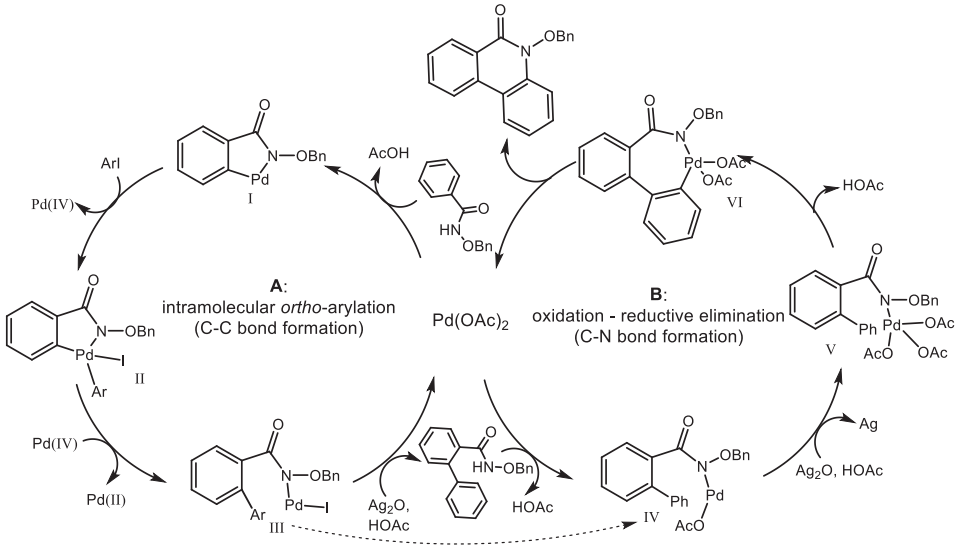

Scheme 16*. Suggested mechanism of dual C-H/N-H activation in the synthesis of phenanthridinones.*

The structural analogues of PJ34, a 2nd generation PARP inhibitor, the **5g-j** have been synthesized to assess their cytotoxic activity, anticancer potential, and tolerance toward healthy cells. A 42% yield of the required chemical **5r** was obtained using *N*-(benzyloxy)benzamide and meta-iodonitrobenzene as an arylating agent. The significant deactivation of aryl iodide by the meta-nitro group can be used to explain the reduced yield. A combination of products with a partially reduced nitro group and a partially removed benzyl protecting group were prepared when the nitro group was reduced by Zn/HCl, Fe(II), and $SnCl_2$. The nitro-group was quantitatively reduced into the amine **5s** while the benzyl protecting group was left intact thanks to the use of a NiB_2 catalyst that was created (***Scheme 17***).

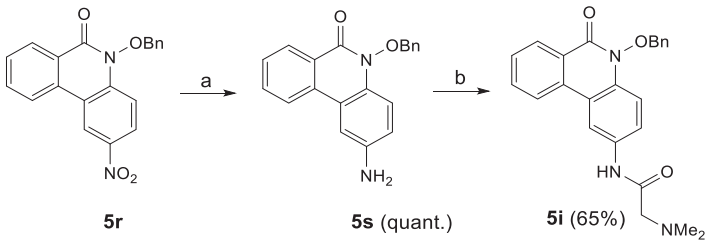

***Scheme 17**. Synthetic strategy towards synthesis of lead compounds, where:(a) NiB_2, N_2H_4 (MeOH), 2h; (b) DCC, DMAP (dry DCM). Adopted and changed from Publication III.*

Molecular models showed that *N*-(benzyloxy) derivatives should be more efficient due to the greater interaction at the catalytic site of the PARP1 enzyme (***Figure 33***). While the phenanthridinone scaffold have similar energy of interaction to PJ34 molecule the presence of *O-(benzyloxy)* substituent leads to strong $\pi - \pi$ stacking interaction with aromatic residues of PARP enzyme. Compound **5h** can indeed be called a most promising candidate in terms of all the parameters (pose of conformation, energy of ligand interaction, and hydrogen bonding with an important amino acid residue). Although compound **5j** does not have specific binding to the receptor, its binding mode practically coincides with that of PJ34, and this factor can be called decisive. Molecular dynamics study confirmed the absence of hydrogen bonds of *N*-dimethylglycine fragment. The compounds **5h** and **5j** were the first candidates for MD. Compound **5h** showed the most promising antitumor activity. At a concentration of 5 µM, this compound inhibits the growth of MDB-MB-231, HepG2 and HeLa by more than 50%, which means that its IC_{50} is expected to be ≤1 µM.

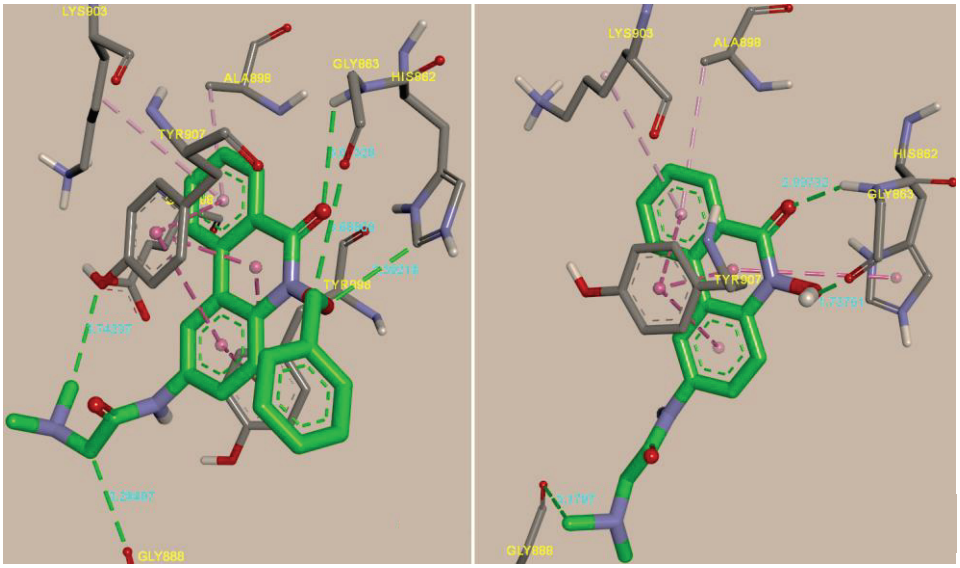

***Figure 33**. Molecular docking of phenanthridinones **5h** (left) and **5j** (right) in CAS of PARP1. Adopted and changed from Publication III.*

The WST-1 assay was used to assess the cytotoxicity of the drugs. After the compounds were applied to NIH 3T3, HepG2, BxPC3, MDB-MD-231, and HeLa cells, the vitality parameters were recorded after 48 hours. The viability of the HeLa cell line was statistically significantly reduced after 48 hours of incubation with compounds **5c–f** at a dosage of 25 mM, in contrast to the noncancer cell line NIH 3T3, where none of the compounds had any statistically significant effects on survival. Only compounds **5f** and **5d** were able to reduce cell survival statistically significantly in HepG2 cells. It is interesting to note that the BxPC3 cells likewise showed statistically significant sensitivity to the toxicity of agents **5b** through **5s**, with agent **5s** being the only one to not significantly reduce cell survival. The substances were employed in the further trials at the concentration of 50 µM to check their cytotoxicity at lower concentration. Compound **5g**, one of the most prospective candidates, was also examined at concentrations of 5 µM and 25 µM. The WST-1 assay results showed that it had a dose-dependent cytotoxic effect on all cell lines and is hazardous to cells at high concentrations (25 µM and 50 µM). However, the toxicity toward noncancer NIH 3T3 cells was minimal at low concentrations (5 µM). A kit for measuring in vitro PARP activity was used to examine a compound's impact on PARP1 activity. The chemicals **5g**, **5h**, and **5j** should have a profound inhibitory effect on the PARP1 enzyme, according to the recommendations of molecular docking. The inhibitory activity of the compounds varied and compound **5h** was the most active with IC_{50} values in the range of 49 nM (***Figure 34***). Compounds **5j** and **5g** had IC_{50} values of 495 nM and 1.36 µM, respectively. This matched the molecular docking prediction and agreed with the cell culture data.

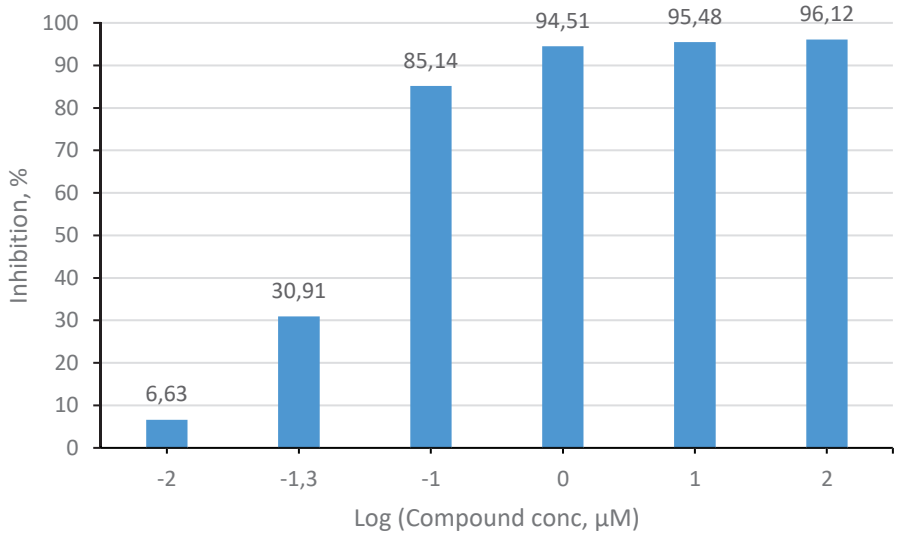

Figure 34*. The colorimetric readout of inhibition of catalytic activity of PARP1 by* ***5g****. Adopted and changed from Publication III.*

PARP-1 has emerged as a key molecular target for novel antitumor agents. In study of this, we synthesized potential inhibitors based on the *N*-(benzyloxy)- and *N*-(hydroxy)phenanthridinones scaffolds. Novel cyclic arylhydroxamic acids, based on phenanthridinone, were derived from *N*-(benzyloxy)benzamides and aryl iodides

using palladium acetate. This synthesis involved the ortho-C-H bond activation of *N*-(benzyloxy)benzamides. The resulting phenanthridinones, modified with electron-withdrawing and donating groups, were obtained in satisfactory yields with possibility of scale up. The cytotoxicity of the novel compounds against four human cancer cell lines (HepG2, BxPC3, MDB-MD-231, and HeLa cell lines) and the healthy fibroblast NIH 3T3 and HEK 293 cell lines have been evaluated. Molecular docking revealed the compounds' potential to form stable complexes with PARP-1, consolidated by further MD simulations. Specific residues in the PARP-1 catalytic centre were identified to play crucial roles in inhibition. Notably, compounds **5g**, **5h**, and **5j** displayed potent anticancer activities, inhibiting PARP-1 at low submicromolar levels. Of these, hydroxamic acid **5h** exhibited the greatest inhibitory effect, a potential lead for further refinement. This research serves as the first evidence of hydroxamic acids as efficient PARP-1 inhibitors.

3.4 Design of oxazolopyrimidines as VEGFR2 inhibitors (Publication I)

Starting from the commercially available 2-aryl-4-(dichloromethylidene)-1,3-oxazol-5(4H)-one **6a**, its reaction with amidine hydrochlorides **6b** or **6c** in the presence of triethylamine yielded imidazol-5(4)-ones **6d** or **6e**. Subsequent heating in pyridine gave oxazolo[*4,5-d*]pyrimidin-7-ones **6g** and **6h** via cyclo-condensation (***Schemes 18)***. To synthesize oxazolo[4,5-*d*]pyrimidine **6f**, we further used the protocol suggested and elaborated by Velihina et al.[236]

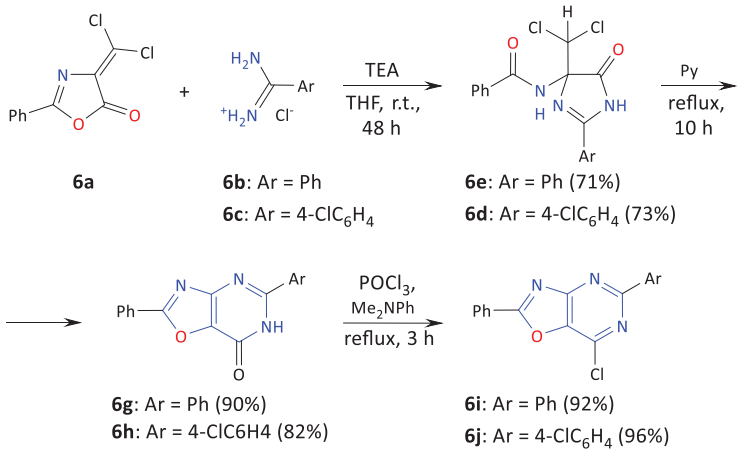

6a

6b: Ar = Ph
6c: Ar = 4-ClC$_6$H$_4$

6e: Ar = Ph (71%)
6d: Ar = 4-ClC$_6$H$_4$ (73%)

6g: Ar = Ph (90%)
6h: Ar = 4-ClC6H4 (82%)

6i: Ar = Ph (92%)
6j: Ar = 4-ClC$_6$H$_4$ (96%)

Scheme 18*. Synthesis of 7-chloro-substituted oxazolo[4,5-d]pyrimidines* ***5a-b****. Adopted and changed from Publication II.*

Further reaction of **6g** and-**6h** with phosphoryl chloride and *N,N*-dimethylaniline yielded 2,5-diaryl-7-chloroxazolo[4,5-*d*]pyrimidines **6i** and **6j**. The target, 7-*N*-Boc-piperazinoxazolo[4,5-*d*]pyrimidine **6f,** was synthesized using tert-butyl piperazine-1-carboxylate. The structural validation of intermediates was performed by NMR, IR, and elemental analyses.

The transformation of **6f** into oxazolo[4,5-*d*]pyrimidines **6i,l** involved a Suzuki-Miyaura cross-coupling with arylboronic acids (***Scheme 19)***. Boc deprotection with CF_3COOH gave oxazolo[4,5-*d*]pyrimidin-7-yl-piperazin-1-ium trifluoroacetates **6m-o**.

Functionalization of 7-chloro-substituted oxazolo[4,5-*d*]pyrimidine **6i** was achieved via a Suzuki-Miyaura reaction with phenyl - (**6p**) or 4-methoxycarbonylphenylboronic acids (**6q**), using $[Pd(\mu\text{-}Cl)Cl(IPr)]_2$, and K_2CO_3 in ethanol (***Scheme 20***). This reaction gave **6r**,**s** in 70% and 79% yields, respectively.

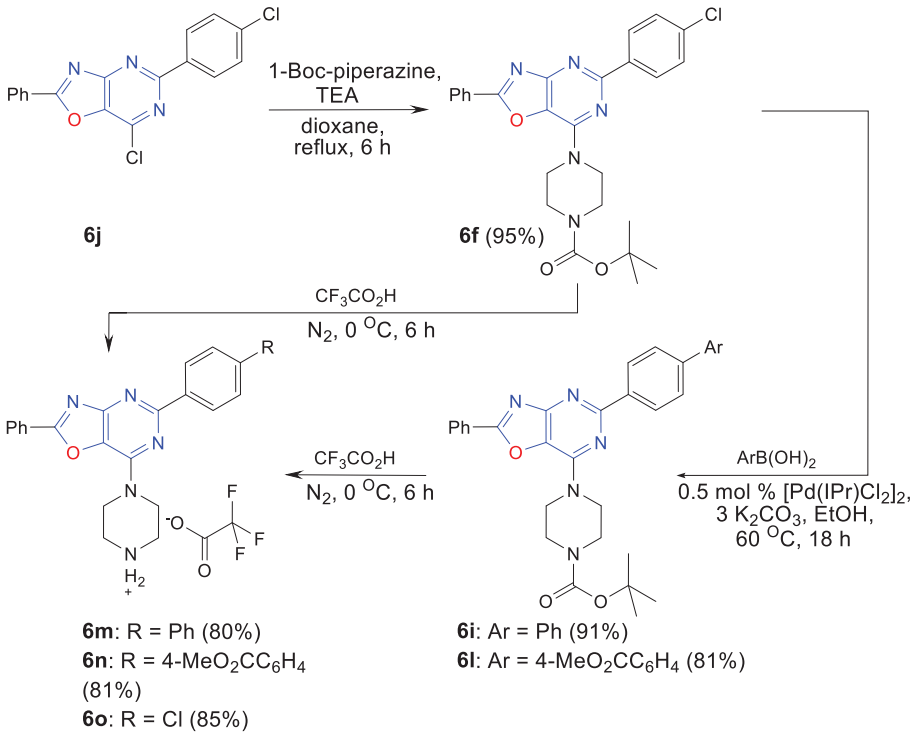

Scheme 19*. Synthesis of oxazolo[4,5-d]pyrimidines* ***6m-o****. Adopted and changed from Publication II.*

Alternatively, synthesis of an isomeric oxazolo[5,4-*d*]pyrimidin-7-one **6v** was achieved by treatment of benzoyl bromide **6t** with silver cyanide to form oxazolo[3,4-*d*][1,3]oxazine **6u** (***Scheme 21***). The subsequent reaction of **6u** with sodium methoxide and then with acetic acid gave 2,5-diphenyl-oxazolo[5,4-*d*]pyrimidin-7-one **6v**.

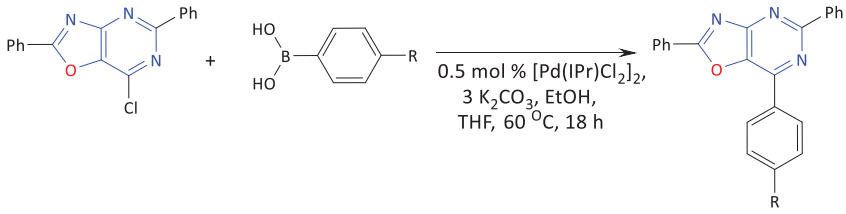

Scheme 20*. Synthesis of 7-aryl-substituted oxazolo[4,5-d]pyrimidines* ***6r,s****. Adopted and changed from Publication II.*

Compound **6v** was then treated with trichlorophosphate in the presence of *N,N*-dimethylaniline, giving 2,5-diphenyl-7-chlor-oxazolo[5,4-*d*]pyrimidine **6w**. 7-aryl-substituted oxazolo[5,4-*d*]pyrimidines **6x**,**z** were obtained similarly to **6r**,**s**.

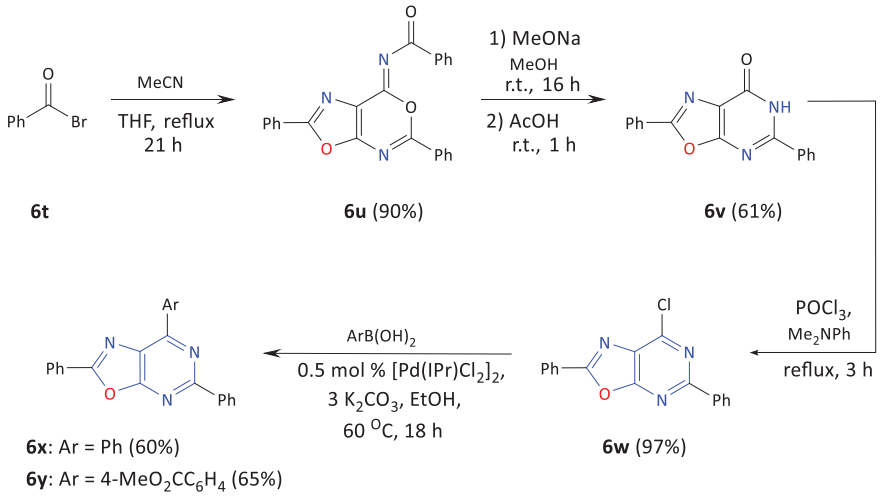

***Scheme 21**. Synthesis of oxazolo[5,4-d]pyrimidines 15.*

The relevance of oxazolopyrimidines in medicinal chemistry is underscored by their interaction with VEGFR2's ATP binding site. A redocking of the known inhibitor, sunitinib, served as a validation step. This reaffirmed our hypothesis that synthesized compounds might share a similar mechanism of action with VEGFR2.

Detailed docking analyses of bioactive compounds **6m-o** (***Figure 35***), highlighted their significant binding energies and complex interplay of hydrophobic and hydrophilic interactions, suggesting their potential as efficient drug candidates. They indicate persistent binding mode of compounds **6m-0** within the active site of VEGFR2, forming stable protein-ligand complexes with predicted ΔG values of -10.1, -9.6, and -9.8 kcal/mol, respectively.

The compounds **6m** and **6n** formed dual hydrogen bonds with amino acid Leu840 and displayed various hydrophobic interactions with several amino acids. Compound **6o**, on the other hand, demonstrated notable interactions with amino acids like Leu840 and Lys838.A comparative analysis of the docking positions (***Figure 35***), of compounds **6m-o** and the known VEGFR2 inhibitor sunitinib shown similar binding modes. To SAR ligand **6r**, characterized by the EWG at C(7) and smaller binding energy than sunitinib, was docked to VEGFR2's active center. Notably, the resulting ligand-protein complex was stabilized predominantly through hydrophobic interactions, diverging significantly from the docking positions of potent ligands **6m-o**.

Electron density calculations further confirmed the pivotal role of the π-system in stabilizing their complexes with aromatic amino acids. Their ability to form hydrogen bonds, particularly due to the lone electron pairs at two nitrogen atoms of pyrimidine, were highlighted. In essence, molecular docking results, combined with electronic structural insights, emphasized the promising therapeutic potential of oxazolopyrimidines.

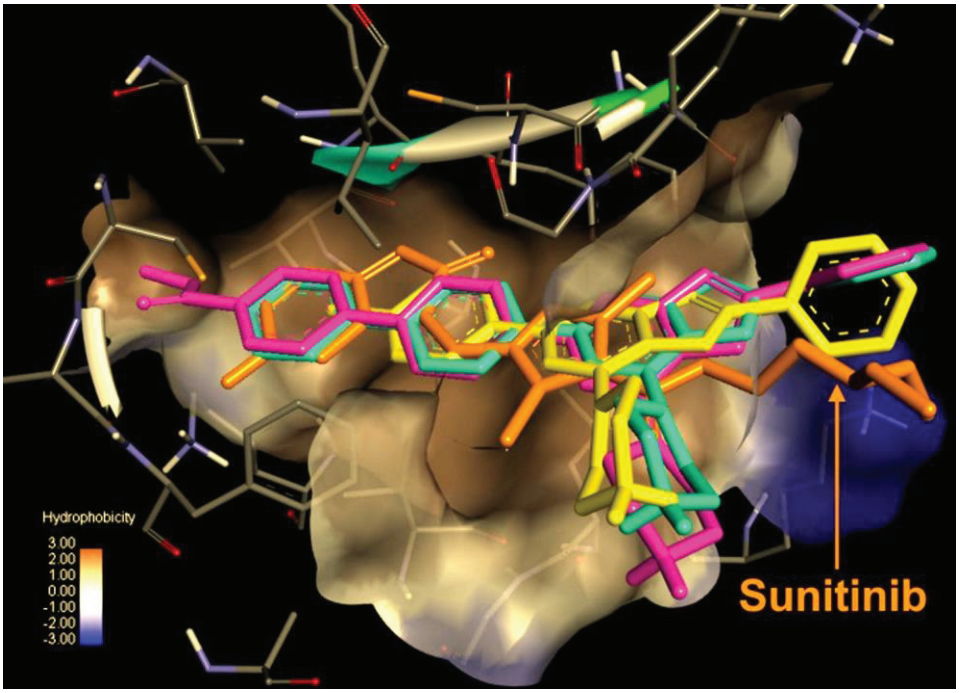

***Figure 35**. Molecular docking of compounds **6m-o** and sunitinib in CAS of VEGFR2. Compounds **6m** – blue, **6n** – violet, **6o** – yellow, sunitinib – orange. Adopted and changed from Publication I.*

The synthesized novel oxazolo[4,5-*d*]pyrimidines and their isomeric oxazolo[5,4-*d*]pyrimidines were designed with acceptor groups at the C(2) and C(5) positions and were further functionalized with either electron-donating (piperazine) or withdrawing (aryl) substituents at C(7).Molecular docking studies revealed that the oxazolo[4,5-*d*]pyrimidines **6m-o**, connected to a positively charged nitrogen in the piperazine moiety, exhibited significant binding energy. These values highlighted their potential as VEGFR2 inhibitors. In contrast, other synthesized compounds primarily formed ligand-protein complexes stabilized by hydrophobic interactions, absent of hydrogen bonding or electrostatic interactions. To determine the therapeutic potential, they were tested against HCT-116, OVCAR-3, and MDA-MB-231 cancer cell lines. Preliminary results indicated that oxazolo[4,5-*d*]pyrimidines **6m-o** exhibited greater cytotoxicity than doxorubicin, further underscoring their potential as antitumor agents. Due to these promising results, compounds **6m-o** emerged as potential candidates for further optimization of anticancer agents.

4 Conclusions

In this doctoral work, a design of drug candidates was developed based on hydroxamic acids and oximes, two classes of organic α-nucleophiles. The synthesized bioactive compounds exhibited enhanced pharmaceutical activity and reduced cytotoxicity. These compounds were prepared from readily available starting material in step-economic manner, with good yields, and chemo- and regioselectivity.

Central to our approach was the concept of target-driven synthesis, which leads to a specific change in chemical structures for better interaction with intended molecular target. This strategy inspired by structures of the existing pharmaceutical agents (Pralidoxime, PJ34) was successfully implemented using robust synthetic procedures. Specifically, our goal to develop α-nucleophiles capable of reactivating AChE and inhibiting PARP used previous experience in drug development. This approach promises to be a valuable contribution to the field of medicinal chemistry.

The specific results are:

- A general strategy for nanodiamonds as a drug delivery platform into the CNS was developed. This approach was tested for the delivery of charged oxime antidotes, with a successful internalization in an *in vitro* model of the blood-brain barrier, using MDCK and HUVEC assays;
- A rational design of *N*-substituted arylhydroxamic acids for treatment of OP poisoning resulted in synthesis of a series of compounds able to cross BBB and restore AChE;
- A series of *N*-(benzyloxy)- and *N*-(hydroxy)phenanthridinones was prepared and systematically examined as potential PARP inhibitors revealing the first-time reported inhibition of PARP1 by hydroxamic acids at submicromolar concentrations and with high cell differentiation;
- Design and preparation of isomeric oxazolo[4,5-*d*]pyrimidines and oxazolo[5,4-*d*]pyrimidines with scaffold modifications for targeting VEGFR2 was achieved with enhanced antitumor activity.

References

[1] Fina, N. J.; Edwards, J. O. The Alpha Effect. A Review. *Int. J. Chem. Kinet.*, **1973**, *5* (1), 1–26. https://doi.org/10.1002/kin.550050102.

[2] Edwards, J. O.; Pearson, R. G. The factors determining nucleophilic reactivities. *J. Am. Chem. Soc.*, **1962**, *84* (1), 16–24. https://doi.org/10.1021/ja00860a005.

[3] Grekov, A. P.; Veselov, V. Y. The α-effect in the chemistry of organic compounds. *Russ. Chem. Rev.*, **1978**, *47* (7), 631–648. https://doi.org/10.1070/RC1978v047n07ABEH002243.

[4] Rappoport, Z.; Liebman, J. F., Eds. *The Chemistry of Hydroxylamines, Oximes and Hydroxamic Acids*. John Wiley & Sons, Ltd., **2009**. https://doi.org10.1002/9780470741962.

[5] Popov, A. F.; Prokop'eva, T. M.; Suprun, I. P.; Simanenko, Yu. S. Reactivity of inorganic α-nucleophiles in the transfer of phosphoryl and phosphonyl groups. *Theor. Exp. Chem.*, **2000**, *36* (4), 208–214. https://doi.org/10.1007/BF02522753.

[6] Palling, D.; Jencks, W. P. Nucleophilic reactivity toward acetyl chloride in water. *J. Am. Chem. Soc.*, **1984**, *106* (17), 4869–4876. https://doi.org/10.1021/ja00329a040.

[7] Hansen, T.; Vermeeren, P.; Bickelhaupt, F. M.; Hamlin, T. A. Origin of the A-effect in S_N2 reactions. *Angew. Chem. Int. Ed.*, **2021**, *60* (38), 20840–20848. https://doi.org/10.1002/anie.202106053.

[8] Ibne-Rasa, K. M.; Edwards, J. O. The mechanism of the oxidation of some aromatic amines by peroxyacetic acid. *J. Am. Chem. Soc.*, **1962**, *84* (5), 763–768. https://doi.org/10.1021/ja00864a018.

[9] Hoz, S.; Buncel, E. Pitfalls in the determination of the α-effect by a two-point analysis. The effect of solvent on the α-effect. *Tetrahedron Lett.*, **1984**, *25* (32), 3411–3414. https://doi.org/10.1016/S0040-4039(01)91033-0.

[10] Bernasconi, C. F.; Leyes, A. E.; Eventova, I.; Rappoport, Z. Kinetics of the Reactions of β-Methoxy-α-Nitrostilbene with Methoxyamine and *N*-Methylmethoxyamine. Direct Observation of the Intermediate in Nucleophilic Vinylic Substitution. *J. Am. Chem. Soc.*, **1995**, *117* (6), 1703–1711. https://doi.org/10.1021/ja00111a006.

[11] Buncel, E.; Um, I.-H. The α-Effect and Its Modulation by Solvent. *ChemInform*, **2004**, *35* (45). https://doi.org/10.1002/chin.200445284.

[12] Moutiers, G.; Le Guével, E.; Cannes, C.; Terrier, F.; Buncel, E. The α-effect in S_NAr Substitutions − Reaction between oximate nucleophiles and 2,4-Dinitrofluorobenzene in aqueous solution. *Eur. J. Org. Chem.*, **2001**, *17*, 3279. https://doi.org/10.1002/1099-0690(200109)2001:17<3279::AID-EJOC3279>3.0.CO;2-9.

[13] Boudjema, H. Application of organized molecular systems for the chemical decomposition of warfare poisonous substances. *J. Russ. Chem. Soc.*, **2007**, *51*, 36–43.

[14] Morales-Rojas, H.; Moss, R. A. Phosphorolytic Reactivity of *o* -Iodosylcarboxylates and Related Nucleophiles. *Chem. Rev.*, **2002**, *102* (7), 2497–2522. https://doi.org/10.1021/cr9405462.

[15] Fountain, K. R.; Felkerson, C. J.; Driskell, J. D.; Lamp, B. D. The α-effect in methyl transfers from *S*-methyldibenzothiophenium fluoroborate to substituted *N*-methylbenzohydroxamates. *J. Org. Chem.*, **2003**, *68* (5), 1810–1814. https://doi.org/10.1021/jo0206263.

[16] DePuy, C. H.; Della, E. W.; Filley, J.; Grabowski, J. J.; Bierbaum, V. M. Absence of an α-effect in the gas-phase nucleophilic reactions of hydroperoxide ion. *J. Am. Chem. Soc.*, **1983**, *105* (8), 2481–2482. https://doi.org/10.1021/ja00346a066.

[17] Buncel, E.; Wilson, H.; Chuaqui, C. Reactivity-Selectivity Correlations: The α-effect in S_{N2} reactions at sp^3 Carbon. The reactions of hydrogen peroxide anion with methyl phenyl sulfates. *J. Am. Chem. Soc.*, **1982**, *104* (18), 4896–4900. https://doi.org/10.1021/ja00382a025.

[18] Simanenko Y; Popov A; Prokop'eva T; Karpichev E; Savelova V; Suprun I; Bunton C. Inorganic anionic Oxygen-containing α-nucleophiles-effective acyl group acceptors: hydroxylamine ranks first among the α-nucleophile series. *Russ. J. Org. Chem.* **2002**, *38* (9), 1286–1298. https://doi.org/10.1023/A:1021699628721.

[19] Patterson, E. v.; Fountain, K. R. On gas phase α-Effects. 1. The gas-phase manifestation and potential set character. *J. Org. Chem.*, **2006**, *71* (21), 8121–8125. https://doi.org/10.1021/jo061275l.

[20] Um, I.-H.; Lee, E.-J.; Seok, J.-A.; Kim, K.-H. The α-effect in reactions of sp-*hybridized* carbon atom: Michael-type reactions of 1-aryl-2-propyn-1-ones with primary amines. *J. Org. Chem.*, **2005**, *70* (19), 7530–7536. https://doi.org/10.1021/jo050624t.

[21] Séguès, B.; Ferez, E.; Rico-Lattes, I.; Rivière, M.; Lattes, A. Chemical decontamination. I. Dephosphorylation of organophosphorus compounds. *Bull. Soc. Chim. Fr.*, **1996**, *133*, 925–937.

[22] Yang, Y. C.; Baker, J. A.; Ward, J. R. Decontamination of Chemical Warfare Agents. *Chem. Rev.*, **1992**, *92* (8), 1729–1743. https://doi.org/10.1021/cr00016a003.

[23] Lossen, H. Ueber Die Oxalohydroxamsäure. *Ann. Chem. Pharm.*, **1869**, *150* (3), 314–322. https://doi.org/10.1002/jlac.18691500304.

[24] Ferry, A.; Malik, G.; Guinchard, X.; Větvička, V.; Crich, D. Synthesis and Evaluation of Di- and Trimeric Hydroxylamine-Based β-(1→3)-Glucan Mimetics. *J. Am. Chem. Soc.*, **2014**, *136* (42), 14852–14857. https://doi.org/10.1021/ja507084t.

[25] Malik, G.; Ferry, A.; Guinchard, X.; Cresteil, T.; Crich, D. *N-O* bond as a glycosidic-bond surrogate: synthetic studies toward polyhydroxylated *N* -alkoxypiperidines. *Chem. Eur. J.* **2013**, *19* (6), 2168–2179. https://doi.org/10.1002/chem.201202374.

[26] Domingos, J. B.; Longhinotti, E.; Brandão, T. A. S.; Bunton, C. A.; Santos, L. S.; Eberlin, M. N.; Nome, F. Mechanisms of nucleophilic substitution reactions of methylated hydroxylamines with bis(2,4-dinitrophenyl)phosphate. mass spectrometric identification of key intermediates. *J. Org. Chem.*, **2004**, *69* (18), 6024–6033. https://doi.org/10.1021/jo0494735.

[27] Zubareva, T. M.; Prokop'eva, T. M.; Kapitanov, I. V.; Belousova, I. A.; Razumova, N. G.; Popov, A. F. Reactivity of N-Alkyl Derivatives of hydroxylamine in decomposition of 4-Nitrophenyl diethylphosphonate in water and in cetyltrimethylammonium bromide micelles. *Theor. Exp. Chem.*, **2007**, *43* (4), 247–254. https://doi.org/10.1007/s11237-007-0029-8.

[28] Singh, N.; Karpichev, Y.; Sharma, R.; Gupta, B.; Sahu, A. K.; Satnami, M. L.; Ghosh, K. K. From α-nucleophiles to functionalized aggregates: exploring the reactivity of hydroxamate ion towards esterolytic reactions in micelles. *Org. Biomol. Chem.*, **2015**, *13* (10), 2827–2848. https://doi.org/10.1039/C4OB02067G.

[29] Hess, R. A.; Hengge, A. C.; Cleland, W. W. Kinetic Isotope effects for acyl transfer from *p*-Nitrophenyl acetate to hydroxylamine show a pH-dependent change in mechanism. *J. Am. Chem. Soc.*, **1997**, *119* (30), 6980–6983. https://doi.org/10.1021/ja970648k.

[30] Bruice, T. C.; Benkovic, S. J. Bioorganic Mechanisms. New York, W.A. Benjamin, 1966.

[31] Sadovskii, Yu. S.; Solomoichenko, T. N.; Turovskaya, M. K.; Kapitanov, I. V.; Piskunova, Zh. P.; Kostrikin, M. L.; Prokop'eva, T. M.; Popov, A. F. Peroxyhydrolysis of 4-Nitrophenyl diethyl phosphate in micellar systems based on imidazolium gemini surfactants. *Theor. Exp. Chem.*, **2012**, *48* (2), 122–128. https://doi.org/10.1007/s11237-012-9249-7.

[32] Golik, J.; Clardy, J.; Dubay, G.; Groenewold, G.; Kawaguchi, H.; Konishi, M.; Krishnan, B.; Ohkuma, H.; Saitoh, K.; Doyle, T. W. Esperamicins, a novel class of potent antitumor antibiotics. 2. Structure of Esperamicin X. *J. Am. Chem. Soc.*, **1987**, *109* (11), 3461–3462. https://doi.org/10.1021/ja00245a048.

[33] Golik, J.; Dubay, G.; Groenewold, G.; Kawaguchi, H.; Konishi, M.; Krishnan, B.; Ohkuma, H.; Saitoh, K.; Doyle, T. W. Esperamicins, a novel class of potent antitumor antibiotics. 3. Structures of Esperamicins A1, A2, and A1b. *J. Am. Chem. Soc.*, **1987**, *109* (11), 3462–3464. https://doi.org/10.1021/ja00245a049.

[34] Lee, M. D.; Dunne, T. S.; Siegel, M. M.; Chang, C. C.; Morton, G. O.; Borders, D. B. Calichemicins, a novel family of antitumor antibiotics. 1. Chemistry and partial structure of Calichemicin. gamma.1I. *J. Am. Chem. Soc.*, **1987**, *109* (11), 3464–3466. https://doi.org/10.1021/ja00245a050.

[35] Berge, J. M.; Copley, R. C. B.; Eggleston, D. S.; Hamprecht, D. W.; Jarvest, R. L.; Mensah, L. M.; O'Hanlon, P. J.; Pope, A. J. Inhibitors of bacterial tyrosyl TRNA synthetase: synthesis of four stereoisomeric analogues of the natural product SB-219383. *Bioorg. Med. Chem. Lett.*, **2000**, *10* (16), 1811–1814. https://doi.org/10.1016/S0960-894X(00)00348-6.

[36] Axerio-Cilies, P.; Castañeda, I. P.; Mirza, A.; Reynisson, J. investigation of the incidence of "undesirable" molecular moieties for high-throughput screening compound libraries in marketed drug compounds. *Eur. J. Med. Chem.*, **2009**, *44* (3), 1128–1134. https://doi.org/10.1016/j.ejmech.2008.06.013.

[37] Yu, B.; Reynisson, J. Bond stability of the "undesirable" heteroatom–heteroatom molecular moieties for high-throughput screening libraries. *Eur. J. Med. Chem.*, **2011**, *46* (12), 5833–5837. https://doi.org/10.1016/j.ejmech.2011.09.044.

[38] Zhang, Y.; Albohy, A.; Zou, Y.; Smutova, V.; Pshezhetsky, A. v.; Cairo, C. W. Identification of selective inhibitors for human neuraminidase isoenzymes using C4,C7-modified 2-deoxy-2,3-didehydro-*N*-acetylneuraminic acid (DANA) analogues. *J Med Chem*, **2013**, *56* (7), 2948–2958. https://doi.org/10.1021/jm301892f.

[39] Benigni, R.; Bossa, C. Mechanisms of chemical carcinogenicity and mutagenicity: A review with implications for predictive toxicology. *Chem. Rev.*, **2011**, *111* (4), 2507–2536. https://doi.org/10.1021/cr100222q.

[40] Benigni, R.; Giuliani, A.; Franke, R.; Gruska, A. Quantitative Structure−Activity Relationships of mutagenic and carcinogenic aromatic amines. *Chem. Rev.*, **2000**, *100* (10), 3697–3714. https://doi.org/10.1021/cr9901079.

[41] Dhanju, S.; Crich, D. Synthesis of *N*,*N*,*O*-trisubstituted hydroxylamines by stepwise reduction and substitution of *O*-Acyl *N*,*N*-Disubstituted hydroxylamines. *Org. Lett.*, **2016**, *18* (8), 1820–1823. https://doi.org/10.1021/acs.orglett.6b00556.

[42] Tidwell, T. T. Schiff bases, and a century of β-lactam synthesis. *Angew. Chem. Int. Ed.*, **2008**, *47* (6), 1016–1020. https://doi.org/10.1002/anie.200702965.

[43] Patai, S. *Carbon-Nitrogen Double Bonds*; Patai, S., Ed.; John Wiley & Sons, Ltd.: Chichester, UK, 1970. https://doi.org/10.1002/9780470771204.

[44] Meyer, V.; Janny, A. Ueber stickstoffhaltige acetonderivate. *Ber. Dtsch. Chem. Ges.* **1882**, *15* (1), 1164–1167. https://doi.org/10.1002/cber.188201501257.

[45] Belmar, J.; Quezada, J.; Jiménez, C. A.; Díaz-Gallifa, P.; Pasán, J.; Ruiz-Pérez, C. Synthesis, Crystal Structures and Tautomerism in Novel Oximes Based on Hydroxyalkylpyrazolones. *New J. Chem.*, **2013**, *37* (7), 2002. https://doi.org/10.1039/c3nj00163f.

[46] Kolandaivel, P. G.; Kuze, N.; Sakaizumi, T.; Ohashi, O.; Iijima, K. Molecular structures and rotational potential energy surfaces of E and Z geometrical isomers of propionaldehyde oxime: Ab Initio and DFT Studies. *J. Phys. Chem. A.*, **1997**, *101* (15), 2873–2878. https://doi.org/10.1021/jp962386z.

[47] Radulović, N. S.; Tasić, M. M.; Mladenović, M. Z. Oximes of 3,7-Dimethylocta-2,6-dienal: green synthesis, preparative separation of all diastereomers and complete assignment of ^{1}H and ^{13}C NMR Spectra. *J. Mol. Struct.*, **2021**, *1227*, 129427. https://doi.org/10.1016/j.molstruc.2020.129427.

[48] Maraković, N.; Knežević, A.; Rončević, I.; Brazzolotto, X.; Kovarik, Z.; Šinko, G. Enantioseparation, *in Vitro* testing, and structural characterization of triple-binding reactivators of organophosphate-inhibited cholinesterases. *Biochem. J.*, **2020**, *477* (15), 2771–2790. https://doi.org/10.1042/BCJ20200192.

[49] Bohle, D. S.; Chua, Z.; Perepichka, I.; Rosadiuk, K. *E*/*Z* Oxime isomerism in PhC(NOH)CN. *Chem. Eur. J.*, **2013**, *19* (13), 4223–4229. https://doi.org/10.1002/chem.201203357.

[50] Tecle, H.; Lauffer, D. J.; Mirzadegan, T.; Moos, W. H.; Moreland, D. W.; Pavia, M. R.; Schwarz, R. D.; Davis, R. E. Synthesis and SAR of bulky 1-Azabicyclo[2.2.1]-3-one oximes as muscarinic receptor subtype selective agonists. *Life Sci.*, **1993**, *52* (5–6), 505–511. https://doi.org/10.1016/0024-3205(93)90308-P.

[51] Brandt, U.; von Jagow, G. Analysis of the binding of *p*-chlorophenyl-methoxybenzyl-ketoxime (CPMB-oxime) to mitochondrial cytochrome *c* reductase. *FEBS Lett.*, **1991**, *287* (1–2), 215–218. https://doi.org/10.1016/0014-5793(91)80054-7.

[52] Kolandaivel, P.; Senthilkumar, K. Ab Initio and DFT studies on structure and stability of aliphatic aldoxime molecules. *J. Mol. Struct.*, **2001**, *535* (1–3), 61–70. https://doi.org/10.1016/S0166-1280(00)00571-6.

[53] Blatt, A. H. The tautomerism of oximes. *J. Org. Chem.*, **1938**, *03* (2), 91–98. https://doi.org/10.1021/jo01219a001.

[54] Vijfhuizen, P. C.; Terlouw, J. K. On the Loss of $CH_3^{\cdot}$ from o-Methylbenzaldoxime. Evidence for An ortho Assisted Oxime-nitrone Isomerization. *Org. Mass Spectrom.*, **1977**, *12* (2), 63–64. https://doi.org/10.1002/oms.1210120203.

[55] Long, J. A.; Harris, N. J.; Lammertsma, K. Formaldehyde oxime-nitrosomethane tautomerism. *J. Org. Chem.*, **2001**, *66* (20), 6762–6767. https://doi.org/10.1021/jo010671v.

[56] Novikov, A. S.; Bolotin, D. S. Tautomerism of amidoximes and other oxime species. *J. Phys. Org. Chem.*, **2018**, *31* (3), e3772. https://doi.org/10.1002/poc.3772.

[57] Roca-López, D.; Darù, A.; Tejero, T.; Merino, P. Revisiting oxime–nitrone tautomerism. evidence of nitrone tautomer participation in oxime nucleophilic addition reactions. *RSC Adv.*, **2016**, *6* (26), 22161–22173. https://doi.org/10.1039/C6RA02638A.

[58] Dignam, K. J.; Hegarty, A. F. Reactivity of 1,3-Dipoles in Aqueous Solution. Part 4. Kinetics and mechanism of isomerisation of amidoximes in aqueous solution. *J. Chem. Soc., Perkin Trans. 2*, **1979**, No. 10, 1437. https://doi.org/10.1039/p29790001437.

[59] Noguchi, M.; Okada, H.; Tanaka, M.; Matsumoto, S.; Kakehi, A.; Yamamoto, H. Mechanistic considerations on the oxime–nitrone isomerization and intramolecular cycloaddition reaction of 3-(Alk-2-enylamino)propionaldehyde Oximes. *Bull. Chem. Soc. Jpn.*, **2001**, *74* (5), 917–925. https://doi.org/10.1246/bcsj.74.917.

[60] Mann, F. George.; Saunders, B. Charles. Practical Organic Chemistry. Longmans **1960**. ISBN:0582442281.

[61] Katritzky Meth-Cohn Otto. Rees Charles W., A. R. *Comprehensive organic functional group transformations*; Pergamon: Oxford, OX; New York, **1995**. ISBN: 9780080406046.

[62] Adams, J. P. Imines, Enamines and Oximes. *J. Chem. Soc. Perkin Trans. 1*, **2000**, No. 2, 125–139. https://doi.org/10.1039/a808142e.

[63] Adams, J. P. Imines, Enamines and Oximes. *Contemp. Org. Synth.*, **1997**, *4* (6), 517. https://doi.org/10.1039/co9970400517.

[64] Beckman, E. Zur Isomerie Der Aldoxime. V. *Chem. Ber.*, **1890**, *23*, 1680–1692.

[65] Beckmann, E. I. Zur kenntniss der oximidoverbindungen. *Liebigs Ann. Chem.*, **1909**, *365* (2-3), 201–214.

[66] Hajipour, A. R.; Mohammadpoor-baltork, I.; Nikbaghat, K.; Imanzadeh, G. Solid-phase synthesis of oximes. *Synth. Commun.*, **1999**, *29* (10), 1697–1701. https://doi.org/10.1080/00397919908086156.

[67] Hajipour, A. R.; Mallakpour, S. E.; Imanzadeh, G. A Rapid and convenient synthesis of oximes in dry media under microwave irradiation. *J. Chem. Res.*, **1999**, No. 3, 228–229. https://doi.org/10.1039/a806359a.

[68] Li, J.-T.; Li, X.-L.; Li, T.-S. Synthesis of oximes under ultrasound irradiation. *Ultrason. Sonochem.*, **2006**, *13* (3), 200–202. https://doi.org/10.1016/j.ultsonch.2005.11.011.

[69] Damljanović, I.; Vukićević, M.; Vukićević, R. D. A Simple synthesis of oximes. *Monatsh. Chem.,* **2006**, *137* (3), 301–305. https://doi.org/10.1007/s00706-005-0427-3.

[70] Hosseini Sarvari, M. ZnO/CH_3 COCl: A New and highly efficient catalyst for dehydration of aldoximes into nitriles under solvent-free condition. *Synthesis*, **2005**, *05*, 787–790. https://doi.org/10.1055/s-2005-861826.

[71] Guo, J.-J.; Jin, T.-S.; Zhang, S.-L.; Li, T.-S. TiO2/SO42–: An efficient and convenient catalyst for preparation of aromatic oximes. *Green Chem.*, **2001**, *3* (4), 193–195. https://doi.org/10.1039/b102067f.

[72] Heaney, F.; Bourke, S.; Cunningham, D.; McArdle, P. Steric control of reactivity: formation of oximes, benzodiazepinone n-oxides and isoxazoloquinolinones. *J. Chem. Soc., Perkin Trans. 2*, **1998**, No. 3, 547. https://doi.org/10.1039/a707857i.

[73] Kad, G. L.; Bhandari, M.; Kaur, J.; Rathee, R.; Singh, J. Solventless preparation of oximes in the solid state and via microwave irradiation. *Green Chem.*, **2001**, *3* (6), 275–277. https://doi.org/10.1039/b107356g.

[74] Saikia, L.; Baruah, J. M.; Thakur, A. J. A Rapid, Convenient, solventless green approach for the synthesis of oximes using grindstone chemistry. *Org. Med. Chem. Lett.*, **2011**, *1* (1), 12. https://doi.org/10.1186/2191-2858-1-12.

[75] Byerley, J. J.; Peters, E. Kinetics and mechanisms of the reaction between carbon monoxide and copper(II) in aqueous solution. *Can. J. Chem.*, **1969**, *47* (2), 313–321. https://doi.org/10.1139/v69-043.

[76] Knifton, J. F. Homogeneous catalyzed reduction of nitro compounds. i. synthesis of oximes. *J. Org. Chem.*, **1973**, *38* (19), 3296–3301. https://doi.org/10.1021/jo00959a011.

[77] Barton, D. H.; Bowles, T.; Husinec, S.; Forbes, J. E.; Llobera, A.; Porter, A. E.; Zard, S. Z. Reductive formylation of oximes; an approach to the synthesis of vinyl isonitriles. *Tetrahedron Lett.*, **1988**, *29* (27), 3343–3346. https://doi.org/10.1016/0040-4039(88)85157-8.

[78] Albanese, D.; Landini, D.; Penso, M. Reduction of allylic nitro compounds to oximes with carbon disulfide under solid-liquid phase-transfer catalysis conditions. *Synthesis*, **1990**, *1990* (04), 333–336. https://doi.org/10.1055/s-1990-26869.

[79] Ono, N. *The Nitro Group in Organic Synthesis*; John Wiley & Sons, **2003**. ISBN: 978-0-471-45846-3.

[80] Iyer, S. NItro compounds. recent advances in synthesis and chemistry. VCH, Weinheim, **1990**.ISBN 3-527-26949-5.

[81] Okamoto, T.; Kobayashi, K.; Oka, S.; Tanimoto, S. A High-yield regiospecific synthesis of keto oximes from aryl-conjugated ethylenes and ethyl nitrite in the presence of cobalt complex and BH^{4-} ion. *J. Org. Chem.*, **1988**, *53* (21), 4897–4901. https://doi.org/10.1021/jo00256a001.

[82] Ohno M; Naruse N; Terasawa I. 7-Cyanoheptanal. *Org. Synth.*, **1969**, *49*, 27. https://doi.org/10.15227/orgsyn.049.0027.

[83] Fileti, M.; Ponzio, G. Umwandlung Der Ketone in β-Diketone. *J. Prakt. Chem.*, **1894**, *51* (1), 498–510. https://doi.org/10.1002/prac.18950510142.

[84] Rüedi, G.; Oberli, M. A.; Nagel, M.; Weymuth, C.; Hansen, H.-J. A Practical and user-friendly method for the selenium-free one-step preparation of 1,2-diketones and their monoxime analogs. *Synlett.*, **2004**, *13*, 2315–2318. https://doi.org/10.1055/s-2004-832815.

[85] Kozłowska, J.; Potaniec, B.; Żarowska, B.; Anioł, M. Synthesis and biological activity of novel o-alkyl derivatives of naringenin and their oximes. *Molecules*, **2017**, *22* (9), 1485. https://doi.org/10.3390/molecules22091485.

[86] Zhmurenko, L. A.; Litvinova, S. A.; Kutepova, I. S.; Nerobkova, L. N.; Mokrov, G. v.; Rebeko, A. G.; Voronina, T. A.; Gudasheva, T. A. Synthesis of dibenzofuranone-oxime derivatives with anticonvulsant, antihypoxic, and anti-ischemic activity. *Pharm. Chem. J.*, **2020**, *53* (11), 997–1004. https://doi.org/10.1007/s11094-020-02112-2.

[87] Robb, E. L.; Baker, M. B. *Organophosphate Toxicity,* Treasure Island (FL): StatPearls Publishing; **2023**. PMID: 29261901.

[88] Wilson, I.; Ginsburg, B. A Powerful Reactivator of alkylphosphate-inhibited acetylcholinesterase. *Biochim. Biophys. Acta*, **1955**, 168–170. https://doi.org/10.1016/0006-3002(55)90040-8.

[89] Grob, D.; Johns, R. J. Use of oximes in the treatment of intoxication by anticholinesterase compounds in normal subjects. *Am J Med*, **1958**, *24* (4), 497–511. https://doi.org/10.1016/0002-9343(58)90290-0.

[90] Purves, D.; Williams, S. M. *Neuroscience. 2nd Edition*; Sinauer Associates, **2001**. ISBN:0-87893-742-0.

[91] Shahbaz, K. Cephalosporins: Pharmacology and Chemistry. *Pharm. Biol. Eval.* **2017**, *4* (6), 234. https://doi.org/10.26510/2394-0859.pbe.2017.36.

[92] Lima, L. M.; Silva, B. N. M. da; Barbosa, G.; Barreiro, E. J. β-Lactam Antibiotics: An Overview from a Medicinal Chemistry Perspective. *Eur. J. Med. Chem.*, **2020**, *208*, 112829. https://doi.org/10.1016/j.ejmech.2020.112829.

[93] Abraham, E. P. The Cephalosporin C Group. *Q. Rev., Chem. Soc.*, **1967**, *21* (2), 231. https://doi.org/10.1039/qr9672100231.

[94] Bui, T.; Preuss, C. v. *Cephalosporins*; Treasure Island (FL): StatPearls Publishing; **2021**. PMID: 31855361.

[95] McSherry, B. A. Technetium-99m-Teboroxime: A New Agent for Myocardial Perfusion Imaging. *J. Nucl. Med. Technol.*, **1991**, *19*, 22–26.

[96] Narra, R. K.; Nunn, A. D.; Kuczynski, B. L.; Feld, T.; Wedeking, P.; Eckelman, W. C. A neutral Technetium-99m complex for myocardial imaging. *J. Nucl. Med.*, **1989**, *30* (11), 1830–1837.

[97] Kane, S. M.; Davis, D. D. *Technetium-99m* Treasure Island (FL): StatPearls Publishing; **2023**.PMID: 32644439.

[98] Ghosh, P. R. FDA approves two new technetium-labelled cardiac agents and a pharmacologic alternative to exercise in stress-thallium studies. *J. Nucl. Med.*, **1991**, *32* (5), 11N, 14N-16N, 19N. PMID: 1827149.

[99] Beanlands, R. S. B.; deKemp, R. A.; Harmsen, E.; Veinot, J. P.; Hartman, N. G.; Ruddy, T. D. Myocardial kinetics of Technetium-99m teboroxime in the presence of postischemic injury, necrosis and low flow reperfusion. *J. Am. Coll. Cardiol.*, **1996**, *28* (2), 487–494. https://doi.org/10.1016/0735-1097(96)00159-3.

[100] Okada, D. R.; Johnson, G.; Okada, R. D. Myocardial clearance of Technetium-99m-Teboroxime in repercussed injured canine myocardium. *EJNMMI Res*, **2014**, *4* (1), 42. https://doi.org/10.1186/s13550-014-0042-6.

[101] Berman, D. S.; Kiat, H.; van Train, K. F.; Friedman, J.; Garcia, E. v.; Maddahi, J. Comparison of SPECT Using Technetium-99m Agents and Thallium-201 and PET for the Assessment of Myocardial Perfusion and Viability. *Am. J. Cardiol.*, **1990**, *66* (13), E72–E79. https://doi.org/10.1016/0002-9149(90)90616-9.

[102] Labonté, C.; Taillefer, R.; Lambert, R.; Basile, F.; TonThat, T.; Jarry, M.; Léveillé, J. Comparison between Technetium-99m-Teboroxime and Thallium-201 dipyridamole planar myocardial perfusion imaging in detection of coronary artery disease. *Am. J. Cardiol.*, **1992**, *69* (1), 90–96. https://doi.org/10.1016/0002-9149(92)90681-N.

[103] Evison, D.; Hinsley, D.; Rice, P. Clinical review regular review chemical weapons. *BMJ*, **2002**, *324* (7333), 332–335. https://doi.org/10.1136/bmj.324.7333.332.

[104] Singh, J. A. Project Coast: Eugenics in apartheid south africa. *Endeavour*, **2008**, *32* (1), 5–9. https://doi.org/10.1016/j.endeavour.2008.01.005.

[105] Mégarbane, B. Le VX Ou l'arme de Destruction Massive Devenue Arme d'assassinat Ciblé. *Reanimation*, **2017**, *26* (5), 405–410. https://doi.org/10.1007/s13546-017-1295-7.

[106] Nakagawa, T.; Tu, A. T. Murders with VX: Aum Shinrikyo in Japan and the assassination of Kim Jong-Nam in Malaysia. *Forensic Toxicol.*, **2018**, *36* (2), 542–544. https://doi.org/10.1007/s11419-018-0426-9.

[107] Carlsen, L. After Salisbury Nerve Agents revisited. *Mol. Inform.*, **2019**, *38* (8–9). https://doi.org/10.1002/minf.201800106.

[108] Steindl, D.; Boehmerle, W.; Körner, R.; Praeger, D.; Haug, M.; Nee, J.; Schreiber, A.; Scheibe, F.; Demin, K.; Jacoby, P.; et al. Novichok Nerve Agent Poisoning. *The Lancet*, **2021**, *397* (10270), 249–252. https://doi.org/10.1016/S0140-6736(20)32644-1.

[109] Bertolote J; Fleischmann A; Eddleston M; Gunnell D. Deaths from pesticide poisoning: a global response. *Br. J. Psychiatry.*, **2006**, *189* (3), 201–203.

[110] Saint-André, G.; Kliachyna, M.; Kodepelly, S.; Louise-Leriche, L.; Gillon, E.; Renard, P.-Y.; Nachon, F.; Baati, R.; Wagner, A. Design, Synthesis and evaluation of new α-nucleophiles for the hydrolysis of organophosphorus nerve agents: application to the reactivation of phosphorylated acetylcholinesterase. *Tetrahedron*, **2011**, *67* (34), 6352–6361. https://doi.org/10.1016/j.tet.2011.05.130.

[111] Walker, P. F. A Century of Chemical Warfare: Building a World Free of Chemical Weapons. *One Hundred Years of Chemical Warfare: Research, Deployment, Consequences*, **2017**, 379–400. https://doi.org/10.1007/978-3-319-51664-6_20.

[112] Tucker, J. B. *Double-Edged Innovations: Preventing the Misuse of Emerging Biological/Chemical Technologies*; 2010.

[113] Okumura, T.; Hisaoka, T.; Yamada, A.; Naito, T.; Isonuma, H.; Okumura, S.; Miura, K.; Sakurada, M.; Maekawa, H.; Ishimatsu, S.; et al. The Tokyo subway sarin attack - lessons learned. *Toxicol. Appl. Pharmacol.*, **2005**, *207* (2), 471–476. https://doi.org/10.1016/j.taap.2005.02.032.

[114] Rosman, Y.; Eisenkraft, A.; Milk, N.; Shiyovich, A.; Ophir, N.; Shrot, S.; Kreiss, Y.; Kassirer, M. Lessons learned from the Syrian sarin attack: evaluation of a clinical syndrome through social media. *Ann. Intern. Med.*, **2014**, *160* (9), 644–648. https://doi.org/10.7326/M13-2799.

[115] Quinn, D. M. Acetylcholinesterase: enzyme structure, reaction dynamics, and virtual transition states. *Chem. Rev.*, **1987**, *87* (5), 955–979. https://doi.org/10.1021/cr00081a005.

[116] Thiermann, H.; Aurbek, N.; Worek, F. Treatment of Nerve Agent poisoning. Issues Toxicol., RSC, **2016**; *27*, 1–42. https://doi.org/10.1039/9781782628071-00001.

[117] Worek, F.; Thiermann, H.; Wille, T. Oximes in Organophosphate Poisoning: 60 Years of Hope and Despair. *Chem. Biol. Interact.*, **2016**, *259*, 93–98. https://doi.org/10.1016/j.cbi.2016.04.032.

[118] Renou, J.; Mercey, G.; Verdelet, T.; Păunescu, E.; Gillon, E.; Arboléas, M.; Loiodice, M.; Kliachyna, M.; Baati, R.; Nachon, F.; et al. Syntheses and *in vitro* evaluations of uncharged reactivators for human acetylcholinesterase inhibited by organophosphorus nerve agents. *Chem. Biol. Interact.*, **2013**, *203* (1), 81–84. https://doi.org/10.1016/j.cbi.2012.09.023.

[119] Mercey, G.; Verdelet, T.; Renou, J.; Kliachyna, M.; Baati, R.; Nachon, F.; Jean, L.; Renard, P. Y. Reactivators of acetylcholinesterase inhibited by organophosphorus Nerve Agents. *Acc. Chem. Res.*, **2012**, *45* (5), 756–766. https://doi.org/10.1021/ar2002864.

[120] Singh, N.; Karpichev, Y.; Tiwari, A. K.; Kuca, K.; Ghosh, K. K. Oxime functionality in surfactant self-assembly: an overview on combating toxicity of organophosphates. *J. Mol. Liq.*, **2015**, *208*, 237–252. https://doi.org/10.1016/j.molliq.2015.04.010.

[121] Franjesevic, A. J.; Sillart, S. B.; Beck, J. M.; Vyas, S.; Callam, C. S.; Hadad, C. M. Resurrection and reactivation of acetylcholinesterase and butyrylcholinesterase. *Chem. Eur. J.*, **2019**, 5337–5371. https://doi.org/10.1002/chem.201805075.

[122] Kuca Kamil; Juna Daniel; Musilek Kamil. Structural requirements of acetylcholinesterase reactivators. *Mini. Rev. Med. Chem.*, **2006**, *6*, 269–277. https://doi.org/10.2174/138955706776073510.

[123] Kovalevsky, A.; Blumenthal, D. K.; Cheng, X.; Taylor, P.; Radić, Z. Limitations in current acetylcholinesterase structure–based design of oxime antidotes for organophosphate poisoning. *Ann. N.-Y. Acad. Sci.*, **2016**, *1378* (1), 41–49. https://doi.org/10.1111/nyas.13128.

[124] Maxwell, D. M.; Koplovitz, I.; Worek, F.; Sweeney, R. E. A Structure-Activity Analysis of the variation in oxime efficacy against Nerve Agents. *Toxicol. Appl. Pharmacol.*, **2008**, *231*, 157–164. https://doi.org/10.1016/j.taap.2008.04.007.

[125] Gorecki, L.; Gerlits, O.; Kong, X.; Cheng, X.; Blumenthal, D. K.; Taylor, P.; Ballatore, C.; Kovalevsky, X. A.; Radić, X. Z. Rational Design, Synthesis, and evaluation of uncharged, "smart" bis-oxime antidotes of organophosphate-inhibited human acetylcholinesterase. *J. Biol. Chem.*, **2020**, *295* (13), 4079–4092. https://doi.org/10.1074/jbc.RA119.012400.

[126] Banks, W. A. From Blood-Brain Barrier to Blood-Brain Interface: new opportunities for CNS drug delivery. *Nat. Rev. Drug. Discov.*, **2016**, *15* (4), 275–292. https://doi.org/10.1038/nrd.2015.21.

[127] Ballabh, P.; Braun, A.; Nedergaard, M. The Blood–Brain Barrier: an overview. *Neurobiol. Dis.*, **2004**, *16* (1), 1–13. https://doi.org/10.1016/j.nbd.2003.12.016.

[128] Abbott, N. J.; Rönnbäck, L.; Hansson, E. Astrocyte–Endothelial Interactions at the Blood–Brain Barrier. *Nat. Rev. Neurosci.*, **2006**, *7* (1), 41–53. https://doi.org/10.1038/nrn1824.

[129] Lin, T.; Zhao, P.; Jiang, Y.; Tang, Y.; Jin, H.; Pan, Z.; He, H.; Yang, V. C.; Huang, Y. Blood-Brain-Barrier-penetrating albumin nanoparticles for biomimetic drug delivery via albumin-binding protein pathways for antiglioma therapy. *ACS Nano*, **2016**, *10* (11), 9999–10012. https://doi.org/10.1021/acsnano.6b04268.

[130] Li, X.; Tsibouklis, J.; Weng, T.; Zhang, B.; Yin, G.; Feng, G.; Cui, Y.; Savina, I. N.; Mikhalovska, L. I.; Sandeman, S. R.; et al. Nano carriers for drug transport across the Blood–Brain Barrier. *J. Drug Target.*, **2016**, 17–28. https://doi.org/10.1080/1061186X.2016.1184272.

[131] Jun, D.; Musilova, L.; Musilek, K.; Kuca, K. *In Vitro* ability of currently available oximes to reactivate organophosphate pesticide-inhibited human acetylcholinesterase and butyrylcholinesterase. *Int. J. Mol. Sci.*, **2011**, *12* (3), 2077–2087. https://doi.org/10.3390/ijms12032077.

[132] Worek, F.; Wille, T.; Koller, M.; Thiermann, H. Toxicology of organophosphorus compounds in view of an increasing terrorist threat. *Arch. Toxicol.*, **2016**, 2131–2145. https://doi.org/10.1007/s00204-016-1772-1.

[133] Lorke, D. E.; Kalasz, H.; Petroianu, G. A.; Tekes, K. Entry of oximes into the brain: a review. *Curr. Med. Chem*., **2008**, 743–753.

[134] Shih, T.-M.; Skovira, J. W.; O'Donnell, J. C.; McDonough, J. H. Central acetylcholinesterase reactivation by oximes improves survival and terminates seizures following nerve agent intoxication; 2009.

[135] Skovira, J. W.; O'Donnell, J. C.; Koplovitz, I.; Kan, R. K.; McDonough, J. H.; Shih, T.-M. Reactivation of brain acetylcholinesterase by monoisonitrosoacetone increases the therapeutic efficacy against nerve agents in *Guinea* pigs. *Chem. Biol. Interact.*, **2010**, *187* (1–3), 318–324. https://doi.org/10.1016/j.cbi.2010.03.010.

[136] Tsung-Ming, S.; Jeffrey, K. A.; John, M. H. Tertiary oximes on brain acetylcholinesterase and central excitatory effects of nerve agents. *Ther. Pharmacol. Clin. Toxicol.*, **2012**, *16* (4), 251–267.

[137] Wei, Z.; qin Liu, Y.; zheng Wang, S.; Yao, L.; fang Nie, H.; an Wang, Y.; Liu, X. Y.; bing Zheng, Z.; Li, S. Conjugates of salicylaldoximes and peripheral site ligands: novel efficient nonquaternary reactivators for nerve agent-inhibited acetylcholinesterase. *Bioorg. Med. Chem.*, **2017**, *25* (16), 4497–4505. https://doi.org/10.1016/j.bmc.2017.06.041.

[138] Sakurada, K.; Ohta, H. No promising antidote 25 years after the Tokyo subway sarin attack: a review. *Leg Med*, **2020**, *47* (101761), 1–6. https://doi.org/10.1016/j.legalmed.2020.101761.

[139] Worek, F.; Aurbek, N.; Thiermann, H. Reactivation of organophosphate-inhibited human AChE by combinations of Obidoxime and HI 6 *in Vitro*. *J. Appl. Toxicol.*, **2007**, *27* (6), 582–588. https://doi.org/10.1002/jat.1241.

[140] Keth, J.; Johann, T.; Frey, H. Hydroxamic Acid: An Underrated Moiety? Marrying Bioinorganic Chemistry and Polymer Science. *Biomacromolecules*, **2020**, *21* (7), 2546–2556. https://doi.org/10.1021/acs.biomac.0c00449.

[141] Smith, G. F. Designing Drugs to Avoid Toxicity. *Prog. Med. Chem.*, **2011**, *50*, 1–47. https://doi.org/10.1016/B978-0-12-381290-2.00001-X.

[142] Kakkar, R. Theoretical Studies on Hydroxamic Acids. *Hydroxamic Acids*; Springer Berlin Heidelberg: Berlin, Heidelberg, **2013**; pp 19–53. https://doi.org/10.1007/978-3-642-38111-9_2.

[143] Harvey, A. E.; Manning, D. L. Spectrophotometric methods of establishing empirical formulas of colored complexes in solution. *J. Am. Chem. Soc.*, **1950**, *72* (10), 4488–4493. https://doi.org/10.1021/ja01166a044.

[144] Bass, V. C.; Yoe, J. H. Hydroxamic acids as colorimetric reagents. *Talanta*, **1966**, *13* (5), 735–744. https://doi.org/10.1016/0039-9140(66)80009-7.

[145] Fazary, A. E. Thermodynamic studies on the protonation equilibria of some hydroxamic acids in $NaNO_3$ solutions in water and in mixtures of water and dioxane. *J. Chem. Eng. Data.*, **2005**, *50* (3), 888–895. https://doi.org/10.1021/je0496185.

[146] Kurzak, B.; Kozłowski, H.; Farkas, E. Hydroxamic and aminohydroxamic acids and their complexes with metal ions. *Coord. Chem. Rev.*, **1992**, *114* (2), 169–200. https://doi.org/10.1016/0010-8545(92)85002-8.

[147] Neilands, J. B. Siderophores: structure and function of microbial iron transport compounds. *J. Biol. Chem.*, **1995**, *270* (45), 26723–26726. https://doi.org/10.1074/jbc.270.45.26723.

[148] Yang, K.; Lou, B. Molecular Diversity of hydroxamic acids: Part I. Solution- and solid-phase synthesis. *Mini Rev. Med. Chem.*, **2003**, *3* (4), 349–360. https://doi.org/10.2174/1389557033488114.

[149] Kurz, T.; Pein, M. K.; Marek, L.; Behrendt, C. T.; Spanier, L.; Kuna, K.; Brücher, K. Microwave-assisted conversion of 4-nitrophenyl esters into *O*-protected hydroxamic acids. *Eur. J. Org. Chem.*, **2009**, *18*, 2939–2942. https://doi.org/10.1002/ejoc.200900201.

[150] Devocelle, M.; McLoughlin, B. M.; Sharkey, C. T.; Fitzgerald, D. J.; Nolan, K. B. A Convenient parallel synthesis of low molecular weight hydroxamic acids using polymer-supported 1-hydroxybenzotriazole. *Org. Biomol. Chem.*, **2003**, *1* (5), 850–853. https://doi.org/10.1039/b211526c.

[151] Richardson, D. R.; Kalinowski, D. S.; Lau, S.; Jansson, P. J.; Lovejoy, D. B. Cancer cell iron metabolism and the development of potent iron chelators as anti-tumour agents. *Biochim. Biophys. Acta Gen. Subj.*, **2009**, *1790* (7), 702–717. https://doi.org/10.1016/j.bbagen.2008.04.003.

[152] Aust, S. D.; White, B. C. Iron chelation prevents tissue injury following ischemia. *Free Radic. Biol. Med.*, **1985**, *1* (1), 1–17. https://doi.org/10.1016/8755-9668(85)90003-1.

[153] Henle, E. S.; Linn, S. Formation, prevention, and repair of DNA damage by iron/hydrogen peroxide. *J. Biol. Chem.*, **1997**, *272* (31), 19095–19098. https://doi.org/10.1074/jbc.272.31.19095.

[154] Hershko, C. Oral iron chelators: new opportunities and new dilemmas. *Haematologica*, **2006**, *91* (10), 1307–1312. https://doi.org/10.3324/%x.

[155] Farkas, E.; Enyedy, É. A.; Csóka, H. Some factors affecting metal ion–monohydroxamate interactions in aqueous solution. *J. Inorg. Biochem.*, **2000**, *79* (1–4), 205–211. https://doi.org/10.1016/S0162-0134(99)00158-0.

[156] Jones, M. M. New developments in therapeutic chelating agents as antidotes for metal poisoning. *Crit. Rev. Toxicol.*, **1991**, *21* (3), 209–233. https://doi.org/10.3109/10408449109089880.

[157] Nagoba, B.; Vedpathak, D. Medical applications of siderophores. *Electron. J. Gen. Med.* **2011**, *8* (3), 229–235. https://doi.org/10.29333/ejgm/82743.

[158] Hašková, P.; Koubková, L.; Vávrová, A.; Macková, E.; Hrušková, K.; Kovaříková, P.; Vávrová, K.; Šimůnek, T. Comparison of various iron chelators used in clinical practice as protecting agents against catecholamine-induced oxidative injury and cardiotoxicity. *Toxicology*, **2011**, *289* (2–3), 122–131. https://doi.org/10.1016/j.tox.2011.08.006.

[159] Hu, X.; Zhu, J.; Srivathsan, S.; Pei, D. Peptidyl hydroxamic acids as methionine aminopeptidase inhibitors. *Bioorg. Med. Chem. Lett.*, **2004**, *14* (1), 77–79. https://doi.org/10.1016/j.bmcl.2003.10.031.

[160] Zhou, T.; Ma, Y.; Kong, X.; Hider, R. C. Design of iron chelators with therapeutic application. *Dalton Trans.*, **2012**, *41* (21), 6371. https://doi.org/10.1039/c2dt12159j.

[161] Sharma, N.; Kumari, M.; Kumar, V.; Chaudhry, S. C. Synthesis, structural characterisation and antibacterial activity of bis(1-phenyl-1,3-butanedionato)non-oxovanadium(iv) hydroxamates. *J. Enzyme Inhib. Med. Chem.*, **2010**, *25* (5), 708–714. https://doi.org/10.3109/14756360903540292.

[162] Lombardi, P. M.; Cole, K. E.; Dowling, D. P.; Christianson, D. W. Structure, mechanism, and inhibition of histone deacetylases and related metalloenzymes. *Curr. Opin. Struct. Biol.*, **2011**, *21* (6), 735–743. https://doi.org/10.1016/j.sbi.2011.08.004.

[163] Saban, N.; Bujak, M. Hydroxyurea and hydroxamic acid derivatives as antitumor drugs. *Cancer Chemother. Pharmacol.*, **2009**, *64* (2), 213–221. https://doi.org/10.1007/s00280-009-0991-z.

[164] Stanetty, C.; Czollner, L.; Koller, I.; Shah, P.; Gaware, R.; Cunha, T. da; Odermatt, A.; Jordis, U.; Kosma, P.; Claßen-Houben, D. Synthesis of novel 3-amino and 29-hydroxamic acid derivatives of glycyrrhetinic acid as selective 11β-hydroxysteroid dehydrogenase 2 inhibitors. *Bioorg. Med. Chem.*, **2010**, *18* (21), 7522–7541. https://doi.org/10.1016/j.bmc.2010.08.046.

[165] Bailey, S.; Fish, P. v.; Billotte, S.; Bordner, J.; Greiling, D.; James, K.; McElroy, A.; Mills, J. E.; Reed, C.; Webster, R. Succinyl hydroxamates as potent and selective non-peptidic inhibitors of procollagen c-proteinase: design, synthesis, and evaluation as topically applied, dermal anti-scarring agents. *Bioorg. Med. Chem. Lett.*, **2008**, *18* (24), 6562–6567. https://doi.org/10.1016/j.bmcl.2008.10.036.

[166] Rajic, Z.; Butula, I.; Zorc, B.; Kraljevic Pavelic, S.; Hock, K.; Pavelic, K.; Naesens, L.; De Clercq, E.; Balzarini, J.; Przyborowska, M.; et al. Cytostatic and antiviral activity evaluations of hydroxamic derivatives of some non-steroidal anti-inflammatory drugs. *Chem. Biol. Drug. Des.*, **2009**, *73* (3), 328–338. https://doi.org/10.1111/j.1747-0285.2009.00774.x.

[167] Barbarić, M.; Uršić, S.; Pilepić, V.; Zorc, B.; Hergold-Brundić, A.; Nagl, A.; Grdiša, M.; Pavelić, K.; Snoeck, R.; Andrei, G.; et al. Synthesis, x-ray crystal structure study, and cytostatic and antiviral evaluation of the novel cycloalkyl- *n* -aryl-hydroxamic acids. *J. Med. Chem.*, **2005**, *48* (3), 884–887. https://doi.org/10.1021/jm040878r.

[168] Villalta-Romero, F.; Gortat, A.; Herrera, A. E.; Arguedas, R.; Quesada, J.; de Melo, R. L.; Calvete, J. J.; Montero, M.; Murillo, R.; Rucavado, A.; et al. Identification of new snake venom metalloproteinase inhibitors using compound screening and rational peptide design. *ACS Med. Chem. Lett.*, **2012**, *3* (7), 540–543. https://doi.org/10.1021/ml300068r.

[169] Alcaraz, M. J.; Megías, J.; García-Arnandis, I.; Clérigues, V.; Guillén, M. I. New molecular targets for the treatment of osteoarthritis. *Biochem. Pharmacol.*, **2010**, *80* (1), 13–21. https://doi.org/10.1016/j.bcp.2010.02.017.

[170] Chen, W.-P.; Bao, J.-P.; Hu, P.-F.; Feng, J.; Wu, L.-D. Alleviation of osteoarthritis by trichostatin a, a histone deacetylase inhibitor, in experimental osteoarthritis. *Mol. Biol. Rep.*, **2010**, *37* (8), 3967–3972. https://doi.org/10.1007/s11033-010-0055-9.

[171] Leissring, M. A.; Malito, E.; Hedouin, S.; Reinstatler, L.; Sahara, T.; Abdul-Hay, S. O.; Choudhry, S.; Maharvi, G. M.; et al. Designed inhibitors of insulin-degrading enzyme regulate the catabolism and activity of insulin. *PLoS One*, **2010**, *5* (5), e10504. https://doi.org/10.1371/journal.pone.0010504.

[172] Lou, B.; Yang, K. Molecular diversity of hydroxamic acids: part II. Potential therapeutic applications. *Mini Rev. Med. Chem.*, **2003**, *3* (6), 609–620. https://doi.org/10.2174/1389557033487872.

[173] Gialeli, C.; Theocharis, A. D.; Karamanos, N. K. Roles of matrix metalloproteinases in cancer progression and their pharmacological targeting. *FEBS J.*, **2011**, *278* (1), 16–27. https://doi.org/10.1111/j.1742-4658.2010.07919.x.

[174] Verma, R. P.; Hansch, C. Matrix metalloproteinases (MMPs): chemical–biological functions and QSARs. *Bioorg. Med. Chem.*, **2007**, *15* (6), 2223–2268. https://doi.org/10.1016/j.bmc.2007.01.011.

[175] Rothenberg, M. L.; Nelson, A. R.; Hande, K. R. New drugs on the horizon: matrix metalloproteinase inhibitors. *Stem Cells*, **1999**, *17* (4), 237–240. https://doi.org/10.1002/stem.170237.

[176] Kodani, S.; Ohnishi-Kameyama, M.; Yoshida, M.; Ochi, K. A New siderophore isolated from Streptomyces SP. TM-34 with potent inhibitory activity against angiotensin-converting enzyme. *Eur. J. Org. Chem.*, **2011**, *17*, 3191–3196. https://doi.org/10.1002/ejoc.201100189.

[177] Paulis, L.; Unger, T. Novel therapeutic targets for hypertension. *Nat. Rev. Cardiol.*, **2010**, *7* (8), 431–441. https://doi.org/10.1038/nrcardio.2010.85.

[178] Stuehr, D. J. Mammalian nitric oxide synthases. *Biochim. Biophys. Acta Bioenerg.*, **1999**, *1411* (2–3), 217–230. https://doi.org/10.1016/S0005-2728(99)00016-X.

[179] Marmion, C. J.; Griffith, D.; Nolan, K. B. Hydroxamic acids − an intriguing family of enzyme inhibitors and biomedical ligands. *Eur. J. Inorg. Chem.*, **2004**, *15*, 3003–3016. https://doi.org/10.1002/ejic.200400221.

[180] Marmion, C. J.; Murphy, T.; Docherty, J. R.; Nolan, K. B. Hydroxamic acids are nitric oxide donors. Facile formation of ruthenium(ii)-nitrosyls and no-mediated activation of guanylate cyclase by hydroxamic acids. *Chem. Commun.*, **2000**, *13*, 1153–1154. https://doi.org/10.1039/b001631o.

[181] Vystorop, I. v.; Konovalova, N. P.; Nelyubina, Yu. v.; Varfolomeev, V. N.; Fedorov, B. S.; Sashenkova, T. E.; Berseneva, E. N.; Lyssenko, K. A.; Kostyanovsky, R. G. Cyclic hydroxamic acids derived from α-amino acids 1. Regioselective synthesis, structure, NO-donor and antimetastatic activities of spirobicyclic hydroxamic acids derived from glycine and Dl-alanine. *Russ. Chem. Bull.*, **2010**, *59* (1), 127–135. https://doi.org/10.1007/s11172-010-0055-x.

[182] Shen, S.; Kozikowski, A. P. Why hydroxamates may not be the best histone deacetylase inhibitors: what some may have forgotten or would rather forget? *ChemMedChem*, **2016**, *11* (1), 15–21. https://doi.org/10.1002/cmdc.201500486.

[183] Thomas, M.; Alsarraf, J.; Araji, N.; Tranoy-Opalinski, I.; Renoux, B.; Papot, S. The Lossen rearrangement from free hydroxamic acids. *Org. Biomol. Chem.*, **2019**, *17* (22), 5420–5427. https://doi.org/10.1039/C9OB00789J.

[184] Harris, L. W.; Stitcher, D. L.; Heyl, W. C. The effects of pretreatments with carbamates, atropine and mecamylamine on survival and on soman-induced alterations in rat and rabbit brain acetylcholine. *Life Sci.*, **1980**, *26* (22), 1885–1891. https://doi.org/10.1016/0024-3205(80)90617-7.

[185] Harris, L. W.; Stitcher, D. L.; Heyl, W. C. Effects of inhibitors of acetylcholine synthesis on brain acetylcholine and survival in soman-intoxicated animals. *Life Sci.*, **1982**, *30* (22), 1867–1873. https://doi.org/10.1016/0024-3205(82)90466-0.

[186] Wilson, I. Acetylcholinesterase XI. Reversibility of tetraethyl pyrophosphate. *J. Biol. Chem.*, **1951**, *190* (1), 111–117. https://doi.org/10.1016/S0021-9258(18)56051-8.

[187] Wilson, I. B.; Meislich, E. K. Reactivation of acetylcholinesterase inhibited by alkylphosphates. *J. Am. Chem. Soc.*, **1953**, *75* (18), 4628–4629. https://doi.org/10.1021/ja01114a546.

[188] Mager, P. P.; das Gupta, S. Quantitative structure-activity relationships of reactivators of phosphylated acetylcholinesterase. Part 2. *Pharmazie*, **1982**, *37* (8), 607–608.

[189] Childs, A. F.; Davies, D. R.; Green, A. L.; Rutland, J. P. The reactivation by oximes and hydroxamic acids of cholinesterase inhibited by organophosphorus compounds. *Br. J. Pharmacol. Chemother.*, **1955**, *10* (4), 462–465. https://doi.org/10.1111/j.1476-5381.1955.tb00106.x.

[190] Askew, B. M. Oximes and atropine in sarin poisoning. *Br. J. Pharmacol. Chemother.*, **1957**, *12* (3), 340–343. https://doi.org/10.1111/j.1476-5381.1957.tb00145.x.

[191] Dultz, L.; Epstein, M. A.; Freeman, G.; Gray, E. H.; Weil, W. B. Studies on a Group of Oximes as Therapeutic Compounds in Sarin Poisoning. *J. Pharmacol. Exp. Ther.*, **1957**, *119* (4), 522–531.

[192] Rutland, J. P. THE EFFECT OF SOME OXIMES IN SARIN POISONING. *Br. J. Pharmacol Chemother*, **1958**, *13* (4), 399–403. https://doi.org/10.1111/j.1476-5381.1958.tb00228.x.

[193] Myers, D. K. Mechanism of the prophylactic action of diacetylmonoxime against sarin poisoning. *Biochim. Biophys. Acta*, **1959**, *34*, 555–557. https://doi.org/10.1016/0006-3002(59)90311-7.

[194] Hobbiger, F. Reactivation of Phosphorylated Acetylcholinesterase. *Handbook of Experimental Pharmacology*. **1963**, 921–988. https://doi.org/10.1007/978-3-642-99875-1_21.

[195] Gorecki, L.; Soukup, O.; Korabecny, J. Countermeasures in organophosphorus intoxication: pitfalls and prospects. *Trends. Pharmacol. Sci.*, **2022**. https://doi.org/10.1016/j.tips.2022.04.008.

[196] Devereaux, A.; Amundson, D. E.; Parrish, J. S.; Lazarus, A. A. Vesicants and nerve agents in chemical warfare. *Postgrad. Med.*, **2002**, *112* (4), 90–96. https://doi.org/10.3810/pgm.2002.10.1334.

[197] Amitai, G.; Gez, R.; Raveh, L.; Bar-Ner, N.; Grauer, E.; Chapman, S. Novel bifunctional hybrid small molecule scavengers for mitigating nerve agents toxicity. *Chem. Biol. Interact.*, **2016**, *259*, 187–204. https://doi.org/10.1016/j.cbi.2016.04.036.

[198] Amitai, G.; Plotnikov, A.; Chapman, S.; Lazar, S.; Gez, R.; Loewenthal, D.; Shurrush, K. A.; Cohen, G.; Solmesky, L. J.; Barr, H.; et al. Non-quaternary oximes detoxify nerve agents and reactivate nerve agent-inhibited human butyrylcholinesterase. *Commun. Biol.*, **2021**, *4* (1), 573. https://doi.org/10.1038/s42003-021-02061-w.

[199] Walkinshaw, D. R.; Yang, X. J. Histone deacetylase inhibitors as novel anticancer therapeutics. *Curr. Oncol.*, **2008**, *15* (5), 237–243. PMCID: PMC2582508.

[200] Rothenberg, M. L.; Nelson, A. R.; Hande, K. R. New Drugs on the Horizon: Matrix Metalloproteinase Inhibitors. *Stem. Cells*, **1999**, *17* (4), 237–240. https://doi.org/10.1002/stem.170237.

[201] Cress, W. D.; Seto, E. Histone Deacetylases, Transcriptional Control, and Cancer. *J. Cell. Physiol.*, **2000**, *184* (1), 1–16. https://doi.org/10.1002/(SICI)1097-4652(200007)184:1<1::AID-JCP1>3.0.CO;2-7.

[202] Mahlknecht, U.; Hoelzer, D. Histone Acetylation Modifiers in the Pathogenesis of Malignant Disease. *Mol. Med.*, **2000**, *6* (8), 623–644.

[203] Duvic, M.; Vu, J. Vorinostat: A New Oral Histone Deacetylase Inhibitor Approved for Cutaneous T-Cell Lymphoma. *Expert Opin. Investig. Drugs*, **2007**, *16* (7), 1111–1120. https://doi.org/10.1517/13543784.16.7.1111.

[204] Nelson, A. R.; Fingleton, B.; Rothenberg, M. L.; Matrisian, L. M. Matrix Metalloproteinases: Biologic Activity and Clinical Implications. *J. Clin. Oncol.* **2000**, *18* (5), 1135–1135. https://doi.org/10.1200/JCO.2000.18.5.1135.

[205] Avendaño C; Menéndez J. Carlos. *Medicinal Chemistry of Anticancer Drugs*, 1st edition.; Elsevier, **2008**. https://doi.org/10.1016/B978-0-444-52824-7.X0001-7.

[206] Shalinsky, D. R.; Brekken, J.; Zou, H.; Mcdermott, C. D.; Forsyth, P.; Edwards, D.; Margosiak, S.; Bender, S.; Truitt, G.; Wood, A.; et al. Broad antitumor and antiangiogenic activities of AG3340, a potent and selective MMP inhibitor undergoing advanced oncology clinical trials. *Ann. N.-Y. Acad. Sci.*, **1999**, *878* (1 INHIBITION OF), 236–270. https://doi.org/10.1111/j.1749-6632.1999.tb07689.x.

[207] Jagtap, P.; Szabo, C. Poly(ADP-Ribose) Polymerase and the therapeutic effects of its inhibitors. *Nat. Rev. Drug Discov.* **2005**, 421–440. https://doi.org/10.1038/nrd1718.

[208] Mateo, J.; Lord, C.; Serra, V.; Tutt, A.; Balmaña, J.; Castroviejo-Bermejo, M.; Cruz, C.; Oaknin, A.; Kaye, S.; de Bono, J. A decade of clinical development of parp inhibitors in perspective. *Ann. Oncol.*, **2019**, *30* (9), 1437–1447. https://doi.org/10.1093/annonc/mdz192/5520938.

[209] Leo, C. P.; Hentschel, B.; Szucs, T. D.; Leo, C. FDA and EMA approvals of new breast cancer drugs—a comparative regulatory analysis. *Cancers (Basel)*, **2020**, *12* (2), 437. https://doi.org/10.3390/cancers12020437.

[210] Banasik, M.; Komura, H.; Shimoyama, M.; Ueda, K. Specific inhibitors of poly(ADP-ribose) synthetase and mono(ADP-ribosyl)transferase. *J. Biol. Chem.*, **1992**, *267* (3), 1569–1575. https://doi.org/10.1016/s0021-9258(18)45983-2.

[211] Bryant, H. E.; Schultz, N.; Thomas, H. D.; Parker, K. M.; Flower, D.; Lopez, E.; Kyle, S.; Meuth, M.; Curtin, N. J.; Helleday, T. Specific killing of BRCA2-deficient tumours with inhibitors of poly(ADP-ribose) polymerase. *Nature*, **2005**, *434* (7035), 913–917. https://doi.org/10.1038/nature03443.

[212] Azad, I.; Ahmad, R.; Khan, T.; Saquib, M.; Hassan, F.; Akhter, Y.; Khan, A. R.; Nasibullah, M. Phenanthridine derivatives as promising new anticancer agents: synthesis, biological evaluation and binding studies. *Future Med. Chem.*, **2020**, *12* (8), 709–739. https://doi.org/10.4155/fmc-2019-0016.

[213] Wan, M.; Zhang, L.; Chen, Y.; Li, Q.; Fan, W.; Xue, Q.; Yan, F.; Song, W. Synthesis and anticancer activity evaluation of novel phenanthridine derivatives. *Front. Oncol.*, **2019**, *9*. https://doi.org/10.3389/fonc.2019.00274.

[214] Wurz, G.; Hofer, O.; Greger, H. Structure and synthesis of phenaglydon, a new quinolone derived phenanthridine alkaloid from glycosmis cyanocarpa. *Nat. Prod. Lett.*, **1993**, *3* (3), 177–182. https://doi.org/10.1080/10575639308043859.

[215] Gandeepan, P.; Parthasarathy, K.; Cheng, C.-H. Synthesis of phenanthrone derivatives from *sec*- alkyl aryl ketones and aryl halides via a palladium-catalyzed dual c–h bond activation and enolate cyclization. *J. Am. Chem. Soc.*, **2010**, *132* (25), 8569–8571. https://doi.org/10.1021/ja1026248.

[216] Inbar-Rozensal, D.; Castiel, A.; Visochek, L.; Castel, D.; Dantzer, F.; Izraeli, S.; Cohen-Armon, M. A Selective eradication of human nonhereditary breast cancer cells by phenanthridine-derived polyADP-ribose polymerase inhibitors. *Breast Cancer Res.*, **2009**, *11* (6). https://doi.org/10.1186/bcr2445.

[217] Yedage, S. L.; Bhanage, B. M. Palladium-catalyzed deaminative phenanthridinone synthesis from aniline via c-h bond activation. *J. Org. Chem.*, **2016**, *81* (10), 4103–4111. https://doi.org/10.1021/acs.joc.6b00378.

[218] Yuan, Z.; Chen, S.; Sun, Q.; Wang, N.; Li, D.; Miao, S.; Gao, C.; Chen, Y.; Tan, C.; Jiang, Y. Olaparib hydroxamic acid derivatives as dual PARP and HDAC inhibitors for cancer therapy. *Bioorg. Med. Chem.*, **2017**, *25* (15), 4100–4109. https://doi.org/10.1016/j.bmc.2017.05.058.

[219] Bauser, M.; Delapierre, G.; Hauswald, M.; Flessner, T.; D'Urso, D.; Hermann, A.; Beyreuther, B.; De Vry, J.; Spreyer, P.; Reissmüller, E.; et al. Discovery and optimization of 2-aryl oxazolo-pyrimidines as adenosine kinase inhibitors using liquid phase parallel synthesis. *Bioorg. Med. Chem. Lett.*, **2004**, *14* (8), 1997–2000. https://doi.org/https://doi.org/10.1016/j.bmcl.2004.01.082.

[220] Köse, M.; Schiedel, A. C.; Bauer, A. A.; Poschenrieder, H.; Burbiel, J. C.; Akkinepally, R. R.; Stachel, H.-D.; Müller, C. E. Focused screening to identify new adenosine kinase inhibitors. *Bioorg. Med. Chem.*, **2016**, *24* (21), 5127–5133. https://doi.org/https://doi.org/10.1016/j.bmc.2016.08.026.

[221] Tuo, W.; Bollier, M.; Leleu-Chavain, N.; Lemaire, L.; Barczyk, A.; Dezitter, X.; Klupsch, F.; Szczepanski, F.; Spencer, J.; Chavatte, P.; et al. Development of novel oxazolo[5,4-*d*]pyrimidines as competitive CB2 neutral antagonists based on scaffold hopping. *Eur. J. Med. Chem.*, **2018**, *146*, 68–78. https://doi.org/https://doi.org/10.1016/j.ejmech.2018.01.034.

[222] Myllymäki, M. J.; Käsnänen, H.; Kataja, A. O.; Lahtela-Kakkonen, M.; Saario, S. M.; Poso, A.; Koskinen, A. M. P. Chiral 3-(4,5-Dihydrooxazol-2-yl)phenyl alkylcarbamates as novel FAAH inhibitors: insight into FAAH enantioselectivity by molecular docking and interaction fields. *Eur. J. Med. Chem.*, **2009**, *44* (10), 4179–4191. https://doi.org/https://doi.org/10.1016/j.ejmech.2009.05.012.

[223] De Coen, L. M.; Roman, B. I.; Movsisyan, M.; Heugebaert, T. S. A.; Stevens, C. V. Synthesis and biological activity of Oxazolopyrimidines. *Eur. J. Org. Chem.*, **2018**, *2018* (19), 2148–2166. https://doi.org/https://doi.org/10.1002/ejoc.201800133.

[224] Miller, D. J.; Ravikumar, K.; Shen, H.; Suh, J.-K.; Kerwin, S. M.; Robertus, J. D. Structure-based design and characterization of novel platforms for ricin and shiga toxin inhibition. *J. Med. Chem.*, **2002**, *45* (1), 90–98. https://doi.org/10.1021/jm010186s.

[225] Al-Husein, B.; Abdalla, M.; Trepte, M.; DeRemer, D. L.; Somanath, P. R. Antiangiogenic therapy for cancer: an update. *Pharmacotherapy: The Journal of Human Pharmacology and Drug Therapy*, **2012**, *32* (12), 1095–1111. https://doi.org/https://doi.org/10.1002/phar.1147.

[226] Dvorak, H. F.; Nagy, J. A.; Feng, D.; Brown, L. F.; Dvorak, A. M. Vascular permeability factor/vascular endothelial growth factor and the significance of microvascular hyperpermeability in angiogenesis. *Vascular Growth Factors and Angiogenesis*; Claesson-Welsh, L., Ed.; Springer Berlin Heidelberg: Berlin, Heidelberg, **1999**; pp 97–132. https://doi.org/10.1007/978-3-642-59953-8_6.

[227] Ferrara, N.; Gerber, H.-P.; Le Couter, J. The Biology of VEGF and its receptors. *Nat. Med.*, **2003**, *9* (6), 669–676. https://doi.org/10.1038/nm0603-669.

[228] Ferrara, N.; Hillan, K. J.; Gerber, H.-P.; Novotny, W. Discovery and development of bevacizumab, an anti-VEGF antibody for treating cancer. *Nat. Rev. Drug. Discov.*, **2004**, *3* (5), 391–400. https://doi.org/10.1038/nrd1381.

[229] Dvorak, H. F. Vascular Permeability Factor/Vascular Endothelial Growth Factor: A Critical Cytokine in Tumor Angiogenesis and a Potential Target for Diagnosis and Therapy. *J. Clin. Oncol.*, **2002**, *20* (21), 4368–4380. https://doi.org/10.1200/JCO.2002.10.088.

[230] Kaipainen, A.; Korhonen, J.; Mustonen, T.; van Hinsbergh, V. W.; Fang, G. H.; Dumont, D.; Breitman, M.; Alitalo, K. Expression of the Fms-like Tyrosine Kinase 4 Gene Becomes Restricted to Lymphatic Endothelium during Development. *PNAS*, **1995**, *92* (8), 3566–3570. https://doi.org/10.1073/pnas.92.8.3566.

[231] Sun, L.; Liang, C.; Shirazian, S.; Zhou, Y.; Miller, T.; Cui, J.; Fukuda, J. Y.; Chu, J.-Y.; Nematalla, A.; Wang, X.; et al. Discovery of 5-[5-Fluoro-2-oxo-1,2- dihydroindol-(3z)-ylidenemethyl]-2,4- dimethyl-1*H*-Pyrrole-3-carboxylic acid (2-diethylaminoethyl)amide, a Novel Tyrosine Kinase Inhibitor Targeting Vascular Endothelial and Platelet-Derived Growth Factor Receptor Tyrosine Kinase. *J. Med. Chem.*, **2003**, *46* (7), 1116–1119. https://doi.org/10.1021/jm0204183.

[232] Renhowe, P. A.; Pecchi, S.; Shafer, C. M.; Machajewski, T. D.; Jazan, E. M.; Taylor, C.; Antonios-McCrea, W.; McBride, C. M.; Frazier, K.; Wiesmann, M.; et al. Design, Structure−Activity Relationships and *in Vivo* Characterization of 4-Amino-3-benzimidazol-2-ylhydroquinolin-2-ones: A Novel Class of Receptor Tyrosine Kinase Inhibitors. *J. Med. Chem.*, **2009**, *52* (2), 278–292. https://doi.org/10.1021/jm800790t.

[233] Deng, Y.-H.; Xu, D.; Su, Y.-X.; Cheng, Y.-J.; Yang, Y.-L.; Wang, X.-Y.; Zhang, J.; You, Q.-D.; Sun, L.-P. Synthesis and Biological Evaluation of Novel Oxazolo[5,4-*d*]pyrimidines as potent VEGFR-2 inhibitors. *Chem. Biodivers.*, **2015**, *12* (4), 528–537. https://doi.org/https://doi.org/10.1002/cbdv.201400270.

[234] Martin-Kohler, A.; Widmer, J.; Bold, G.; Meyer, T.; Séquin, U.; Traxler, P. Furo[2,3-*d*]pyrimidines and oxazolo[5,4-*d*]pyrimidines as inhibitors of receptor tyrosine kinases (RTK). *Helv. Chim. Acta.*, **2004**, *87* (4), 956–975. https://doi.org/https://doi.org/10.1002/hlca.200490089.

[235] Scattolin, T.; Bortolamiol, E.; Visentin, F.; Palazzolo, S.; Caligiuri, I.; Perin, T.; Canzonieri, V.; Demitri, N.; Rizzolio, F.; Togni, A. Palladium(II)-*H*3-allyl complexes bearing *N*-trifluoromethyl *N*-heterocyclic carbenes: a new generation of anticancer agents that restrain the growth of high-grade serous ovarian cancer tumoroids. *Chem. Eur. J.*, **2020**, *26* (51), 11868–11876. https://doi.org/https://doi.org/10.1002/chem.202002199.

[236] Velihina, Y.; Kachaeva, M.; Pilyo, S.; Mitiukhin, O.; Zhirnov, V.; Brovarets, V. Synthesis, characterization, and *in vitro* anticancer evaluation of 7-(1,4-Diazepan)- substituted [1,3]oxazolo[4,5-*d*]pyrimidines. *Chem. Res. J.* **2018**, *3*, 81–93. ISSN: 2455-8990.

[237] Nance, E.; Pun, S. H.; Saigal, R.; Sellers, D. L. Drug delivery to the Central Nervous System. *Nat. Rev. Mater.*, **2022**, *7*, 314–331. https://doi.org/10.1038/s41578-021-00394-w.

[238] Barbu, E.; Molnàr, É.; Tsibouklis, J.; Górecki, D. C. The potential for nanoparticle-based drug delivery to the brain: overcoming the blood-brain barrier. *Expert Opin. Drug Deliv.*, **2009**, 553–565. https://doi.org/10.1517/17425240902939143.

[239] Shenderova, O. A.; McGuire, G. E. Science and engineering of nanodiamond particle surfaces for biological applications (review). *Biointerphases*, **2015**, *10* (3), 30802. https://doi.org/10.1116/1.4927679.

[240] Wolfbeis, O. S. An Overview of nanoparticles commonly used in fluorescent bioimaging. *Chem. Soc. Rev.* RSC. ***2015***, 4743–4768. https://doi.org/10.1039/c4cs00392f.

[241] Vaijayanthimala, V.; Lee, D. K.; Kim, S. v; Yen, A.; Tsai, N.; Ho, D.; Chang, H. C.; Shenderova, O. Nanodiamond-mediated drug delivery and imaging: challenges and opportunities. *Expert. Opin. Drug. Deliv.*, **2015**, *12* (5), 735–749. https://doi.org/10.1517/17425247.2015.992412.

[242] Kaur, R.; Badea, I. Nanodiamonds as novel nanomaterials for biomedical applications: drug delivery and imaging systems. *Int. J. Nanomedicine*, **2013**, *8*, 203–220. https://doi.org/10.2147/IJN.S37348.

[243] Turcheniuk, K.; Mochalin, V. N. Biomedical applications of nanodiamond (review). *Nanotechnology*, **2017**, *28* (25), 252001. https://doi.org/10.1088/1361-6528/aa6ae4.

[244] Giammarco, J.; Mochalin, V. N.; Haeckel, J.; Gogotsi, Y. The adsorption of tetracycline and vancomycin onto nanodiamond with controlled release. *J. Colloid. Interface. Sci.*, **2016**, *468*, 253–261. https://doi.org/10.1016/j.jcis.2016.01.062.

[245] Mochalin, V. N.; Pentecost, A.; Li, X. M.; Neitzel, I.; Nelson, M.; Wei, C.; He, T.; Guo, F.; Gogotsi, Y. Adsorption of drugs on nanodiamond: toward development of a drug delivery platform. *Mol. Pharm.*, **2013**, *10* (10), 3728–3735. https://doi.org/10.1021/mp400213z.

[246] An, F. F.; Zhang, X. H. Strategies for preparing albumin-based nanoparticles for multifunctional bioimaging and drug delivery. *Theranostics*, **2017**, *7* (15), 3667–3689. https://doi.org/10.7150/thno.19365.

[247] Georgakilas, V.; Perman, J. A.; Tucek, J.; Zboril, R. Broad family of carbon nanoallotropes: classification, chemistry, and applications of fullerenes, carbon dots, nanotubes, graphene, nanodiamonds, and combined superstructures. *Chem. Rev.*, **2015**, *115* (11), 4744–4822. https://doi.org/10.1021/cr500304f.

[248] Chang, S. L. Y.; Reineck, P.; Krueger, A.; Mochalin, V. N. Ultrasmall nanodiamonds: perspectives and questions. *ACS Nano*, **2022**. https://doi.org/10.1021/acsnano.2c00197.

[249] Beltz, J.; Pfaff, A.; Abdullahi, I. M.; Cristea, A.; Mochalin, V. N.; Ercal, N. Effect of nanodiamond surface chemistry on adsorption and release of tiopronin. *Diam. Relat. Mater.*, **2019**, *100*, 107590. https://doi.org/10.1016/j.diamond.2019.107590.

[250] Krueger, A.; Lang, D. Functionality Is key: recent progress in the surface modification of nanodiamond. *Adv. Funct. Mater.*, **2012**, *22* (5), 890–906. https://doi.org/10.1002/adfm.201102670.

[251] Danilenko V. On the history of the discovery of nanodiamond synthesis. *Phys. Solid State.,* **2004**, *46*, 581–584. https://doi.org/10.1134/1.1711431.

[252] Zhang, X.; Hu, W.; Li, J.; Tao, L.; Wei, Y. A comparative study of cellular uptake and cytotoxicity of multi-walled carbon nanotubes, graphene oxide, and nanodiamond. *Toxicol. Res. (Camb)*, **2012**, *1* (1), 62–68. https://doi.org/10.1039/c2tx20006f.

[253] Mochalin, V. N.; Shenderova, O.; Ho, D.; Gogotsi, Y. The properties and applications of nanodiamonds. *Nat. Nanotechnol.*, **2012**, *7* (1), 11–23. https://doi.org/10.1038/nnano.2011.209.

[254] Setyawati, M. I.; Mochalin, V. N.; Leong, D. T. Tuning endothelial permeability with functionalized nanodiamonds. *ACS Nano*, **2016**, *10* (1), 1170–1181. https://doi.org/10.1021/acsnano.5b06487.

[255] Li, X.; Shao, J.; Qin, Y.; Shao, C.; Zheng, T.; Ye, L. TAT-conjugated nanodiamond for the enhanced delivery of doxorubicin. *J. Mater. Chem.*, **2011**, *21* (22), 7966–7973. https://doi.org/10.1039/c1jm10653h.

[256] Roy, U.; Drozd, V.; Durygin, A.; Rodriguez, J.; Barber, P.; Atluri, V.; Liu, X.; Voss, T. G.; Saxena, S.; Nair, M. Characterization of nanodiamond-based anti-HIV drug delivery to the brain. *Sci. Rep.*, **2018**, *8* (1). https://doi.org/10.1038/s41598-017-16703-9.

[257] Moscariello, P.; Raabe, M.; Liu, W.; Bernhardt, S.; Qi, H.; Kaiser, U.; Wu, Y.; Weil, T.; Luhmann, H. J.; Hedrich, J. Unraveling *In Vivo* brain transport of protein-coated fluorescent nanodiamonds. *Small*, **2019**, *15* (42). https://doi.org/10.1002/smll.201902992.

[258] Llu, K. K.; Zheng, W. W.; Wang, C. C.; CMu, Y. C.; Cheng, C. L.; Lo, Y. S.; Chen, C.; Chao, J. I. Covalent linkage of nanodiamond-paclitaxel for drug delivery and cancer therapy. *Nanotechnology*, **2010**, *21* (31). https://doi.org/10.1088/0957-4484/21/31/315106.

[259] Kümmerer, K.; Menz, J.; Schubert, T.; Thielemans, W. Biodegradability of organic nanoparticles in the aqueous environment. *Chemosphere*, **2011**, *82* (10), 1387–1392. https://doi.org/10.1016/j.chemosphere.2010.11.069.

[260] Friedrich, J.; Längin, A.; Kümmerer, K. Comparison of an electrochemical and luminescence-based oxygen measuring system for use in the biodegradability testing according to Closed Bottle Test (OECD 301D). *Clean. (Weinh)*, **2013**, *41* (3), 251–257. https://doi.org/10.1002/clen.201100558.

[261] OECD. *OECD Test Guidelines for Chemicals*. 1992.

[262] Kitano, M. Updating of OECD guidelines for the testing of chemicals. *Water Sci. Technol.*, **1992**, *25* (11), 465–472. https://doi.org/10.2166/wst.1992.0327.

[263] Helmbrecht, H.; Joseph, A.; McKenna, M.; Zhang, M.; Nance, E. Governing transport principles for nanotherapeutic application in the brain. *Curr. Opin. Chem. Eng.*, **2020**, *30*, 112–119. https://doi.org/10.1016/j.coche.2020.08.010.

[264] Finger, V.; Kucera, T.; Kafkova, R.; Muckova, L.; Dolezal, R.; Kubes, J.; Novak, M.; Prchal, L.; Lakatos, L.; Andrs, M.; et al. 2,6-Disubstituted 7-(naphthalen-2-ylmethyl)-7*H*-purines as a new class of potent antitubercular agents inhibiting DprE1. *Eur. J. Med. Chem.*, **2023**, *258*, 115611. https://doi.org/10.1016/j.ejmech.2023.115611.

[265] Rankovic, Z. CNS Drug Design: Balancing Physicochemical Properties for Optimal Brain Exposure. *J. Med. Chem.*, **2015**, *58* (6), 2584–2608. https://doi.org/10.1021/jm501535r.

[266] Soukup, O.; Jun, D.; Zdarova-Karasova, J.; Patocka, J.; Musilek, K.; Korabecny, J.; Krusek, J.; Kaniakova, M.; Sepsova, V.; Mandikova, J.; et al. A Resurrection of 7-MEOTA: A Comparison with Tacrine. *Curr. Alzheimer. Res.*, **2013**, *10* (8), 893–906. https://doi.org/10.2174/1567205011310080011.

[267] Jun, D.; Musilova, L.; Pohanka, M.; Jung, Y. S.; Bostik, P.; Kuca, K. reactivation of human acetylcholinesterase and butyrylcholinesterase inhibited by leptophos-oxon with different oxime reactivators in vitro. *Int. J Mol. Sci.*, **2010**, *11* (8), 2856–2863. https://doi.org/10.3390/ijms11082856.

[268] Ellman, G. L.; Courtney, K. D.; Andres, V.; Featherstone, R. M. A new and rapid colorimetric determination of acetylcholinesterase activity. *Biochem. Pharmacol.*, **1961**, *7*, 88–95.

[269] Di, L.; Kerns, E. H.; Fan, K.; McConnell, O. J.; Carter, G. T. High throughput artificial membrane permeability assay for blood–brain barrier. *Eur. J. Med. Chem.*, **2003**, *38* (3), 223–232. https://doi.org/10.1016/S0223-5234(03)00012-6.

[270] OECD. *OECD Guideline for Testing of Chemicals*; 1992.

[271] Wang, G.; Yuan, T.; Li, D. One-Pot Formation of C-C and C-N bonds through palladium-catalyzed dual C-H activation: synthesis of phenanthridinones. *Angew. Chem. Int. Ed.*, **2011**, *50* (6), 1380–1383. https://doi.org/10.1002/anie.201005874.

Acknowledgements

This research was conducted within the Department of Chemistry and Biotechnology at the School of Science, Tallinn University of Technology. It was funded by the NATO Science for Peace and Security (SPS) Program (VNT19018). Additional financial support was provided by the Dora Plus T1.2 long-term mobility scholarship and the T1.1 short-term mobility scholarships, courtesy of The Archimedes Foundation, Estonia. I am also thankful for the support from the ASTRA "TUT Institutional Development Program for 2016–2022" and the Graduate School in Biomedicine and Biotechnology, funded by the European Regional Development Fund under program ASTRA 2014-2020.4.01.16-0032 in Estonia.

I would like to express my profound gratitude to Dr. Yevgen Karpichev for his consistent mentorship and guidance, especially during the early challenges of my doctoral studies. His unwavering dedication and visionary approach have been crucial to the successful completion of my research. I am also deeply thankful to Dr. Dzmitry Kananovich for his thorough review and invaluable feedback on my thesis.

Abstract

Design of AChE reactivators and PARP inhibitors based on hydroxamic acids and oximes

Since the pioneering work by Edwards and Pearson on the α-effect in reactivity, the concept of supernucleophiles has been extensively studied and remains an important subject of modern physical organic chemistry.

Despite their widespread application in organic synthesis due to their low cost, versatility, and well-studied chemistry, hydroxamic acids and oximes, typical supernucleophiles, face challenges in medicinal chemistry due to their presumably fragile N-O bond, detrimental to compound chemical stability, drug efficiency, and metabolite safety. This study aims to demonstrate the utility of hydroxamic acids and oximes in drug design through adressing two medical problems: organophosphate (OP) poisoning and the development of anticancer agents. For OP poisoning treatment, nanodiamond-grafted oximes were prepared and studied to overcome BBB limitations, based on visualization of tight junctions and actin cytoskeleton with confocal microscopy to follow internalization and localization of the nanoparticles and their aggregates inside the MDCK and HUVEC cells. Optimization of antidote structure and surface modification techniques can further enhance the efficacy of the nanodiamond-based reactivators of human acelylcholinesterase (AChE) inhibited by OPs. A rational design of *N*-substituted aryl hydroxamic acids was lead to optimization of their reactivation capacity for AChE inhibited by OPs; the *N*-butyl derivatives were shown to have a better-balanced combination of properties.

For anticancer activity, the cyclic aryl hydroxamic acids, *N*-(benzyloxy)- and *N*-(hydroxy)phenanthridinones, were prepared and investigated for the first time as PARP inhibitors aside from their well-known application as HDAC inhibitors. The oxazolopyrimidine scaffold was explored due to its versatility in drug design. Isomeric oxazolo[4,5-*d*]pyrimidines and oxazolo[5,4-*d*]pyrimidines were designed to inhibit VEGFR2 and modulation of their antitumor activity was possible by structural modification, offering prospects for therapeutic use.

In conclusion, this study expands the horizons of α-nucleophiles in drug design and involved preparation of various substituted oximes and hydroxamic acids, oxazolopyrimidines with valuable theraupetic properties thereby enriching drug libraries with valuable candidates.

Lühikokkuvõte

Hüdroksaamhapetel ja oksiimidel põhinevate AChE reaktivaatorite ja PARP inhibiitorite disain

Alates Edwardsi ja Pearsoni teedrajavast tööst reaktiivsuse α-efekti valdkonnas, on supernukleofiilide kontseptsiooni põhjalikult uuritud ning see on tänapäevase füüsikalise orgaanilise keemia üheks tähtsaimaks uurimisobjektiks.

Tänu supernukleofiilide madalale hinnale, mitmekülgsusele ja põhjalikult uuritud keemiale on need orgaanilises sünteesis laialdaselt kasutusel. Vaatamata sellele, on tüüpiliste supernukleofiilide – hüdroksaamhapete ja oksiimide kasutamine meditsiinilises keemias tõsine väljakutse, nende eeldatavalt nõrga N-O sideme tõttu, mis vähendab ühendite keemilist stabiilsust, potentsiaalsete ravimite efektiivsust ja kaasnevate metaboliitide ohutust. Selle uuringu eesmärgiks on demonstreerida hüdroksaamhapete ja oksiimide kasulikkust ravimite väljatöötamisel, käsitledes kahte meditsiinilist probleemi: orgaanilise fosfaadi (OP) mürgistust ja vähivastaste ainete väljatöötamist. OP-mürgistuse raviks valmistati ette ja uuriti nanoteemandiga poogitud oksiime, et ületada BBB piirangud, mis põhinevad tugevate ühenduste ja aktiini tsütoskeleti visualiseerimisel konfokaalmikroskoopiaga, et jälgida nanoosakeste ja nende agregaatide sisestamist ja lokalisatsiooni MDCK ja HUVEC rakkudes. Antidoodi struktuuri ja pinna modifitseerimise tehnikate optimeerimine võib veelgi suurendada OP-de poolt inhibeeritud inimese atselüülkoliinesteraasi (AChE) nanoteemandipõhiste reaktivaatorite efektiivsust. *N*-asendatud arüülhüdroksaamhapete ratsionaalne disain viis nende reaktiveerimisvõime optimeerimiseni OP-de poolt inhibeeritud AChE suhtes. Näidati, et *N*-butüülderivaatidel on paremini tasakaalustatud omaduste kombinatsioon.

Vähivastase aktiivsuse uurimise eesmärgil valmistati tsüklilised arüülhüdroksaamhapped, *N*-(bensüüloksü)- ja *N*-(hüdroksü)fenantridinoonid ning neid katsetati esmakordselt PARP inhibiitoritena, lisaks nende hästituntud kasutusele HDAC inhibiitoritena. Oksasolopürimidiini struktuuri uuriti selle mitmekülgsuse tõttu ravimite väljatöötamisel. Isomeersed oksasolo[4,5-*d*]pürimidiinid ja oksasolo[5,4-*d*]pürimidiinid disainiti inhibeerimaks VEGFR2 ning nende kasvajavastase toime moduleerimine oli läbi struktuuri muutuste võimalik, pakkudes väljavaateid terapeutiliseks kasutamiseks.

Kokkuvõtteks, antud uuring laiendab α-nukleofiilide kasutusvõimalusi ravimite väljatöötamisel ja erinevate asendatud oksiimide ja hüdroksaamhapete sünteesi võimalusi, rikastades seeläbi väärtuslike terapeutiliste omadustega oksasolopürimidiinidel põhinevate ravimite raamatukogusid väärtuslike ravimikandidaatidega.

Appendix 1

Publication I

Velihina, Ye.; Scattolin,Th.; Bondar, D.; Pil'o, S.; Obernikhina, N.; Kachkovskyi, O.; Semenyuta, I.; Caligiuri, I.; Rizzolio, F.; Brovarets, V.; Karpichev, Y.; Nolan S. P. Synthesis, in silico and in vitro Evaluation of Novel Oxazolopyrimidines as Promising Anticancer Agents. *Helv. Chim. Acta*, 2020, 103 (12), #e2000169.

Reprinted from the permission of John Wiley & Sons.

Check for updates

DOI: 10.1002/hlca.202000169

FULL PAPER

HELVETICA chimica acta

Synthesis, *in silico* and *in vitro* Evaluation of Novel Oxazolopyrimidines as Promising Anticancer Agents

Yevheniia Velihina,[a, b] Thomas Scattolin,[c] Denys Bondar,[a] Stepan Pil'o,[b] Nataliya Obernikhina,[d] Olesksiy Kachkovskyi,[b] Ivan Semenyuta,[b] Isabella Caligiuri,[e] Flavio Rizzolio,[e, f] Volodymyr Brovarets,*[b] Yevgen Karpichev,*[a] and Steven P. Nolan*[c]

[a] Department of Chemistry and Biotechnology, School of Science, Tallinn University of Technology, Akadeemia tee 15, EE-12618 Tallinn, Estonia, e-mail: yevgen.karpichev@taltech.ee

[b] V.P. Kukhar Institute of Bioorganic Chemistry and Petrochemistry, National Academy of Science of Ukraine, Murmanska str. 1, UA-02094 Kyiv-94, Ukraine, e-mail: brovarets@bpci.kiev.ua

[c] Department of Chemistry, Ghent University, Krijgslaan 281, BE-9000 Gent, Belgium, e-mail: Steven.Nolan@UGent.be

[d] O.O. Bogomolets National Medical University, T. Shevchenko Blvd. 13, UA-01601, Kyiv, Ukraine

[e] Pathology Unit, Department of Molecular Biology and Translational Research, Centro di Riferimento Oncologico di Aviano (CRO) IRCCS, via Franco Gallini 2, IT-33081 Aviano, Italy

[f] Department of Molecular Sciences and Nanosystems, Università Ca' Foscari, Campus Scientifico, Via Torino 155, IT-30174 Venezia-Mestre, Italy

Dedicated to Prof. *Antonio Togni* on the occasion of his 65th birthday and retirement

New potential bioactive oxazolopyrimidines have been synthesized using two main approaches: the pyrimidine ring annulation on a functionalized oxazole and the benzoyl bromide trimerization followed by rearrangement and formation of the oxazolo[5,4-*d*]pyrimidine scaffold. The docking analyzes have shown that 7-piperazine substituted oxazolo[4,5-*d*]pyrimidines **8a**–**8c** could be potential VEGFR2 inhibitors with high free energy of ligand–protein complex formation (ΔG: −10.1, −9.6, −9.8 kcal/mol, respectively). *In vitro* antitumor assays confirmed theoretical predictions that oxazolo[4,5-*d*]pyrimidines **8a**–**8c** containing positively charged piperazine moiety should demonstrate significantly higher cytotoxic effects. 4-[5-(4-Chlorophenyl)-2-phenyl[1,3]oxazolo[4,5-*d*]pyrimidin-7-yl]piperazin-1-ium trifluoroacetate (**8c**) exhibited a slightly higher antiproliferative effect (IC_{50} = 0.21 μM) than doxorubicin (IC_{50} = 0.36 μM) on MDA-MB-231 cell line and has relatively good results on OVCAR-3 (IC_{50} = 1.7 μM) and HCT-116 (IC_{50} = 0.24 μM) cells.

Keywords: antitumor agents, donor-acceptor systems, molecular docking, oxazolopyrimidines, *Suzuki-Miyaura* reaction.

Introduction

The oxazolopyrimidine architecture represents an universal scaffold used in the design of bioactive ligands against enzymes or receptors such as adenosine kinase (AK) inhibitors,[1,2] cannabinoid receptor 2 (CB2) neutral antagonists,[3] fatty acid amide hydrolase (FAAH) inhibitors,[4] endothelial differentiation gene receptor 1 (EDG-1) agonist[5] and purinergic G protein-coupled (P2Y1) receptor antagonist.[6] Thus, among the numerous heterocyclic moieties of biological and pharmacological interest, this pharmacophore represents an important structural motif in oncology and infectious disease treatments.

Cancer is a general term for malignant diseases characterized by uncontrolled abnormal cell growth.

Supporting information for this article is available on the WWW under https://doi.org/10.1002/hlca.202000169

© 2020 Wiley-VHCA AG, Zurich, Switzerland

There is substantial preclinical and clinical evidence that angiogenesis plays a role in tumor development and growth/progression. A large number of cancers have been reported to be dependent on angiogenesis and respond well to anti-angiogenic therapies. These include cancers of the breast, colon, lung, and bladder as well as renal cell carcinoma and non-small cell lung cancer. Additionally, some of these cancers require the vascular endothelial growth factor (VEGF) for their survival. Anti-angiogenic therapies target angiogenesis by two main mechanisms: blocking the receptor tyrosine kinases intracellularly or neutralizing angiogenic factors such as VEGF or its receptors.[7]

The VEGF family consists of 6 secreted glycoproteins, VEGF–A, VEGF–B, VEGF–C, VEGF–D, VEGF–E and placenta growth factor.[8] VEGF mediates angiogenesis through several different tyrosine kinase domain receptors. VEGFR1 (Flt-1) is critical in developmental angiogenesis, as well as other processes including monocyte migration, recruitment of endothelial cell (EC) progenitors, and inducing growth factors from liver sinusoidal ECs.[9,10] VEGFR2 (KDR and the murine homologue Flk-1) mediates the majority of the downstream effects of VEGF–A in angiogenesis, including microvascular permeability, EC proliferation, and survival.[9,11] TheVEGFR3 is expressed throughout the embryonic vasculature and later is limited to lymphatic ECs.[12] The various members of the VEGF family have differing binding affinities for each of these receptors, which have helped in elucidating the functions of each of these receptors.

Three major classes of agents which target VEGF have been developed: monoclonal antibodies (Bevacizumab), VEGF decoy receptor (Aflibercept), and small molecule tyrosine kinase inhibitors (Imatinib, Sorafenib, Sunitinib, Pazopanib, Axitinib).[7] Among tyrosine kinase inhibitors (TKIs), there are bicyclic *N*-containing heterocycles that bind with the hinge region of the enzyme through H-bonds as mimic of the purine ring of ATP.[13,14] In this context, oxazolo[5,4-*d*]pyrimidines, which can be considered as 9-oxapurine analogs of nucleobases, have been reported as potent VEGFR2 inhibitors.[15,16] Therefore, synthesis and modification of drugs based on the oxazolopyrimidine scaffold as well as other organic and metal compounds with anticancer properties is currently a pressing issue.[17]

We have recently reported *in vitro* studies of 7-piperazine- and 7-diazepan substituted [1,3]oxazolo[4,5-*d*]pyrimidines against a panel of different cancer cell lines, which have exhibited growth inhibitory, cytostatic and cytotoxic effects at submicromolar and micromolar concentrations.[18,19] To further explore the structure–biological activity relationship of this scaffold, oxazolo[4,5-*d*]pyrimidines and oxazolo[5,4-*d*]pyrimidines with phenyl group at C(2), aryl or biaryl substituents at C(5) and electron donating (piperazine) or withdrawing groups (aryl residues) at C(7) were developed as potential VEGFR2 inhibitors. Since this receptor is a mediator of growth and proliferation of the colon, ovarian, and breast cancer cells,[20,21] their biological activity were investigated on HCT-116, OVCAR-3 and MDA-MB-231 lines of the above-mentioned cancer cells.

Results and Discussion

Synthesis of Target Oxazolopyrimidines

The synthesis of new oxazolo[4,5-*d*]pyrimidine **6** was accomplished in analogy to previously reported derivatives as depicted in *Schemes 1* and *2*.[22,23] Compound **6** is obtained by the sequence of reactions starting from available 2-aryl-4-(dichloromethylidene)-1,3-oxazol-5(4*H*)-one **1**.[24] Treatment of **1** with amidine hydrochlorides **2a** or **2b** in the presence of triethylamine led to substituted imidazol-5(4)-ones **3a**/**3b**, which on heating in pyridine underwent cyclo-condensation followed by recyclization affording the corresponding oxazolo[4,5-*d*]pyrimidin-7-ones **4a**/**4b**.

The reaction of compounds **4a**/**4b** with trichlorophosphate in the presence of *N*,*N*-dimethylaniline proceeded 2,5-diaryl-7-chlor-oxazolo[4,5-d]pyrimidines **5a**/**5b**. Compound **5b** was converted into desired 7-*N*-Boc-piperazine-substituted oxazolo[4,5-*d*]pyrimidine **6** by reaction with *tert*-butyl piperazine-1-carboxylate. Since the structures of the intermediates **3a**, **4a** and

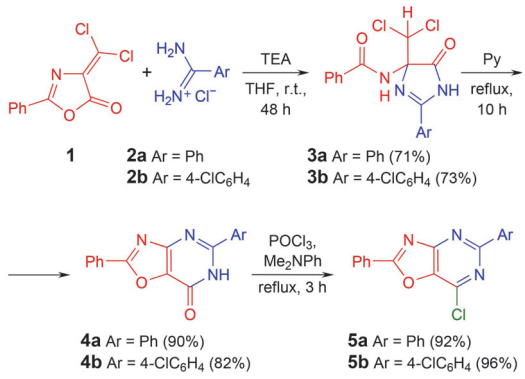

Scheme 1. Synthesis of 7-chloro-substituted oxazolo[4,5-*d*]pyrimidines **5a**/**5b**.

© 2020 Wiley-VHCA AG, Zurich, Switzerland

15222675, 2020, 12, Downloaded from https://onlinelibrary.wiley.com/doi/10.1002/hlca.202000169 by Tallin Technical University, Wiley Online Library on [03/06/2023]. See the Terms and Conditions (https://onlinelibrary.wiley.com/terms-and-conditions) on Wiley Online Library for rules of use; OA articles are governed by the applicable Creative Commons License

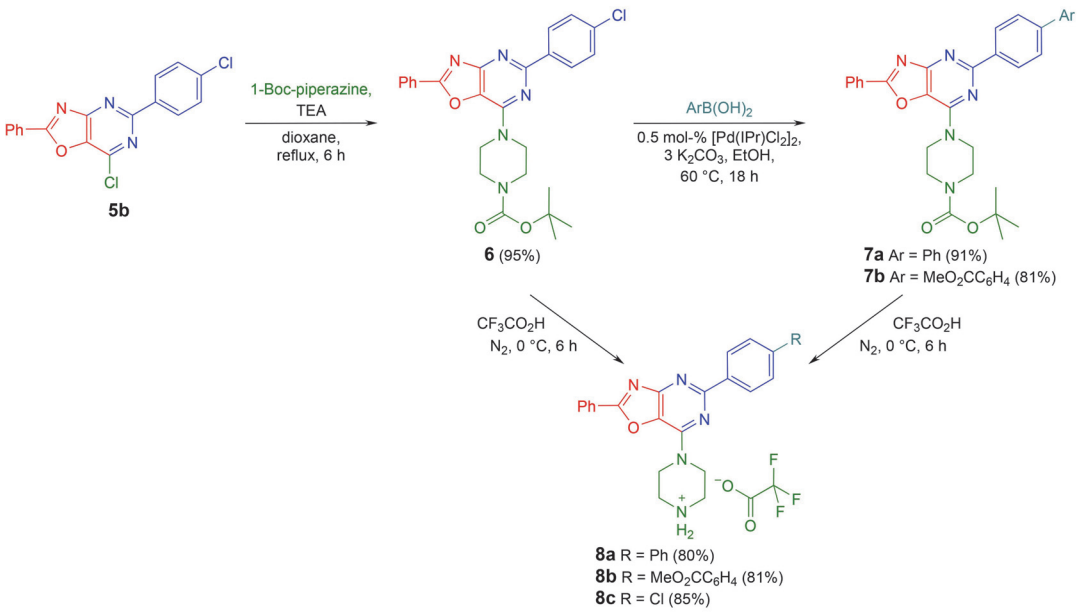

Scheme 2. Synthesis of oxazolo[4,5-*d*]pyrimidines **8a**–**8c**. IPr = 1,3-bis(2,6-diisopropylphenyl)imidazol-2-ylidene.

5a were reliably established earlier,[25,26] the structures of congeners **3b**, **4b** and **5b** were confirmed by ^{1}H- and ^{13}C-NMR, IR spectra and elemental analysis. NH signals of **3b** are appear at 12.08 and 9.29 ppm in the ^{1}H-NMR spectra and at 3427–3204 cm^{-1} in the IR spectra, while the NH signal of **4b** can be observed at 13.15 ppm and 3064 cm^{-1}, respectively. ^{1}H-NMR spectrum of **6** in (D_6)-DMSO revealed a singlet at 1.48 ppm due to the 1-Boc-piperazine moiety.

Compounds **7a** and **7b** were obtained by *Suzuki–Miyaura* cross coupling reaction of 7-*N*-Boc-piperazine-substituted oxazolo[4,5-*d*]pyrimidine **6** with the corresponding arylboronic acids in the presence of [Pd(μ-Cl)Cl(IPr)]$_2$ (0.5 mol-%), EtOH and K_2CO_3 (IPr = 1,3-bis(2,6-diisopropylphenyl)imidazol-2-ylidene; *Scheme 2*).[27–30] *N*-Boc-protection was removed by reacting **6** or **7a**/**7b** with CF_3COOH under an inert atmosphere resulting in the formation of oxazolo[4,5-*d*]pyrimidin-7-yl)-piperazin-1-ium trifluoroacetates **8a**–**8c**. Compounds **8a**–**8c** reveal in their ^{1}H-NMR spectra a resonance at 9.04–9.16 ppm corresponding to H_2N^+ functionality in the piperazine moiety, and their ^{19}F-NMR spectra in (D_6) DMSO revealed a singlet at −73.5 ppm.

Functionalization of 7-chloro-substituted oxazolo [4,5-*d*]pyrimidine **5a** was also carried out by *Suzuki–Miyaura* reaction with phenyl-(**9a**) or 4-methoxycarbonylphenylboronic acids (**9b**) in the presence of [Pd(μ-Cl)Cl(IPr)]$_2$, EtOH and K_2CO_3 (*Scheme 3*) affording products **10a**–**10b** in high yield.

The isomeric oxazolo[5,4-*d*]pyrimidin-7-one **13** was synthesized using the route improved by *Dounchis* (*Scheme 4*).[31] The reaction of benzoyl bromide **11** with silver cyanide led to 7*H*-[1,3]oxazolo[5,4-*d*][1,3] oxazine **12**. Treatment of the trimer **12** with sodium methoxide followed by stirring with acetic acid afforded 2,5-diphenyl-oxazolo[5,4-*d*]pyrimidin-7-one **13**.

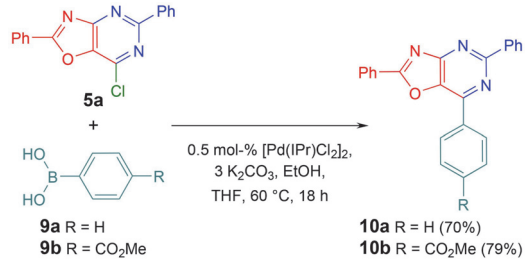

Scheme 3. Synthesis of 7-aryl-substituted oxazolo[4,5-*d*]pyrimidines **10**. IPr = 1,3-bis(2,6-diisopropylphenyl)imidazol-2-ylidene.

© 2020 Wiley-VHCA AG, Zurich, Switzerland

15222675, 2020, 12, Downloaded from https://onlinelibrary.wiley.com/doi/10.1002/hlca.202000169 by Tallin Technical University, Wiley Online Library on [03/06/2023]. See the Terms and Conditions (https://onlinelibrary.wiley.com/terms-and-conditions) on Wiley Online Library for rules of use; OA articles are governed by the applicable Creative Commons License

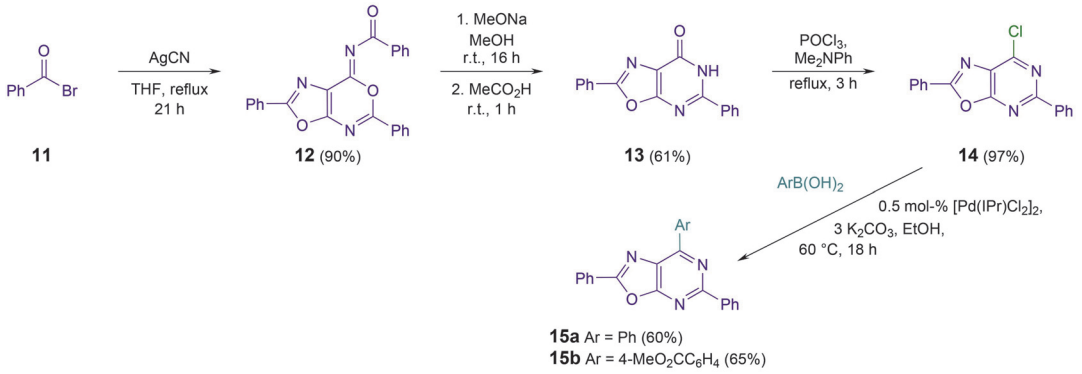

Scheme 4. Synthesis of oxazolo[5,4-*d*]pyrimidines **15**. IPr = 1,3-bis(2,6-diisopropylphenyl)imidazol-2-ylidene.

The reaction of compound **13** with trichlorophosphate in the presence of *N*,*N*-dimethylaniline gave 7-chloro-2,5-diphenyl[1,3]oxazolo[5,4-*d*]pyrimidine (**14**). 7-Aryl-substituted oxazolo[5,4-*d*]pyrimidines **15a**/**15b** were obtained under the same conditions as their isomers **10a**/**10b** described above.

Molecular Docking

It is known that oxazolopyrimidine-containing compounds are inhibitors of the VEGFR2 and interact with ATP binding site.[15,16] The docking validation was conducted by redocking sunitinib-ligand into the active site VEGFR2 (PDB ID: 4AGD). The obtained ligand-protein complex showed $\Delta G = -9.8$ kcal/mol (*Table 1*). RMSD value for all atoms did not exceed 2 Å. It was assumed that all studied compounds containing the oxazolopyrimidine moiety have a similar molecular mechanism of action. Therefore, the molecular docking of the studied compounds was performed similarly using the VEGFR2 crystal structure (*Table 1*).

Table 1. Molecular docking results.

Compound	ΔG, kcal/mol	Number of H-bonds and electrostatic interactions
Sunitinib	−9.8	3
5a	−9.1	0
8a	−10.1	3
8b	−9.6	4
8c	−9.8	3
10a	−9.5	0
10b	−9.6	0
14	−8.8	0
15a	−9.2	0
15b	−9.1	0

Docking analysis of potential biologically active compounds **8a**–**8c** with the highest binding energy −10.1, −9.6, −9.8 kcal/mol respectively is presented in *Figures 1* and *2*.

Each piperazine group of compounds **8a** and **8b** (*Figure 1*) forms two H-bonds (2.46–3.24 Å) with amino acid Leu840. The phenyl ring at C(2) of each compound forms the electrostatic interactions (4.13–4.57 Å) with amino acid Lys838. The phenyl rings at C(5) of compounds **8a** and **8b** are characterized by forming of the many hydrophobic π-alkyl interactions (3.56–5.47 Å) with amino acids Leu840, Val848, Ala866, Val899, Cys919, Leu1035 and Cys1045. Moreover, **8b** forms an additional hydrogen bond between the carboxyl group and the amino acid Glu885.

Piperazine moiety of ligand **8c** forms a H-bond (2.48 Å) with amino acid Leu840. The phenyl group at C(2) forms the electrostatic interaction (4.68 Å) with amino acid Lys838. The phenyl group at C(5) is characterized by forming of the five hydrophobic π-alkyl interactions (3.46–4.46 Å) with amino acids Leu840, Val848, Ala866 and Leu1035. Also, the chlorine atom forms one H-bond (3.77 Å) with amino acids Lys868 and two π-alkyl hydrophobic interactions (4.39–4.42 Å) with amino acids Val916, Val 899.

Thus, the docking results show a similar binding mode of compounds **8a**–**8c** in the active site VEGFR2 with the formation of stable protein-ligand complexes with predicted $\Delta G = -10.1$, −9.6, −9.8 kcal/mol, respectively (see *Table 1*).

© 2020 Wiley-VHCA AG, Zurich, Switzerland

15222675, 2020, 12, Downloaded from https://onlinelibrary.wiley.com/doi/10.1002/hlca.202000169 by Tallin Technical University, Wiley Online Library on [03/06/2023]. See the Terms and Conditions (https://onlinelibrary.wiley.com/terms-and-conditions) on Wiley Online Library for rules of use; OA articles are governed by the applicable Creative Commons License

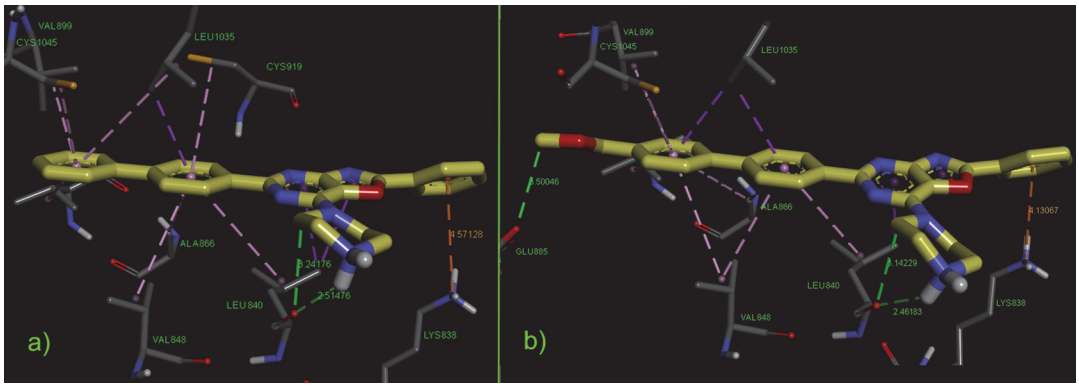

Figure 1. Molecular docking of compounds **8a** (a) and **8b** (b) into the active site VEGFR2.

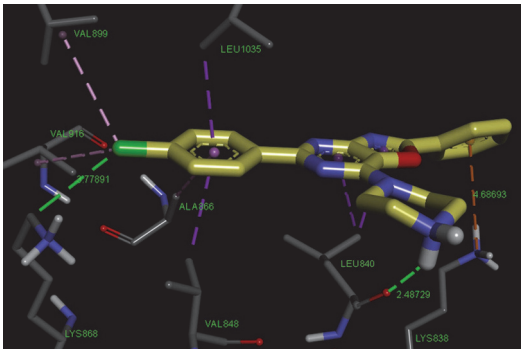

Figure 2. Molecular docking of compounds **8c** into the active site VEGFR2.

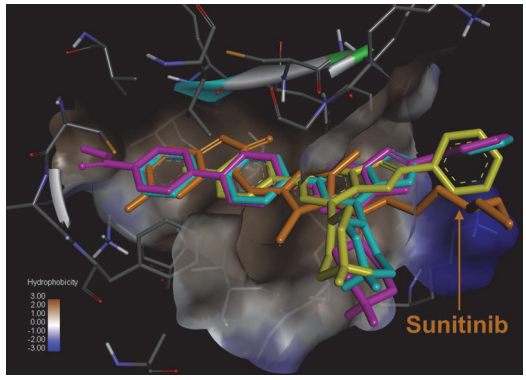

Figure 3. The docking position of compounds **8a**–**8c** and sunitinib (co-crystallized with VEGFR2) in VEGFR2 active site. Compound **8a**: light blue, **8b**: violet, **8c**: yellow, sunitinib: orange.

Figure 3 shows the similar binding mode of compounds **8a**–**8c** and VEGFR2 inhibitor sunitinib in the active site of the protein.

To investigate the structure–biological activity relationship of the oxazolopyrimidine scaffold, the ligand **10a** with an acceptor group at C(7) and a binding energy lower than that of the reference molecule sunitinib was docked to the active center of the VEGFR2 (*Figure 4*).

Figure 4 shows that the formed ligand-protein complex is stabilized mainly by hydrophobic interactions (3.71–5.46 Å) with no evidence of hydrogen bonds and electrostatic interactions. The localization of ligand **10a** was significantly different in comparison with docking position of the highly effective ligands **8a**–**8c** in the VEGFR2 active site.

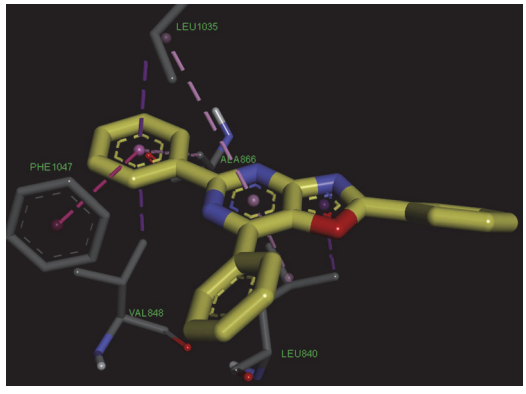

Figure 4. Molecular docking of compound **10a** into the active site VEGFR2.

© 2020 Wiley-VHCA AG, Zurich, Switzerland

15222675, 2020, 12, Downloaded from https://onlinelibrary.wiley.com/doi/10.1002/hlca.202000169 by Tallin Technical University, Wiley Online Library on [03/06/2023]. See the Terms and Conditions (https://onlinelibrary.wiley.com/terms-and-conditions) on Wiley Online Library for rules of use; OA articles are governed by the applicable Creative Commons License

Electron Structure of the Oxazolopyrimidine Derivatives

As can be seen from *Figure 4*, careful analysis of molecular docking calculations illustrates essential contribution of π-system of the studied compounds, interaction of the π-electrons can additionally stabilize the generated complex of compounds with the suitable fragments of biomolecules (proteins). In addition, *N*-heterocycles with di-coordinated nitrogen atoms (and hence with the lone electron pair – LEP) could generate hydrogen bonds with amino acids.

We may optimistically suppose that the biological activity (or affinity) of conjugated heterocycles is primarily determined by its donor/acceptor properties; their complex with protein fragments can be stabilized by π–π-stack interactions and H-bond formation. Donor–acceptor properties of any conjugated molecule can be estimated quantitatively by changes of the relative positions of their frontier molecular orbitals: highest occupied molecular orbital (HOMO) and lowest unoccupied molecular orbital (LUMO) by the following index ϕ_0[32,33].

When $\phi_0 = 0.5$, the donor and acceptor properties are mutually balanced; an increase of the parameter ($\phi_0 > 0.5$) indicates a predominately donor nature; if $\phi_0 < 0.5$, the frontier molecular orbitals are shifted downward, indicating a predominantly acceptor character. Here, the compounds were optimized before calculation by DFT/6-31 (d,p)/wB97XD method using package GAUSSIAN 03;[34] obtained values of the substituted oxazolopyrimidines are collected in *Table 2*.

It follows from *Table 2* that:

Table 2. Electron characteristics of oxazolopyrimidines (**5a**, **8a**–**8c**, **10a**/**10b**, **15a**/**15b**).

Compound	ε(MO) [eV] HOMO	LUMO	Δ[a]	ϕ_0[b]
Model molecule[c]	−8.963	0.544	9.507	0.43
5a	−8.320	−0.457	7.862	0.39
8a	−7.520	0.121	7.399	0.48
8b	−7.599	−0.450	7.149	0.44
8c	−7.786	−0.014	7.772	0.46
10a	−8.053	−0.436	7.617	0.41
10b	−8.148	−0.686	7.742	0.39
15a	−7.833	−0.432	7.401	0.42
15b	−7.943	−0.674	7.269	0.40

[a] Δ = εLUMO−εHOMO is energy gap.
[b] $\phi_0 = (\varepsilon LUMO-\alpha)/\Delta$.[11,12]
[c] 2,5,7-trimethyloxazolo[4,5-*d*]pyrimidine.

1) introduction of the phenyl substituents (compounds **5a**, **10a**/**10b**, **15a**/**15b**) decreases their donor ability compared to the model molecule;
2) introduction of the donor methoxycarbonyl group (compounds **10b** and **15b**) additionally increases donor properties of the molecules;
3) replacement of the phenyl ring by the piperazine fragment (compounds **8a**–**8c**) is accompanied by an increase of the parameter ϕ_0.

The calculations of the electron structure show that the studied compounds can generate a stable complex with the aromatic fragments of phenylalanine, tyrosine or tryptophan. Additionally, the aryl substituents could act as the additional centers for the formation of complexes with the fragments of the proteins.

Since the LEPs at the nitrogen atoms in the pyrimidine heterocycle can form hydrogen bonds (see *Figures 1*–3), the binding energies of these bonds are undoubtedly dependent on the position of the corresponding *n*-level (LEP level). The performed calculations show that *n*-level is positioned relatively high. This causes the some mixing of *n*→π* - and π→π* transitions (see in detail in the *Supporting Information*). Consequently, LEP can effectively generate the hydrogen bonds, which is consistent with the molecular docking modeling.

In vitro *Anticancer Activity*

The ability of all new synthesized oxazolopyrimidines (**8a**–**8c**, **10a**/**10b**, **15a**/**15b**) and their precursors (**5a**, **14**) to inhibit cell proliferation of ovarian (OVCAR-3), colon (HCT-116) and breast (MDA-MB-231) cancer cells was analyzed after 96 h treatment. All oxazolopyrimidines are sparingly soluble in water, and for this reason the stock solutions for biological investigations were prepared in dimethyl sulfoxide. The data obtained on these three cell lines along with data for doxorubicin, a known antineoplastic drug, are summarized in *Table 3*. Oxazolo[4,5-*d*]pyrimidines **8a**–**8c** exhibited cytotoxic effect against all three cancer cell lines and compound **10b** showed activity against two of them. Other compounds, including precursors, exhibiting $\Delta G \leq -9.5$ kcal/mol (see *Table 1*), have not demonstrated an effect on the growth of the studied cancer cell lines.

It is worth noting that oxazolo[4,5-*d*]pyrimidines **8b**/**8c** displayed a slightly higher antiproliferative activity (IC_{50}: 0.24 ± 0.05 μM and 0.21 ± 0.03 μM, respectively) than doxorubicin (IC_{50} = 0.36 ± 0.03 μM) on MDA-MB-231 and have relatively good results on OVCAR-3 (IC_{50}: 1.8 ± 0.3 μM and 1.7 ± 0.2 μM) and HCT-

© 2020 Wiley-VHCA AG, Zurich, Switzerland

15222675, 2020, 12, Downloaded from https://onlinelibrary.wiley.com/doi/10.1002/hlca.202000169 by Tallin Technical University, Wiley Online Library on [03/06/2023]. See the Terms and Conditions (https://onlinelibrary.wiley.com/terms-and-conditions) on Wiley Online Library for rules of use; OA articles are governed by the applicable Creative Commons License

Table 3. Effects of the studied compounds on proliferation of different cancer cell lines after 96 h of incubation.

Compound	IC_{50} [μM] OVCAR3	HCT-116	MDA-MB-231
Doxorubicin	0.0021 ± 0.0004	0.10 ± 0.01	0.36 ± 0.03
5a	> 100	> 100	> 100
8a	5.3 ± 0.3	3.9 ± 0.4	1.4 ± 0.3
8b	1.8 ± 0.3	3.9 ± 0.3	0.24 ± 0.05
8c	1.7 ± 0.2	0.24 ± 0.03	0.21 ± 0.03
10a	> 100	> 100	> 100
10b	43 ± 4	> 100	22 ± 2
14	> 100	> 100	> 100
15a	> 100	> 100	> 100
15b	> 100	> 100	> 100

116 (IC_{50}: 3.9 ± 0.3 μM and 0.24 ± 0.03 μM). At the same time, compound **8a** exhibited lower activity than the previous two, but also inhibited the growth of OVCAR-3, HCT-116, and MDA-MB-231 at micromolar concentrations (IC_{50}: 5.3 ± 0.3 μM, 3.9 ± 0.4 μM and 1.4 ± 0.3 μM, respectively).

Methyl 4-(2,5-diphenyl[1,3]oxazolo[4,5-*d*]pyrimidin-7-yl)benzoate (**10b**), with the same free energy of ligand–protein complex as **8c** ($\Delta G = -9.6$ kcal/mol, see *Table 1*), also showed cytotoxic effect on OVCAR-3 and MDA-MB-231 only at 43 ± 4 μM and 22 ± 2 μM, respectively.

It can be concluded that piperazine fragment containing a positively charged nitrogen atom play a significant role in the cytotoxicity of oxazolo[4,5-*d*] pyrimidines **8a**–**8c**.

Conclusions

In order to investigate the structure-biological activity relationship of the oxazolopyrimidine framework, new oxazolo[4,5-*d*]pyrimidines and isomeric oxazolo[5,4-*d*] pyrimidines containing acceptor groups at C(2) and C(5), and electron donating (piperazine) or withdrawing substituents (aryl residues) at C(7) have been synthesized.

The docking results show that oxazolo[4,5-*d*]pyrimidines **8a**–**8c** with nitrogen atom at the piperazine moiety bearing positive charge could be potential VEGFR2 inhibitors with the highest binding energy (ΔG: −10.1, −9.6, −9.8 kcal/mol,respectively). In the other cases, the nature of the ligand-protein interaction differs: the formed ligand-protein complexes are stabilized mainly by hydrophobic interactions, without any hydrogen bonds and electrostatic interactions.

The introduction of piperazine moiety increases the donor-acceptor parameter (ϕ_0) of oxazolopyrimidines **8a**–**8c** in the range: 0.48, 0.44, 0.46, respectively, which is inversely proportional to the obtained results of their anticancer activity on all studied cancer cell lines.

Oxazolo[4,5-*d*]pyrimidines **8a**–**8c** containing positively charged piperazine moiety displayed the best cytotoxicity effects showing in some cases similar or even better activity than doxorubicin. Prospects for these molecules as potential anticancer agents are very attractive and will be the subject of future studies.

Experimental Section

Materials and Methods

Commercially available reagents were used without purification. The reagents and the solvents were purchased from *Sigma–Aldrich* or *Eurisotop*. The solvents used were purified by distillation over the drying agents indicated: THF (Na/benzophenone), DMF, MeCN (CaH_2), MeOH (Mg). Reaction monitoring by thin layer chromatography was performed on precoated alumina plates SiO_2 *60* F_{254} from *Merck*. Melting points were determined on a *Fisher–Johns* (compounds **3b**, **4b**, **5b**, **6**) or a *Stuart SMP40* apparatus (compounds **7a**/**7b**, **8a**–**8c**, **10a**/**10b**, **15a**/**15b**) and are uncorrected. Infrared (IR) spectra were recorded on a *Bruker Tensor 27* (compounds **7a**/**7b**, **8a**–**8c**, **10a**/**10b**, **15a**/**15b**) or a *Vertex-70* spectrometer from KBr pellets (compounds **3b**, **4b**, **5b**, **6**). ^{1}H- and ^{13}C-NMR spectra were recorded on a *Bruker Avance II* (296.2 K, 400 and 101 MHz, resp.) or *500 MHz Agilent DD2* (353.2 K, 500 and 126 MHz, resp.; only for compounds **4b**, **6**, **8c**) spectrometers, with tetramethylsilane (TMS)

© 2020 Wiley-VHCA AG, Zurich, Switzerland

15222675, 2020, 12, Downloaded from https://onlinelibrary.wiley.com/doi/10.1002/hlca.202000169 by Tallin Technical University, Wiley Online Library on [03/06/2023]. See the Terms and Conditions (https://onlinelibrary.wiley.com/terms-and-conditions) on Wiley Online Library for rules of use; OA articles are governed by the applicable Creative Commons License

as internal standard. All ^{1}H signals are reported in ppm with the internal chloroform signal at 7.26 ppm or dimethyl sulfoxide at 2.50 ppm as internal reference. Data are reported as follows: chemical shift, multiplicity (*s*=*singlet*, *d*=*doublet*, *t*=*triplet*, *q*=*quartet*, *m*=*multiplet*), integration, and assignment. Broad signals are indicated as *br*. Coupling constants (*J*) are given in Hertz [Hz]. All ^{13}C-NMR signals are reported in ppm with the internal chloroform signal at 77.16 ppm or dimethyl sulfoxide at 39.52 ppm as internal references. The LC- or HR-MS identification of compounds was conducted on an *Agilent 1200 Series* system equipped (compounds **3b**, **4b**, **5b**, **6**) with a diode array and a *G6130 A* mass-spectrometer (atmospheric pressure electrospray ionization) or on an *Agilent 6540 UHD Accurate-Mass Q-TOF LC/MS G6540 A* mass-spectrometer (compounds **7a**/**7b**, **8a**–**8c**, **10a**/**10b**, **15a**/**15b**). Elemental analyses were carried out on a *Vario MACRO Cube/Elementar* instrument. DFT calculations were performed by DFT/6-31 (d,p)/wB97XD method using package GAUSSIAN 03.[33]

Molecular Docking

The docking preparation of the protein with ligands was done by AutoDock Tools (ADT) (ver. 1.5.6).[35] The crystal structure (PDB ID: 4AGD) of VEGFR-2 was used for the docking of nine studied compounds. Water molecules and ligand were removed from the 4AGD crystal structure using Accelrys DS (ver. 4.0).[36] The protein was prepared by adding all hydrogens using the 'no Bond Order method' (ADT). *Gasteiger* partial charge calculation method was used and the created files were saved in PDBQT format. The created ligand structures were saved in Mol2 format using ChemAxon Marvin Sketch 5.3.735.[37] All ligands optimization and energy minimization were performed by Avogadro v1.1.1[38] using Auto Optimization Tool by applying the MMFF94s force field. Partial charges and torsion angles of ligands were changed by ADT and saved in PDBQT format. AutoDock Vina 1.1.2[39] program was applied to docking. The box center (x=45.434, y=−3.366, z=−13.177) and the grid map (40*40*40 points) with a grid spacing of 1 Å were used. The visualization of protein-ligand interactions was performed by Accelrys DS program.

Cell Viability Assays

Cell viability inhibition assays were carried out using human colon HCT-116, ovarian OVCAR-3, breast MDA-MB-231 cancer cells. Cells were obtained from ATCC (Manassas, VA). Cells were grown in accordance with the supplier and maintained at 37 °C in a humidified atmosphere of 5 % carbon dioxide. Five hundred cells were plated in 96 wells and treated with six different concentrations (0.001, 0.01, 0.1, 1, 10 and 100 μM) of the synthesized compounds. After 96 hours from the treatment, cell viability was measured with Cell Titer glow assay (*Promega*, Madison, WI, USA) with a *Tecan M1000* instrument. IC_{50} values were calculated from logistical dose response curves. Averages were obtained from triplicates, and error bars are standard deviations.

General Procedure for the Synthesis of N-*[4-(Dichloromethyl)-5-oxo-2-aryl-4,5-dihydro-1*H-*imidazol-4-yl]benzamides* **3a** *and* **3b**

To a solution of 1,3-oxazol-5(4*H*)-one **1** (62-66 mmol, 1.00 equiv.), prepared by the literature procedure,[24] in dry THF (100 mL) was added one of the amidine hydrochlorides **2a,b** (62-66 mmol, 1.00 equiv.) followed by Et_3N (64-68 mmol, 1.03 equiv.). The mixture was stirred at r.t. for 48 h. The precipitate that formed was collected by filtration, washed with H_2O, and dried.

***N*-[4(5)-(Dichloromethyl)-5(4)-oxo-2-phenyl-4,5-dihydro-1*H*-imidazol-4(5)-yl]benzamide** (**3a**). Compound **3a** was prepared as described above following the *General Procedure*, starting from 2-aryl-4-(dichloromethylidene)-1,3-oxazol-5(4*H*)-one (**1**; 15.01 g, 62 mmol, 1.00 equiv.), benzamidine hydrochloride (**2a**; 9.71 g, 62 mmol, 1.00 equiv.), and Et_3N (9 mL, 64 mmol, 1.03 equiv.). Yield: 15.94 g, 71 %. Spectral and elemental analysis data are identical to literature reports.[26]

***N*-[2-(4-Chlorophenyl)-4(5)-(dichloromethyl)-5(4)-oxo-4,5-dihydro-1*H*-imidazol-4(5)-yl]benzamide** (**3b**). Compound **3b** was prepared as described above following the *General Procedure*, starting from compound **1** (16.00 g, 66 mmol, 1.00 equiv.), 4-chlorobenzamidine hydrochloride (**2b**; 12.63 g, 66 mmol, 1.00 equiv.), and Et_3N (9.50 mL, 68 mmol, 1.03 equiv.). Compound **3b** was obtained as light grey solid. Yield: 19.11 g, 73 %. M.p. 144–146 °C. IR (KBr): 3427–3204 (NH, assoc.), 1785 (C=O), 1649 (NC=O), 1614, 1475, 1285, 1093, 923, 841, 712, 689, 645, 466. ^{1}H-NMR (400 MHz, (D_6)DMSO): 12.08 (*s*, 1 H, NH); 9.29 (*s*, 1 H, NH); 8.06 (*d*, J=8.4, 2 H, ArH); 7.83–7.81 (*m*, 2 H, ArH); 7.66 (*d*, J=8.6, 2 H, ArH); 7.59 (*dd*, J=8.4, 6.3, 1 H, ArH); 7.51 (*t*, J=7.5, 2 H, ArH); 6.46 (*s*, 1 H, $CHCl_2$). ^{13}C-NMR (101 MHz, (D_6)DMSO): 178.13;

© 2020 Wiley-VHCA AG, Zurich, Switzerland

15222675, 2020, 12, Downloaded from https://onlinelibrary.wiley.com/doi/10.1002/hlca.202000169 by Tallin Technical University, Wiley Online Library on [03/06/2023]. See the Terms and Conditions (https://onlinelibrary.wiley.com/terms-and-conditions) on Wiley Online Library for rules of use; OA articles are governed by the applicable Creative Commons License

166.16; 137.66; 132.63; 132.21; 130.12; 129.26; 129.15; 128.50; 127.74; 126.65; 81.29; 71.99. MS: 398.0 ($[M+H]^+$, $C_{17}H_{13}Cl_3N_3O_2^+$; calc. 397.7). Anal. calc. for $C_{17}H_{12}Cl_3N_3O_2$ (396.66): C 51.48, H 3.05, N 10.59; found: C 51.40, H 3.12, N 10.45.

*General Procedure for the Synthesis of 2-Phenyl[1,3]-oxazolo[4,5-*d*]pyrimidin-7(*6*H)-ones* **4a** *and* **4b**

A solution of one of the compounds **3a** or **3b** (48 mmol) in pyridine (60 mL) was refluxed for 10 h. The pyridine was removed *in vacuo*. The residue was treated with H_2O, filtered, dried, and recrystallized.

2,5-Diphenyl[1,3]oxazolo[4,5-*d*]pyrimidin-7(6*H*)-one (**4a**). Compound **4a** was prepared according to the above *General Procedure*, starting from **3a** (17.38 g, 48 mmol). Purification by recrystallization (DMF) gave white crystals. Yield: 12.50 g, 90%. Spectral and elemental analysis data are identical to literature reports.[27–30]

5-(4-Chlorophenyl)-2-phenyl[1,3]oxazolo[4,5-*d*]-pyrimidin-7(6*H*)-one (**4b**). Compound **4b** was prepared according to the above *General Procedure*, starting from **3b** (19.10 g, 48 mmol). Purification by recrystallization (DMF) gave white crystals. Yield: 12.74 g, 82%. M.p. 294–296 °C. IR (KBr): 3064 (NH), 1690 (NC=O), 1601, 1484, 1342, 1262, 920, 837, 717, 683, 545, 462. ^{1}H-NMR (500 MHz, 353.2 K, (D_6)DMSO): 8.19–8.13 (*m*, 4 H, ArH); 7.69–7.56 (*m*, 5 H, ArH). ^{13}C-NMR (126 MHz, (D_6)DMSO): 164.59; 158.23; 154.59; 151.52; 136.13; 132.10; 131.66; 130.68; 129.32; 128.80; 128.14; 127.06; 125.29. MS: 324.0 ($[M+H]^+$, $C_{17}H_{11}ClN_3O_2^+$; calc. 324.7). Anal. calc. for $C_{17}H_{10}ClN_3O_2$ (323.74): C 63.07, H 3.11, N 12.98; found: C 63.00, H 3.17, N 12.91.

*General Procedure for the Synthesis of 7-Chloro-2-phenyl [1,3]oxazolo[4,5-*d*]pyrimidines* **5a** *and* **5b**

A mixture of one of the compounds **4a** or **4b** (39 mmol, 1.00 equiv.), $POCl_3$ (75 mL), and Me_2NPh (78 mmol, 2.00 equiv.) was refluxed for 3 h. After evaporation of $POCl_3$ excess, the solid residue was recrystallized from 1,4-dioxane.

7-Chloro-2,5-diphenyl[1,3]oxazolo[4,5-*d*]pyrimidine (**5a**). Compound **5a** was prepared as described above in the *General Procedure*, starting from **4a** (11.28 g, 39 mmol, 1.00 equiv.), $POCl_3$ (75 mL), and Me_2NPh (10 mL, 78 mmol, 2.00 equiv.). Yield: 11.04 g, 92%. Spectral and elemental analysis data are identical to literature reports.[27–30]

7-Chloro-5-(4-chlorophenyl)-2-phenyl[1,3]oxazolo[4,5-*d*]pyrimidine (**5b**). Compound **5b** was prepared as described above in the *General Procedure*, starting from **4b** (12.63 g, 39 mmol, 1.00 equiv.), $POCl_3$ (75 mL), and Me_2NPh (10 mL, 78 mmol, 2.00 equiv.). Light pink solid. Yield: 12.81 g, 96%. M.p. 241–243 °C. IR (KBr): 1609, 1538, 1487, 1378, 1221, 1086, 908, 842, 708, 682, 481. ^{1}H-NMR (400 MHz, $CDCl_3$): 8.44 (*dd*, *J* = 39.4, 7.8, 4 H, ArH); 7.71–7.46 (*m*, 5 H, ArH). ^{13}C-NMR (101 MHz, $CDCl_3$): 169.03; 163.96; 161.26; 141.58; 138.29; 137.64; 134.78; 134.20; 130.17; 129.50; 129.20; 129.05; 125.20. MS: 344.0 ($[M+H]^+$, $C_{17}H_{10}Cl_2N_3O^+$; calc. 343.2). Anal. calc. for $C_{17}H_9Cl_2N_3O$ (342.19): C 59.67, H 2.65, N 12.28; found: C 59.56, H 2.66, N 12.20.

***tert*-Butyl 4-[5-(4-chlorophenyl)-2-phenyl[1,3]oxazolo[4,5-*d*]pyrimidin-7-yl]piperazine-1-carboxylate** (**6**). The synthesis of compound **6** was accomplished in analogy to previously reported derivatives.[18,19] A mixture of compound **5b** (5.50 g, 16 mmol, 1.00 equiv.), 1-Boc-piperazine (2.98 g, 16 mmol, 1.00 equiv.), and Et_3N (2 mL, 16 mmol, 1.00 equiv.) in dioxane (50 ml) was refluxed for 6 h. After removal of the solvent, the residue was triturated with water, filtered off, dried, and recrystallized from MeCN obtaining white solid. Yield: 7.48 g, 95%. M.p. 248–250 °C. IR (KBr): 3065–2880 (CH_2 (piperazine)), 1693, 1620, 1547, 1479, 1364, 1289, 1173, 1131, 1084, 1011, 930, 848, 776, 686. ^{1}H-NMR (500 MHz, 353.2 K, (D_6) DMSO): 8.40–8.37 (*m*, 2 H, ArH); 8.28 (*dd*, *J* = 5.2, 3.4, 2 H, ArH); 7.72–7.63 (*m*, 3 H, ArH); 7.53–7.50 (*m*, 2 H, ArH); 4.07 (*dd*, *J* = 6.2, 4.4, 4 H, piperazine); 3.63 (*dd*, *J* = 6.2, 4.5, 4 H, piperazine); 1.48 (*s*, 9 H, Me_3CO_2C). ^{13}C-NMR (126 MHz, (D_6)DMSO): 164.24; 161.42; 158.19; 153.57; 147.58; 136.35; 134.54; 132.23; 129.07; 128.73; 127.79; 127.70; 127.39; 125.28; 78.80; 44.19; 42.67; 27.67. MS: 492.0 ($[M+H]^+$, $C_{26}H_{26}ClN_5O_3^+$; calc. 493.0). Anal. calc. for $C_{26}H_{26}ClN_5O_3$ (491.98): C 63.48, H 5.33, N 14.23; found: C 63.44, H 5.30, N 14.18.

*General Procedure for the Synthesis of 5-Biaryl-Substituted tert-Butyl 4-([1,3]oxazolo[4,5-*d*]pyrimidin-7-yl)piperazine-1-carboxylates* **7a** *and* **7b**

A mixture of compound **6** (1.00 g, 2 mmol, 1.00 equiv.), arylboronic acid (4 mmol, 2.00 equiv.), K_2CO_3 (6 mmol, 3.00 equiv.), $[Pd(IPr)Cl_2]_2$ (10 μmol, 0.005 equiv.), and absolute EtOH (20 mL) was stirred at 60 °C for 18 h. The precipitate was collected by filtration, washed

© 2020 Wiley-VHCA AG, Zurich, Switzerland

15222675, 2020, 12, Downloaded from https://onlinelibrary.wiley.com/doi/10.1002/hlca.202000169 by Tallin Technical University, Wiley Online Library on [03/06/2023]. See the Terms and Conditions (https://onlinelibrary.wiley.com/terms-and-conditions) on Wiley Online Library for rules of use; OA articles are governed by the applicable Creative Commons License

with water and ethanol and then dissolved in CH_2Cl_2 and passed through a microfilter. The solvent was removed *in vacuo*.

***tert*-Butyl 4-[5-([1,1′-biphenyl]-4-yl)-2-phenyl-[1,3]oxazolo[4,5-*d*]pyrimidin-7-yl]piperazine-1-carboxylate** (**7a**). Compound **7a** was prepared as described above in the *General Procedure*, starting from **6** (1.00 g, 2 mmol, 1.00 equiv.), phenylboronic acid (0.49 g, 4 mmol, 2.00 equiv.), K_2CO_3 (0.83 g, 6 mmol, 3.00 equiv.), $[Pd(IPr)Cl_2]_2$ (11 mg, 10 μmol, 0.005 equiv.), and absolute EtOH (20 mL). White solid. Yield: 0.97 g, 91 %. M.p. 288.3 °C. IR (KBr): 3451–2973 (CH_2 (piperazine)), 1698, 1617, 1547, 1474, 1375, 1251, 1169, 1056, 1013, 930, 854, 769, 696. ^{1}H-NMR (400 MHz, $CDCl_3$): 8.56–8.52 (*m*, 2 H, ArH); 8.26–8.22 (*m*, 2 H, ArH); 7.71–7.65 (*m*, 4 H, ArH); 7.62–7.51 (*m*, 3 H, ArH); 7.50–7.43 (*m*, 2 H, ArH); 7.40–7.34 (*m*, 1 H, ArH); 4.08 (*dd*, *J* = 6.2, 4.3, 4 H, piperazine); 3.68 (*dd*, *J* = 10.3, 5.3, 4 H, piperazine); 1.53 (*s*, 9 H, Me_3CO_2C). ^{13}C-NMR (101 MHz, $CDCl_3$): 165.15; 162.69; 160.51; 154.79; 148.03; 142.82; 140.84; 137.02; 132.70; 129.77; 129.21; 128.93; 128.90; 128.16; 127.66; 127.26; 127.06; 126.26; 80.50; 45.07; 28.58. HR-MS: 534.2493 ($[M+H]^+$, $C_{32}H_{32}N_5O_3^+$; calc. 534.2500). Anal. calc. for $C_{32}H_{31}N_5O_3$ (533.64): C 72.03, H 5.86, N 13.12; found: C 71.99, H 5.84, N 13.02.

***tert*-Butyl 4-{5-[4′-(methoxycarbonyl)[1,1′-biphenyl]-4-yl]-2-phenyl[1,3]oxazolo[4,5-*d*]pyrimidin-7-yl}piperazine-1-carboxylate** (**7b**). Compound 7b was prepared as described above in the *General Procedure*, starting from 6 (1.00 g, 2 mmol, 1.00 equiv.), 4-(methoxycarbonyl)phenylboronic acid (0.72 g, 4 mmol, 2.00 equiv.), K_2CO_3 (0.83 g, 6 mmol, 3.00 equiv.), $[Pd(IPr)Cl_2]_2$ (11 mg, 10 μmol, 0.005 equiv.) and absolute EtOH (20 mL). White solid. Yield: 0.96 g, 81 %. M.p. 280.3 °C. IR (KBr): 3450–2973 (CH_2 (piperazine)), 1720(C=O), 1693, 1608, 1545, 1426, 1377, 1278, 1172, 1058, 1026, 931, 844, 774, 693. ^{1}H-NMR (400 MHz, $CDCl_3$): 8.55 (*d*, *J* = 8.2, 2 H, ArH); 8.24 (*d*, *J* = 7.5, 2 H, ArH); 8.12 (*d*, *J* = 8.3, 2 H, ArH); 7.73–7.69 (*m*, 4 H, ArH); 7.61–7.52 (*m*, 3 H, ArH); 4.11–4.06 (*m*, 4 H, piperazine); 3.94 (*s*, 3 H, MeO_2C); 3.72–3.65 (*m*, 4 H, piperazine); 1.53 (*s*, 9 H, Me_3CO_2C). ^{13}C-NMR (101 MHz, $CDCl_3$): 167.11; 165.22; 162.67; 160.24; 154.78; 148.04; 145.22; 141.47; 137.85; 132.76; 130.24; 129.22; 129.18; 129.01; 128.22; 128.17; 127.21; 127.13; 126.20; 80.53; 52.28; 45.06; 28.57. HR-MS: 592.2535 ($[M+H]^+$, $C_{34}H_{34}N_5O_5^+$; calc. 592.2554). Anal. calc. for $C_{34}H_{33}N_5O_5$ (591.67): C 69.02, H 5.62, N 11.84; found: C 68.98, H 5.60, N 11.78.

General Procedure for the Synthesis of 4-([1,3]-Oxazolo[4,5-d]pyrimidin-7-yl)piperazin-1-ium Trifluoroacetates **8a–8c**

To a mixture of **6** (2 mmol) or **7a**/**7b** (1 mmol) and 1,4-dioxane (5 mL) while stirring at 0 °C under an inert atmosphere (Ar) was added an excess of trifluoroacetic acid (5 mL). The solution was stirred at r.t. for 5 h. The excess of trifluoroacetic acid and 1,4-dioxane were removed under reduced pressure at 70 °C. The solid was washed with water, dried, and recrystallized from MeCN/DMF.

4-[5-([1,1′-Biphenyl]-4-yl)-2-phenyl[1,3]oxazolo[4,5-*d*]pyrimidin-7-yl]piperazin-1-ium Trifluoroacetate (**8a**). Compound **8a** was prepared as described above in the *General Procedure*, starting from **7a** (0.53 g, 1 mmol), 1,4-dioxane (5 mL), and an excess of trifluoroacetic acid (5 mL). White solid. Yield: 0.44 g, 80 %. M.p. 288.5 °C. IR (KBr): 3427–3009 (NH_2^+, CH_2 (piperazine)), 1681, 1620, 1548, 1452 1379, 1201, 1130, 1025, 930, 769, 720, 695. ^{1}H-NMR (400 MHz, (D_6) DMSO): 9.16 (br. *s*, 2 H, NH_2^+ (piperazine)); 8.45 (*d*, *J* = 8.5, 2 H, ArH); 8.29 (*d*, *J* = 7.1, 2 H, ArH); 7.81–7.69 (*m*, 5 H, ArH); 7.68–7.61 (*m*, 2 H, ArH); 7.55–7.47 (*m*, 2 H, ArH); 7.41 (*ddd*, *J* = 6.5, 4.4, 1.1, 1 H, ArH); 4.33–4.21 (*m*, 4 H, piperazine); 3.47–3.36 (*m*, 4 H, piperazine). ^{13}C-NMR (101 MHz, (D_6)DMSO): 164.66; 161.97; 159.06; 158.34; 147.42; 141.81; 139.49; 136.49; 133.07; 129.38; 129.04; 128.43; 127.96; 127.93; 126.76; 126.68; 125.43; 42.62. ^{19}F-NMR (376 MHz, (D_6)DMSO): −73.54. HR-MS: 434.1962 ($[M+H]^+$, $C_{27}H_{25}N_5O^+$; calc. 434.1975). Anal. calc. for $C_{29}H_{24}F_3N_5O_3$ (546.55): C 63.62, H 4.42, N 12.79; found: C 63.59, H 4.47, N 12.76.

4-{5-[4′-(Methoxycarbonyl)[1,1′-biphenyl]-4-yl]-2-phenyl[1,3]oxazolo[4,5-*d*]pyrimidin-7-yl}piperazin-1-ium Trifluoroacetate (8b). Compound 8b was prepared as described above in the *General Procedure*, starting from 7b (0.59 g, 1 mmol), 1,4-dioxane (5 mL), and an excess of trifluoroacetic acid (5 mL). White solid. Yield: 0.49 g, 81 %. M.p. 243.9 °C. IR (KBr): 3422–2522 (NH_2^+, CH_2 (piperazine)), 1721(C=O), 1667, 1625, 1548, 1482, 1376, 1278, 1208, 1132, 1024, 935, 833, 773, 720, 693. ^{1}H-NMR (400 MHz, (D_6)DMSO): 9.16 (br. *s*, 2 H, NH_2^+ (piperazine)); 8.46 (*d*, *J* = 8.4, 2 H, ArH); 8.29 (*d*, *J* = 7.1, 2 H, ArH); 8.06 (*d*, *J* = 8.4, 2 H, ArH); 7.89 (*d*, *J* = 8.4, 2 H, ArH); 7.84 (*d*, *J* = 8.5, 2 H, ArH); 7.76–7.70 (*m*, 1 H, ArH); 7.69–7.61 (*m*, 2 H, ArH); 4.26 (*s*, 4 H, piperazine); 3.89 (*s*, 3 H, MeO_2C); 3.40 (*s*, 4 H, piperazine). ^{13}C-NMR (101 MHz, (D_6)DMSO): 166.01; 164.66; 161.93; 160.98; 158.81; 147.40; 143.92; 140.29;

© 2020 Wiley-VHCA AG, Zurich, Switzerland

15222675, 2020, 12, Downloaded from https://onlinelibrary.wiley.com/doi/10.1002/hlca.202000169 by Tallin Technical University, Wiley Online Library on [03/06/2023]. See the Terms and Conditions (https://onlinelibrary.wiley.com/terms-and-conditions) on Wiley Online Library for rules of use; OA articles are governed by the applicable Creative Commons License

137.32; 133.08; 129.83; 129.54; 129.37; 128.71; 128.48; 127.95; 126.98; 125.40; 52.21; 42.63. ^{19}F-NMR (376 MHz, (D$_6$)DMSO): 73.56. HR-MS: 492.2017 ([*M*+H]$^+$, $C_{29}H_{27}N_5O_3^+$; calc. 492.2030). Anal. calc. for $C_{31}H_{26}F_3N_5O_5$ (605.58): C 61.49, H 4.33, N 11.56; found: C 61.4, H 4.29, N 11.50.

4-[5-(4-Chlorophenyl)-2-phenyl[1,3]oxazolo[4,5-*d*]pyrimidin-7-yl]piperazin-1-ium Trifluoroacetate (**8c**). Compound **8c** was prepared as described above in the *General Procedure*, starting from **6** (0.98 g, 2 mmol), 1,4-dioxane (5 mL), and an excess of trifluoroacetic acid (5 mL). White solid. Yield: 0.86 g, 85%. M.p. 258.6 °C. IR (KBr): 3417–2509 (NH_2^+, CH_2 (piperazine)), 1718, 1674, 1622, 1545, 1452, 1358, 1283, 1207, 1127, 1021, 930, 832, 767, 694. ^{1}H-NMR (500 MHz, 353.2 K, (D$_6$)DMSO): 9.04 (br. *s*, 2 H, NH_2^+ (piperazine)); 8.40 (*dd*, *J*=8.9, 2.1, 2 H, ArH); 8.33–8.29 (*m*, 2 H, ArH); 7.73 (*dd*, *J*=8.4, 6.3, 1 H, ArH); 7.70–7.65 (*m*, 2 H, ArH); 7.55 (*dd*, *J*=8.9, 2.3, 2 H, ArH); 4.31–4.24 (*m*, 4 H, piperazine); 3.42–3.36 (*m*, 4 H, piperazine). ^{13}C-NMR (126 MHz, 80 °C, (D$_6$)DMSO): 164.59; 161.77; 158.26; 147.29; 136.18; 134.83; 132.60; 129.22; 128.92; 128.02; 127.84; 127.60; 125.20; 42.38; 41.56. ^{19}F-NMR (376 MHz, (D$_6$)DMSO): 73.52. HR-MS: 392.1264 ([*M*+H]$^+$, $C_{21}H_{20}ClN_5O^+$; calc. 392.1273). Anal. calc. for $C_{23}H_{19}F_3ClN_5O_3$ (505.89): C 54.61, H 3.79, N 13.84; found: C 54.56, H 3.81, N 13.86.

*General Procedure for the Synthesis of 2,5,7-Triaryl[1,3]-oxazolo[4,5-*d*]pyrimidines* **10a** *and* **10b**

To a solution of 7-chloro-substituted [1,3]oxazolo[4,5-*d*]pyrimidine **5a** (0.31 g, 1 mmol, 1.00 equiv.) in THF (7 mL) and EtOH (1 mL) were added one of the arylboronic acids **9a**/**9b** (2 mmol, 2.00 equiv.), K_2CO_3 (3 mmol, 3.00 equiv.), followed by $[Pd(IPr)Cl_2]_2$ (0.005 equiv.). The mixture was stirred at 60 °C for 18 h. The precipitate was collected by filtration, washed with water, ethanol, and dried.

2,5,7-Triphenyl[1,3]oxazolo[4,5-*d*]pyrimidine (**10a**). Compound **10a** was prepared as described above in the *General Procedure*, starting from **5a** (0.31 g, 1 mmol, 1.00 equiv.) in THF (7 mL) and EtOH (1 mL), phenylboronic acid **9a** (0.25 g, 2 mmol, 2.00 equiv.), K_2CO_3 (0.42 g, 3 mmol, 3.00 equiv.), and $[Pd(IPr)Cl_2]_2$ (6 mg, 5 μmol, 0.005 equiv.). White solid. Yield: 0.25 g, 70%. M.p. 268.5 °C. IR (KBr): 1613, 1546, 1485, 1448, 1396, 1363, 1216, 1021, 922, 763, 689. ^{1}H-NMR (400 MHz, $CDCl_3$): 8.70 (*dd*, *J*=7.9, 1.7, 2 H, ArH); 8.63 (*d*, *J*=7.0, 2 H, ArH); 8.42 (*d*, *J*=7.1, 2 H, ArH); 7.69–7.56 (*m*, 6 H, ArH); 7.56–7.46 (*m*, 3 H, ArH). ^{13}C-NMR (101 MHz, $CDCl_3$): 168.16; 164.32; 161.53; 146.76; 138.48; 137.78; 133.86; 133.55; 131.74; 130.59; 129.37; 129.18; 129.04; 128.91; 128.68; 128.63; 125.89. HR-MS: 350.1279 ([*M*+H]$^+$, $C_{23}H_{16}N_3O^+$; calc. 350.1288). Anal. calc. for $C_{23}H_{15}N_3O$ (349.40): C 79.07, H 4.33, N 12.03; found: C 79.03, H 4.36, N 11.95.

Methyl 4-(2,5-Diphenyl[1,3]oxazolo[4,5-*d*]pyrimidin-7-yl)benzoate (**10b**). Compound **10b** was prepared as described above in the *General Procedure*, starting from **5a** (0.31 g, 1 mmol, 1.00 equiv.) in THF (7 mL) and EtOH (1 mL), 4-(methoxycarbonyl)phenylboronic acid **9b** (0.36 g, 2 mmol, 2.00 equiv.), K_2CO_3 (0.42 g, 3 mmol, 3.00 equiv.), $[Pd(IPr)Cl_2]_2$ (6 mg, 5 μmol, 0.005 equiv.). White solid. Yield: 0.32 g, 79%. M.p. 272.2 °C. IR (KBr): 1718 (C=O), 1602, 1544 1394, 1358, 1283, 1217, 1115, 1020, 918, 767, 695. ^{1}H-NMR (400 MHz, $CDCl_3$): 8.69–8.62 (*m*, 4 H, ArH); 8.40 (*dd*, *J*=5.3, 3.3, 2 H, ArH); 8.29–8.26 (*m*, 2 H, ArH); 7.70–7.65 (*m*, 1 H, ArH); 7.64–7.57 (*m*, 2 H, ArH); 7.56–7.47 (*m*, 3 H, ArH); 3.98 (*s*, 3 H, MeO_2C). ^{13}C-NMR (101 MHz, $CDCl_3$): 168.45; 166.59; 164.65; 161.67; 145.36; 138.60; 137.83; 137.48; 133.77; 132.64; 130.76; 130.29; 129.43; 128.98; 128.89; 128.67; 125.65; 52.57. HR-MS: 408.1331 ([*M*+H]$^+$, $C_{25}H_{18}N_3O_3^+$; calc. 408.1343). Anal. calc. for $C_{25}H_{17}N_3O_3$ (407.43): C 73.70, H 4.21, N 10.31; found: C 73.65, H 4.20, N 10.35.

***N*-[(7*Z*)-2,5-Diphenyl-7*H*-[1,3]oxazolo[5,4-*d*][1,3]-oxazin-7-ylidene]benzamide** (**12**). Compound **12** was prepared by a literature procedure[13]. A solution of benzoyl bromide **11** (7 mL, 59 mmol, 3.00 equiv.) in anhydrous ether (35 mL), in which was suspended silver cyanide (7.96 g, 59 mmol, 3.00 equiv.), was stirred and refluxed for 21 h. The solids were collected and washed with cold ether. Yellow product was dissolved in hot chloroform and separated from the silver salts. The solvent was removed *in vacuo*. Yield: 6.96 g, 90%. ^{1}H-NMR (400 MHz, (D$_6$)DMSO): 8.14–8.02 (*m*, 6 H, ArH); 7.72–7.54 (*m*, 9 H, ArH). ^{13}C-NMR (100 MHz, (D$_6$)DMSO): 174.70; 160.95; 160.20; 159.53; 145.84; 133.96; 133.48; 133.42; 133.23; 129.51; 129.36; 128.80; 128.69; 128.08; 126.74; 125.28; 117.70.

2,5-Diphenyl[1,3]oxazolo[5,4-*d*]pyrimidin-7(6*H*)-one (**13**). Compound **13** was obtained by a published procedure.[13] Trimer **12** (7.00 g, 18 mmol, 1.00 equiv.) was stirred at r.t. for 16 h in anhydrous methanol (70 mL) containing sodium methoxide (2.16 g, 36 mmol, 2.00 equiv.). The solid was filtered, washed with methanol and dried. The resulting sodium salt

© 2020 Wiley-VHCA AG, Zurich, Switzerland

15222675, 2020, 12, Downloaded from https://onlinelibrary.wiley.com/doi/10.1002/hlca.202000169 by Tallin Technical University, Wiley Online Library on [03/06/2023]. See the Terms and Conditions (https://onlinelibrary.wiley.com/terms-and-conditions) on Wiley Online Library for rules of use; OA articles are governed by the applicable Creative Commons License

was converted into **13** by stirring in 50% aqueous acetic acid (50 mL) at r.t. for 1 h. Yield: 3.18 g, 61%. ^{1}H-NMR (400 MHz, (D_6)DMSO): 13.12 (*s*, 1 H, NH); 8.18–8.11 (*m*, 4 H, ArH); 7.65–7.56 (*m*, 6 H, ArH). ^{13}C-NMR (100 MHz, (D_6)DMSO): 163.90; 158.50; 155.63; 132.07; 131.81; 129.40; 128.83; 128.12; 126.70; 125.98.

7-Chloro-2,5-diphenyl[1,3]oxazolo[5,4-*d*]pyrimidine (**14**). A mixture of compound **13** (4.12 g, 14 mmol, 1.00 equiv.), $POCl_3$ (50 ml), and Me_2NPh (4 mL, 28 mmol, 2.00 equiv.) was refluxed for 3 h. After evaporation of $POCl_3$ excess the solid residue was recrystallized from 1,4-dioxane. Yield: 4.18 g, 97%. M.p. 209–211 °C.[13] ^{1}H-NMR (400 MHz, (D_6)DMSO): 8.43–8.39 (*m*, 2 H, ArH); 8.30–8.28 (*m*, 2 H, ArH); 7.78–7.73 (*m*, 1 H, ArH); 7.71–7.67 (*m*, 2 H, ArH); 7.62–7.56 (*m*, 3 H, ArH). ^{13}C-NMR (100 MHz, (D_6)DMSO): 166.19; 162.99; 159.36; 148.96; 135.29; 133.51; 131.70; 129.63; 129.46; 129.08; 128.11; 128.06; 125.00.

*General Procedure for the Synthesis of 2,5,7-Triaryl-[1,3]-oxazolo[5,4-*d*]pyrimidines* **15a** *and* **15b**

A mixture of 7-chloro-substituted [1,3]oxazolo[5,4-*d*]-pyrimidine **14** (0.31 g, 1 mmol, 1.00 equiv.), arylboronic acid (2 mmol, 2.00 equiv.), K_2CO_3 (3 mmol, 3.00 equiv.), EtOH (6 mL) and $[Pd(IPr)Cl_2]_2$ (5 μmol, 0.005 equiv.) was stirred at 60 °C for 18 h. The precipitate was collected by filtration, washed with water, ethanol, and dried.

2,5,7-Triphenyl[1,3]oxazolo[5,4-*d*]pyrimidine (**15a**). Compound **15a** was prepared as described above in the *General Procedure*, starting from **14** (0.31 g, 1 mmol, 1.00 equiv.), EtOH (6 mL), phenylboronic acid **9a** (0.25 g, 2 mmol, 2.00 equiv.), K_2CO_3 (0.42 g, 3 mmol, 3.00 equiv.), and $[Pd(IPr)Cl_2]_2$ (6 mg, 5 μmol, 0.005 equiv.). White solid. Yield: 0.21 g, 60%. M.p. 288.7 °C. IR (KBr): 1615, 1569, 1450, 1392, 1365, 1271, 1022, 963, 916, 760, 687. ^{1}H-NMR (400 MHz, ($CDCl_3$): 8.96 (*d*, *J* = 6.7, 2 H, ArH); 8.66 (*dd*, *J* = 7.7, 1.8, 2 H, ArH); 8.38 (*dd*, *J* = 7.3, 1.1, 2 H, ArH); 7.65–7.49 (*m*, 9 H, ArH). ^{13}C-NMR (101 MHz, $CDCl_3$): 167.26; 162.52; 160.08; 154.84; 137.47; 135.32; 132.74; 131.60; 130.89; 129.84; 129.24; 128.89; 128.74; 128.65; 128.31; 128.05; 126.22. HR-MS: 350.1279 ($[M+H]^+$, $C_{23}H_{16}N_3O^+$; calc. 350.1288). Anal. calc. for $C_{23}H_{15}N_3O$ (349.40): C 79.07, H 4.33, N 12.03; found: C 79.00, H 4.33, N 11.98.

Methyl 4-(2,5-Diphenyl[1,3]oxazolo[5,4-*d*]pyrimidin-7-yl)benzoate (**15b**). Compound **15b** was prepared as described above in the *General Procedure*, starting from compound **14** (0.31 g, 1 mmol, 1.00 equiv.), EtOH (1 mL), 4-(methoxycarbonyl)phenylboronic acid **9b** (0.36 g, 2 mmol, 2.00 equiv.), K_2CO_3 (0.42 g, 3 mmol, 3.00 equiv.), and $[Pd(IPr)Cl_2]_2$ (6 mg, 5 μmol, 0.005 equiv.) White solid. Yield: 0.27 g, 65%. M.p. 277.5 °C. IR (KBr): 1722 (C=O), 1615, 1538, 1392, 1361, 1278, 1107, 1020, 962, 767, 700. ^{1}H-NMR (400 MHz, ($CDCl_3$): 9.04–9.01 (*m*, 2 H, ArH); 8.66–8.61 (*m*, 2 H, ArH); 8.42–8.33 (*m*, 2 H, ArH); 8.29–8.21 (*m*, 2 H, ArH); 7.68–7.48 (*m*, 6 H, ArH); 3.99 (*s*, 3 H, MeO_2C). ^{13}C-NMR (101 MHz, $CDCl_3$): 167.43; 166.88; 163.03; 160.23; 153.43; 139.33; 137.22; 133.00; 132.41; 131.08; 130.03; 129.69; 129.33; 128.81; 128.67; 128.58; 128.44; 126.01; 52.51. HR-MS: 408.1331 ($[M+H]^+$, $C_{25}H_{18}N_3O_3^+$; calc. 408.1343). Anal. calc. for $C_{25}H_{17}N_3O_3$ (407.43): C 73.70, H 4.21, N 10.31; found: C 73.66, H 4.22, N 10.20.

Acknowledgements

Authors thank *Indrek Reile* for assistance with NMR studies. Support from COST Action CA15106: 'C–H Activation in Organic Synthesis' (CHAOS) is gratefully acknowledged. *Ye. V.* thanks the European Regional Development Fund (Dora Plus Programme) for financial support. *S. P. N.* acknowledges the financial support from the BOF fund (starting and senior grants).

Author Contribution Statement

The project and experiments were designed by *Ye. V.*, *T. S.*, *S. P.*, *Y. K.*, *V. B.*, and *S. P. N.* The experimental work was performed by *Ye. V.*, *D. B.*, and *T. S.*, the biological research was carried out by *I. C.* and *F. R.*, and the computational work was conducted by *I. S.*, *O. K.*, and *N. O.* All authors contributed to the manuscript writing and review process.

References

[1] M. Bauser, G. Delapierre, M. Hauswald, T. Flessner, D. D'Urso, A. Hermann, B. Beyreuther, J. De Vry, P. Spreyer, E. Reissmüller, H. Meier, 'Discovery and optimization of 2-aryl oxazolo-pyrimidines as adenosine kinase inhibitors using liquid phase parallel synthesis', *Bioorg. Med. Chem. Lett.* **2004**, *14*, 1997–2000.

[2] M. Köse, A. C. Schiedel, A. A. Bauer, H. Poschenrieder, J. C. Burbiel, R. R. Akkinepally, H.-D. Stachel, C. E. Müller,

© 2020 Wiley-VHCA AG, Zurich, Switzerland

15222675, 2020, 12, Downloaded from https://onlinelibrary.wiley.com/doi/10.1002/hlca.202000169 by Tallin Technical University, Wiley Online Library on [03/06/2023]. See the Terms and Conditions (https://onlinelibrary.wiley.com/terms-and-conditions) on Wiley Online Library for rules of use; OA articles are governed by the applicable Creative Commons License

'Focused screening to identify new adenosine kinase inhibitors', *Bioorg. Med. Chem.* **2016**, *24*, 5127–5133.
[3] W. Tuo, M. Bollier, N. Leleu-Chavain, L. Lemaire, A. Barczyk, X. Dezitter, F. Klupsch, F. Szczepanski, J. Spencer, P. Chavatte, R. Millet, 'Development of novel oxazolo[5,4-*d*] pyrimidines as competitive CB_2 neutral antagonists based on scaffold hopping', *Eur. J. Med. Chem.* **2018**, *146*, 68–78.
[4] M. J. Myllymäki, H. Käsnänen, A. O. Kataja, M. Lahtela-Kakkonen, S. M. Saario, A. Poso, A. M. P. Koskinen, 'Chiral 3-(4,5-dihydrooxazol-2-yl)phenyl alkylcarbamates as novel FAAH inhibitors: Insight into FAAH enantioselectivity by molecular docking and interaction fields', *Eur. J. Med. Chem.* **2009**, *44*, 4179–4191.
[5] V. Briand, S. Gratzer, T. Huebschle, P. Janiak, D. Kadereit, A. Parkar, B. Poirier, M. Schaefer, P. Wohlfart, '{4-[5-(3-Chlorophenoxy)-oxazolo[5,4-d]pyrimidin-2-yl]-2,6-dimethyl-phenoxy]-acetic acid for use in the prevention or treatment of acute kidney injury', 2015, WO/2015/055694A1.
[6] D. J. Miller, K. Ravikumar, H. Shen, J.-K. Suh, S. M. Kerwin, J. D. Robertus, 'Structure-Based Design and Characterization of Novel Platforms for Ricin and Shiga Toxin Inhibition', *J. Med. Chem.* **2002**, *45*, 90–98.
[7] B. Al-Husein, M. Abdalla, M. Trepte, D. L. DeRemer, P. R. Somanath, 'Antiangiogenic Therapy for Cancer: An Update', *Pharmacotherapy* **2012**, *32*, 1095–1111.
[8] H. F. Dvorak, L. F. Brown, M. Detmar, A. M. Dvorak, 'Vascular permeability factor/vascular endothelial growth factor, microvascular hyperpermeability, and angiogenesis', *Am. J. Pathol.* **1995**, *146*, 1029–1039.
[9] N. Ferrara, H.-P. Gerber, J. LeCouter, 'The biology of VEGF and its receptors', *Nat. Med.* **2003**, *9*, 669–676.
[10] N. Ferrara, K. J. Hillan, H.-P. Gerber, W. Novotny, 'Discovery and development of bevacizumab, an anti-VEGF antibody for treating cancer', *Nat. Rev. Drug Discovery* **2004**, *3*, 391–400.
[11] H. F. Dvorak, 'Vascular Permeability Factor/Vascular Endothelial Growth Factor: A Critical Cytokine in Tumor Angiogenesis and a Potential Target for Diagnosis and Therapy', *J. Clin. Oncol.* **2002**, *20*, 4368–4380.
[12] A. Kaipainen, J. Korhonen, T. Mustonen, V. W. van Hinsbergh, G. H. Fang, D. Dumont, M. Breitman, K. Alitalo, 'Expression of the fms-like tyrosine kinase 4 gene becomes restricted to lymphatic endothelium during development', *Proc. Natl. Acad. Sci. USA* **1995**, *92*, 3566–3570.
[13] L. Sun, C. Liang, S. Shirazian, Y. Zhou, T. Miller, J. Cui, J. Y. Fukuda, J.-Y. Chu, A. Nematalla, X. Wang, H. Chen, A. Sistla, T. C. Luu, F. Tang, J. Wei, C. Tang, 'Discovery of 5-[5-Fluoro-2-oxo-1,2-dihydroindol-(3*Z*)-ylidenemethyl]-2,4-dimethyl-1*H*-pyrrole-3-carboxylic Acid (2-Diethylaminoethyl)amide, a Novel Tyrosine Kinase Inhibitor Targeting Vascular Endothelial and Platelet-Derived Growth Factor Receptor Tyrosine Kinase', *J. Med. Chem.* **2003**, *46*, 1116–1119.
[14] P. A. Renhowe, S. Pecchi, C. M. Shafer, T. D. Machajewski, E. M. Jazan, C. Taylor, W. Antonios-McCrea, C. M. McBride, K. Frazier, M. Wiesmann, G. R. Lapointe, P. H. Feucht, R. L. Warne, C. C. Heise, D. Menezes, K. Aardalen, H. Ye, M. He, V. Le, J. Vora, J. M. Jansen, M. E. Wernette-Hammond, A. L. Harris, 'Design, Structure–Activity Relationships and in Vivo Characterization of 4-Amino-3-benzimidazol-2-ylhydroquinolin-2-ones: A Novel Class of Receptor Tyrosine Kinase Inhibitors', *J. Med. Chem.* **2009**, *52*, 278–292.
[15] Y.-H. Deng, D. Xu, Y.-X. Su, Y.-J. Cheng, Y.-L. Yang, X.-Y. Wang, J. Zhang, Q.-D. You, L.-P. Sun, 'Synthesis and Biological Evaluation of Novel Oxazolo[5,4-*d*]pyrimidines as Potent VEGFR-2 Inhibitors', *Chem. Biodiversity* **2015**, *12*, 528–537.
[16] A. Martin-Kohler, J. Widmer, G. Bold, T. Meyer, U. Séquin, P. Traxler, 'Furo[2,3-*d*]pyrimidines and Oxazolo[5,4-*d*]pyrimidines as Inhibitors of Receptor Tyrosine Kinases (RTK)', *Helv. Chim. Acta* **2004**, *87*, 956–975.
[17] T. Scattolin, E. Bortolamiol, F. Visentin, S. Palazzolo, I. Caligiuri, T. Perin, V. Canzonieri, N. Demitri, F. Rizzolio, A. Togni, 'Palladium(II)-η^3-Allyl Complexes Bearing *N*-Trifluoromethyl *N*-Heterocyclic Carbenes: A New Generation of Anticancer Agents that Testrain the Growth of High-Grade Serous Ovarian Cancer Tumoroids', *Chem. Eur. J.* **2020**, *26*, 11868–11876.
[18] Y. S. Velihina, M. V. Kachaeva, S. G. Pilyo, V. V. Zhirnov, V. S. Brovarets, 'Synthesis, Characterization, and *In Vitro* Anticancer Evaluation of 7-Piperazin-Substituted [1,3]Oxazolo [4,5-D]pyrimidines', *Der Pharm. Chem.* **2018**, *10*, 1–10.
[19] Y. S. Velihina, M. V. Kachaeva, S. G. Pilyo, O. P. Mitiukhin, V. V. Zhirnov, V. S. Brovarets, 'Synthesis, Characterization, and *In Vitro* Anticancer Evaluation of 7-(1,4-Diazepan)-substituted [1,3]oxazolo[4,5-*d*]pyrimidines', *Chem. Res. J.* **2018**, *3*, 81–93.
[20] H. Lal Goel, A. M. Mercurio, 'VEGF targets the tumour cell', *Nat. Rev. Cancer* **2013**, *13*, 871–882.
[21] C. O. Madu, S. Wang, C. O. Madu, Y. Lu, 'Angiogenesis in Breast Cancer Progression, Diagnosis, and Treatment', *J. Cancer* **2020**, *11*, 4474–4494.
[22] M. V. Kachaeva, S. G. Pilyo, V. B. Zhirnov, V. S. Brovarets, 'Synthesis, characterization, and *In Vitro* anticancer evaluation of 2-substituted 5-arylsulfonyl-1,3-oxazole-4-carbonitriles', *Med. Chem. Res.* **2019**, *28*, 71–80.
[23] M. V. Kachaeva, N. V. Obernikhina, E. S. Veligina, M. Y. Zhuravlova, Y. O. Prostota, O. D. Kachkovsky, V. S. Brovarets, 'Estimation of biological affinity of nitrogen-containing conjugated heterocyclic pharmacophores', *Chem. Heterocycl. Compd.* **2019**, *55*, 448–454.
[24] B. S. Drach, G. N. Miskevich, 'Interaction of the Azlactone of α-Benzamide-β,β-dichloroacrylic acid with amines and alcohols', *Russ. J. Org. Chem.* **1974**, *10*, 2315 (Chem. Abstr. **1975**, 82, 72843).
[25] T. K. Vinogradova, G. N. Mis'kevich, B. S. Drach, 'Reaction of functional derivatives of 3,3-dichloro-2-acylaminoacrylic acids with benzamidine', *Russ. J. Org. Chem.* **1980**, *16*, 1869. (Chem. Abstr. **1981**, 94, 84010e).
[26] V. M. Sviripa, A. A. Gakh, V. S. Brovarets, A. V. Gutov, B. S. Drach, 'Original Approach to New Derivatives of [1,3] Oxazolo[4,5-*d*]pyrimidine', *Synthesis* **2006**, 3462.
[27] O. Diebolt, P. Braunstein, S. P. Nolan, C. S. J. Cazin, 'Room-temperature activation of aryl chlorides in Suzuki–Miyaura coupling using a $[Pd(\mu\text{-}Cl)Cl(NHC)]_2$ complex (NHC = *N*-heterocyclic carbene)', *Chem. Commun.* **2008**, 3190–3192.
[28] N. Marion, S. P. Nolan, 'Well-Defined N-Heterocyclic Carbenes–Palladium(II) Precatalysts for Cross-Coupling Reactions', *Acc. Chem. Res.* **2008**, *41*, 1440–1449.
[29] T. Scattolin, S. P. Nolan, 'Synthetic Routes to Late Transition Metal–NHC Complexes', *Trends Chem.* **2020**, *2*, 721–736.
[30] T. Zhou, S. Ma, F. Nahra, A. M. C. Obled, A. Poater, L. Cavallo, C. S. J. Cazin, S. P. Nolan, M. Szostak, '[Pd(NHC)(μ-

 © 2020 Wiley-VHCA AG, Zurich, Switzerland

15222675, 2020, 12, Downloaded from https://onlinelibrary.wiley.com/doi/10.1002/hlca.202000169 by Tallin Technical University, Wiley Online Library on [03/06/2023]. See the Terms and Conditions (https://onlinelibrary.wiley.com/terms-and-conditions) on Wiley Online Library for rules of use; OA articles are governed by the applicable Creative Commons License

Cl)Cl]$_2$: Versatile and Highly Reactive Complexes for Cross-Coupling Reactions that Avoid Formation of Inactive Pd(I) Off-Cycle Products', *iScience* **2020**, *23*, 101377.
[31] H. Dounchis, 'Structure of aroyl isocyanide trimers', *J. Org. Chem.* **1972**, *87*, 2583–2587.
[32] N. Obernikhina, M. Kachaeva, V. Shchodryi, Y. Prostota, O. Kachkovsky, V. Brovarets, Z. Tkachuk, 'Topological Index of Conjugated Heterocyclic Compounds as Their Donor/Acceptor Parameter', *Polycyclic Aromat. Compd.* **2019**, *40*, 1196–1209.
[33] N. Obernikhina, O. Pavlenko, A. Kachkovsky, V. Brovarets, 'Quantum-Chemical and Experimental Estimation of Non-Bonding Level (Fermi Level) and π-Electron Afinity of Conjugated Systems', *Polycyclic Aromat. Compd.* **2020**, https://doi.org/10.1080/10406638.2019.1710855.
[34] Gaussian 03, Revision B.05, M. J. Frisch, G. W. Trucks, H. B. Schlegel, G. E. Scuseria, M. A. Robb, J. R. Cheeseman, J. A. Montgomery Jr., T. Vreven, K. N. Kudin, J. C. Burant, J. M. Millam, S. S. Iyengar, J. Tomasi, V. Barone, B. Mennucci, M. Cossi, G. Scalmani, N. Rega, G. A. Petersson, H. Nakatsuji, M. Hada, M. Ehara, K. Toyota, R. Fukuda, J. Hasegawa, M. Ishida, T. Nakajima, Y. Honda, O. Kitao, H. Nakai, M. Klene, X. Li, J. E. Knox, H. P. Hratchian, J. B. Cross, V. Bakken, C. Adamo, J. Jaramillo, R. Gomperts, R. E. Stratmann, O. Yazyev, A. J. Austin, R. Cammi, C. Pomelli, J. W. Ochterski, P. Y. Ayala, K. Morokuma, G. A. Voth, P. Salvador, J. J. Dannenberg, V. G. Zakrzewski, S. Dapprich, A. D. Daniels, M. C. Strain, O. Farkas, D. K. Malick, A. D. Rabuck, K. Raghavachari, J. B. Foresman, J. V. Ortiz, Q. Cui, A. G. Baboul, S. Clifford, J. Cioslowski, B. B. Stefanov, G. Liu, A. Liashenko, P. Piskorz, I. Komaromi, R. L. Martin, D. J. Fox, T. Keith, M. A. Al-Laham, C. Y. Peng, A. Nanayakkara, M. Challacombe, P. M. W. Gill, B. Johnson, W. Chen, M. W. Wong, C. Gonzalez, and J. A. Pople, Gaussian, Inc., Wallingford CT, 2003.
[35] M. F. Sanner, 'Python: a programming language for software integration and development', *J. Mol. Graphics Modell.* **1999**, *17*, 57–61.
[36] Dassault Systèmes BIOVIA, Discovery Studio Visualizer, v4.0.100.13345, San Diego: Dassault Systèmes, 2020.
[37] M. Sketch 5.3.735, 2017, ChemAxon. http://www.chemaxon.com.
[38] M. D. Hanwell, D. E. Curtis, D. C. Lonie, T. Vandermeersch, E. Zurek, G. R. Hutchison, 'Avogadro: an advanced semantic chemical editor, visualization, and analysis platform', *J. Cheminf.* **2012**, *4*, 17.
[39] O. Trott, A. J. Olson, 'AutoDock Vina: improving the speed and accuracy of docking with a new scoring function, efficient optimization, and multithreading', *J. Comput. Chem.* **2010**, *31*, 455–461.

Received September 2, 2020
Accepted October 9, 2020

 © 2020 Wiley-VHCA AG, Zurich, Switzerland

15222675, 2020, 12, Downloaded from https://onlinelibrary.wiley.com/doi/10.1002/hlca.202000169 by Tallin Technical University, Wiley Online Library on [03/06/2023]. See the Terms and Conditions (https://onlinelibrary.wiley.com/terms-and-conditions) on Wiley Online Library for rules of use; OA articles are governed by the applicable Creative Commons License

Appendix 2

Publication II

Bondar, D.; Kapitanov, I. V.; Pulkrabkova, L.; Soukup, O.; Jun, D.; Botelho, F. D.; França, T. C. C.; Kuča, K.; Karpichev, Y. N-substituted arylhydroxamic acids as acetylcholinesterase reactivators. *Chem.-Biol. Interact.*, **2022**, 110078.

Reprinted from the permission of Elsevier.

Chemico-Biological Interactions 365 (2022) 110078

Contents lists available at ScienceDirect

Chemico-Biological Interactions

journal homepage: www.elsevier.com/locate/chembioint

Research paper

N-substituted arylhydroxamic acids as acetylcholinesterase reactivators

Denys Bondar [a], Illia V. Kapitanov [a,1], Lenka Pulkrabkova [b], Ondřej Soukup [b,c], Daniel Jun [c], Fernanda D. Botelho [d], Tanos C.C. França [d,e], Kamil Kuča [e], Yevgen Karpichev [a,*]

[a] Department of Chemistry and Biotechnology, Tallinn University of Technology, Akadeemia Tee 15, 12618, Tallinn, Estonia
[b] Biomedical Research Center, University Hospital Hradec Kralove, Sokolska 581, 500 05, Hradec Kralove, Czech Republic
[c] Department of Toxicology and Military Pharmacy, Faculty of Military Health Sciences, University of Defense, Trebesska 1575, 500 01, Hradec Kralove, Czech Republic
[d] Laboratory of Molecular Modeling Applied to the Chemical and Biological Defense (LMCBD), Military Institute of Engineering, Rio de Janeiro, RJ, Brazil
[e] Department of Chemistry, Faculty of Science, University of Hradec Kralove, Rokitanskeho 62, 500 03 Hradec Kralove, Czech Republic

ARTICLE INFO

Keywords:
Hydroxamic acids
Organophosphorus toxicants
Acetylcholine esterase
BBB permeability
Reactivation capacity
Molecular docking

ABSTRACT

The problem of the efficient treatment of acute organophosphorus (OP) poisoning needs more efforts in the development of a versatile antidote, applicable for treatment of the injuries of both peripheral and central nervous systems. A series of *N*–H, *N*-methyl, *N*-butyl, and *N*-phenyl derivatives of benzhydroxamic (**1a-1d**), 3-methoxybenzhydroxamic (**2a-2d**), 4-methoxybenzhydroxamic (**3a-3d**) acids, and corresponding salycilhydroxamates (**4a-4d**) was prepared. Their predicted hydrophobicity (log *P*) was evaluated as regards to BBB score by the open access cheminformatics tools; prediction of the passive transport across the BBB was found by means on the parallel artificial membrane permeability assay (PAMPA). The data on reactivation capacity of human acetylcholinesterase (*Hss*AChE) inhibited by GB, VX, and paraoxon was supported by molecular docking study on binding to the active site of the AChE, viability study against mammalian cells (Chinese hamster ovary CHO–K1), and biodegradability (Closed Bottle test OECD 301D). Among the studied compounds, *N*-butyl derivatives have better balanced combination of properties; among them, *N*-butylsalicylhydroxamic acid is most promising. The studied compounds demonstrate modest reactivation capacity; change of *N*–H by *N*–Me ensures the reactivation capacity in studied concentrations on all studied OP substrates; among *N*-butyl derivatives, the *N*-butylsalicylhydroxamic acid demonstrates most promising results within the series. The found regularities may lead to selection of perspective structures to complement current formulations for medical countermeasures against poisoning by organophosphorus toxicants.

1. Introduction

In the last years, the threat of using chemical warfare agents (CWA) dramatically increased [1–4]. The widely published numerous incidents with CWA in Syria in 2013 and 2017 [5] and use of the CWA for political poisoning and assassination highlighted this risk [6]. The most remarkable acts of using CWA in the terrorist attacks and assassination attempt incidents include organophosphorus (OP) nerve agents: GB (Sarin) [7], VX [8], or, more recently Novichok [9,10] agents, see Fig. 1. At the same time, poisoning caused by the commonly used organophosphorus pesticides (Fig. 1), leads to numerous lethal cases among agricultural workers [11].

The nerve agents, e.g. phosphonofluoridates (G-type agents) or VX-type CWA, as well as OP pesticides (Fig. 1) are the cholinesterase inhibitors. Blocking of acetylcholinesterase (AChE) catalytic activity is considered as the main mechanism for nerve agents' toxicity and occurs via nucleophilic attack of the *Ser* hydroxyl group of the serine at active site of AChE at phosphorus atom. It causes overstimulation of cholinergic nervous system, resulting in ataxia, muscle spasms, nervous overstimulation, and breath arrest [1].

Prompt and efficient treatment of victim exposure raises the chance of survival and increases the quality of posttreatment life. In the case of irreversibly OP-inhibited AChE, the only available way of reactivation includes administration of quaternary oxime antidotes, see Fig. 1 [1–3]. The overall medical countermeasures against poisoning by OPs generally involve carbamates (pyridostigmine) for pretreatment, oximes-based AChE reactivators, anticholinergic (atropine) and neuroprotective (benzodiazepines) drugs for post-exposure treatment [12].

* Corresponding author.
E-mail address: yevgen.karpichev@taltech.ee (Y. Karpichev).
[1] Current address: Gemini PharmChem Mannheim GmbH, 68305 Mannheim, Germany.

https://doi.org/10.1016/j.cbi.2022.110078
Received 26 June 2022; Received in revised form 23 July 2022; Accepted 26 July 2022
Available online 5 August 2022
0009-2797/© 2022 Elsevier B.V. All rights reserved.

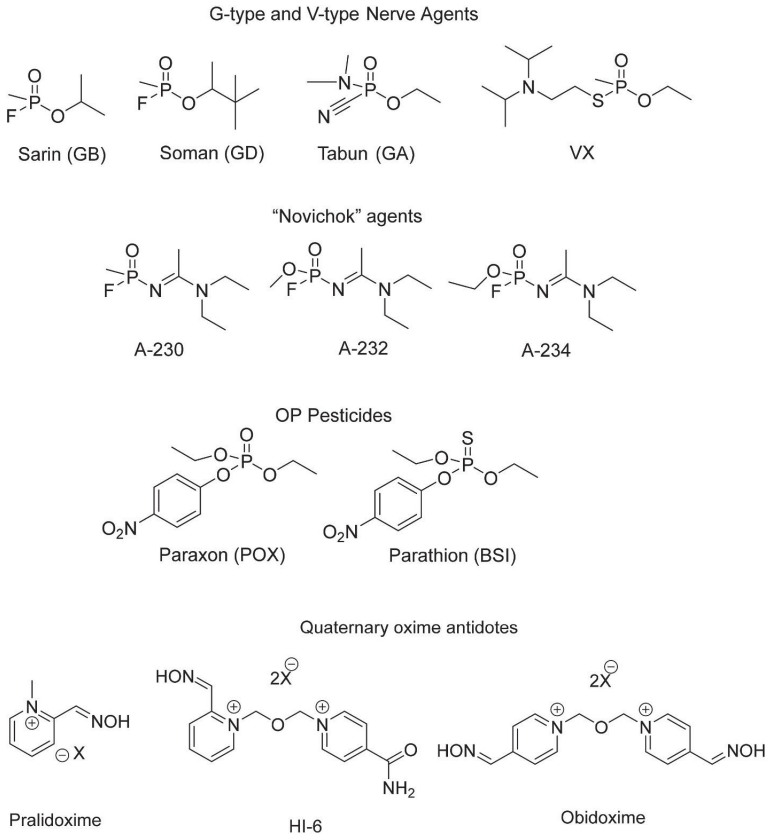

Fig. 1. Structures of typical OP toxicants and examples of quaternary oxime antidotes.

Such drug combination ensures a protection of peripheral nervous system and counteract acute effects of the lethal doses of the toxicants. At the same time, the neuroprotectants do not protect the central nervous system with the risk to have brain damage becoming irreversible. Among new therapeutic approaches for pre- and post-exposure treatments are means of detoxification of OP molecules before they reach their molecular targets e.g. catalytic (bio)scavengers designed for crossing the blood–brain barrier and reactivate OP-inhibited AChE in the CNS [1,13]. Therefore, the problem of the efficient treatment of acute OP poisoning needs further efforts in the development of a versatile antidote, applicable for treatment of the injuries of both peripheral and central nervous systems and capable to restore the activity of AChE inhibited by hardly reactivated compounds like tabun and Novichoks [14].

After more than 80 years passed since the discovery of the first nerve agent Tabun (GA) [1,3], the problem of designing an antidote able to prevent brain injury is not solved. Under these circumstances, the development of antidotes-reactivators of the OP-inhibited AChE with high reactivation capacity and ability to penetrate the blood-brain barrier (BBB) to central nervous system (CNS) is the major concern. Taking into account rising threat of the terrorist attacks against the civilians and further proliferation of CWAs by the rogue states, the pursuit of new antidotes must be intensified to prevent and limit possible damage [4].

Quaternary pyridinium oxime antidotes currently used for OP poisoning treatment [15] show insufficient capacity of coming across the BBB, and this disadvantage affects their ability to restore AChE activity in brain system [16]. Non-quaternary oximes can be a promising alternative to better penetrate through BBB into the CNS but, despite numerous attempts to develop uncharged reactivators, this problem is far from being solved [17–19].

Along with oximes, hydroxamic acids were among the first candidates used for AChE reactivation [20] and they have high potential for a broad range of the pharmaceutical applications [21,22]. Unlike non-quaternary oximes, hydroxamic moiety exhibits lower basicity (pK_a) and can be easily deprotonated into alpha nucleophilic (hydroxamate) species under the physiologically relevant conditions [23–25]. The relatively low reactivity of hydroxamates, compared with oximes, can be explained by lower electronic density at the nucleophilic center and low acidity [23]. The quaternary oximes have higher pK_a and nucleophilicity, exhibiting higher reactivation capacity over hydroxamic acids, however due to charged quaternary nitrogen they do not penetrate effectively through BBB. The quaternary pyridinium oximes with basicity (pK_a), comparable to the hydroxamic acids have higher nucleophilic reactivity towards electrophilic center [26] since the Brønsted slopes for the reaction of oximes with $pK_a < 9$ towards electrophilic centers are remarkably higher than those for hydroxamic acids. Non-charged (tertiary) oximes have the highest nucleophilic reactivity (due to levelling off the Brønsted relationship, the nucleophilicity of the oximes with $pK_a > 9$ changes insufficiently following the β value for corresponding substrate [26,27]). At the same time, they undergo deprotonation to form oximate ion at high pH, hardly accessible at moderately basic pH, which this makes them less effective nucleophilic reagent under physiological conditions.

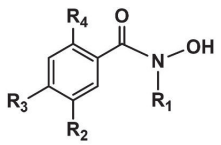

1a-1d: R_2=R_3=R_4=H; R_1=H (**1a**), Me (**1b**), Bu (**1c**), Ph (**1d**)

2a-2d: R_2=OMe;R_3=R_4=H; R_1= H (**2a**), Me (**2b**), Bu (**2c**), Ph(**2d**)

3a-3d: R_3=OMe;R_2=R_4=H; R_1= H (**3a**), Me (**3b**), Bu (**3c**), Ph (**3d**)

4a-4d: R_4=OH; R_2=R_3=H; R_1= H (**4a**), Me (**4b**), Bu (**4c**), Ph (**4d**)

Fig. 2. Arylhydroxamic acids (**1a-1d) – (4a-4d)** studied in the present work.

The action of highly active scavengers on the basis of oximes or hydroxamic acids will more likely be stoichiometric than catalytic [28]. An obstacle for a wider application of unsubstituted hydroxamic acid is their ability to undergo Lossen rearrangement to convert activated O-phosphorylated intermediates into the corresponding product (isocyanate, in essence), known as a "suicide" nucleophilic attack [29]. Meanwhile, the Lossen rearrangement could be prevented by introduction of a substituents at nitrogen atom of the hydroxamic moiety, resulting in a possibility of a catalytic mechanism with regeneration of the *N*-substituted hydroxamic acid, leading to a design of antidotes based on hydroxamic scaffold [30–32]. In addition, variation of the substituent at nitrogen atom could allow us to control physicochemical properties (in essence, hydrophilicity) of hydroxamic antidotes, and, as a result, to modulate permeability across the BBB to enter the CNS. Different substituents also should differently effect reactivation capacity and basicity of the resulting antidote. This approach allows us to explore a scope of different building blocks and achieve desired efficacy of the reactivator.

In this study, we aimed to prepare a series of the substituted benzhydroxamic acids with improved properties based on comprehensive structure analysis and evaluate experimentally reactivation capacity of OP-inhibited AChE for selected compounds. We focused on four series of the aryl hydroxamic acids (Fig. 2): (1) benzhydroxamic acids **1a-1d** as a standard series with no substituent in the aromatic ring; (2) 3-methoxy benzhydroxamic acids **2a-2d**, a series where electron-donating group is not conjugated with nucleophilic moiety; (3) 4-methoxybenzhydroxamic acids **3a-3d**, a series where electron-donating group is conjugated with nucleophilic moiety and (4) salicylhydroxamic acids **4a-4d**, where hydroxyl group in *ortho* position is involved in the intramolecular H-bonding, which favors nucleophilic attack. Choice of methoxy group as a substituent is caused by their effect on π-electronic system at nucleophilic center. Variation of the substituent at nitrogen atom (H → Me → n-Bu → Ph) allows us to evaluate effect of hydrophobicity on BBB score. The present study includes evaluation of AChE reactivation capacity, cell viability, biodegradation tests for selected compounds, and molecular docking study.

The found regularities are to use in the further improvement of the structures of perspective antidotes.

2. Materials and methods

2.1. Materials

All commercial chemicals and solvents were purchased from Sigma Aldrich, Alfa Aesar, or TCI Europe and used without further purification. Deionized water from a Milli-Q system was used in all sample preparation. Silica gel 60 F254 plates were used for TLC. Pralidoxime chloride was prepared at Department of Toxicology and Military Pharmacy, Faculty of Military Health Sciences, University of Defence (Hradec Kralove, Czech Republic). Phenomenex octadecylsilane-bonded silica gel SPE column was purchased from Chromservis s.r.o. (Prague, Czech Republic). Sarin (isopropyl methylphosphonofluoridate) and VX (*O*-ethyl *S*-diisopropylaminomethyl methylphosphonothiolate) were obtained from Military Technical Institute in Brno (Brno, Czech Republic) and its purity was higher than 95%. Paraoxon (diethyl 4-nitrophenyl phosphate) of analytical purity was purchased from Sigma-Aldrich.

2.2. Synthesis and characterization of products

The hydroxamic acids reported in this work have been prepared according to Scheme 1. The synthetic procedures, R_f, yields, m.p., HRMS data, ^{1}H and ^{13}C NMR spectra of the obtained products are collected in ESI. Melting points were determined with Stuart SMP40 apparatus with parameters for the melting point analysis set at 2 °C per minute ramp; values are expressed in °C. The HRMS identification of compounds was performed on an Agilent 6540 UHD Accurate-Mass Q-TOF LC/MS

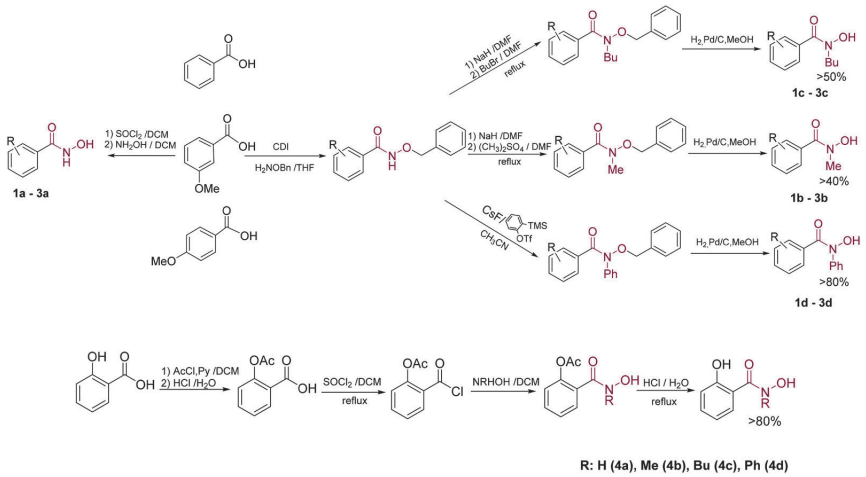

Scheme 1. General routes of the preparation of benzhydroxamic (**1a-1d**), 3-methoxybenzhydroxamic (**2a-2d**), 4-methoxybenzohydroxamic acids (**3a-3d)** (top), and salicylhydroxamic acids (**4a-4d)** (bottom).

G6540A Mass Spectrometer. Bruker Avance III 400 MHz spectrometer operating at 400 MHz for ^{1}H NMR and 101 MHz for ^{13}C NMR. Samples were run in deuterated chloroform ($CDCl_3$) or deuterated dimethyl sulfoxide (DMSO-d_6) where appropriate. All chemical shifts δ are reported in parts per million (ppm) are relative to the internal standard TMS and coupling constants (J) are measured in Hertz (Hz).

2.3. Methods

2.3.1. Evaluation of hydrophobicity and BBB penetration ability

The predicted $P_{o/w}$ values was calculated by means of the open access cheminformatics tools: www.chemicalize.com [33], Molinspiration Cheminformatics free web services, Slovensky Grob, Slovakia (www.molinspiration.com), and www.vcclab.org [34]. The BBB score values were calculated by using Blood-Brain Barrier Predictor (www.cbligand.org), version 0.9; this predictor was built by applying the support vector machine (SVM) and LiCABEDS algorithms [35].

The experimental prediction of the passive transport of the studied compounds across the BBB was carried out using the parallel artificial membrane permeability assay (PAMPA) [36]. In this high-throughput screening tool, a non-cell-based in vitro assay carried out in a coated 96-well membrane filter. The filter membrane of the donor plate was coated with PBL (Polar Brain Lipid, Avanti, USA) in dodecane (4 μl of 20 mg/mL PBL in dodecane) and the acceptor well was filled with 300 μl of PBS (pH 7.4; VA). The tested compounds were dissolved first in DMSO and subsequently diluted with PBS (pH 7.4) to final concentrations of 100 μM in the donor wells. Concentration of DMSO did not exceed 0.5% (v/v) in the donor solution. The final concentration of DMSO did not exceed 0.5% (v/v) in the donor solution. About 300 μL of the donor solution was added to the donor wells (VD) and the donor filter plate was carefully put on the acceptor plate so that coated membrane was "in touch" with both donor solution and acceptor buffer. In principle, test compound diffused from the donor well through the lipid membrane (Area = 0.28 cm^2) to the acceptor well.

The concentration of the drug in both donor and the acceptor wells were assessed after 3, 4, 5, and 6 h of incubation in quadruplicate using the UV plate reader Spark (Tecan Group Ltd, Switzerland) at the maximum absorption wavelength of each compound.

Besides that, solution of theoretical compound concentration, simulating the equilibrium state established if the membrane were ideally permeable was prepared and assessed as well. Concentration of the compounds in the donor and acceptor well and equilibrium concentration were calculated from the standard curve and expressed as the permeability (Pe) according to the equation:

$$\log Pe = \log\left\{ C \times -\ln\left(1 - \frac{[compound]_{acceptor}}{[compound]_{equilibrium}}\right)\right\} \quad (1)$$

where. $C = \left(\frac{V_D \times V_A}{(V_D + V_A) \times Area \times Time}\right)$

2.3.2. Aerobic biodegradation testing using CBT

Effluent from wastewater treatment plant was collected from a municipal wastewater treatment plant in Tallinn, Estonia (Paljassaare wastewater treatment plant, 59°27′55.5"N 24°42′08.8"E). Aerobic biodegradation testing was done using modified closed bottle test (CBT) (OECD 301D) [37]. CBT setup with modification where biological oxygen consumption is measured with an optode oxygen sensor system using PTFE-lined PSt3 oxygen sensor spots (Fibox 3 PreSens, Regensburg, Germany) allows measuring BOD without opening the flasks and thereby reducing the number of parallels needed for each compound and increasing test throughput. It has also shown to improve reproducibility compared to the original OECD 301D guideline [38]. The CBT experiment was carried out according to the protocol published previously [37,39].

2.3.3. In vitro cell viability assessment

Standard MTT assay (Sigma Aldrich) was used according to the manufacturer's protocol on the CHO–K1 (Chinese hamster ovary, ECACC, Salisbury, UK) in order to compare the effect of different compound within the series. The cells were cultured according to ECACC recommended conditions and seeded in a density of 8 000 per well as described previously [40–42]. Briefly, tested compounds were dissolved in the growth medium (F-12). Cells were exposed to a tested compound for 24 h. Then the medium was replaced by a medium containing 10 μM of MTT and cells were allowed to produce formazan for another approximately 3 h under surveillance. Thereafter, medium with MTT was sucked out and crystals of formazan were dissolved in DMSO (100 μL). Cell viability was assessed spectrophotometrically by the amount of formazan produced. Absorbance was measured at 570 nm with 650 nm reference wavelength on Synergy HT (BioTek, USA). IC_{50} was then calculated from the control - subtracted triplicates using non-linear regression (four parameters) of GraphPad Prism 5 software. Final IC_{50} and SEM value was obtained as a mean of 2 independent measurements.

2.3.4. Reactivation assay

Reactivation potency of new oximes and standard reactivator 2-PAM was evaluated on human recombinant AChE. Enzyme was inhibited by the solution of appropriate cholinesterase inhibitor – Sarin (GB), VX and paraoxon in propan-2-ol at concentration 0.01 mM for 60 min. Excess of inhibitor was subsequently removed using octadecylsilane-bonded silica gel SPE cartridge. Inhibited enzyme was incubated for 10 min with solution of reactivator in concentrations 0.1 mM and 0.01 mM at 37 °C. The reaction was started by addition of substrate acetylthiocholine. Activity of AChE was then measured spectrophotometrically at 412 nm by the modified method according of Ellman et al. [43] reported in our previous papers [44,45].

Each concentration of reactivator was assayed in triplicate. The obtained data were used to compute reactivation potency (R; Equation (2)). Results were corrected for oximolysis and inhibition of AChE by reactivator.

$$R = \left(1 - \frac{\Delta A0 - \Delta Ar}{\Delta A0 - \Delta Ai}\right) \times 100\ [\%] \quad (2)$$

ΔA_0 indicates absorbance change caused by intact AChE (phosphate buffer was used instead of AChE inhibitor solution), ΔA_i indicates absorbance change provided by cholinesterase exposed inhibitors and ΔA_r indicates absorbance change caused by AChE incubated with solution of reactivator.

2.3.5. Molecular docking study

The molecular docking was performed based on the procedures published [46,47].

Construction of Ligands. Before construction of the tridimensional structures each molecule was submitted to the server Chemicalize (www.chemicalize.org) in order to investigate their protonation states at pH = 7.4 [33]. After that, the tridimensional structures of the two most abundant species at pH = 7.4 for each molecule were built using the software PC Spartan Pro® [48]. The structures were optimized by the AM1 (*Austin Model 1*) semi-empirical method [49] and the atomic charges were calculated.

Docking energy calculations. After charges calculations, the docking energies of the ligands bound to *Hss*AChE complexed with Sarin, VX and Paraoxon were obtained using the software Molegro Virtual Docker (MVD)® [50]. Due to the stochastic nature of the docking algorithm, 10 runs were performed for each compound in each protein and 30 poses (conformation and orientation of the ligand) were returned so the proximity between the P atom of the nerve agent and the ligand nucleophile atom could be analyzed. The best pose of each compound was selected according to this distance (d_{NP}); the angle between the nucleophile, the P atom and the O atom of Ser203 (θ_{NPO}); the energy

interaction between the ligand and the protein (E_{inter}); and the hydrogen bonds (H-bond) between the ligand and close residues. It was also analyzed if the protonation state of each compound made any difference in the general interaction between the compound and the proteins.

Human acetylcholinesterase (HssAChE) inhibited by Sarin (GB). The model of *Hss*AChE inhibited by GB (*Hss*AChE-GB) used in this work was constructed from the crystallographic structure of AChE from *Mus Musculus* (*Mm*AChE) inhibited by GB, available in RSCB PDB Protein Data Bank (http://www.rcsb.org/pdb/home/home.do) under the code 2Y2V. The primary structures of the enzymes *Mm*AChE and *Hss*AChE were aligned using the BLAST tool from UniProt Data Bank (www.uniprot.org). As these two enzymes present 93% of identity, with 100% of identity in the active sites, the mismatching residues were mutated in order to obtain *Hss*AChE-GB. This model was validated using the server PDBSum (www.ebi.ac.uk/pdbsum), where the Ramachandran plot and also the topology analysis for the protein were obtained. The binding site for the docking studies was restricted into a sphere with a radius of 13 Å, coordinates X = 30.15; Y = 20.98; Z = 12.20, and the residues 6 Å closest to the OP were considered flexible.

HssAChE inhibited by VX (HssAChE-VX). The model of *Hss*AChE-VX was constructed from the crystallographic structure of *Hss*AChE inhibited by VX available in RSCB PDB Protein Data Bank (http://www.rcsb.org/pdb/home/home.do) under the code 6CQZ. The software BIOVIA Discovery Studio (Dessault Systèmes, Discovery Studio Visualizer, v. 4.5.0, 2005) was used to fix the structure of VX and also to make the bond with Ser203 and optimize the receptor with CHARMM force field. This model was validated using the server PDBSum (www.ebi.ac.uk/pdbsum/), where Ramachandran plot and topology analysis for the protein were obtained. The binding site for docking studies was restricted into a sphere with a radius of 10 Å, coordinates X = 56.01; Y = −15.67; Z = 346.95, and the residues 6 Å closest to the OP were considered flexible.

HssAChE inhibited by Paraoxon (PON) (HssAChE-PON). The model of *Hss*AChE-PON was constructed from the crystallographic structure of *Hss*AChE inhibited by PON and complexed with HI-6 available in RSCB PDB Protein Data Bank (www.rcsb.org/pdb/home/home.do) under the code 5HF9. The software BIOVIA Discovery Studio (Dessault Systèmes, Discovery Studio Visualizer, v. 4.5.0, 2005) was used to fix the structure of PON and also to make the bond with Ser203 and optimize the receptor with CHARMM force field. This model was validated using the server PDBSum (www.ebi.ac.uk/pdbsum/), where the Ramachandran plot and also the topology analysis for the protein were obtained. The binding site for the dockings was restricted into a sphere with a radius of 13 Å, coordinates X = −8.99; Y = −42.17; Z = 26.46, and the residues 6 Å closest to the OP were considered flexible.

3. Results and discussion

3.1. Hydrophobicity and BBB permeability: regularities and choice of target molecules for screening

In order to select the most promising structures with ability to successfully cross the BBB, the recognized online tools were used to performed screening of series **1–4** of aryl hydroxamic acids, evaluated correlation BBB score on hydrophobicity with variation of the substituents from methyl (Me) to hexadecyl (Cet) chain length. Unsubstituted hydroxamic acids, as well as *N*-phenyl derivative of aryl hydroxamic acid (as substrate with bulky and hydrophobic ligand), were also analyzed, see Figs. S1–S12 and Tables S1–S4.

The analysis of the predicted properties of the synthesized compounds is collected in ESI (Figs. S1–S12, Tables S1–S4). The chain extension leads to a better interaction with the membrane resulted in the leveling-off the efficiency the higher homologues of therapeutic substances [51]. It was reported for a series of pyridinium oxime antidotes that elongation of the alkyl chain does not result in increased reactivation capacity and, in some cases, resulted in lower efficacy [14],

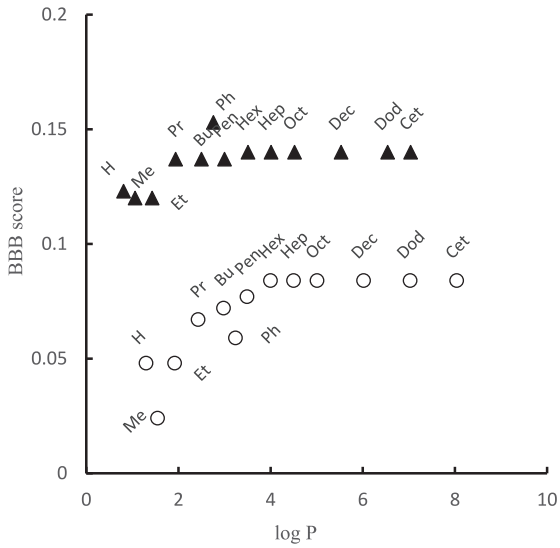

Fig. 3. Correlation of calculated parameters BBB score (by www.cbligand.org) *vs* partitioning coefficient octanol - water log *P* (by www.molinspiration.com) for the series of *N*-substituted benzyl hydroxamic acids (▲) and salycilhydroxamic acids (○).

while experimental data proves decreased permeability across the BBB [52]. This "cut-off" effect is a phenomenon observed when a weaker efficiency or an inefficiency is observed on the higher homologues of therapeutic substances. It may be assigned to a low water solubility,

Table 1
Partitioning coefficients octanol/water (log $P_{o/w}$), lypophilicity (log *D*), and BBB score for studied hydroxamic acids (**1a-1d) – (4a-4d)**.

Entry #	log $P_{o/w}$ [a]	logD[b]	BBB score[c]
1a	0.81 (MI); 0.82 (Ch); 0.17 (VCC); 0.26 [54]	0.81	0.123
1b	1.06 (MI); 1.044 (Ch); 0.57 (VCC); 1.148 [54]	1.03	0.120
1c	2.50 (MI); 2.34 (Ch); 1.79 (VCC)	2.35	0.137
1d	2.76(MI); 2.70 (Ch); 1.78 (VCC)	2.67; 0.0998 [55]	0.153
2a	0.85 (MI); 0.663 (Ch); 0.35 (VCC)	0.62	0.047
2b	1.09 (MI); 0.887 (Ch); 0.89(VCC)	0.88	0.061
2c	2.53 (MI); 2.21 (Ch); 1.93 (VCC)	2.19	0.110
2d	2.79 (MI); 2.55 (Ch); 1.87 (VCC)	2.50	0.092
3a	0.87 (MI); 0.668 (Ch); 0.36 (VCC); 1.205 [54]	0.66	0.047
3b	1.11 (MI); 0.887 (Ch); 0.91 (VCC)	0.88	0.061
3c	2.55 (MI); 2.21 (Ch); 1.95 (VCC)	2.20	0.110
3d	2.81 (MI); 2.55 (Ch); 1.89 (VCC)	2.51	0.092
4a	1.30 (MI); 1.167 (Ch); 0.21 (VCC); 0.689 [54]	1.06	0.048
4b	1.55 (MI); 1.39 (Ch); 0.69 (VCC)-	1.28	0.024
4c	2.98 (MI); 2.715 (Ch); 1.87 (VCC)	2.60	0.072
4d	3.24 (MI); 2.40 (Ch); 2.03 (VCC); 2.428 [54]	2.20	0.059

Note.
[a] Calculated using https://chemicalize.com/(Ch), https://www.molinspiration.com (MI), or http://www.vcclab.org/(VCC) [34].
[b] (Ch) - calculated using https://chemicalize.com/.
[c] Calculated using Blood-Brain Barrier Predictor (www.cbligand.org), version 0.9; this predictor was built by applying the support vector machine (SVM) and LiCABEDS algorithms [35].

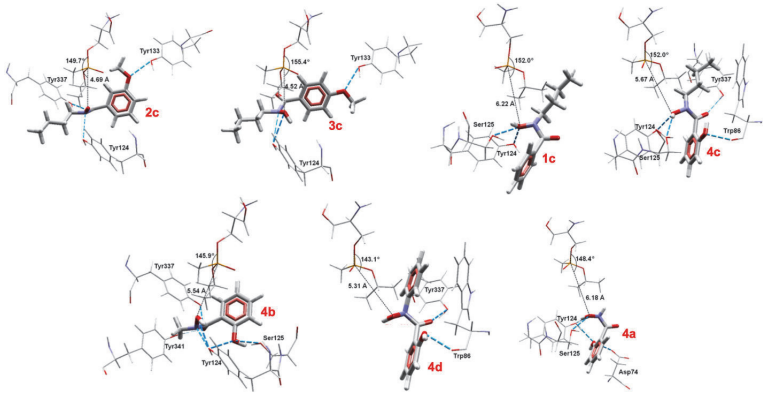

Fig. 4. Best docking poses of studied *N*-butylbenzhydroxamic acids **1c, 2c**, and **3c** and salicylhydroxamic acids **4a-4d** inside *Hss*AChE-GB.

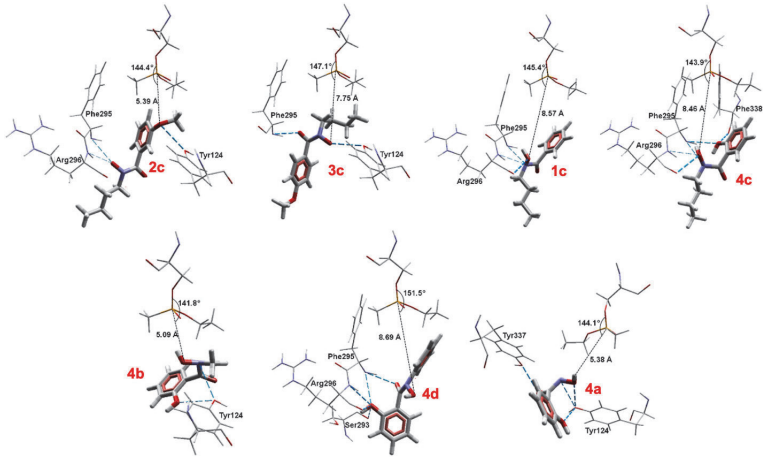

Fig. 5. Best docking poses studied *N*-butylbenzhydroxamic acids **1c, 2c,** and **3c** and salicylhydroxamic acids **4a - 4d** inside *Hss*AChE-VX.

aggregate formation, interaction with a cell membrane, etc. Among the criteria of selection of the most prospective structures there is a requirement to follow the balance of properties (hydrophobicity, BBB score, toxicity, biodegradability, reactivation capacity).

Extension of the chain length of *N*-substituted hydroxamic acids leads to decreasing the solubility in water. Alkyl substituents starting from hexyl and longer are too hydrophobic and could be deposited in the BBB instead transporting it across the barrier. As it was reported by Bunton et al. [53], the *N*-lauryl hydroxamic acid was studied in the comicelles only, to ensure its solubilization by the co-surfactant. The analysis based on the prediction tools shows that butyl chain length would be optimal, since it reveals more remarkable hydrophobic properties compared to unsubstituted analogs and *N*-methyl derivatives, but do not reach the "plateau" in the graph BBB score *vs* log P (Fig. 3 and S1–S12). The *N*-phenyl derivative deviates from the regularities for *N*-alkyl derivatives, which may relate to participation in π-π stacking. It is expected that there are *N*-butyl hydroxamic acids to be the candidates to restore the inhibited AChE exhibiting the advantages in permeability across the BBB and inability to undergo the Lossen rearrangement.

For further study the following structures were selected (i) unsubstituted (*N*–H) hydroxamic acids (undergo Lossen rearrangement), (ii) *N*-methyl derivatives (similar hydrophobicity to the *N*–H hydroxamic acid but methyl group at nitrogen atom prevents undergoing Lossen rearrangement); (iii) *N*-butyl hydroxamic acids as those having highest hydrophobicity before reaching leveling-off on the BBB score *vs* log *P* dependences (Fig. 3 and Figs. S1–S12), and (iv) aryl hydroxamic acids with phenyl group at nitrogen atom, a bulky substituent that have similar hydrophobicity to the *N*-butyl derivatives but may be additionally involved in the π-π stacking interaction. Predicted properties of the selected compounds are shown in Table 1 (see also Figs. 4-6).

It should be noted that the hydrophobicity between pairs "*N*–H – *N*-methyl hydroxamic acids" and "*N*-butyl – *N*-phenyl hydroxamic acids" changes for about one order of magnitude or more, which can clearly indicate an effect of the hydrophobicity on other evaluated properties.

The predicted tendency was supported by the experimental evaluation of the passive transport prediction across the BBB carried out by means of PAMPA assay, carried out for the *N*-butyl derivatives (**1c, 2c**, **3c**, **4c**) and the series of salycilhydroxamic acids (**4a** - **4d**) with variable substituent at nitrogen atom. The results collected at Table 2 demonstrate that all selected compounds have high predicted BBB permeation. The data confirm above-mentioned conclusion that *N*-butyl derivatives possess high BBB permeability (Table 2). The experimental values of *Pe* are shown to follow the order **3c** < **1c** < **2c** < **4c**, demonstrating the salicylhydroxamic derivative to be the most prospective *N*-butyl hydroxamic acid to cross the BBB. In the series of salicylhydroxamic acid studied, the *N*–H and *N*-methyl derivatives do not show considerable

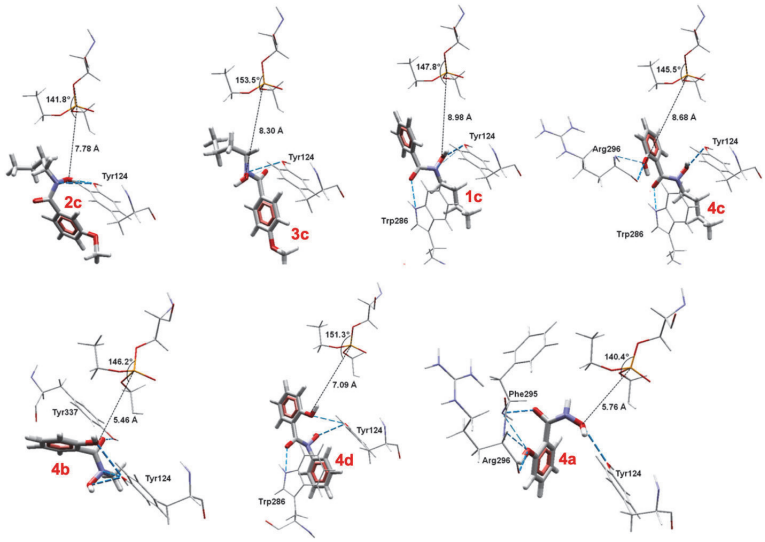

Fig. 6. Best docking poses of studied *N*-butylbenzhydroxamic acids **1c, 2c,** and **3c** and salicylhydroxamic acids **4a-4d** inside *Hss*AChE-PON.

Table 2
Prediction of BBB penetration of studied compounds expressed as *Pe* ± SEM.

Compound	*Pe* ± SEM ($\times 10^{-6}$ cm s^{-1})	n	CNS (+/-)	Tendency
4a	5.64 ± 0.87	3	CNS (+)	
4b	5.58 ± 0.81	3	CNS (+)	
4d	12.63 ± 1.71	2	CNS (+)	
4c	**29.03 ± 0.95**	2	**CNS (+)**	
2c	23.75 ± 1.38	2	CNS (+)	
1c	11.69 ± 2.15	2	CNS (+)	
3c	7.06 ± 2.94	2	CNS (+)	

Notes: n = number of measurements;
CNS + (high BBB permeation predicted): *Pe* ($\times 10^{-6}$ cm s^{-1}) > 4.0
CNS - (low BBB permeation predicted): *Pe* ($\times 10^{-6}$ cm s^{-1}) < 2.0
CNS +/- (BBB permeation uncertain): *Pe* ($\times 10^{-6}$ cm s^{-1}) from 4.0 to 2.0

difference in the *Pe* values, whereas *N*-phenyl salicylhydroxamic acid reveals more than double advantage in the *Pe* values, yielding only the *N*-butyl derivative: **4a** ≈ **4b** < **4d** < **4c** (Table 2). The salicylhydroxamic acid **4c** is the most promising compound in terms of the BBB permeability in the series of both *N*-substituted salicylhydroxamic acids and *N*-butyl derivatives studied in the present work.

3.2. Molecular docking

3.2.1. Selections of structures for docking studies

Since the *N*-butyl hydroxamic acids are considered as the compounds with best optimized hydrophobicity, the structures **1c, 2c, 3c** and **4c** were selected for molecular docking calculations. To study change of properties in series H → Me → n-Bu → Ph substituted salicylhydroxamic acids (**4a-4d**) were selected as promising examples, where intramolecular catalysis by *ortho*-hydroxyl group close to the reactive center could be expected.

The *N*-butylbenzhydroxamic acids **1c**, **2c**, **3c** and salicylhydroxamic acids **4a-4d** have been submitted to the Chemicalize server (www.chemicalize.com) to verify their protonation states at pH = 7.4. It was verified that the predominant species for all molecules were the neutral ones, and the second most abundant species were single charged anions due to deprotonation of a hydrogen atom attached to an oxygen atom. For molecules having an OH group bound to the aromatic ring (salicylhydroxamic acids **4a-4d**), it was counted as the deprotonated group, despite the controversies related to this issue [23,56]. For the other molecules (**1c**, **2c**, and **3c**), the deprotonated group was the hydroxamic acid moiety. The regularities on pK_a of the hydroxamic acids will be discussed below. Table 3 shows the percentages of the two most abundant species for each molecule, according to Chemicalize (www.chemic

Table 3
Protonation results.

HA	Protonation state	Distribution at pH = 7.4
1c	HA	87.24%
	A^-	12.76%
2c	HA	86.37%
	A^-	13.63%
3c	HA	88.28%
	A^-	11.72%
4a	HA	78.04%
	A^-	18.26%
4b	HA	78.01%
	A^-	18.91%
4c	HA	76.67%
	A^-	18.72%
4d	HA	62.97%
	A^-	27.09%

alize.com).

Docking studies for all the compounds listed in Table 3 were performed on *Hss*AChE-GB, *Hss*AChE-VX and *Hss*AChE-PON.

3.2.2. Docking energy calculations

The ligand-protein interaction energies (intermolecular and H-bonds) were calculated in order to get a better understanding of the variations between the binding modes of each compound and the molecular factors responsible for the reactivation. Table 3 lists, for each *Hss*AChE-OP complex, the interatomic distances between the nucleophile of the ligand and the P atom (d_{NucP}), the angle formed by these two atoms and Ser203 oxygen atom (θ_{NucPO}), the residues interacting with the ligand through hydrogen bonds, and the interaction energy values (E_{inter}). In order to enhance the chances of a successful nucleophilic attack to the nerve agent bound to Ser203, d_{NP} has to be smaller than 9 Å and θ_{NPO} has to be between 140° and 180° [57]. Ligand conformations that did not meet those two requirements were not considered and, the one that combined shorter d_{NP} and lower E_{inter} was selected as the best pose for the ligand.

The compounds studied presented negative values of binding energy for all systems, showing stabilization of the ligands inside the three *Hss*AChE-OP complexes. It was noticed that the protonation state did not lead to substantial differences among poses for the same molecule, so the data presented in Table 4 refer to the neutral species since they are the most abundant ones for all ligands. For *Hss*AchE-GB, the compounds with the smallest interaction energies were **3c**, **4d**, and **4c**. The same ligands were also the ones with smallest interaction energies with *Hss*AchE-VX. For *Hss*AchE-PON, the best three ligands were **2c**, **4d**, and **4c**, showing that **4d** and **4c** seem to show promising *Hss*AchE reactivation properties. Although **4a** and **4b** presented the highest interaction energies with the three *Hss*AchE, the distances between the nucleophiles of these two molecules and the P atom are relatively smaller than other values in the tables and the H-bond interactions are stable (low E_{Hbond} values), so these two compounds can also show good *Hss*AchE reactivation properties since that the smaller d_{NP} the bigger the chances for the nucleophile attacking to the P atom and removal of the nerve agent. The residues Tyr124, Ser125, Tyr133 and Tyr337 are the most important ones, contributing for stabilization of the ligands inside *Hss*AChE-GB through hydrogen bonding. For HssAChE-VX, the most important residues interacting with the ligands through hydrogen bonding are Tyr124, Phe295 and Arg296 while for *Hss*AChE-PON, the correspondent residues are Tyr124, Trp286 and Arg296.

Calculated parameters d_{NucP} (Å) and θ_{NucPO} (°) satisfy general requirements for configuration of reactivators. Considering the ratio E_{Hbond} (kcal/mol)/E_{inter} (kcal/mol) for every case of every substance the best ratio E_{Hbond} (kcal/mol)/E_{inter} (kcal/mol) is demonstrated by butylhydroxamic acid, it is always having the highest value:

Table 4
Docking results for interaction of the studied N-butylbenzhydroxamates **1c, 2c, 3c** and salicylhydroxamates **4a-4d** with human cholinesterase (*Hss*AChE) inhibited by GB, VX, and POX.

Ligand	d_{NucP} (Å)	θ_{NucPO} (°)	H-bond interactions	E_{Hbond} (kcal/mol)	E_{inter} (kcal/mol)
	***Hss*AChE-GB**				
1c	6.22	151.96	Tyr124, Ser125	−5.00	−95.97
2c	4.69	149.70	Tyr124, Tyr133, Tyr337	−6.38	−96.72
3c	4.52	155.42	Tyr124 (2), Tyr133	−6.40	−101.36
4a	6.18	148.35	Asp74, Tyr124 (2), Ser125	−8.84	−76.22
4b	5.54	145.90	Tyr124(3), Ser125, Tyr337, Tyr341	−12.57	−75.92
4c	5.67	151.95	Trp86, Tyr124, Ser125, Tyr337	−7.96	−99.49
4d	5.31	143.10	Trp86, Tyr337	−5.00	−100.11
			***Hss*AChE-VX**		
1c	8.57	145.35	Phe295, Arg296 (2)	−4.41	−94.48
2c	5.39	144.40	Tyr124, Phe295, Arg296	−4.00	−92.80
3c	7.75	147.14	Tyr124, Phe295	−4.14	−103.88
4a	5.38	144.07	Tyr124 (3), Tyr337	−7.25	−79.65
4b	5.09	141.80	Tyr124 (2)	−2.47	−76.28
4c	8.46	143.87	Phe295 (2), Arg296 (2), Phe338	−8.58	−101.89
4d	8.69	151.52	Ser293, Phe295 (2), Arg296 (2)	−7.53	−109.42
			HssAChE-PON		
1c	8.98	147.76	Tyr 124 (2), Trp286	−4.93	−105.25
2c	7.78	141.84	Tyr 124 (2)	−4.58	−108.84
3c	8.30	153.52	Tyr 124 (2)	−1.98	−102.54
4a	5.76	140.40	Tyr124, Phe295 (2), Arg296 (2)	−9.02	−78.31
4b	5.46	146.20	Tyr 124 (3), Tyr337	−9.30	−80.41
4c	8.68	145.46	Tyr 124, Trp286 (2), Arg296 (2)	−7.81	−108.91
4d	7.09	151.25	Tyr 124 (2), Trp286	−5.40	−115.98

- in the series of *N*-butyl derivatives with comparable E_{inter} (kcal/mol) the E_{Hbond} (kcal/mol) parameter is always bigger for *N*-butyl salicylhydroxamic acid;
- in the series of salicylhydroxamic acids the optimal ratio E_{Hbond} (kcal/mol)/E_{inter} (kcal/mol) is demonstrated by *N*-butyl substituted derivatives: *N*–H and *N*-methyl have low E_{inter}. In comparison with *N*-phenyl derivative, the *N*-butyl salicylhydroxamic acids has higher E_{Hbond}.

3.3. Role of acid dissociation constants (pK_a)

Being typical organic α-nucleophiles hydroxamic acids exhibit relatively low pK_a similar to 2-PAM, but have an uncharged nature [23],

Table 5
Acid dissociation constants (pK_a), cell viability (IC_{50}, mM), reactivation capacity towards human *AChE* inhibited by nerve agents (GB, VX) and organophosphorus pesticide paraoxon (PON) for studied hydroxamic acids **(1a-1d) – (4a-4d)**.

Entry #	pK_a [a]	IC_{50} [b], mM	Reactivation capacity, (% ± SD) [c]					
			GB		VX		POX	
			100 μM	10 μM	100 μM	10 μM	100 μM	10 μM
1a	8.86 ± 0.04(P) [23] 7.04 (Ch)	4.8 ± 1.6	0.93 ± 0.96	1.32 ± 1.14	0.59 ± 0.34	0.20 ± 0.10	2.02 ± 0.06	1.81 ± 0.50
1b	9.04 (Ch)	9.8 ± 2.3	0.51 ± 1.20	0.26 ± 0.45	0.84 ± 0.28	0.49 ± 0.86	1.36 ± 0.59	1.20 ± 0.02
1c	8.83 (Ch)	1.8 ± 0.6	0.27 ± 1.22	–	0.53 ± 0.02	0.64 ± 0.01	2.37 ± 0.07	1.64 ± 0.38
1d	8.45 (Ch)	1.0 ± 0.1	1.13 ± 0.53	0.82 ± 0.02	0.88 ± 0.62	0.62 ± 0.31	0.86 ± 0.29	0.69 ± 0.00
2a	6.57 (Ch)	2.7 ± 0.7	2.09 ± 0.18	0.96 ± 1.09	–	–	1.99 ± 0.88	1.18 ± 0.14
2b	9.0 (Ch)	4.5 ± 0.2	1.62 ± 0.04	2.82 ± 0.60	0.52 ± 0.01	0.52 ± 0.01	1.19 ± 0.88	1.87 ± 0.37
2c	8.8 (Ch)	1.4 ± 0.2	1.16 ± 1.29	1.58 ± 1.44	1.74 ± 0.26	1.84 ± 0.29	0.64 ± 0.01	0.49 ± 0.32
2d	8.4 (Ch)	>0.35 [b]	1.85 ± 0.92	1.6 ± 0.03	0.50 ± 0.01	0.50 ± 0.01	1.25 ± 0.38	1.43 ± 0.98
3a	9.12 ± 0.06(P) [23] 7.06 (Ch)	3.7 ± 1.4	–	0.97 ± 0.97	–	0.36 ± 0.31	2.95 ± 0.37	2.54 ± 0.11
3b	9.09 (Ch)	1.9 ± 0.0	1.50 ± 2.37	1.99 ± 0.93	0.18 ± 0.63	0.52 ± 0.01	2.23 ± 0.79	1.04 ± 0.28
3c	8.88 (Ch)	1.3 ± 0.1	1.74 ± 0.59	0.29 ± 1.11	0.53 ± 0.01	0.51 ± 0.01	1.33 ± 0.04	1.15 ± 0.26
3d	8.44 (Ch)	>0.1 [b]	1.31 ± 0.55	0.88 ± 0.91	0.36 ± 0.31	0.36 ± 0.31	1.24 ± 0.06	0.55 ± 0.34
4a	9.57 ± 0.06(P) [23] 7.52 ± 0.02(P) [23] 7.96; 9.30 (Ch)	1.8 ± 0.4	0.1 ± 0.07	0.97 ± 1.65	0.19 ± 0.01	–	1.65 ± 0.06	0.71 ± 0.42
4b	7.96; 9.18 (Ch)	5.8 ± 1.0	0.25 ± 1.26	1.41 ± 0.64	0.60 ± 0.35	0.41 ± 0.37	1.14 ± 0.18	0.10 ± 0.71
4c	7.93; 8.99 (Ch)	0.60 ± 0.04	2.33 ± 0.78	0.96 ± 0.97	2.92 ± 0.45	2.17 ± 0.36	3.29 ± 0.09	1.79 ± 0.51
4d	7.66; 8.60 (Ch)	1.2 ± 0.3	1.07 ± 0.07	1.38 ± 0.52	0.40 ± 0.34	0.98 ± 0.36	0.72 ± 0.39	0.80 ± 0.47

Note: [a] determined by potentiometric (P) method reported in Ref. [23], or (Ch) - calculated using https://chemicalize.com; [b] studied against CHO–K1 cell line; mean ± SEM (mM); n = 2; interval value is shown for the compounds that did not reach the 50% decrease in the viability upon exposure to the highest concentration tested; [c] "-" – there is no experimental data.

which favors diffusion over the BBB into the CNS. Non-quaternary (tertiary) oximes used to study as reactivators [18,19] reveal higher pK_a compared to quaternary oximes and to hydroxamic acids. The salicylhydroxamic acid has two OH groups capable for deprotonation to form anionic O-nucleophiles. An early point of view considered phenolic OH-group to deprotonate first [58], which led to a confusing point of view that the phenol proton is more acid than a hydroxamic acid proton. Currently, there is a general agreement to distinguish the two pK_a, a lower one (pK_a ca. 7.5) is to be ascribed to the hydroxamic acid, and the more basic proton (ca. 10.0–10.5) to the phenolic OH group, as it was clearly indicated in the papers on last two decades [23,56,59]. The acidity of studied compounds **1**–**4** (Table 4) followed the above-mentioned common regularity, and they are expected to deprotonate under physiological conditions (see also Table 1).

3.4. Effect of structure on cell viability

The cytotoxicity of any compound is important since it co-determines its maximum therapeutic dose [1]. Generally, introduction of the *N*-methyl group leads to less toxic compounds. Thus, changing of *N*–H on *N*-methyl group decreases toxicity from 2 to 3 times, except the compound **3b,** for which the toxicity was found to be increased twice. Unsurprisingly, in the case of more hydrophobic substituent's the toxicity increases (Table 5) as demonstrated by an extension of the substituent from *N*-methyl to *N*-butyl. At the same time, *N*-butyl derivatives are commonly less toxic, than their *N*-phenyl analogs, except the case of *N*-butyl salicylhydroxamic acid **4c**. However, it can be stated that the IC_{50} values in the range of millimoles indicate very low cytotoxicity compared to standard oxime reactivators [42].

3.5. Reactivation capacity towards human AChE

The selected hydroxamic acids exhibit modest activity towards all studied OPs (Table 5, Fig. 7). As comparted to *N*–H compounds, the *N*-methyl hydroxamic acids demonstrate reactivation capacity in all studied cases, compare **2a** and **2b**, **3a** and **3b**, **4a** and **4b.** Relatively higher reactivation capacity of the *N*-butyl substituted acids, especially towards VX should be highlighted. Among *N*-butyl derivatives, the *N*-butylsalicylhydroxamic acid **4c** shows more promising results.

We did not recognized regularities in reactivation capacity of *N*-phenyl hydroxamic acids, in comparison to *N*-butyl compounds. However, considering higher toxicity of the *N*-phenyl hydroxamic acids, introduction of phenyl substituent seems to be less attractive.

While studied reactivation capacities of the synthesized compounds **2**–**4** do not reach levels of the standard antidotes [1,14,16], but, in essence, *N*- butylhydroxamic acids have a potential ability to enter the CNS through BBB and restore activity of the AChE, along with an assumed turnover pathway for AChE reactivation.

3.6. Biodegradation of N-butyl derivatives

The combination of the optimal BBB scores, reactivation capacity, and toxicity assessment of studied substances shows advantages of *N*-butyl substituted hydroxamic acids **1c**, **2c**, **3c**, **4c** over other derivatives and allows us to select them to biodegradation study.

The *N*–H arylhydroxamic acids are known to undergo biodegradation, even enhanced up to nearly full mineralization in the presence of additional carbon source (glucose) or with the coexistence of carbon source (glucose) and nitrogen source (peptone) [60]. At the same time, there was a concern regarding the photochemistry of acyclic hydroxamic acids was shown to involve the generation of reactive acyl aminoxyl radical intermediates which may have biological consequences such as reactions with DNA [61]. A more recent study shows that biotransformation of salicylhydroxamic acid in the liver tissues is defined by the ability to chelate metal ions, including inhibiting metal-dependent enzymes [62]. The model enzyme cocktails demonstrate intracellular degradation of hydroxamic acids with different rates. Among aryl hydroxamic acids, heterocyclic compounds transform faster that benzhydroxamic acid, exceeding, it their turn, the acetohydroxamic acid [63].

The *N*-butyl substituted hydroxamic acids were chosen for CBT test in order to evaluate their biodegradability Such an approach may allow us to evaluate the overall process of biodegradation and give an indirect information on the possible circulation time of the corresponding antidotes in blood. Among the four *N*-butyl derivatives, only the benzhydroxamic acid derivative **1c** passed the test (Table 6, Fig. S.13). Introduction of the butyl substituent to the nitrogen atom of other aryl hydroxamic acids prevents readily biodegradability of the molecule. However, both 3-methoxy **2c** and 4-methoxy **3c** derivatives show similar biodegradability level passing the 20% threshold required for

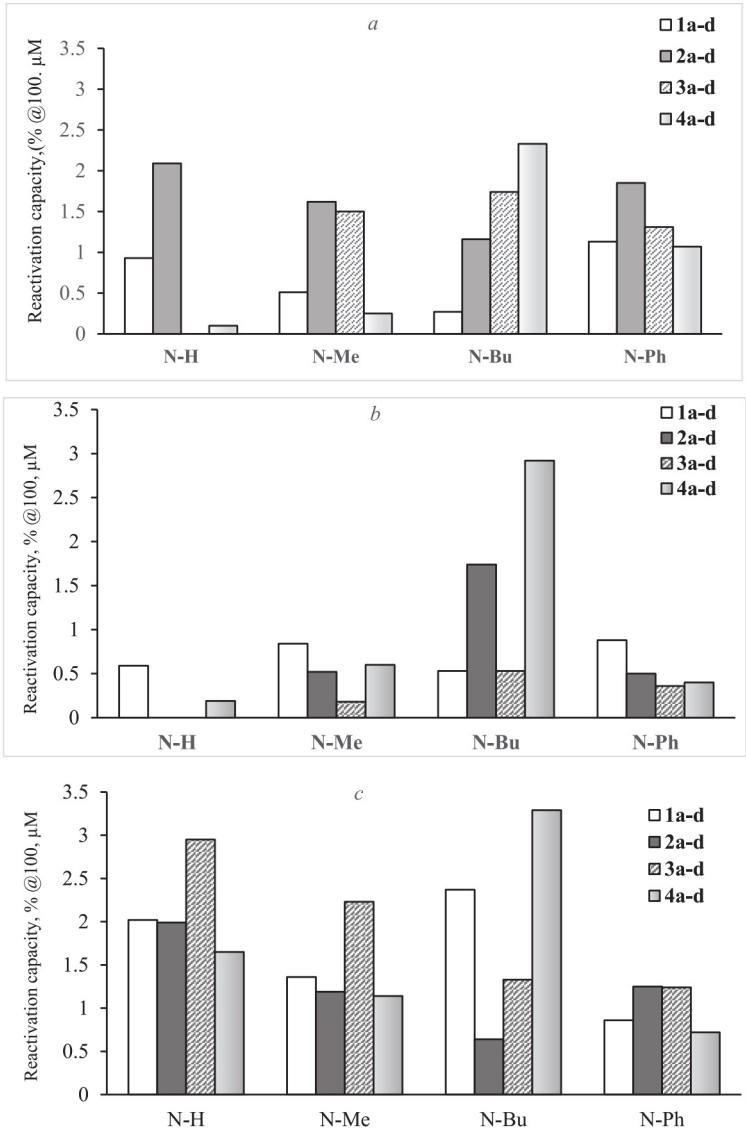

Fig. 7. Potency of hydroxamates **1(a–d) – 4(a–d)** to reactivate recombinant human AcChE (% @100 μM) inhibited by GB (*a*), VX (*b*), and PON (*c*).

Table 6
CBT results on biodegradability of *N*-butyl substituted hydroxamic acids **1c - 4c**.

Structures	D% 28 days	D% 33 days
1c	**70**	**73**
2c	**25**	**27**
3c	**26**	**28**
4c	**13**	**14**

Note. D% is a per cent of biodegradation of the studied compound.

inherently biodegradable compounds, see Table 6 and Figs. S14 and S15. The lowest biodegradability was demonstrated by salicylhydroxamic acid **4c** (Fig. S16), which did not pass the 20% biodegradability threshold and can be classified as non-biodegradable in terms of the experiment window. Meanwhile, combined with the cell viability data, the **4c** can be mentioned rather persistent than toxic, even since its toxicity is the highest in the series of *N*-butyl derivatives (shown as IC_{50} values against CHO–K1, see Table 5): **4c** < **3c** ≈ **2c** < **1**.

The salicylhydroxamic derivative can be expected to reveal biodegradability in more concentrated inoculum or in the case of the extension of CBT window. At the same time, lower, as compared to other compounds in this study, biodegradability may allow the compound **4c** to stay intact in the blood flow for longer period prior its possible enzymatic transformation/decomposition.

Taking into account its remarkable, as compared to other studied structures, reactivation capacity (in particular, towards VX-inhibited AChE, Table 5 and Fig. 7) along with other above-mentioned properties, it makes compound **4c** a suitable candidate for further investigation.

4. Conclusions

A series of arylhydroxamic acids with variable substituent at nitrogen atom (H → Me → n-Bu → Ph) have been prepared and evaluated as regards to their predicted hydrophobicity, BBB score, and molecular docking study on binding human acetylcholinesterase (*Hss*AChE) binding to the active site of the enzyme inhibited by GB, VX, or PON. The data on cell viability, AChE reactivation capacity and biodegradability lead to the structure-activity relationship for the series of hydroxamic acids.

(i) more hydrophobic aryl hydroxamic acids (log *P*) have better predicted abilities to come across the BBB; elongation of the substituent at nitrogen atom of hydroxamic acids results in facilitation of the permeability through BBB (predicted BBB score increases), while for the chain length longer than *N*-butyl or *N*-hexyl the leveling-off is observed; the study on the passive transport with non-cell-based in vitro PAMPA assay experimentally confirms that the *N*-butylsalicyl hydroxamic acids reveals the highest permeability in the series on both *N*-butyl derivative and salicylhydroxamic acids studied.

(ii) the calculated molecular docking parameters satisfy general requirements for configuration of reactivators; studies show that *N*-butyl derivatives have the optimal ratio E_{Hbond}/E_{inter}; in comparison with *N*-phenyl derivative, the *N*-butyl salicylhydroxamic acids has higher E_{Hbond}.

(iii) the studied compounds demonstrate modest reactivation capacity; change of *N*–H by *N*–Me ensures the reactivation capacity in studied concentrations on all studied OP substrates; among *N*-butyl derivatives, the *N*-butylsalicylhydroxamic acid shows most promising results; the change of *N*-butyl by *N*-phenyl does not result in significant changes in reactivation capacity but leads to higher toxicity of the compounds.

(iv) *N*-methyl derivatives reveal lower toxicity as compared to *N*–H compounds, while further extension of the substituent chain length leads to an increase in toxicity.

(iv) among the studied compounds, *N*-butyl derivatives have a better-balanced combination of properties; among them, *N*-butylsalicylhydroxamic acid is most promising.

(v) *N*-salicylhydroxamic acid found the lowest biodegradability in the series of *N*-butyl derivatives.

The found regularities may lead to further improvement of the structures of prospective antidotes and to select perspective structures to complement current formulations for medical countermeasures against poisoning by organophosphorus toxicants.

Author statement

Denys Bondar: Methodology; Investigation (synthesis and characterization of studied compounds), Validation; Data curation; Visualization; Writing- Original draft preparation. **Illia V. Kapitanov**: Conceptualization; Methodology; Writing- Original draft preparation. **Lenka Pulkrabkova**: Investigation (permeability study). **Ondřej Soukup**: Methodology, Investigation (permeability study, cell viability); Resources; Writing- Reviewing and Editing; **Daniel Jun**: Investigation (reactivation), Resources. **Fernanda D. Botelho**: Investigation (Molecular docking). **Tanos C.C. França**: Conceptualization; Formal analysis; Writing- Reviewing and Editing. **Kamil Kuča**: Conceptualization, Resources, Funding acquisition; Writing- Reviewing and Editing. **Yevgen Karpichev**: Conceptualization, Methodology; Resources; Funding acquisition; Writing- Reviewing and Editing.

Declaration of competing interest

The authors declare that they have no known competing financial interests or personal relationships that could have appeared to influence the work reported in this paper.

Data availability

Data will be made available on request.

Acknowledgement

DB and YK acknowledge NATO SPS MYP No. G5565 (DEFIR) for financial support. OS and DJ acknowledge funding from the grant of Czech Science Foundation no 22-12859S. The authors express their appreciation to Mrs. L. Krbálek for excellent technical support, Zeba Usmani for her help in using CBT facility, and Lucie Junová for assistance in biomedical experiments.

Appendix A. Supplementary data

Supplementary data to this article can be found online at https://doi.org/10.1016/j.cbi.2022.110078.

References

[1] Handbook of Toxicology of Chemical Warfare Agents, third ed., Academic Press, 2020 https://doi.org/10.1016/C2018-0-04837-9.
[2] J.D. Figueroa-Villar, E.C. Petronilho, K. Kuca, T.C.C. Franca, Review about structure and evaluation of reactivators of acetylcholinesterase inhibited with neurotoxic organophosphorus compounds, Curr. Med. Chem. 28 (2021) 1422–1442, https://doi.org/10.2174/0929867327666200425213215.
[3] P.F. Walker, A century of chemical warfare: building a world free of chemical weapons, in: B. Friedrich, D. Hoffmann, J. Renn, F. Schmaltz, M. Wolf (Eds.), One Hundred Years of Chemical Warfare: Research, Deployment, Consequences, Springer International Publishing, Cham, 2017, pp. 379–400.
[4] F. Worek, T. Wille, M. Koller, H. Thiermann, Toxicology of organophosphorus compounds in view of an increasing terrorist threat, Arch. Toxicol. 90 (2016) 2131–2145, https://doi.org/10.1007/s00204-016-1772-1.
[5] J. Brooks, T.B. Erickson, S. Kayden, R. Ruiz, S. Wilkinson, F.M. Burkle, Responding to chemical weapons violations in Syria: legal, health, and humanitarian recommendations, Conflict and Health 12 (2018) 7, https://doi.org/10.1186/s13031-018-0143-3.
[6] M. Guidotti, F. Trifiro, Chemical risk and chemical warfare agents: science and technology against humankind, Toxicol. Environ. Chem. 98 (2016) 1018–1025, https://doi.org/10.1080/02772248.2014.996153.
[7] T. Okumura, T. Hisaoka, A. Yamada, T. Naito, H. Isonuma, S. Okumura, K. Miura, M. Sakurada, H. Maekawa, S. Ishimatsu, N. Takasu, K. Suzuki, The Tokyo subway sarin attack - lessons learned, Toxicol. Appl. Pharmacol. 207 (2005) 471–476, https://doi.org/10.1016/j.taap.2005.02.032.
[8] T. Nakagawa, A.T. Tu, Murders with VX: Aum Shinrikyo in Japan and the assassination of Kim Jong-Nam in Malaysia, Forensic Toxicol 36 (2018) 542–544, https://doi.org/10.1007/s11419-018-0426-9.
[9] L. Carlsen, After Salisbury nerve agents revisited, Mol. Inform. 38 (2019), 1800106, https://doi.org/10.1002/minf.201800106.
[10] D. Steindl, W. Boehmerle, R. Korner, D. Praeger, M. Haug, J. Nee, A. Schreiber, F. Scheibe, K. Demin, P. Jacoby, R. Tauber, S. Hartwig, M. Endres, K.U. Eckardt, Novichok nerve agent poisoning, Lancet 397 (2021) 249–252, https://doi.org/10.1016/S0140-6736(20)32644-1.
[11] J. Bertolote, A. Fleischmann, M. Eddleston, D. Gunnell, Deaths from pesticide poisoning: a global response, Br. J. Psychiatry 189 (2006) 201–203, https://doi.org/10.1192/bjp.bp.105.020834.
[12] L. Gorecki, O. Soukup, J. Korabecny, Countermeasures in organophosphorus intoxication: pitfalls and prospects, Trends Pharmacol. Sci. 43 (2022) 593–606, https://doi.org/10.1016/j.tips.2022.04.008.
[13] P. Masson, F. Nachon, Cholinesterase reactivators and bioscavengers for pre- and post-exposure treatments of organophosphorus poisoning, J. Neurochem. 142 (2017) 26–40, https://doi.org/10.1111/jnc.14026.
[14] K. Sakurada, H. Ohta, No promising antidote 25 years after the Tokyo subway sarin attack: a review, Leg. Med. 47 (2020), 101761, https://doi.org/10.1016/j.legalmed.2020.101761.
[15] J. Dhuguru, E. Zviagin, R. Skouta, FDA-approved oximes and their significance in medicinal chemistry, Pharmaceuticals 15 (2022) 66, https://doi.org/10.3390/ph15010066.
[16] K. Kuca, D. Jun, K. Musilek, Structural requirements of acetylcholinesterase reactivators, Mini Rev. Med. Chem. 6 (2006) 269–277, https://doi.org/10.2174/138955706776073510.
[17] T. Zorbaz, A. Braiki, N. Marakovic, J. Renou, E. de la Mora, N.M. Hrvat, M. Katalinic, I. Silman, J.L. Sussman, G. Mercey, C. Gomez, R. Mougeot, B. Perez, R. Baati, F. Nachon, M. Weik, L. Jean, Z. Kovarik, P.Y. Renard, Potent 3-hydroxy-2-pyridine aldoxime reactivators of organophosphate-inhibited cholinesterases with

predicted blood-brain barrier penetration, Chem. Eur.J. 24 (2018) 9675–9691, https://doi.org/10.1002/chem.201801394.
[18] M.N.F. Norrrahim, M. Razak, N.A.A. Shah, H. Kasim, W.Y.W. Yusoff, N.A. Halim, S. A.M. Nor, S.H. Jamal, K.K. Ong, W.Z.W. Yunus, V.F. Knight, N.A.M. Kasim, Recent developments on oximes to improve the blood brain barrier penetration for the treatment of organophosphorus poisoning: a review, RSC Adv 10 (2020) 4465–4489, https://doi.org/10.1039/C9RA08599H.
[19] G. Amitai, A. Plotnikov, S. Chapman, S. Lazar, R. Gez, D. Loewenthal, K. A. Shurrush, G. Cohen, L.J. Solmesky, H. Barr, A.J. Russell, Non-quaternary oximes detoxify nerve agents and reactivate nerve agent-inhibited human butyrylcholinesterase, Commun. Biol. 4 (2021) 573, https://doi.org/10.1038/s42003-021-02061-wio.
[20] A.F. Childs, D.R. Davies, A.L. Green, J.P. Rutland, The reactivation by oximes and hydroxamic acids of cholinesterase inhibited by organo-phosphorus compounds, Br. J. Pharmacol. Chemother. 10 (1955) 462–465, https://doi.org/10.1111/j.1476-5381.1955.tb00106.x.
[21] Z. Syed, S.K, A. Dongre, M. Sogani, A review on hydroxamic acids: widespectrum chemotherapeutic agents, Int. J. Biol. Biomed. Eng. 14 (2020) 75–88, https://doi.org/10.46300/91011.2020.14.12.
[22] S. Bertrand, J.-J. Hélesbeux, G. Larcher, O. Duval, Hydroxamate, a key pharmacophore exhibiting a wide range of biological activities, Mini Rev. Med. Chem. 13 (2013) 1311–1326, https://doi.org/10.2174/13895575113139990007.
[23] Y.S. Simanenko, T.M. Prokop'eva, A.F. Popov, C.A. Bunton, E.A. Karpichev, V. A. Savelova, K.K. Ghosh, O-Nucleophilicity of hydroxamate ions in reactions with ethyl 4-nitrophenyl ethylphosphonate, diethyl 4-nitrophenyl phosphate, and 4-nitrophenyl 4-toluenesulfonate, Russ. J. Org. Chem. 40 (2004) 1337–1350, https://doi.org/10.1007/s11178-005-0017-1.
[24] N. Singh, Y. Karpichev, R. Sharma, B. Gupta, A.K. Sahu, M.L. Satnami, K.K. Ghosh, From alpha-nucleophiles to functionalized aggregates: exploring the reactivity of hydroxamate ion towards esterolytic reactions in micelles, Org. Biomol. Chem. 13 (2015) 2827–2848, https://doi.org/10.1039/C4OB02067G.
[25] R. Swidler, G.M. Steinberg, The kinetics of the reaction of isopropyl methylphosphonofluoridate (Sarin) with benzohydroxamic acid, J. Am. Chem. Soc. 78 (1956) 3594–3598, https://doi.org/10.1021/ja01596a011.
[26] T.M. Prokop'eva, Y.S. Simanenko, I.P. Suprun, V.A. Savelova, T.M. Zubareva, E. A. Karpichev, Nucleophilic substitution at a four-coordinate sulfur atom: VI. Reactivity of oximate ions, Russ. J. Org. Chem. 37 (2001) 655–666, https://doi.org/10.1023/A:1012487415041.
[27] F. Terrier, P. Rodriguez-Dafonte, E. Le Guevel, G. Moutiers, Revisiting the reactivity of oximate alpha-nucleophiles with electrophilic phosphorus centers. Relevance to detoxification of sarin, soman and DFP under mild conditions, Org. Biomol. Chem. 4 (2006) 4352–4363, https://doi.org/10.1039/B609658C.
[28] A. Bierwisch, M. Koller, F. Worek, S. Kubik, Pathways for the reactions between neurotoxic organophosphorus compounds and oximes or hydroxamic acids, Eur. J. Org. Chem. (2016) 5831–5838, https://doi.org/10.1002/ejoc.201601053, 2016.
[29] E.S. Orth, P.L.F. da Silva, R.S. Mello, C.A. Bunton, H.M.S. Milagre, M.N. Eberlin, H. D. Fiedler, F. Nome, Suicide nucleophilic attack: reactions of benzohydroxamate anion with bis(2,4-dinitrophenyl) phosphate, J. Org. Chem. 74 (2009) 5011–5016, https://doi.org/10.1021/jo9007354.
[30] V.E. Semenov, I.V. Zueva, S.V. Lushchekina, O.A. Lenina, L.M. Gubaidullina, L. F. Saifina, M.M. Shulaeva, R.M. Kayumova, A.F. Saifina, A.T. Gubaidullin, S. A. Kondrashova, S.K. Latypov, P. Masson, K.A. Petrov, 6-Methyluracil derivatives as peripheral site ligand-hydroxamic acid conjugates: reactivation for paraoxon-inhibited acetylcholinesterase, Eur. J. Med. Chem. 185 (2019), 111787, https://doi.org/10.1016/j.ejmech.2019.111787.
[31] B.E. Hackley, R. Plapinger, M. Stolberg, T. Wagner-Jauregg, Acceleration of the hydrolysis of organic fluorophosphates and fluorophosphonates with hydroxamic acids, J. Am. Chem. Soc. 77 (1955) 3651–3653, https://doi.org/10.1021/ja01618a072.
[32] G. Amitai, R. Gez, L. Raveh, N. Bar-Ner, E. Grauer, S. Chapman, Novel bifunctional hybrid small molecule scavengers for mitigating nerve agents toxicity, Chem. Biol. Interact. 259 (2016) 187–204, https://doi.org/10.1016/j.cbi.2016.04.036.
[33] M. Swain, chemicalize.org, J. Chem. Inf. Model. 52 (2012) 613–615, https://doi.org/10.1021/ci300046g.
[34] I.V. Tetko, V.Y. Tanchuk, Application of associative neural networks for prediction of lipophilicity in ALOGPS 2.1 program, J. Chem. Inf. Comput. Sci. 42 (2002) 1136–1145, https://doi.org/10.1021/ci025515j.
[35] H.B. Liu, L.R. Wang, M.L. Lv, R.R. Pei, P.B. Li, Z. Pei, Y.G. Wang, W.W. Su, X.Q. Xie, AlzPlatform: an Alzheimer's disease domain-specific chemogenomics knowledgebase for polypharmacology and target identification research, J. Chem. Inf. Model. 54 (2014) 1050–1060, https://doi.org/10.1021/ci500004h.
[36] L. Di, E.H. Kerns, K. Fan, O.J. McConnell, G.T. Carter, High throughput artificial membrane permeability assay for blood-brain barrier, Eur. J. Med. Chem. 38 (2003) 223–232, https://doi.org/10.1016/S0223-5234(03)00012-6.
[37] J. Friedrich, A. Langin, K. Kummerer, Comparison of an electrochemical and luminescence-based oxygen measuring system for use in the biodegradability testing according to closed bottle test (OECD 301D), CLEAN-Soil Air Water 41 (2013) 251–257, https://doi.org/10.1002/clen.201100558.
[38] OECD, Test No. 301: Ready Biodegradability, OECD Guidelines for the Testing of Chemicals, Section 3, OECD Publishing, Paris, 1992, https://doi.org/10.1787/9789264070349-en.
[39] S.J. Pandya, I.V. Kapitanov, Z. Usmani, R. Sahu, D. Sinha, N. Gathergood, K. K. Ghosh, Y. Karpichev, An example of green surfactant systems based on inherently biodegradable IL-derived amphiphilic oximes, J. Mol. Liquids 305 (2020), 112857, https://doi.org/10.1016/j.molliq.2020.112857.
[40] G. Karabanovich, J. Roh, O. Soukup, I. Pavkova, M. Pasdiorova, V. Tambor, J. Stolarikova, M. Vejsova, K. Vavrova, V. Klimesova, A. Hrabalek, Tetrazole regioisomers in the development of nitro group-containing antitubercular agents, MedChemComm 6 (2015) 174–181 (Tetrazole regioisomers in the development of nitro group-containing antitubercular agents).
[41] D. Malinak, R. Dolezal, J. Marek, S. Salajkova, O. Soukup, M. Vejsova, J. Korabecny, J. Honegr, M. Penhaker, K. Musilek, K. Kuca, 6-Hydroxyquinolinium salts differing in the length of alkyl side-chain: synthesis and antimicrobial activity, Bioorg. Med. Chem. Lett. 24 (2014) 5238–5241, https://doi.org/10.1016/j.bmcl.2014.09.060.
[42] O. Soukup, J. Korabecny, D. Malinak, E. Nepovimova, N.L. Pham, K. Musilek, M. Hrabinova, V. Hepnarova, R. Dolezal, P. Pavek, P. Jost, T. Kobrlova, J. Jankockova, L. Gorecki, M. Psotka, T.D. Nguyen, K. Box, B. Outhwaite, M. Ceckova, A. Sorf, D. Jun, K. Kuca, In vitro and in silico evaluation of non-quaternary reactivators of AChE as antidotes of organophosphorus poisoning - a new hope or a blind alley? Med. Chem. 14 (2018) 281–292, https://doi.org/10.2174/1573406414666180112105657.
[43] G.L. Ellman, K.D. Courtney, V. Andres Jr., R.M. Feather-Stone, A new and rapid colorimetric determination of acetylcholinesterase activity, Biochem. Pharmacol. 7 (1961) 88–95, https://doi.org/10.1016/0006-2952(61)90145-9.
[44] D. Jun, L. Musilova, K. Musilek, K. Kuca, In vitro ability of currently available oximes to reactivate organophosphate pesticide-inhibited human acetylcholinesterase and butyrylcholinesterase, Int. J. Mol. Sci. 12 (2011) 2077–2087, https://doi.org/10.3390/ijms12032077.
[45] D. Jun, L. Musilova, M. Pohanka, Y.S. Jung, P. Bostik, K. Kuca, Reactivation of human acetylcholinesterase and butyrylcholinesterase inhibited by leptophos-oxon with different oxime reactivators in vitro, Int. J. Mol. Sci. 11 (2010) 2856–2863, https://doi.org/10.3390/ijms11082856.
[46] J. de Almeida, T.R.C. Guizado, A.P. Guimaraes, T.C. Ramalho, A.S. Goncalves, M. C. de Koning, T.C.C. Franca, Docking and molecular dynamics studies of peripheral site ligand-oximes as reactivators of sarin-inhibited human acetylcholinesterase, J. Biomol. Struct. Dyn. 34 (2016) 2632–2642, https://doi.org/10.1080/07391102.2015.1124807.
[47] R.L. de Paula, J. de Almeida, S.F.A. Cavalcante, A.S. Goncalves, A.B.C. Simas, T.C. C. Franca, M. Valis, K. Kuca, E. Nepovimova, J.M. Granjeiro, Molecular modeling and in vitro studies of a neutral oxime as a potential reactivator for acetylcholinesterase inhibited by paraoxon, Molecules 23 (2018) 2954, https://doi.org/10.3390/molecules23112954.
[48] PC SPARTAN pro molecular modeling for the desktop, Chem. Eng. News 77 (1999) 2, https://doi.org/10.1021/cen-v077n017.p002.
[49] M.J.S. Dewar, E.G. Zoebisch, E.F. Healy, J.J.P. Stewart, The development and use of quantum-mechanical molecular-models .76. AM1 - a new general-purpose quantum-mechanical molecular-model, J. Am. Chem. Soc. 107 (1985) 3902–3909, https://doi.org/10.1021/ja00299a024.
[50] R. Thomsen, M.H. Christensen, MolDock: a new technique for high-accuracy molecular docking, J Med. Chem. 49 (2006) 3315–3321, https://doi.org/10.1021/jm051197e.
[51] D.K.A. Kusumahastuti, M. Sihtmae, I.V. Kapitanov, Y. Karpichev, N. Gathergood, A. Kahru, Toxicity profiling of 24 L-phenylalanine derived ionic liquids based on pyridinium, imidazolium and cholinium cations and varying alkyl chains using rapid screening *Vibrio fischeri* bioassay, Ecotoxicol. Environ. Saf. 172 (2019) 556–565, https://doi.org/10.1016/j.ecoenv.2018.12.076.
[52] S. Okuno, K. Sakurada, H. Ohta, H. Ikegaya, Y. Kazui, T. Akutsu, T. Takatori, K. Iwadate, Blood-brain barrier penetration of novel pyridinealdoxime methiodide (PAM)-type oximes examined by brain microdialysis with LC-MS/MS, Toxicol. Appl. Pharmacol. 227 (2008) 8–15, https://doi.org/10.1016/j.taap.2007.09.021.
[53] C.A. Bunton, F.H. Hamed, L.S. Romsted, Quantitative treatment of reaction-rates in functional micelles and comicelles, J. Phys. Chem. 86 (1982) 2103–2108, https://doi.org/10.1021/j100208a040.
[54] C. Hansch, A. Leo, D. Hoekman, Exploring QSAR: Hydrophobic, Electronic, Steric Constants, American Chemical Society, DC, 1995.
[55] A. Dixit, Lipophilicity (LogD7.4) of N-aryl benzo hydroxamic acids, GJPPS 4 (2018) 107–109, https://doi.org/10.19080/GJPPS.2018.04.555648.
[56] E.C. O'Brien, E. Farkas, M.J. Gil, D. Fitzgerald, A. Castineras, K.B. Nolan, Metal complexes of salicylhydroxamic acid (H2Sha), anthranilic hydroxamic acid and benzohydroxamic acid. Crystal and molecular structure of [Cu(phen)2(Cl)] Cl·H2Sha, a model for a peroxidase-inhibitor complex, J. Inorg. Biochem. 79 (2000) 47–51, https://doi.org/10.1016/S0162-0134(99)00245-7.
[57] J.A.V. da Silva, E. Nepovimova, T.C. Ramalho, K. Kuca, T.C.C. Franca, Molecular modeling studies on the interactions of 7-methoxytacrine-4-pyridinealdoxime, 4-PA, 2-PAM, and obidoxime with VX-inhibited human acetylcholinesterase: a near attack conformation approach, J. Enzyme Inhib. Med. Chem. 34 (2019) 1018–1029, https://doi.org/10.1080/14756366.2019.1609953.
[58] E.D. Bergmann, Z. Tashma, J. Katzhendler, The nature of the ionic dissociation of salicylhydroxamic acid, Isr. J. Chem. 13 (1975) 229–233, https://doi.org/10.1002/ijch.197500033.
[59] K.H. Sharp, P.C.E. Moody, K.A. Brown, E.L. Raven, Crystal structure of the ascorbate peroxidase-salicylhydroxamic acid complex, Biochemistry 43 (2004) 8644–8651, https://doi.org/10.1021/bi049343q.
[60] Z. Wenjun, G. Wenqi, M. Guangjun, Effect of Co-metabolism on Biodegradation of Hydroxamic Acid, in: 2011 International Conference on Electric Technology and Civil Engineering, ICETCE), 2011, pp. 5900–5903, https://doi.org/10.1109/ICETCE.2011.5776497.

[61] E. Lipczynskakochany, The photolability of hydroxamic acids and its importance to the human environment, Sci. Total Environ. 100 (1991) 469–482, https://doi.org/10.1016/0048-9697(91)90388-U.
[62] T.N. Bogatyrenko, Z.V. Kuropteva, L.M. Baider, V.R. Bogatyrenko, B.S. Fedorov, N. P. Konovalova, On the possibility of the nitric oxide formation upon biotransformation of hydroxamic acids, Russ. Chem. Bull. 60 (2011) 1162–1165, https://doi.org/10.1007/s11172-011-0182-z.
[63] H.P.S. Makkar, O.P. Sharma, R.K. Dawra, Enzymatic degradation of hydroxamate in rumen microbes, JDS 66 (1983) 2337–2342, https://doi.org/10.3168/jds.S0022-0302(83)82090-6.

Appendix 3

Publication III

Bondar, D.; Bragina, O.; Lee, J. Y.; Semenyuta, I.; Järving, I.; Brovarets, V.; Wipf, P.; Bahar, I.; Karpichev, Y. Hydroxamic Acids as PARP-1 Inhibitors: Molecular Design and Anticancer Activity of Novel Phenanthridinones, *Helv. Chim. Acta,* #e202300133.

Reprinted from the permission of John Wiley & Sons.

Check for updates

doi.org/10.1002/hlca.202300133

RESEARCH ARTICLE

HELVETICA chimica acta

Hydroxamic Acids as PARP-1 Inhibitors: Molecular Design and Anticancer Activity of Novel Phenanthridinones

Denys Bondar,[a] Olga Bragina,[a] Ji Young Lee,[b] Ivan Semenyuta,[c] Ivar Järving,[a] Volodymyr Brovarets,[c] Peter Wipf,*[d, e] Ivet Bahar,[b] and Yevgen Karpichev*[a]

[a] Department of Chemistry and Biotechnology, Tallinn University of Technology (TalTech), Akadeemia tee 15, EE-12618 Tallinn, Estonia, e-mail: yevgen.karpichev@taltech.ee

[b] Laufer Center for Physical and Quantitative Biology, and Department of Biochemistry and Cell Biology, School of Medicine, Stony Brook University, NY, 11794, USA

[c] V.P. Kukhar Institute of Bioorganic Chemistry and Petrochemistry, National Academy of Science of Ukraine, Akademika Kukharia Str. 1, UA-02094 Kyiv, Ukraine

[d] Department of Chemistry, School of Arts & Sciences, University of Pittsburgh, Pittsburgh, PA 15260, USA, e-mail: pwipf@pitt.edu

[e] School of Pharmacy, University of Eastern Finland, SF-70211 Kuopio, Finland

Dedicated to Prof. *Andrea Vasella* in honor of his 80th birthday and in recognition of his exemplary mentor- and scholarship

Poly(ADP-ribose)polymerase-1 (PARP-1) is a promising target for antitumor agents. This study presents the first evidence of hydroxamic acids as efficient PARP inhibitors. Molecular docking and molecular dynamics simulations revealed that *N*–O substituted phenanthridinones form a complex interplay with PARP-1. A series of cyclic aryl hydroxamic acids, *N*-(benzyloxy)- and *N*-(hydroxy)phenanthridinones, were prepared through a ligand-free methodology from *N*-(benzyloxy)benzamides using dual C–H/N–H bond activation. Three of the computed hit compounds exhibited significant activity in cell-based and enzymatic assays, inhibiting PARP-1 in the low-nanomolar range. The antiproliferative activity of all prepared compounds and the reference compounds PJ34 and Olaparib was evaluated in cancer cells (HepG2, BxPC3, MDA-MD-231, and HeLa) and in noncancer cell lines (NIH 3T3 and HEK 293). An *N*-(benzyloxy)- and an *N*-(hydroxy)phenanthridinone showed the most promising properties as leads for developing therapeutics with a submicromolar activity window. The study highlights the potential utility of this scaffold for PARP inhibitors and the importance of target-specific design to minimize toxicity and side effects.

Keywords: antitumor agents, hydroxamic acids, molecular dynamics, PARP-1, phenanthridinones, PJ34.

Introduction

Poly(ADP-ribose)polymerase-1 (PARP-1) is involved in numerous cellular processes, including DNA repair and cell death, and is one of the most promising current molecular targets for the development of anticancer drugs.[1,2] Early examples of 1st generation PARP-1 inhibitors were developed based on the observations that nicotinamide, a secondary product of the PARP-1-catalyzed reaction, caused moderate inhibition of poly ADP-ribosylation. Since then, many pharmacological PARP-1 inhibitors and drug candidates have been developed that structurally mimic nicotinamide and share two general properties; namely catalytic inhibition of PARP-1 and locking or 'trapping' PARP-1 on damaged DNA.[3,4] A decade later, more efficient 2nd and 3rd generation PARP-1 inhibitors were developed that contain quinazoline and related scaffolds (isoqui-

Supporting information for this article is available on the WWW under https://doi.org/10.1002/hlca.202300133

© 2023 Wiley-VHCA AG, Zurich, Switzerland

nolines, quinazolinediones, phthalazinones, and phenanthridines), and bear a carboxamide in the second (condensed) aromatic ring (*Figure 1*).[5]

Since the discovery of the PARP family of enzymes as potential molecular drug targets in the 1990s, a substantial number of inhibitors and inhibition strategies have emerged (*Figure S1*).[9] PARP inhibitors can act as single-agent cancer therapeutics in tumors in which certain DNA repair pathways are disrupted, focusing the attention of the medicinal chemistry research community on the target-specific design of new PARP-targeting antitumor agents.[10,11] Over the last decade, clinical trials also led to the regulatory approval of several PARP inhibitors for breast and ovarian cancer.[3] Four PARP inhibitors of the 3rd generation (olaparib, rucaparib, niraparib, and talazoparib) have been approved by the US Food and Drug Administration (FDA) for clinical use as single agents, with veliparib expected to receive approval following promising Phase III trial results.[12] At the same time, clinical trials of some PARP-1 inhibitors have been discontinued due to their high toxicity and side effects. One example is iniparib (BSI-201), which failed in a Phase III trial of patients with squamous non-small cell lung cancer and a Phase II trial against platinum-resistant ovarian cancer.[13]

Phenanthridinones contain the benzamide core unit essential to inhibition of PARP-1. They are frequently found as building blocks in a variety of alkaloids (*e.g.*, phenaglydon[14]) and biologically active pharmaceutical agents, including PJ34, a 2nd generation PARP-1 inhibitor (*Figure 1*).[7] Their main advantages include good water-solubility, a wide range of therapeutic effects, and the ready synthetic access from inexpensive commercial starting materials.[15] In particular, the phenanthridinone **PJ34** demonstrated significant cytotoxicity towards cancer cells, and its selective anticancer activity could be key to the development of more efficient and targeted cancer treatments, especially in the final stages of the disease when the immune system is weakened and traditional chemotherapeutics (e.g., doxorubicin) elicit high non-selective cytotoxicity.[7,16–18] The tolerance of healthy cells to antitumor agents is another crucial factor in drug design. Inhibition of PARP-1 activity to block the replication of damaged DNA may be a reliable strategy for the development of new anti-cancer agents.[19]

Hydroxamic acids are a class of α-nucleophiles[20–22] with high pharmaceutical potential.[23–25] The hydroxamic acid moiety has been shown to be a key structural element in the design of potent and selective inhibitors of various metal-dependent enzymes, including histone deacetylases (HDAC).[26] However, due to their relatively low *in vivo* stability,[27] inhibitors containing the hydroxamic acid moiety need further medicinal chemistry optimization.[28] Among the synthetic strategies, the direct *N*-substitution (*Scheme 1,a*), the acylation of an appropriate *N–O* derivative (*Scheme 1,b*), and the direct oxidation of the corresponding amide (*Scheme 1,c*) were reported to allow for the preparation of a wide range of biologically active hydroxamic acids.[24] Furthermore, hydroxamic acids have been explored for the design of multifunctional hybrid anticancer agents,[29] including dual PARP-1/2 and HDAC inhibitors.[30,31] The latter demonstrated high but non-selective cytotoxicity that could be explained by the ability of hydroxamic acids to chelate intracellular metal ions.[27] The activity of *N–*OH species is generally enhanced if the nitrogen atom is not comprised in a cyclic structure, and non-selective cytotoxicity is rarely observed for bioactive

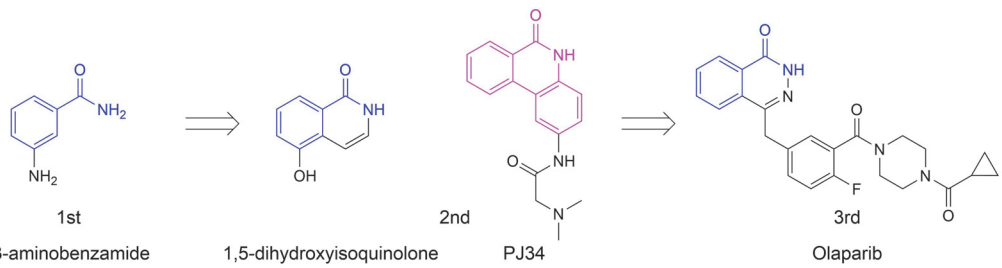

Figure 1. Sequential development of 1st, 2nd, and 3rd generation PARP inhibitors; the benzamide fragment is highlighted in *blue*; the phenanthridinone core in the PJ34 structure is highlighted in *pink*. The IC_{50} values for 3-aminobenzamide,[6] 1,5-dihydroxyisoquinolone,[5] PJ34,[7] and Olaparib[8] are literature data.

© 2023 Wiley-VHCA AG, Zurich, Switzerland

15222675, 2023, 10, Downloaded from https://onlinelibrary.wiley.com/doi/10.1002/hlca.202300133 by Tallin Technical University, Wiley Online Library on [09/11/2023]. See the Terms and Conditions (https://onlinelibrary.wiley.com/terms-and-conditions) on Wiley Online Library for rules of use; OA articles are governed by the applicable Creative Commons License

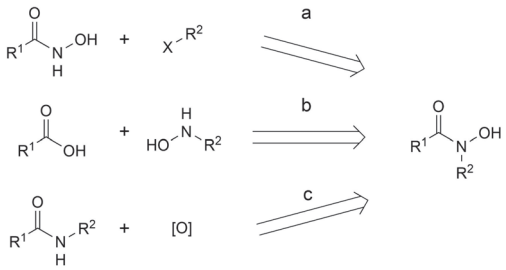

Scheme 1. Synthetic strategies for the preparation of hydroxamic acids. Reaction conditions: R^1, R^2 = alkyl chains, H; X = OH, halogens; [O] = oxidant.

heterocycles containing endocyclic *N*–OH (*N*–OR) groups.[32]

Accordingly, *N*-hydroxy derivatives of benzamide and other aryl hydroxamic acids and their *O*-substituted analogs have not been considered as a scaffold for drug design, and, to the best of our knowledge, systematic studies of *N*–O substituted phenanthridinones as potential PARP-1 inhibitors have not been reported to date.[33]

The aim of this work was to evaluate the potency of the suggested compounds as potential PARP-1 inhibitors using integrated computational studies, develop and optimize the synthesis of a series of *N*-(benzyloxy)- and *N*-(hydroxy)-phenanthridines from *N*-(benzyloxy)benzamides (*Table 1*), and identify potential drug candidates through an analysis of the experimental data. Furthermore, we determined the antiproliferative activity of these compounds against four human malignant cell lines (hepatocyte carcinoma HepG2, pancreatic cancer BxPC3, human breast adenocarcinoma MDA-MD-231, and HeLa) as well as human embryonic kidney cells HEK 293 and the mouse embryonic fibroblast NIH 3T3. The inhibitory activities of the selected compounds, labeled as **4c**, **4e**, and **4h**, were further evaluated by a universal PARP-1 colorimetric assay.

Results and Discussion

Small-molecule targeted drugs remain the primary therapeutic option for cancer treatment,[34] and this work is emphasizing the phenanthridinone core due to its relatively low molecular weight and unique physiochemical properties. Despite the availability of numerous classical reactions to obtain the phenanthridinone moiety,[35–38] for medicinal chemistry applications there is still a need to develop more cost-effective, eco-friendly, and efficient synthetic pathways. To the best of our knowledge, *N*-(benzyloxy)benzamides (*e.g.*, structures **1a**–**1f** in *Table 1*) as precursors of *N*-substituted phenanthridinones and their derivatives as potential anticancer agents have not yet been explored, and no reports on their investigation as PARP-1 inhibitors are available in the literature.

Table 1. Structures of *N*-(benzyloxy)benzamides (**1a**–**1f**), *N*-(benzyloxy)- phenanthridinones (**2a**–**2k**; **3a**, **3b**; **4c**, **4e**, and **4g**) and *N*-(hydroxy)phenanthridinones (**4a**, **4b**, **4d**, **4f** and **4h**) synthesized in the present study.

Compound[a]	R	R^1	R^2
1a	–	H	–
1b	–	3-MeO	–
1c	–	4-MeO	–
1d	–	5-OAc	–
1e	–	6-NO_2	–
1f	–	2,3,4,5-F	–
2a	Bn	H	H
2b	Bn	5-MeO	H
2c	Bn	5-MeO	3-NO_2
2d	Bn	6-MeO	H
2e	Bn	8-HO	H
2f	Bn	6-NO_2	H
2g	Bn	H	3-I
2h	Bn	5,6,7,8-F	H
2i	Bn	H	2-NO_2
2j	Bn	H	3-NO_2
2k	Bn	8-HO	2-NO_2
3a	Bn	H	2-NH_2·HCl
3b	Bn	H	3-NH_2·HCl
4a	H	H	H
4b	H	5-MeO	H
4c	Bn	H	2-MeO
4d	H	H	2-MeO
4e	Bn	H	2-NHC(O)CH_2NMe_2
4f	H	H	2-NHC(O)CH_2NMe_2
4g	Bn	H	3-NHC(O)CH_2NMe_2
4h	H	H	3-NHC(O)CH_2NMe_2

[a] Highlighted compounds are distinguished by their antiproliferative activities. The R group refers to structures in *Scheme 1* where N-OH has been replaced with N-OR.

N-(Benzyloxy)benzamides **1a**–**1f** are converted to phenanthridinones **2a**–**2k** in a reaction with unsubstituted iodobenzene, halophenols, or aryl iodides with strongly electron-withdrawing groups such as –NO_2. The selective reduction of the nitro group in **2j** and **2k** yields the corresponding aminated *N*-(benzyloxy)phenanthridinones **3a** and **3b**, which serve as precursors for *N*–OBn (**4e** and **4g**) and *N*–OH (**4f**

© 2023 Wiley-VHCA AG, Zurich, Switzerland

15222675, 2023, 10, Downloaded from https://onlinelibrary.wiley.com/doi/10.1002/hlca.202300133 by Tallin Technical University, Wiley Online Library on [09/11/2023]. See the Terms and Conditions (https://onlinelibrary.wiley.com/terms-and-conditions) on Wiley Online Library for rules of use; OA articles are governed by the applicable Creative Commons License

and **4h**), products that resemble PJ34. The *Experimental Section* provides a comprehensive account of the optimizations of the synthetic procedures.

Compound series **4**, which includes analogs of PJ34 with *N*–OBn and *N*–OH moieties, were chosen for analysis by molecular docking and molecular dynamics. The computed structures also bear MeO-substituents in place of the 2-(*N,N*-dimethylamino)acetamide group (*Figure 2*).

Compound Design and Molecular Docking Simulations

In the interest of gaining a molecular understanding of the properties of these compounds, their interactions with the catalytic domain of PARP-1 were studied by molecular docking simulations and compared to those of PJ34. We validated the *in silico* binding of PJ34 into the catalytic domain of PARP-1 (PDB ID: 4UXB)[39] by performing multiple docking simulations and verifying the reproducibility of the results. *Figure 3,A* shows the localization of PJ34 in the catalytic domain of PARP-1. The corresponding binding energy is estimated to be −9.0 kcal/mol.

Compounds **4a**–**4h** were docked into the catalytic domain of PARP-1. *Figure 3,B–3,D* illustrate the energetically favorable binding poses that were observed for these compounds. *Table S2* lists the results from the analysis of the interactions between the aryl hydroxamic acid derivatives and PARP-1 in these poses. These results indicate the high affinity of these compounds to form complexes with PARP-1, with binding energies varying in the range from −8.6 to −9.6 kcal/mol. Compounds **4c**, **4e** and **4g** are distinguished by their highest affinities (−9.5 ± 0.1 kcal/mol). Complexes with compounds **4c**–**4h** are noteworthy by the formation of multiple hydrogen bonds, 1–2 coulombic interactions and 6 to 8 hydrophobic contacts, as listed in *Table S2* (see also *Figure 3* caption).

Based on the data from molecular docking simulations, we suggest that the binding affinities of compounds **4c**–**4h** to the catalytic center of PARP-1 are comparable to that of PJ34. The most important amino acids involved in the interactions that stabilize the binding of these compounds are His862, Glu863, Gly888, Tyr889 and Gly988. Hydrophobic contacts involve the side chains of His862, Tyr896, Phe897, Ala898, Lys903 and Tyr907.

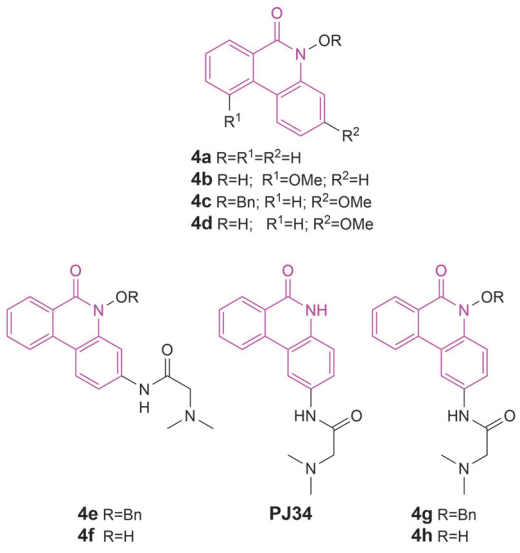

Figure 2. The phenanthridinones **4a**–**4h** studied in this work. The phenanthridinone core is highlighted in *pink*.

Analysis of the Dynamics of PARP-1 Complexes with Compounds **4c**, **4e**, *and* **4h**

Having confirmed that compounds **4e**, **4c** and **4h** are among the most promising candidates in the studied series, we performed a more in-depth analysis of the molecular interactions and binding characteristics of these compounds in extensive molecular dynamics (MD) simulations. As input structures for simulations, we used the crystallographically resolved PARP-1 complexed with PJ34 (PDB id: 4UXB), and its complexes with **4c**, **4e**, and **4h** modeled using this X-ray structure. The initial poses of compounds **4c**, **4e**, and **4h** were obtained by structurally aligning their phenanthridinone scaffold against that of PJ34, as illustrated in *Figure 4,A*. Five independent runs (200 ns each; total 1 μs) were performed for each compound. All four small molecules (PJ34, **4c**, **4e** and **4h**) were observed to remain stably bound in the catalytic site during the course of the simulations, while they exhibited fluctuations in their binding poses and energetics, which were specific to different compounds, as described below.

As shown in *Figure 4,B*, the phenanthridinone scaffold demonstrates highly stable contacts (within 4 Å distance) during almost the entire duration of the simulations in all four compounds (atom numbers 1–15 refer to the scaffold, see panel *4,C*). However, there are some interesting differences between the compounds. First, we note that **4h** is different from others for its high propensity to make persistent/stable

© 2023 Wiley-VHCA AG, Zurich, Switzerland

15222675, 2023, 10, Downloaded from https://onlinelibrary.wiley.com/doi/10.1002/hlca.202300133 by Tallin Technical University, Wiley Online Library on [09/11/2023]. See the Terms and Conditions (https://onlinelibrary.wiley.com/terms-and-conditions) on Wiley Online Library for rules of use; OA articles are governed by the applicable Creative Commons License

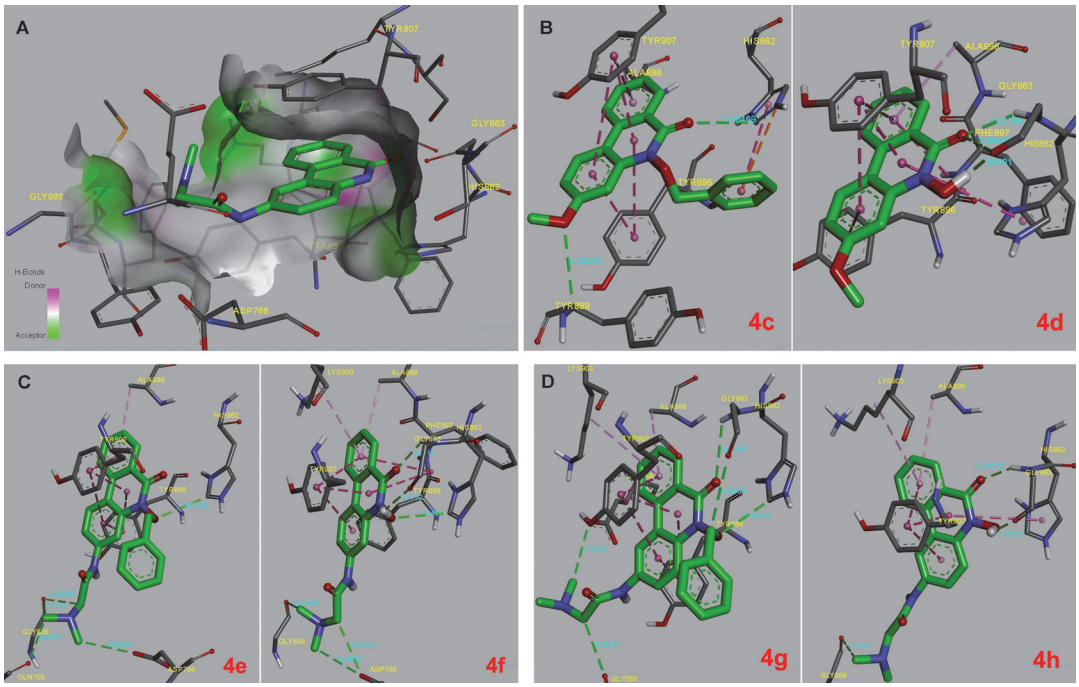

Figure 3. Binding poses of PJ34 (A) and compounds **4c**–**4h** (B–D) in the PARP-1 catalytic pocket. A. The binding pose of PJ34 (*thick green stick* representation) is obtained by using the PDB structure resolved for the complex with PJ34 and further redocking and energy-minimization. Several residues lining the catalytic pocket (His862, Glu863, Tyr907, Gly888, Asp766 and Tyr898) are displayed in *thin sticks* (*gray*) and labeled. B–D. Binding of **4c** (−9.4 kcal/mol) (*left*) and **4d** (−8.6 kcal/mol) (*right*) (panel B), **4e** (−9.6 kcal/mol) (*left*) and **4f** (−8.8 kcal/mol) (*right*) (panel C), and **4g** (−9.5 kcal/mol) (*left*) and **4h** (−8.9 kcal/mol) (*right*) (panel D) in the catalytic domain of PARP-1. Panels A–D illustrate energetically favorable poses in support of the strong binding affinity of these compounds. The compounds in B are stabilized by 2–3 hydrogen bonds or close contacts (1.96–3.70 Å) involving His862, Gly863 and Tyr889, one electrostatic interaction (within 4.51 Å) involving His862, and the eight hydrophobic contacts involving Tyr907, Lys903, Tyr896, Ala898, His862 and Phe897. In panel C, four hydrogen bonds involving His862, Glu863, Gly888, Asp766 and Gln759 and hydrophobic contacts made by Tyr907, Lys903, Tyr896, Ala898, His862, and Phe897 are observed. The poses in panel D are stabilized by hydrogen bonds with His862, Glu863, Gly888, Asp766 and Gln759 and hydrophobic contacts with Tyr907, Lys903, Tyr896, Ala898, His862, and Phe897.

contacts (*blue triangles*). Both **4h** and **4e** have a *N,N*-dimethylglycine amide moiety attached at the position R^2 (atoms 19–21) while **4c** does not feature such a moiety (*Table 1* and *Figure 2*), but atoms 19, 21, 22 in **4h** exhibit stronger interactions than their counterparts in **4e** within a 4.0 Å cutoff distance range, suggesting that **4h** enjoys a higher adaptability due to the absence of the benzyl group at position R (compared to **4e**); however, the oxygen atom 17 in **4e** in the same R^2 group is engaged in stronger interactions compared to **4h**. In the case of close-distance (3.0 Å cutoff) interactions, **4h** again displays persistent contacts at its oxygen atom 23 (which distinguishes it from PJ34), and all four compounds exhibit strong contacts at their oxygen atom 1.

On the side of PARP-1 (see right panels in *Figure 4,B*), residues involved in the most persistent contacts are His862, Gly863, Y896, F897, K903, Ser904 and Tyr907, which is generally consistent with the docking simulations. Among them, His862, Ser904, and Tyr907 again exhibit stronger binding to **4h** than **4c**/**4e**. The association with PJ34 is also strong, but the oxygen atom 23 of **4h**, which is not present in PJ34, provides an advantage compared to PJ34.

Even though the individual interactions of **4h** (and PJ34) are stronger (or more persistent, based on their total contact durations) compared to those of **4c**/**4e**, the latter two compounds have an additional ring at the R position (atoms 24–30), which overall results in a stronger association with the catalytic pocket, as can

 © 2023 Wiley-VHCA AG, Zurich, Switzerland

15222675, 2023, 10, Downloaded from https://onlinelibrary.wiley.com/doi/10.1002/hlca.202300133 by Tallin Technical University, Wiley Online Library on [09/11/2023]. See the Terms and Conditions (https://onlinelibrary.wiley.com/terms-and-conditions) on Wiley Online Library for rules of use; OA articles are governed by the applicable Creative Commons License

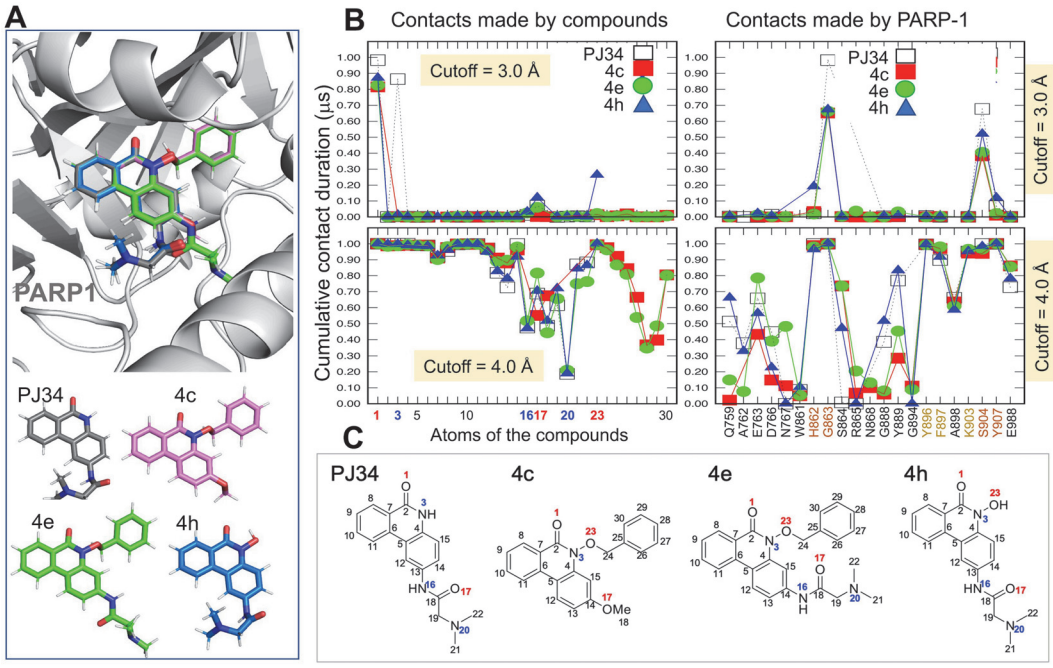

Figure 4. Initial structures adopted in MD simulations (A) and statistical analysis of most persistent (longer duration) contacts (B). Panel A displays the starting conformation at the catalytic pocket. At the bottom, their separate 3D structures are shown. The conformation of PJ34-bound PARP-1 refers to the crystal structure of the PARP-1–PJ34 complex (PDB id: 4UXB). Panel B displays the contacts made by the compounds (*left*) (see the atom index in panel C; oxygen and nitrogen atoms are labelled *in red and blue*, respectively) and those made by the PARP-1 residues (*right*) based on two cutoff distances (3 Å top, and 4 Å bottom) for atom–atom contacts. The residues along the *x*-axis were selected when the residue made contacts of 0.1 μs or longer duration with any of the four compounds, PJ34, **4c**, **4e**, or **4h**, within a 4.0 Å cutoff distance. The *cumulative results* from five runs of 200 ns conducted for each of the complexes are shown, hence the range of the ordinate measures up to 1 μs.

be seen in the interaction energy profiles recorded throughout the complete duration of five runs for each compound (*Figure 5*).

The histograms in *Figure 5* (*right panels*) indicate the higher binding affinity of **4c** and **4e** (-9.52 ± 0.22 and -9.43 ± 0.20 kcal/mol, respectively) compared to PJ34 and **4h**, which exhibit average affinities of -8.14 ± 0.14 and -8.15 ± 0.15 kcal/mol, respectively. The comparable energies of PJ34 and **4h**, and the higher stability of **4c** and **4e** are also consistent with the results from docking simulations (see *Table S2*). Note that the binding affinities of PJ34 and **4h** found in the MD simulations are not as strong as those observed in the optimal binding poses from docking simulations (which were estimated as -9.0 to -8.9 kcal/mol). The MD results represent the average behavior over microseconds of simulations. The data in *Figure 5* confirm that such highly favorable poses are occasionally visited (see the fluctuations in the binding affinities as a function of time on the *left panels* in *Figure 5* or their histograms on the *right* panels), but the average affinity is lower than those of **4c** and **4e** by about 1.3 kcal/mol. This is predominantly due to additional contacts made by the benzyl ring (at position R). This type of higher affinity concurrently entails a low selectivity, however, and therefore potential off-target effects. *Figure 6,A* displays representative snapshots from simulations, and panel B again confirms that the more favorable interactions of compounds **4c** and **4e** mostly originate from their higher propensity of hydrophobic contacts to which their additional benzyl rings contribute.

Further examination of hydrogen bond formation patterns showed that the oxygen atom 1 of **4c**/**4e**/**4h** as well as PJ34 strongly associates with the Gly863 backbone, underscoring the critical role of Gly863. In

 © 2023 Wiley-VHCA AG, Zurich, Switzerland

15222675, 2023, 10, Downloaded from https://onlinelibrary.wiley.com/doi/10.1002/hlca.202300133 by Tallin Technical University, Wiley Online Library on [09/11/2023]. See the Terms and Conditions (https://onlinelibrary.wiley.com/terms-and-conditions) on Wiley Online Library for rules of use; OA articles are governed by the applicable Creative Commons License

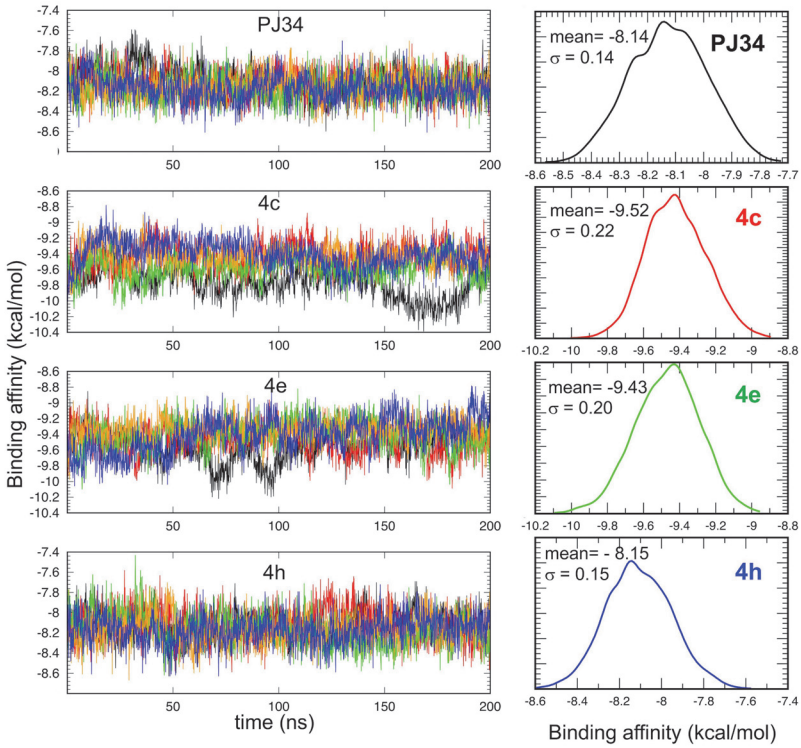

Figure 5. Time evolution of binding affinities observed in MD simulations of PARP-1 complexed with the four lead compounds (left), and the histograms of the observed binding affinities (right). A set of five curves is displayed for each compound on the left panels, referring to five independent runs conducted for each system. The histograms on the right are obtained by compiling the snapshots from all five trajectories for each compound. The average binding affinities (in kcal/mol) and the corresponding standard deviations are indicated in each case. Binding affinities were calculated with PRODIGY-LIG software using MD snapshots (10,000 snapshots for each compound) as input (here, cutoff distance is 10.5 Å).

contrast, **4h** exhibits stronger association with S904 compared to **4c**/**4e**. The oxygen atom 23 of **4h** makes contact with His862, and another oxygen atom 17 of **4h** makes contact with Tyr907, while **4c**/**4e** has negligible contacts. **4h** exhibits stronger hydrogen bonds with His862, Gly863, Ser904, and Tyr907 compared to **4c**/**4e** (*Figure 7*).

Overall, the phenanthridinone scaffold ensures a stable binding pose in all four compounds **4c**, **4e**, **4h**, and PJ34. Compound **4h** shows stronger hydrogen bonds compared to **4c**/**4e**, and **4e** exhibits stronger interactions than **4c** in the distance range of 4.0 Å as **4c** lacks the dimethyl glycine moiety. However, **4c**/**4e** end up having higher affinities than **4h** in a distance range of 10.5 Å due to their more extensive hydrophobic contacts, partly contributed by their additional benzyl moiety.

Optimization of the Synthetic Protocols

The envisioned synthesis pathway toward the target inhibitors involved using various aryl iodides to form the phenanthridinone scaffold. To optimize the conversion, a cross-coupling reaction with iodobenzene was performed on *N*-(benzyloxy)benzamide (**1a**) as a model compound (*Scheme 2*). Multiple reaction parameters, including catalyst type and loading, oxidants, solvents, reaction temperature, and time, were examined to optimize the conditions and yield higher amounts of the targeted product.

© 2023 Wiley-VHCA AG, Zurich, Switzerland

15222675, 2023, 10, Downloaded from https://onlinelibrary.wiley.com/doi/10.1002/hlca.202300133 by Tallin Technical University, Wiley Online Library on [09/11/2023]. See the Terms and Conditions (https://onlinelibrary.wiley.com/terms-and-conditions) on Wiley Online Library for rules of use; OA articles are governed by the applicable Creative Commons License

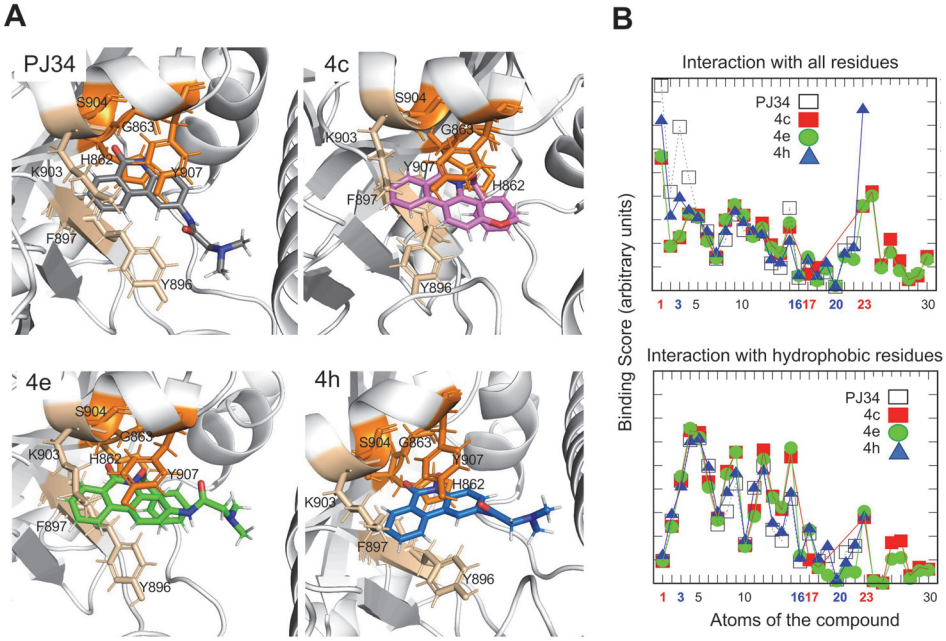

Figure 6. Representative snapshots displaying the equilibrated poses of the four compounds observed in MD simulations (A), and their interactions (B). The compounds are shown by the same color code used in *Figures 4*–5. Panel B shows that the higher affinity of compounds **4c** and **4e** is predominantly due to more favorable contacts with hydrophobic residues (*bottom*). In particular, atoms 8, 9, 12, 13, 14, and 15 of **4c**/**4e** exhibit stronger interactions than their counterparts in **4h**, in addition to the additional 24–30 atoms unique to these two compounds. The binding score is defined as $\Sigma\ (1/d_{ki})^2$ where k is frame/snapshot index and d_{ki} is corresponding distance between the compound and the residue i summed over all snapshots n (10,000 compiled from five independent runs for each compound), provided that they make atom–atom contacts of $d_{ki} < 4.0$ Å.

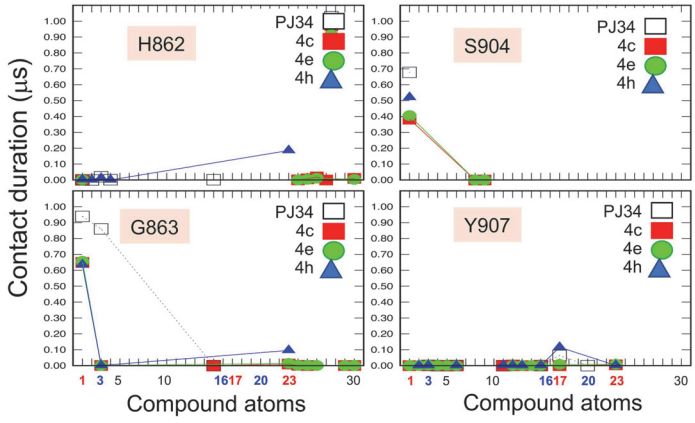

Duration of hydrogen bond (μs)
Geometry parameters 160° & 3.0 Å

	PJ34	4c	4e	4h
H862	0.00	0.00	0.00	0.10
G863	0.83	0.30	0.29	0.34
S904	0.33	0.26	0.27	0.34
Y907	0.03	0.00	0.00	0.06

Figure 7. The ability of compound **4h** to engage in close interactions typical of hydrogen bonds with selected PARP-1 residues. Comparative analysis of the propensity of close contacts made by the four compounds indicates the higher ability of **4h** to form hydrogen bonds with the PARP-1 catalytic pocket residues His862, Ser904, Gly863 and Tyr907 compared to the other compounds, except for the stronger ability of PJ34 to closely interact with Gly863. The table on the right shows the total duration of hydrogen bonds using a cutoff distance of 3.0 Å between donor and acceptor and a 160° angle.

© 2023 Wiley-VHCA AG, Zurich, Switzerland

15222675, 2023, 10, Downloaded from https://onlinelibrary.wiley.com/doi/10.1002/hlca.202300133 by Tallin Technical University, Wiley Online Library on [09/11/2023]. See the Terms and Conditions (https://onlinelibrary.wiley.com/terms-and-conditions) on Wiley Online Library for rules of use; OA articles are governed by the applicable Creative Commons License

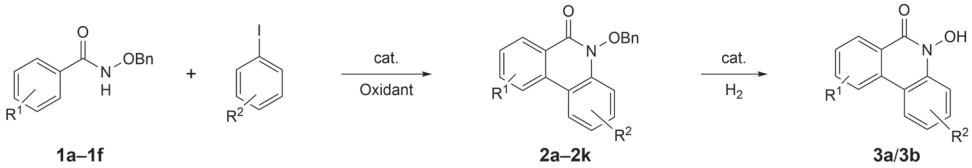

1a–1f 2a–2k 3a/3b

Scheme 2. Synthesis of *N*-(benzyloxy)- (**2a**–**2k**) and *N*-(hydroxy)phenylanthridinones (**3a**, **3b**).

The first step was carried out using the following conditions: **1a** (0.2 mmol), iodobenzene (0.4 mmol), and silver nitrate (0.4 mmol, 2.0 equiv.) with $PdCl_2$ (10 mol-%) as a catalyst in glacial acetic acid (1 mL) under an argon atmosphere (*Scheme 3*). The reaction mixture was degassed three to four times by evacuation with a vacuum pump followed by flushing with argon. The resulting suspension was heated at reflux for 24 h under an argon flow to obtain the desired product **2a** in 36% yield.

The reaction progress was monitored by thin-layer chromatography (TLC), and the consumption of the initial compound and the formation of phenanthridinone **2a**, the desired product, were detected at 254 nm and 366 nm, respectively. To optimize the reaction conditions, various catalysts, including Co(II) compounds, were evaluated as a possible earth-abundant metal alternatives to Pd.[40] $Co(OAc)_2$ did not show any catalytic activity at a loading of up to 20 mol-% of starting material **1a**, while the pyridine-based catalyst $Cl–Co(dmH)_2Py$ completely decomposed the *N*-(benzyloxy)benzamide **1a** through a Lossen rearrangement, due to the basic nature of the organic ligand (*Table S3*).

Despite the higher content of Pd in $PdCl_2$ as compared to $Pd(OAc)_2$, the former proved to be less active and offered a considerably lower yield, which allowed us to select $Pd(OAc)_2$ as the most efficient catalyst among those screened. The variation of the oxidant type and content, as well as the solvent, demonstrated that silver oxide provided very good yields of **2a** (*Table S4*, *Entries 5*–*7*). Using a two-fold excess of Ag_2O as an oxidant resulted in the best yield (87%) under the tested reaction conditions. According to these results, acetic acid was shown to be more efficient as a solvent and provided the best medium for the desired transformation. The use of formic or propionic acid as solvent caused lower yields of product **2a** (*Table S4*, *Entries 8* and *9*).

Reducing the amount of $Pd(OAc)_2$ catalyst from 10 mol-% to 5 mol-% caused a slight decline in product yield from 87% to 82%, which is still acceptable for synthetic purposes. However, lowering the catalyst amount to 2.5 mol-% resulted in a significant drop in yield to 51% (see *Table S5*, *Entry 3*). Notably, in the absence of the catalyst, formation of **2a** was not observed.

Finally, the reaction temperature and the reaction time were optimized. The decrease of the reaction temperature from 120 °C to 100 °C led to a twofold decrease in the reaction yield (*Table S5*, *Entry 5*). A further decrease in the reaction temperature to 80 °C resulted in the complete suppression of the transformation (*Table S5*, *Entry 6*). The decrease in the reaction time to 12 h also led to a twofold decrease in the product yield (*Table S5*, *Entry 7*). Finally, increasing the reaction time to 48 h and 72 h led to a slight decrease in the yield of **2a** (*Table S5*, *Entries 8* and *9*) possibly because of the decomposition of product **2a**.

The desired compounds were obtained by the optimized synthetic procedure in moderate to good yields (see *Experimental Section*). The reaction likely occurred through a cascade Pd-catalyzed dual C–H and C–N bond activation.[41] The variation of substituents on the *N*-(benzyloxy)benzamide demonstrated that *N*-(benzyloxy)benzamides with electron-donating groups (*e.g.* –OH, –OMe) were transformed into the corresponding products **2b**–**2e** in good yields, while the substrates bearing electron-withdrawing groups such as -F, $-NO_2$ provided products **2h** and **2f** in considerably lower yields (23% and 43%, respectively). The aryl iodides with –I and $–NO_2$ groups provided moderate yields of **2g**, **2i** and **2j**, and aryl iodides with electron-withdrawing groups (–I, $–NO_2$, –CN) in the

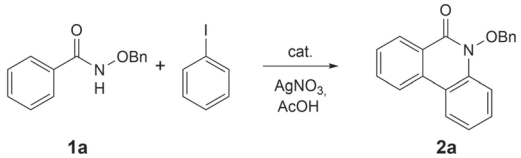

1a 2a

Scheme 3. Synthesis of **2a** used for catalyst optimization.

© 2023 Wiley-VHCA AG, Zurich, Switzerland

15222675, 2023, 10, Downloaded from https://onlinelibrary.wiley.com/doi/10.1002/hlca.202300133 by Tallin Technical University, Wiley Online Library on [09/11/2023]. See the Terms and Conditions (https://onlinelibrary.wiley.com/terms-and-conditions) on Wiley Online Library for rules of use; OA articles are governed by the applicable Creative Commons License

ortho-position did not undergo the transformation at all and were recovered intact. Reaction of compound **1a** with *para*-iodonitrobenzene as source of aryl groups at 120 °C resulted in <40% yield of **2i** (*Scheme 4*); a minor product of double *ortho*-arylation, **2ii**, was isolated when the reaction mixture was kept at a lower temperature.

The cytotoxicity screening of the novel *N*-(benzyloxy)phenanthridinones demonstrated that two analogs, **2a** and **2e**, caused a significant decrease in cancer cell viability (see below). To understand the effect of the benzyl group on the biological activity of compounds, *N*-(hydroxy)phenanthridinones **4a**, **4b**, and **4d** were prepared by a selective hydrogenolysis of the benzyl protective group[25] in the corresponding *N*-(benzyloxy)phenanthridinones **2a**, **2b**, and **4c** with Pd/C in MeOH (*Scheme 5*).

The synthesis of compounds **4e**–**4h** as structural analogues of the 2nd generation PARP inhibitor PJ34 was developed starting from *N*-(benzyloxy)benzamide **1a** and using *meta*-iodonitrobenzene as an arylating agent to obtain the desired intermediate **2j** in 42% yield after the first step (*Scheme 6*). The lower yield can be explained by the strong deactivation of the aryl iodide by the *meta*-nitro group. The reduction of the nitro group with Zn/HCl, Fe(II), and $SnCl_2$ resulted in a mixture of products with a partially reduced nitro group and a partially removed benzyl protective group. To ensure a controlled reduction, a NiB_2 catalyst was used, resulting in a quantitative reduction of the nitro group to amines **3a** and **3b** while the benzyl group was kept intact.

After obtaining amine derivatives **3a** and **3b**, the 2-(*N,N*-dimethylamino)acetamide was attached to the phenanthridinone core using *N,N*-dicyclohexylcarbodiimide (DCC) as a coupling agent and 4-dimethylaminopyridine (DMAP) as a catalyst at room temperature (r.t.) in dry dichloromethane (CH_2Cl_2) to form

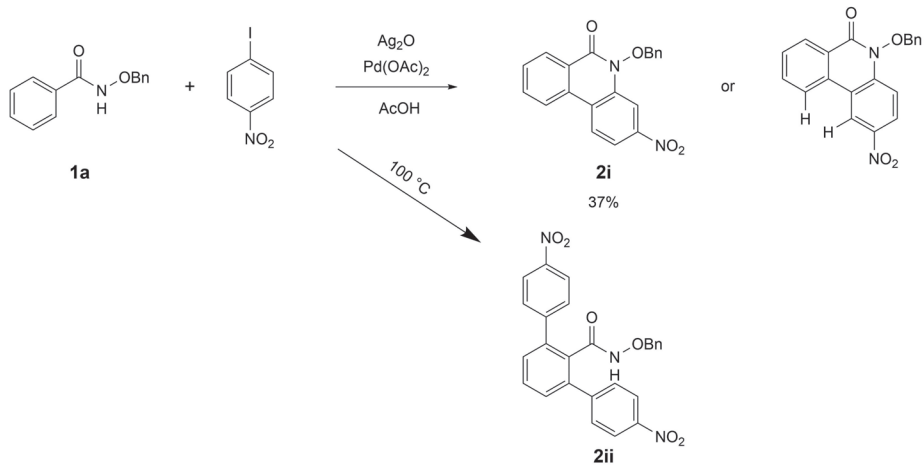

Scheme 4. Reaction of *N*-(benzyloxy)benzamides with *para*-iodonitrobenzene.

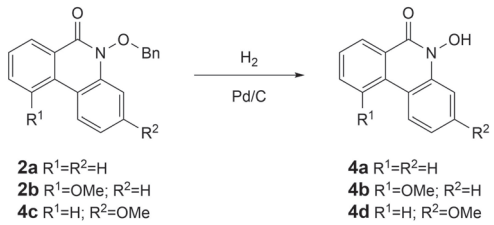

Scheme 5. Selective hydrogenation of compounds **2a**, **2b**, and **4c**. Reaction conditions: 1 bar, MeOH, 12 h.

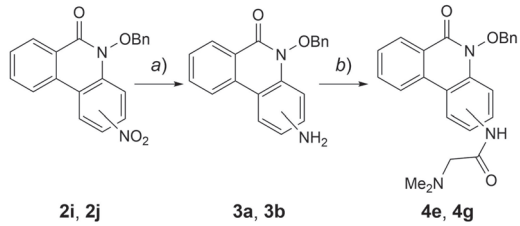

Scheme 6. Synthesis of *N*–OBn phenanthridinones **4e**, **4g**. *a*) NiB_2, N_2H_4 (MeOH); *b*) DCC, DMAP (dry CH_2Cl_2).

© 2023 Wiley-VHCA AG, Zurich, Switzerland

15222675, 2023, 10, Downloaded from https://onlinelibrary.wiley.com/doi/10.1002/hlca.202300133 by Tallin Technical University, Wiley Online Library on [09/11/2023]. See the Terms and Conditions (https://onlinelibrary.wiley.com/terms-and-conditions) on Wiley Online Library for rules of use; OA articles are governed by the applicable Creative Commons License

products **4e** and **4g** in 67% and 65% yield, respectively. Compounds **4f** and **4h** were prepared by removal of the benzyl protective group.

PARP-1 Inhibition Study

The selected compounds **4e**, **4c**, and **4h** were further tested for their capacity to inhibit PARP-1 activity with Olaparib as a positive control using the PARP/Apoptosis Universal Colorimetric Assay Kit.[42] The screening of these compounds was performed at concentrations of 0.001, 0.01, 0.05, 0.1, 1, 10, and 100 μM in triplicate ($n=3$) measurements. Compound **4c** showed 8.6, 11.7, 13.2, 24.7, 34.5, 65.1 and 68.8% inhibition, and **4e** showed 5.5, 14.7, 24.3, 37.9, 69.1, 78.1 and 95.5% inhibition at these respective concentrations; furthermore, **4h** showed 6.5, 8.1, 24.1, 79.6, 87.1, 94.2, and 97.1% inhibition, respectively (*Figure 8*). The tested compounds demonstrated a dose-dependent inhibition of the catalytic activity of PARP-1 in a cell-free system. The IC_{50} values were found to be 1.36 μM (**4c**), 494.8 nM (**4e**), and 48.9 nM (**4h**), confirming that compounds **4e** and **4h** exhibited a remarkable inhibitory effect against PARP-1. The activity of **4h** exceeds that of PJ34 reported recently in the literature,[9,39] but is inferior to Olaparib, which demonstrated an IC_{50} of 4.9 nM in the experiment with the PARP-1 enzyme kit (*Figure 8*).

Since hydroxamic acids are well known inhibitors of metal-dependent enzymes (such as histone deacetylases, see above), targeting HDAC could be one of the possible mechanisms of action for the products of the benzyl group deprotection, *i.e.*, *N*–OH phenanthridinones. Thus, we determined the inhibitory activity of **4h**, the most active inhibitor of the PARP-1 enzyme, using a fluorogenic HDAC1 assay and obtained an IC_{50} of 4.2 nM (*Figure 9*). This assay confirms that cyclic hydroxamic acids can be potential HDAC inhibitors and inhibit other molecular targets. Therefore, the potential action against two molecular targets, PARP-1 and HDAC1, of our novel *N*–OH phenanthridinones *vs* the inhibition of PARP-1 demonstrated by *N*–OBn derivatives requires further investigation and will be presented in a future study.

Evaluation of Cytotoxicity: Cell Viability Measurements

The choice of cancer cells lines to study cell viability against the extended compound series **2a**–**2j**, **3a**/**3b**, and **4a**–**4h** using PJ34 and Olaparib as positive controls was made based on recent studies documenting their sensitivity to PARP1 inhibition. Thus, pancreatic cancer cells BXPC-3 were reported to be exquisitely sensitive to PARP inhibition,[43], and the HepG2 line was proposed to undergo apoptosis through the mitochondrial pathway.[44] MDA-MB-231 is a BRCA-proficient TNBC cell line, and, thus, may be less sensitive to PARP inhibition but provides us with insights into the main mechanism of action.[45] Therefore, to determine the cytotoxicity of compounds **2a**–**2f** and PJ34 at the concentration of 25 μM, the cell lines HEK 293, NIH 3T3, HeLa, BxPC3, HepG2, MDA-MB-231 were used. All compounds were incubated for 48 h with cells.[46] The determination of cell viability was performed using the WST-1 assay, and HEK 293 cells were used as a control. Notably, HEK 293 is not a

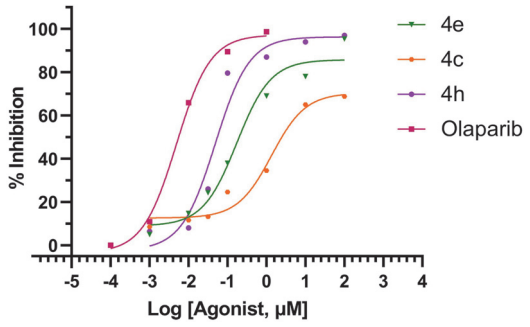

Figure 8. Inhibition of PARP-1 catalytic activity by compounds **4e** in *green*, **4c** in *amber*, and **4h** in *violet*, Olaparib in *purple*. Concentration–response curves are a representation of the colorimetric readout of the inhibition of the catalytic activity of PARP-1 based on three independent experiments in triplicate ($n=3$). The IC_{50} value calculated from each data set is indicated.

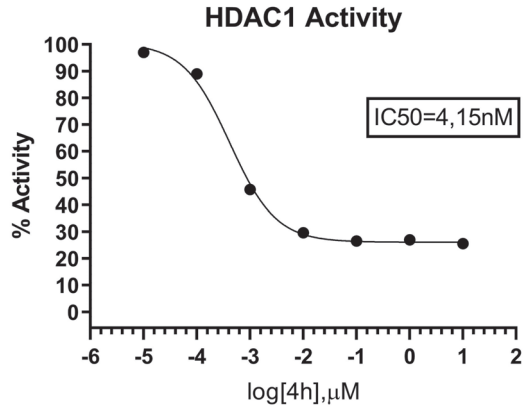

Figure 9. Inhibition of HDAC1 catalytic activity by compound **4h** determined with an HDAC1 colorimetric enzyme assay.

© 2023 Wiley-VHCA AG, Zurich, Switzerland

15222675, 2023, 10, Downloaded from https://onlinelibrary.wiley.com/doi/10.1002/hlca.202300133 by Tallin Technical University, Wiley Online Library on [09/11/2023]. See the Terms and Conditions (https://onlinelibrary.wiley.com/terms-and-conditions) on Wiley Online Library for rules of use; OA articles are governed by the applicable Creative Commons License

regular human cell model; these cells are immortalized by the known oncogene but are not yet malignant. Conversely, NIH 3T3 cells originate from mouse embryonic fibroblasts (MEFs) and can overcome cellular senescence and spontaneously immortalize when cultured under certain conditions.[47]

The cytotoxicity of all components used in HEK 293 and NIH 3T3 cells was very similar and different from that of malignant cells (*Figure 10,A*). Compounds **2a**, **2b**, and **2e** exhibited the highest cytotoxicity against all malignant cell lines. Two compounds, **2d** and **2f**, showed a statistically significant increase in cytotoxicity against malignant cells (correspondingly, HeLa 52% and 60%, BxPC3 50% and 71%, HepG2 90% and 88%, MDA-MB-231 70% and 84%), but did not reduce the viability of malignant cells as much as **2a**, **2b** and **2e**. An exception were HepG2 cells, which did not show a high level of cell death in the presence of compounds **2b**, **2d**, and **2f**. Interestingly, PJ34 led to a decrease in the viability of BxPC3 (65%), HepG2 (41%), and MDA-MB-231 (43%) cells, but not HeLa (84%), which may be due to an insufficient concentration of PJ34 to demonstrate significant cytotoxic effect against these cells.[7]

For a more in-depth study, compounds **2a** and **2b** were selected, and their *N*–OH analogs **4a** and **4b** were prepared (*Figure 10,B*). In subsequent experiments, concentrations of 50 μM were used.

A comparison of cell survival as a function of treatment with compounds **2a** and **4a** demonstrated that the removal of the benzyl protecting group may led to a decrease in the survival of the control, non-malignant cell lines HEK 293 (119% and 81%, respectively) and NIH 3T3 (109% and 53%, respectively; *Figure 10,B*). In contrast, the survival of HeLa (43% and 97%, respectively) and HepG2 cells (71% and 97%, respectively) increased. Similarly, a decrease in the survival of HEK 293 cells (98% and 60%, respectively), was observed for compounds **2b** and **4b**. Interestingly, the survival of NIH 3T3 (88% and 87%, respectively), HeLa (58% and 51%, respectively), and BxPC3 (45% and 35%, respectively) cells did not change when the benzyl protection group was removed to obtain **4b** from **2b**, but the survival of HepG2 cells decreased almost twofold (110% and 59%, respectively; *Figure 10,B*). Moreover, increasing the concentration of compound **2b** to 50 μM led to a slight decrease in the survival of HepG2 cells (89% at concentration 25 μM and 59% at 50 μM; *Figure 10,A* and *10,B*). This suggested that the cytotoxicity of *N*-(hydroxy)phenanthridinones against the studied cancer cell lines is expected to remain similar to the corresponding *N*-(benzyloxy)-derivatives, but there was a concern regarding the toxicity towards non-cancer cell lines.

The analysis of the cytotoxicity of compounds **2g**–**2j**, **3a**, **3b**, and **4c**–**4h** is presented in *Figure 11,A* and *11,B*. Compounds **3b**, **4c**, **4e**, and **4h** show the most promising results under these conditions; the remainder of the studied phenanthridinones did not exhibit statistically significant discriminatory effects between the survival of control cells (HEK 293 and NIH 3T3) and cancer cells (HeLa, HepG2 and MDA-MB-231). Compound **4c** did not change the viability of HEK 293 (92%) and NIH 3T3 (108%) cells, but significantly ($p < 0.0001$) reduced the survival of HeLa (26%) and MDA-MB-231 (48%) cells; the survival of HepG2 cells decreased by 40% ($p = 0.001$). Compound **4h** reduced the survival of HEK 293 (66%) and NIH 3T3 (79%) cells, but also significantly ($p < 0.0001$) decreased the survival of HeLa (26%), MDA-MB-231(34%) and HepG2 (14%) cells. Compound **3b** reduced the viability of HeLa (22%) and MDA-MD-231 (35%) with a remarkable effect on the survival of HepG2 (10%) but it was toxic towards NIH 3T3 (19%).

Compound **4e** exhibited extremely high cytotoxicity (<10%) against all cell lines studied at a concentration of 25 μM, including non-malignant cells. To investigate whether compound **4e** exhibited specificity toward cancer cells under dilution conditions, experiments at lower concentrations were performed to compare its effectiveness and selectivity towards oncogenic cells. For subsequent experiments, concentrations of 25 μM and 5 μM were used with compounds **4e**, PJ34 and Olaparib (see *Figure 12*). Compound **4e** at a concentration of 25 μM was found to be toxic and led to cell death in all cases, while Olaparib and PJ34 at the same concentration strongly inhibited non-cancer HEK 293 and NIH 3T3 cell lines. Remarkably, at 5 μM concentration, Olaparib and PJ34 still mostly suppressed non-oncogenic cells, while compound **4e** promoted the survival of non-malignant HEK 293 (124%) and NIH 3T3 (111%) cell lines but strongly ($p < 0.0001$) reduced the survival of HeLa (32%), MDA-MB-231 (30%) and HepG2 (42%) cells. Therefore, the WST-1 assay demonstrated that compound **4e** exhibited a dose-dependent cytotoxic activity and superior tumor differentiation to Olaparib and PJ34.

These results cast light on the molecular origins of the behavior observed in *Figure 8*. First, the relative inhibitory activities of **4e** and **4c** may be rationalized by the slightly stronger binding of **4e**, due to its additional dimethyl moiety. We also note in *Figure 6,B*

© 2023 Wiley-VHCA AG, Zurich, Switzerland

15222675, 2023, 10, Downloaded from https://onlinelibrary.wiley.com/doi/10.1002/hlca.202300133 by Tallin Technical University, Wiley Online Library on [09/11/2023]. See the Terms and Conditions (https://onlinelibrary.wiley.com/terms-and-conditions) on Wiley Online Library for rules of use; OA articles are governed by the applicable Creative Commons License

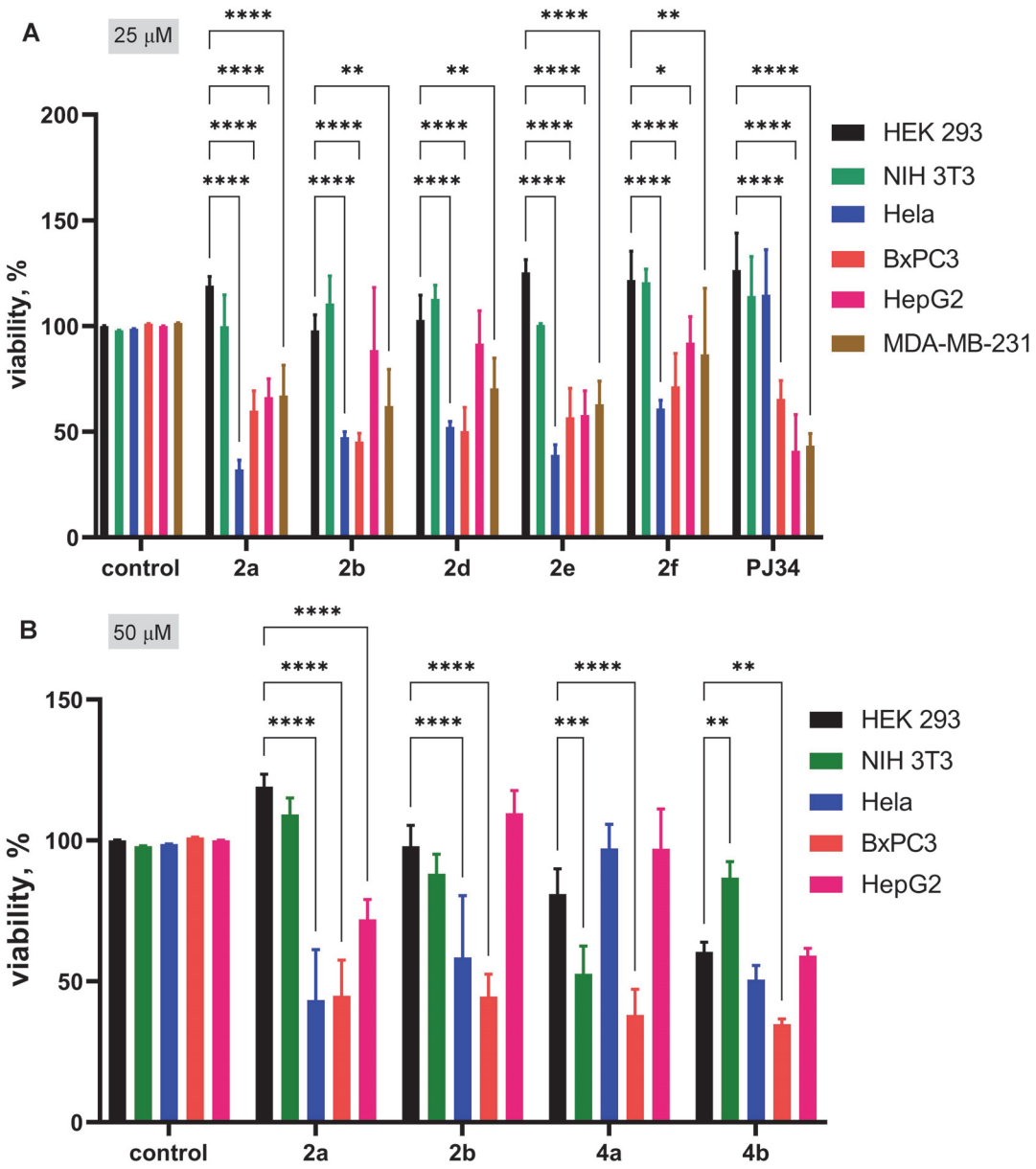

Figure 10. Results from cytotoxicity assays for compounds **2a**–**2f** and **4a**, **4b**. A. Cell viability data (WST-1 assay) after 48 h of 25 μM of **2a**, **2b**, **2d**, **2e**, **2f** and PJ34 exposure. B. Cell viability data after 48 h of exposure with 50 μM of **2a**, **2b**, **4a**, **4b**. In all panels, data of cells treated with solvent are used as control (100% viability, $n \geq 3$). Bars are mean + SD, asterisks indicate a significant difference between HEK 293 and other cell lines ($P < 0.05$ is represented as *, $P < .01$ as **, $P < .001$ as *** and $P < .0001$ as ****). 50% viability is indicated by the *dashed line* for visual comparison.

lower panel that several residues have a higher propensity to make long-lived contacts with **4e** compared to their contacts with **4c**. Examples of such residues are E763, D766, N767, and Y889, which

© 2023 Wiley-VHCA AG, Zurich, Switzerland

15222675, 2023, 10, Downloaded from https://onlinelibrary.wiley.com/doi/10.1002/hlca.202300133 by Tallin Technical University, Wiley Online Library on [09/11/2023]. See the Terms and Conditions (https://onlinelibrary.wiley.com/terms-and-conditions) on Wiley Online Library for rules of use; OA articles are governed by the applicable Creative Commons License

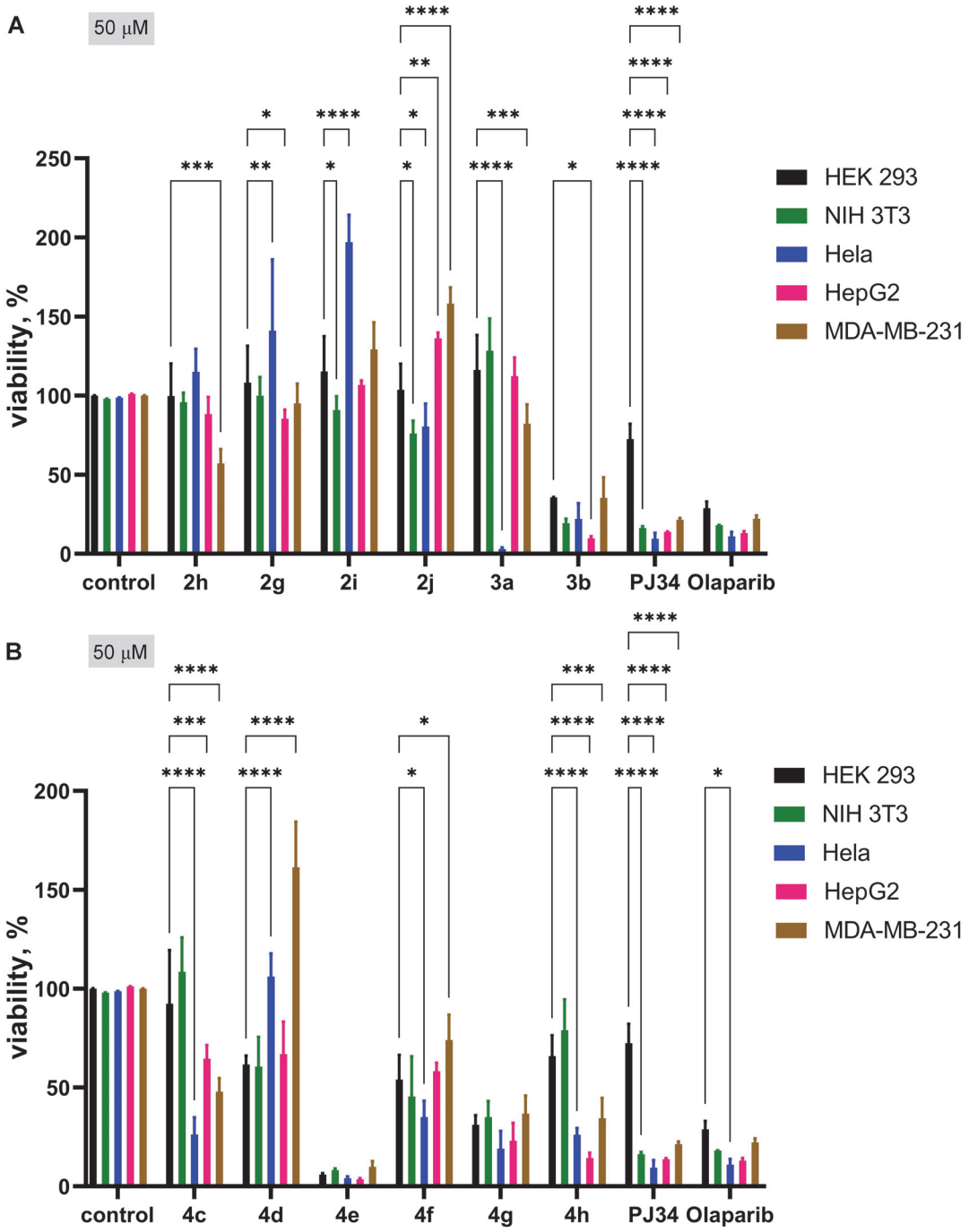

Figure 11. Results from cytotoxicity assays for compounds **2g**–**2j**, **3a**/**3b**, and **4c**–**4h**. A. Cell viability data after 48 h of exposure to **2h**, **2g**, **2i**, **2j**, **3a**, and **3b** at 50 μM concentration. B. Cell viability data after 48 h exposure to 50 μM of **4c**, **4d**, **4e**, **4f**, **4g**, and **4h**. 50% viability is indicated by the *dashed line* for visual comparison.

© 2023 Wiley-VHCA AG, Zurich, Switzerland

15222675, 2023, 10, Downloaded from https://onlinelibrary.wiley.com/doi/10.1002/hlca.202300133 by Tallin Technical University, Wiley Online Library on [09/11/2023]. See the Terms and Conditions (https://onlinelibrary.wiley.com/terms-and-conditions) on Wiley Online Library for rules of use; OA articles are governed by the applicable Creative Commons License

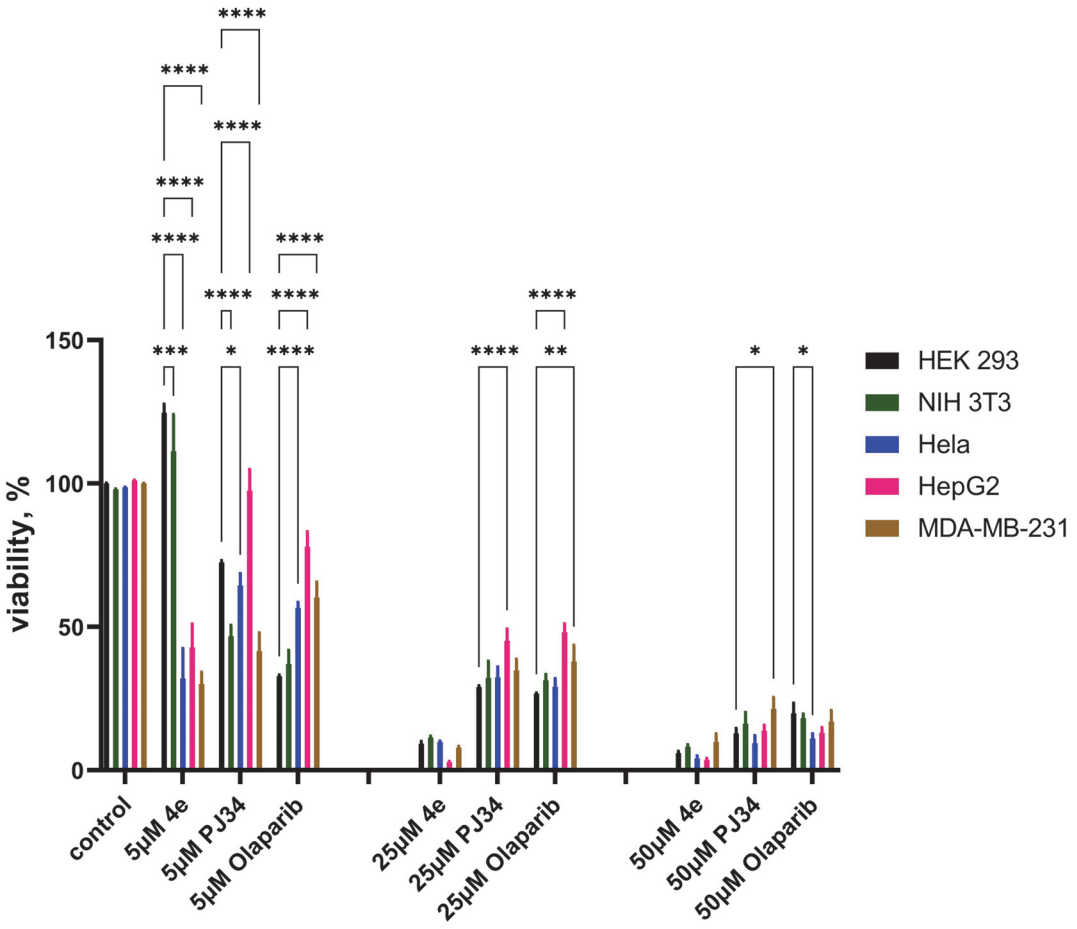

Figure 12. Results from cytotoxicity assays for **4e**, PJ34 and Olaparib. Cell viability data after 48 h of exposure at 5, 25, and 50 μM concentrations. Asterisks indicate a significant difference between HEK 293 and other cell lines ($P < 0.05$ is represented as *, $P < .01$ as **, $P < .001$ as *** and $P < .0001$ as ****).

apparently make contacts with the dimethyl glycine group (see lower left panel in *Figure 6,B*). The higher ability of **4e** to partially inhibit PARP-1 at the lowest concentration range may be attributed to its higher propensity to make a diverse set of contacts, favored by its relatively large size, in addition to its stronger short-range interactions that stabilize the bound pose.

At low concentrations, **4e** is experimentally observed to have a stronger inhibitory effect than **4h** as well, which is supported by our computational study that demonstrated that **4e** has a higher binding affinity at long distance ranges than **4h**, mainly due to its additional benzyl ring. On the other hand, **4h** shows a stronger dependence on concentration compared to **4c**/**4e**. At the same time, at higher concentrations, **4h** shows stronger inhibition, which can be explained by its ability to engage in more effective interactions, *e.g.*, hydrogen bonds (*Figures 5,B* and *7*) once it is bound to the catalytic pocket. At low concentrations, an important factor would be the encounter between compound and target, and relatively strong long-range interactions assist in recognizing the binding pocket. At a high concentration, the ability to make strong and long-lasting contacts by possibly inserting deeper into the pocket (as is the case for the 'smaller' **4h**) and

 © 2023 Wiley-VHCA AG, Zurich, Switzerland

15222675, 2023, 10, Downloaded from https://onlinelibrary.wiley.com/doi/10.1002/hlca.202300133 by Tallin Technical University, Wiley Online Library on [09/11/2023]. See the Terms and Conditions (https://onlinelibrary.wiley.com/terms-and-conditions) on Wiley Online Library for rules of use; OA articles are governed by the applicable Creative Commons License

form strong close contacts (*e.g.*, hydrogen bonds) appear to play a more important role.

The ability of the investigated compounds to inhibit PARP-1 in cells is dependent on several factors (*e.g.*, cell type). Generally, the *N*-(benzyloxy)- and *N*-(hydroxy)phenanthridinones **4c**–**4h** exhibited cytotoxic effects against the malignant cells studied. The introduction of a dimethylglycine moiety into the phenanthridinone scaffold appears to enhance the anticancer activity of the compounds. Furthermore, the selectivity and anticancer activity were also affected by the position of the dimethylglycine fragment at the R^2 position (**4e** and **4f** *vs.* **4g** and **4h**; *Table 1* and *Figure 2*), and the presence or absence of the benzyl group at the R position in (*N*-(benzyloxy)- *vs.* *N*-(hydroxy) analog pairs **4e** *vs.* **4f** and **4g** *vs.* **4h**).

Conclusions

PARP-1 is a key molecular target for the discovery of novel synthetic antitumor agents. To investigate the potential anticancer activity of *N*-(benzyloxy)- and *N*-(hydroxy)phenanthridinones, we used integrated computational studies to explore the binding modes and interactions of the suggested candidates with the catalytic domain of PARP-1. Molecular docking indicated that the designed phenanthridinones may form highly stable complexes with PARP-1, with estimated binding affinities of up to −9.6 kcal/mol. The differential behavior of the proposed hits at different distance ranges can be attributed to a complex balance of H-bonding and hydrophobic interactions between the compounds and the catalytic site of PARP-1. The dose-dependent PARP-1 inhibition by the computed structures with IC_{50} values of 1.357 μM (**4c**), 494.8 nM (**4e**), and 48.9 nM (**4h**), consolidated these results. MD simulations further validated the affinity of compounds **4c**, **4e**, and **4h**, which were either comparable to Olaparib or higher than that of PJ34. Notably, residues His862, Glu863, Gly888, Tyr889, Y896, F897, K903, S904, Y907, and Glu988 in the catalytic core of PARP-1 were distinguished by a high propensity to engage in strongly stabilizing interactions with the lead structures in the complexes. We developed an efficient synthetic protocol for preparing these PARP-1 inhibitors, involving ligand-free C–H/N–H activation of *N*-(benzyloxy)benzamides and aryl iodides using palladium acetate as a catalyst. The reaction can be scaled up to the gram level, and a series of phenanthridinones with electron-withdrawing and donating substituents were obtained in moderate to good yields. The results of cell viability experiments conducted on HepG2, BxPC3, MDA-MD-231, and HeLa cancer cells, as well as nonmalignant HEK 293 and NIH 3T3 cell lines, revealed that all test compounds exhibited antitumor activity that was either comparable or superior to that of PJ34 in the respective experiments.

Our findings indicate that hit compounds **4c**, **4e**, and **4h** exhibit significant anticancer activities in both cell-based and cell-free assays, inhibiting PARP-1 at nanomolar concentrations. Among these compounds, the phenanthridinones **4e** and **4h** demonstrate the most promising properties at the lowest concentrations and could serve as lead structures for the further development of potential drugs with nanomolar potencies. Our study is the first experimental evidence of the potential therapeutic utility of hydroxamic acids as efficient PARP-1 inhibitors.

Experimental Section

Computational Methods

Molecular Docking. The crystal structure of the PARP-1 was obtained from the Protein Data Bank (PDB ID: 4UXB),[48] prepared using AutoDock Tools (ADT) 1.5.6 and saved in PDBQT format.[49] The ChemAxon Marvin Sketch 5.3.735 program was used to create, generate conformations, optimize, and save all ligands in Mol2 format.[1] The energy minimization and optimization of the ligands were performed by software Avogadro v1.2.0,[51] using the Auto Optimization Tool (MMFF94s force field).[52] Partial charges by the Gasteiger method for all ligands were calculated with ADT and saved in PDBQT format. Docking simulations were performed using the AutoDock Vina 1.1.2 program.[53] The co-crystallized ligand PJ34 was set as the box center of the grid map (30*30*30 points) with 1 Å grid spacing. The analysis and visualization of ligand-protein interactions were performed by Accelrys DS.[54] The validation of the molecular docking of inhibitor PJ34 into the catalytic domain of PARP1 was conducted by redocking. The obtained ligand-protein complex demonstrated estimated binding energies of about −9.0 kcal/mol. The RMSD value for all atoms was calculated as 0.35 Å.

[1] Marvin Sketch was used for drawing, displaying and optimization chemical structures.[50]

© 2023 Wiley-VHCA AG, Zurich, Switzerland

15222675, 2023, 10, Downloaded from https://onlinelibrary.wiley.com/doi/10.1002/hlca.202300133 by Tallin Technical University, Wiley Online Library on [09/11/2023]. See the Terms and Conditions (https://onlinelibrary.wiley.com/terms-and-conditions) on Wiley Online Library for rules of use; OA articles are governed by the applicable Creative Commons License

Compound modeling and initial binding pose for PJ34, **4c**, **4e**, *and* **4h**. The 3-D structures of three compounds, **4c**, **4e**, **4h**, and their force fields were generated using CHARMM-GUI Ligand Reader & Modeler.[55] The structure and pose of PJ34 was obtained from PDB 4UXB.[45] Compounds **4c**, **4e**, and **4h** were structurally aligned against PJ34 by superposing their phenanthridinone scaffold, and the same PARP-1 conformation from PDB 4UXB was used for initiating the simulations with all the compounds. Alignment was performed using PyMOL 2.3.5.[56]

Molecular dynamics simulations of PJ34, **4c**, **4e**, *and* **4h**. All atom MD systems were set up using CHARMM-GUI Solution Builder.[57] Simulations were performed using the MD simulation package NAMD[58] with the CHARMM36m force field [59] for proteins, the TIP3P water model,[60] and the CGenFF force field[61] for the compounds. Five independent runs of 200 ns (total 1 μs) were performed for each compound, PJ34, **4c**, **4e**, and **4h**. Typically, a given simulation system comprised one PARP-1 catalytic domain and one compound, 18,652 water molecules, 52 Na^+ ions, and 53 Cl^- ions (0.15 M NaCl concentration), *i.e.*, a total of 61,652 atoms in a 87 Å×87 Å×87 Å box. We relaxed the systems using the equilibration steps in CHARMM-GUI and performed NPT dynamics for 200 ns with 2 fs time step. Nosé-Hoover constant pressure (1 bar) and temperature (300 K) were used. Contact duration between the target and compound and their hydrogen bond formation were analyzed using VMD 1.9.4.[62] Data visualization was performed using PyMOL 2.3.5[56] and Gnuplot.[63] Binding affinities were calculated using PRODIGY-LIG software,[64] using as input the snapshots from MD simulations.

Synthetic Chemistry Methods

All chemicals and solvents were purchased from Sigma–Aldrich. Melting points (M.p.) were determined with a Stuart SMP40 apparatus with parameters for the melting point analysis set at a 2 °C/ min ramp; values are expressed in °C. The HR-MS identification of compounds was performed on an Agilent 6540 UHD Accurate-Mass Q-TOF LC/MS G6540 A Mass Spectrometer. ^{1}H- and ^{13}C-NMR spectra were recorded on a Bruker Avance III spectrometer operating at 400 MHz for ^{1}H-NMR and 101 MHz for ^{13}C-NMR.

General Synthetic Procedures

The synthesis of novel phenanthridinone-based PAPR1 inhibitors consists of four main steps: (1) synthesis of *N*-(benzyloxy)benzamides; (2) synthesis of *N*-(benzyloxy)phenanthridinones; (3) reduction of the nitro group; (4) synthesis of the lead compounds.

General Procedure 1 (GP1). Synthesis of N-(Benzyloxy)benzamides (**1a–1f**)

_N_-(Benzyloxy)benzamide (*Scheme 7*; **1a**).

To a solution of the corresponding acid (10.0 mmol) in 25 mL of dry tetrahydrofuran (THF) at room temperature (r.t.) was added white, powdery 1,1′-carbonyldiimidazole (CDI; 15.0 mmol). The mixture was vigorously stirred under nitrogen at r.t. for 1 h and then *N*-benzylhydroxylamine (12 mmol) was added dropwise for 30 min. After being stirred at ambient conditions for 12 h, the resulting mixture was concentrated *in vacuo*. The residue was acidified with hydrochloric acid to pH 1 and diluted with 25 mL of dichloromethane (CH_2Cl_2) and the layers were separated. The aqueous layer was washed with brine and 25 mL of CH_2Cl_2 for a second time. The combined organic layers were dried over sodium sulfate and concentrated *in vacuo*. The crude product was recrystallized using ethyl acetate (AcOEt)/hexanes. The final compound was obtained as a white solid in 82% yield: M.p. 104 °C. HR-EI-MS: 250.0835 ($[M+Na]^+$; calc. 250.0838). ^{1}H-NMR (400 MHz, $CDCl_3$): 9.41 (s, 1H), 7.60–7.53 (m, 2H), 7.34 (t, J = 7.4, 1H), 7.28–7.19 (m, 7H), 4.86 (s, 2H). ^{13}C-NMR (101 MHz, $CDCl_3$): 166.5 (*C*(O)NH), 135.4 (CH_2C_{Bn}), 131.0 (CH_{Ar}), 131.0 (CH_{Bn}), 129.3 (CH_{Ar}), 128.7 (CH_{Ar}), 128.6 (C(O)C_{Ar}), 128.6 (CH_{Bn}), 127.2 (CH_{Bn}), 78.3 (CH_2Ph).

***N*-(Benzyloxy)-3-methoxybenzamide** (**1b**). Compound **1b** was prepared according to *GP1* and obtained as a viscous, slowly crystallizing oil in 91% yield. M.p. 112 °C. HR-EI-MS: 258.1121 ($[M+H]^+$; calc. 258.1125). ^{1}H-NMR (400 MHz, $CDCl_3$): 8.82 (s, 1H), 7.43 (dd, J = 6.4, 3.4, 2H), 7.37 (dd, J = 5.1, 2.2, 3H), 7.29–

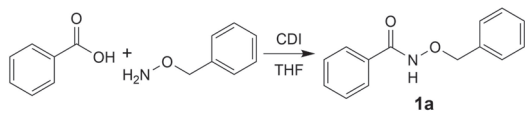

1a

Scheme 7. Synthesis of *N*-(benzyloxy)benzamide (**1a**).

© 2023 Wiley-VHCA AG, Zurich, Switzerland

15222675, 2023, 10, Downloaded from https://onlinelibrary.wiley.com/doi/10.1002/hlca.202300133 by Tallin Technical University, Wiley Online Library on [09/11/2023]. See the Terms and Conditions (https://onlinelibrary.wiley.com/terms-and-conditions) on Wiley Online Library for rules of use; OA articles are governed by the applicable Creative Commons License

7.23 (m, 2H), 7.17 (dt, J = 7.6, 1.2, 1H), 7.02 (dd, J = 7.7, 2.2, 1H), 5.01 (s, 2H), 3.80 (s, 3H). ^{13}C-NMR (101 MHz, $CDCl_3$): 166.4 (*C*(O)NH),159.9 (CH_3OC_{Ar}), 135.3 (CH_2C_{Bn}), 133.4 (C(O)C_{Ar}), 129.8 (CH_{Bn}), 129.5 (CH_{Bn}), 128.9 (CH_{Bn}), 128.8 (CH_{Ar}), 119.0 (CH_{Ar}), 118.4 (CH_{Ar}), 112.4 (CH_{Ar}), 78.5 (CH_2Ph), 55.5 (OCH_3).

***N*-(Benzyloxy)-4-methoxybenzamide** (**1c**). Compound **1c** was prepared according to *GP1* and obtained as a white solid in 96% yield. M.p. 131 °C. HR-EI-MS: 258.1120 ($[M+H]^+$; calc. 258.1125). ^{1}H-NMR (400 MHz, $CDCl_3$): 8.71 (s, 1H), 7.65 (dd, J = 9.4, 2.5, 2H), 7.47–7.40 (m, 2H), 7.37 (dd, J = 6.6, 1.4, 3H), 6.91–6.83 (m, 2H), 5.00 (s, 2H), 3.82 (s, 3H). ^{13}C-NMR (101 MHz, $CDCl_3$): 166.4 (*C*(O)NH), 162.7 (CH_3OC_{Ar}), 135.5 (CH_2C_{Bn}), 129.4 (C(O)C_{Ar}), 129.1 (CH_{Bn}), 128.9 (CH_{Bn}), 128.8 (CH_{Bn}), 124.2 (CH_{Ar}), 114.0 (CH_{Ar}), 78.5 (CH_2Ph), 55.5 (OCH_3).

2-[(Benzyloxy)carbamoyl)]phenyl Acetate (**1d**). Compound **1d** was prepared according to *GP1* and obtained as a white crystalline (needles) solid in 76% yield. M.p. 128 °C. HR-EI-MS: 286.1069 ($[M+H]^+$; calc. 286.1074). ^{1}H-NMR (400 MHz, $CDCl_3$): 8.70 (s, 1H), 7.74–7.67 (m, 1H), 7.51–7.44 (m, 2H), 7.43–7.36 (m, 5H), 7.29 (dd, J = 7.6, 1.1, 2H), 7.09 (dd, J = 8.1, 1.2, 1H), 5.01 (s, 2H), 2.10 (s, 3H). ^{13}C-NMR (101 MHz, $CDCl_3$): 169.1 (CH_3C(O)O), 148.2 (*C*(O)NH), 132.6 (CH_3C(O)OC_{Ar}), 130.0 (CH_2C_{Bn}), 129.3 (C(O)C_{Ar}), 129.0 (CH_{Bn}), 128.9 (CH_{Bn}), 128.5 (CH_{Bn}), 128.1 (CH_{Ar}), 126.4 (CH_{Ar}), 123.4 (CH_{Ar}), 119.1 (CH_{Ar}), 78.3 (CH_2Ph), 21.0 (CH_3C(O)O).

***N*-(Benzyloxy)-4-nitrobenzamide** (**1e**). Compound **1e** was prepared according to *GP1* and obtained as a yellowish solid in 79% yield. M.p. 166 °C. HR-EI-MS: 295.069 ($[M+Na]^+$; calc. 295.0689). ^{1}H-NMR (400 MHz, DMSO-d_6): 12.11 (s, 1H), 8.34–8.29 (m, 2H), 7.99–7.95 (m, 2H), 7.50–7.44 (m, 2H), 7.40 (t, J = 6.9, 3H), 4.96 (s, 2H). ^{13}C-NMR (101 MHz, DMSO-d_6): 162.6 (*C*(O)NH), 149.3 ($C_{Ar}NO_2$), 138.0 (CH_{Ar}), 135.7 (CH_2C_{Bn}), 129.1 (C(O)C_{Ar}), 128.7 (CH_{Bn}), 128.5 (CH_{Bn}), 128.4 (CH_{Bn}), 123.7 (CH_{Ar}), 77.2 (CH_2Ph).

***N*-(Benzyloxy)-2,3,4,5-tetrafluorobenzamide** (**1f**). Compound **1f** was prepared according to *GP1* and obtained as a white powder in 76% yield. M.p. 146 °C. HR-EI-MS: 300.0648 ($[M+Na]^+$; calc. 300.0642). ^{1}H-NMR (400 MHz, $CDCl_3$): 9.14 (s, 1H), 7.67 (q, J = 8.5, 1H), 7.45–7.34 (m, 6H), 5.02 (s, 2H). ^{13}C-NMR (101 MHz, $CDCl_3$): 159.1 (*C*(O)NH), 147.6 (dm, $^1J_{CF}$ = 251.1) (CF_{Ar}), 146.0 (dm, $^1J_{CF}$ = 247.1) (CF_{Ar}), 143.0 (dm, $^1J_{CF}$ = 259.7) (CF_{Ar}), 141.0 (dm, $^1J_{CF}$ = 260.2) (CF_{Ar}), 135.0 (CH_2C_{Bn}), 129.4 (C(O)C_{Ar}), 129.2 (CH_{Bn}), 129.0 (CH_{Bn}), 115.5 (CH_{Bn}), 113.0 (d, $^2J_{CF}$ = 21.2) (CH_{Ar}), 78.9 (CH_2Ph).

General Procedure 2 (*GP2*). *Synthesis of* N-*(benzyloxy)phenanthridinones* (**2a**–**2k**)

5-(Benzyloxy)phenanthridin-6(5*H*)-one (*Scheme 8*; **2a**).

To a solution of the corresponding *N*-(benzyloxy)benzamide **1a** (2.0 mmol) in 25 mL of glacial acetic acid at r.t. was added (3.5 mmol) iodobenzene, followed by grey, powdery silver oxide (4 mmol) and palladium catalyst (5 mol-%). The obtained mixture was degassed and flushed with nitrogen three times. After being heated at 120 °C for 24 h, the resulting mixture was concentrated *in vacuo*. The resulting residue was filtered on a short pad with Celite and CH_2Cl_2 as an eluent, followed by concentration by rotary evaporation. The crude product was purified by column chromatography using petroleum ether (PE)/AcOEt (4:1) as an eluent. The product was obtained as crystals in 82% yield. M.p. 145 °C. HR-EI-MS: ($[M+H]^+$; calc. 302.1176) 302.1175. ^{1}H-NMR (400 MHz, $CDCl_3$): 8.60 (dd, J = 8.0, 1.5, 1H), 8.33–8.23 (m, 2H), 7.80 (ddd, J = 8.4, 7.2, 1.4, 1H), 7.72–7.61 (m, 4H), 7.55 (ddd, J = 8.4, 7.2, 1.4, 1H), 7.46–7.40 (m, 3H), 7.34 (ddd, J = 8.2, 7.2, 1.2, 1H), 5.31 (s, 2H). ^{13}C-NMR (101 MHz, $CDCl_3$): 157.7 (*C*(O)N), 136.6 (C_{Ar}N), 134.2 (CH_2C_{Bn}), 133.2 (CH_{Ar}), 132.8 (CH_{Ar}), 130.0 (CH_{Ar}), 130.0 (CH_{Ar}), 129.3 (CH_{Bn}), 128.8 (C_{Ar}), 128.7 (CH_{Bn}), 128.3 (C_{Ar}), 126.6 (CH_{Ar}), 123.3(CH_{Ar}), 123.3 (CH_{Ar}), 122.1 (C_{Ar}), 118.6 (CH_{Bn}), 113.1 (CH_{Ar}), 77.2 (CH_2Ph).

5-(Benzyloxy)-10-methoxyphenanthridin-6(5*H*)-one (**2b**). Compound **2b** was synthesized according to *GP2* and obtained as a white powder in 86% yield. M.p. 152 °C. HR-EI-MS: 332.1276 ($[M+H]^+$; calc. 332.1281). ^{1}H-NMR (400 MHz, $CDCl_3$): 8.20 (dd, J = 12.5, 8.6, 2H), 8.02 (d, J = 2.8, 1H), 7.71 (d, J = 8.4, 1H), 7.67 (d, J = 7.6, 2H), 7.51 (t, J = 8.5, 1H), 7.48–7.36 (m, 4H),

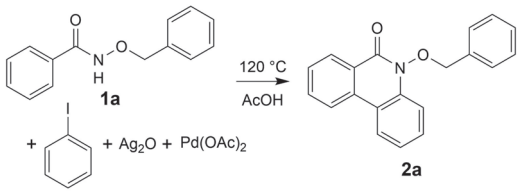

Scheme 8. Synthesis of 5-(benzyloxy)phenanthridin-6(5*H*)-one (**2a**).

© 2023 Wiley-VHCA AG, Zurich, Switzerland

15222675, 2023, 10, Downloaded from https://onlinelibrary.wiley.com/doi/10.1002/hlca.202300133 by Tallin Technical University, Wiley Online Library on [09/11/2023]. See the Terms and Conditions (https://onlinelibrary.wiley.com/terms-and-conditions) on Wiley Online Library for rules of use; OA articles are governed by the applicable Creative Commons License

7.33 (t, J=7.7, 1H), 5.31 (s, 2H), 3.99 (s, 3H). ^{13}C-NMR (101 MHz, $CDCl_3$): 159.7 (*C*(O)N), 157.5 ($C_{Ar}OCH_3$), 135.4 (C_{Ar}N),134.2 (CH_2C_{Bn}), 130.0 (CH_{Ar}), 129.3 (CH_{Bn}), 128.9 (C_{Ar}), 128.8 (CH_{Bn}), 127.8 (C_{Ar}), 126.7 (CH_{Ar}), 123.9 (CH_{Ar}), 123.4 (CH_{Ar}), 122.7 (CH_{Ar}), 122.6 (C_{Ar}), 118.6 (CH_{Bn}), 113.1 (CH_{Ar}), 108.9 (CH_{Ar}), 77.2 (CH_2Ph), 55.9 (OCH_3).

5-(Benzyloxy)-10-methoxy-2-nitrophenanthridin-6(5*H*)-one (**2c**). Compound **2c** was synthesized according to *GP2* and obtained as a greenish powder in 64% yield. M.p. 168 °C. HR-EI-MS: 377.1136 ([M+H]$^+$; calc. 377.1132). ^{1}H-NMR (400 MHz, $CDCl_3$): 9.05 (d, J=2.4, 1H), 8.34–8.25 (m, 2H), 8.01 (d, J=2.8, 1H), 7.73 (d, J=9.2, 1H), 7.64–7.56 (m, 2H), 7.51–7.38 (m, 4H), 5.34 (s, 2H), 4.01 (s, 3H). ^{13}C-NMR (101 MHz, $CDCl_3$): 160.8 (*C*(O)N), 157.6 ($C_{Ar}OCH_3$), 143.4 ($C_{Ar}NO_2$), 139.6 (C_{Ar}N), 133.5 (CH_2C_{Bn}), 130.1 (CH_{Ar}), 129.7 (CH_{Bn}), 129.00 (C_{Ar}), 128.2 (CH_{Bn}), 125.3 (C_{Ar}), 124.4 (CH_{Ar}), 123.6 (CH_{Ar}), 123.3 (C_{Ar}), 118.9 (CH_{Ar}), 118.7 (CH_{Bn}), 113.8 (CH_{Ar}), 109.4 (CH_{Ar}), 78.00 (CH_2Ph), 56.0 (OCH_3).

5-(Benzyloxy)-9-methoxyphenanthridin-6(5*H*)-one (**2d**). Compound **2d** was synthesized according to *GP2* and obtained as a white powder in 72% yield. M.p. 161 °C. HR-EI-MS: 332.1279 ([M+H]$^+$; calc. 332.1281). ^{1}H-NMR (400 MHz, $CDCl_3$): 8.52 (d, J=8.8, 1H), 8.20 (d, J=6.8, 1H), 7.72–7.62 (m, 4H), 7.59–7.51 (m, 1H), 7.47–7.40 (m, 3H), 7.32 (dd, J=8.2, 7.1, 1H), 7.19 (dd, J=8.9, 2.4, 1H), 5.30 (s, 2H), 4.01 (s, 3H). ^{13}C-NMR (101 MHz, $CDCl_3$): 163.3 (*C*(O)N), 157.6 ($C_{Ar}OCH_3$), 137.0 (C_{Ar}N), 135.2 (CH_2C_{Bn}), 134.3 (CH_{Ar}), 130.8 (CH_{Ar}), 130.2 (C_{Ar}), 130.0 (CH_{Bn}), 129.3 (C_{Ar}), 128.8 (CH_{Bn}), 123.3 (CH_{Ar}), 123.0 (CH_{Ar}), 120.1 (C_{Ar}), 118.3 (CH_{Ar}), 116.1 (CH_{Bn}), 113.2 (CH_{Ar}), 105.1 (CH_{Ar}), 77.23 (CH_2Ph), 55.8 (OCH_3).

5-(Benzyloxy)-7-hydroxyphenanthridin-6(5*H*)-one (**2e**). Compound **2e** was synthesized according to *GP2* and obtained as a white powder in 74% yield. M.p. 154 °C. HR-EI-MS: 318.1121 ([M+H]$^+$; calc. 318.1125). ^{1}H-NMR (400 MHz, $CDCl_3$): 12.79 (s, 1H), 8.23 (dd, J=8.1, 1.4, 1H), 7.75–7.63 (m, 5H), 7.60–7.52 (m, 1H), 7.48–7.41 (m, 3H), 7.36 (t, J=7.7, 1H), 7.07 (dd, J=8.0, 1.1, 1H), 5.30 (s, 2H). ^{13}C-NMR (101 MHz, $CDCl_3$): 162.3 (*C*(O)N), 161.7 (C_{Ar}OH), 135.6 (C_{Ar}N), 134.9 (CH_2C_{Bn}), 134.2 (CH_{Ar}), 133.8 (CH_{Ar}), 130.2 (C_{Ar}), 130.0 (CH_{Bn}), 129.5 (C_{Ar}), 128.9 (CH_{Bn}), 124.1 (CH_{Ar}), 123.9 (CH_{Ar}), 119.2 (C_{Ar}), 115.5 (CH_{Ar}), 113.3 (CH_{Ar}), 112.3 (CH_{Bn}), 110.9 (CH_{Ar}), 77.7 (CH_2Ph).

5-(Benzyloxy)-9-nitrophenanthridin-6(5*H*)-one (**2f**). Compound **2f** was synthesized according to *GP2* and obtained as a yellowish powder in 78% yield. M.p. 163 °C. HR-EI-MS: 347.1023 ([M+H]$^+$; calc. 347.1026). ^{1}H-NMR (400 MHz, DMSO-d_6): 8.78 (d, J=8.9, 1H), 8.68 (d, J=8.1, 1H), 8.47 (dd, J=8.0, 1.4, 1H), 8.30 (d, J=2.3, 1H), 8.14 (dd, J=8.8, 2.4, 1H), 8.00 (ddd, J=8.4, 7.3, 1.5, 1H), 7.90–7.81 (m, 1H), 7.66–7.58 (m, 2H), 7.50–7.36 (m, 3H), 5.35 (s, 2H). ^{13}C-NMR (101 MHz, DMSO-d_6): 156.3 (*C*(O)N), 150.7 ($C_{Ar}NO_2$), 137.1 (C_{Ar}N), 134.4 (CH_2C_{Bn}), 133.7 (CH_{Ar}), 131.6 (C_{Ar}), 130.7 (CH_{Bn}), 130.5 (C_{Ar}), 130.0 (CH_{Bn}), 129.6 (CH_{Ar}), 128.9 (CH_{Ar}), 124.0 (CH_{Ar}), 123.7 (C_{Ar}), 121.9 (CH_{Ar}), 118.0 (CH_{Ar}), 117.4 (CH_{Bn}), 113.6 (CH_{Ar}), 77.6 (CH_2Ph).

5-(Benzyloxy)-2-iodophenanthridin-6(5*H*)-one (**2g**). Compound **2g** was synthesized according to *GP2* and obtained as a grey viscous solid in 75% yield. M.p. 173 °C. HR-EI-MS: 428.0124 ([M+H]$^+$; calc. 428.0142). ^{1}H-NMR (400 MHz, $CDCl_3$): 8.64–8.53 (m, 4H), 8.23 (d, J=7.7, 2H), 7.86–7.76 (m, 4H), 7.75–7.58 (m, 7H), 7.48–7.37 (m, 9H), 5.29 (s, 4H). ^{13}C-NMR (101 MHz, $CDCl_3$): 157.4 (*C*(O)N), 138.5 (C_{Ar}N), 136.2 (CH_{Ar}), 133.9 (CH_2C_{Bn}), 133.0 (C_{Ar}), 132.1 (C_{Ar}),131.9 (CH_{Bn}), 130.0 (C_{Ar}), 129.5 (CH_{Bn}), 128.9 (CH_{Ar}), 128.8 (CH_{Ar}), 126.7 (CH_{Ar}), 122.2 (CH_{Ar}), 122.1 (CH_{Bn}), 120.6 (CH_{Ar}), 115.2 (CH_{Ar}), 86.6 (Cl_{Ar}), 77.4 (CH_2Ph).

5-(Benzyloxy)-7,8,9,10-tetrafluorophenanthridin-6(5*H*)-one (**2h**). Compound **2h** was synthesized according to *GP2* and obtained as a white solid in 23% yield. M.p. 141 °C. HR-EI-MS: 374.0790 ([M+H]$^+$; calc. 374.0799). ^{1}H-NMR (400 MHz, $CDCl_3$): 8.59 (dt, J=8.4, 1.9, 1H), 7.71 (dd, J=8.4, 1.4, 1H), 7.63 (t, J=8.1, 3H), 7.51–7.31 (m, 5H), 5.26 (s, 2H). ^{13}C-NMR (101 MHz, $CDCl_3$): 153.2 (*C*(O)N), 148.3 (dm, $^1J_{CF}$=259.5) (CF_{Ar}), 144.9 (dm, $^1J_{CF}$=249.9) (CF_{Ar}), 143.8 (dm, $^1J_{CF}$=259.7) (CF_{Ar}), 139.8 (q, $^1J_{CF}$=259.6) (CF_{Ar}), 136.3 (C_{Ar}N), 133.6 (CH_2C_{Bn}), 131.5 (C_{Ar}), 131.2 (CH_{Bn}), 130.1 (CH_{Ar}), 129.67 (C_{Ar}), 128.9 (CH_{Bn}), 127.7 (q, $^2J_{CF}$= 19.4) (C_{Ar}), 124.1 (CH_{Ar}), 114.2 (CH_{Ar}), 113.0 (CH_{Bn}), 112.0 (CH_{Ar}), 77.4 (CH_2Ph).

5-(Benzyloxy)-3-nitrophenanthridin-6(5*H*)-one (**2i**). Compound **2i** was synthesized according to *GP2* and obtained as a yellowish solid in 42% yield. M.p. 154 °C. HR-EI-MS: 347.1030 ([M+H]$^+$; calc. 347.1026). ^{1}H-NMR (400 MHz, $CDCl_3$): 8.65 (ddd, J=7.9, 1.5, 0.6, 1H), 8.50 (d, J=2.3, 1H), 8.40–8.29 (m, 2H), 8.13 (dd, J=8.8, 2.3, 1H), 7.89 (ddd, J=8.3, 7.2, 1.5, 1H), 7.77 (ddd, J=8.2, 7.2, 1.1, 1H), 7.68–7.58 (m, 2H), 7.46–7.34 (m, 3H), 5.38 (s, 2H). ^{13}C-NMR (101 MHz, $CDCl_3$): 156.5 (*C*(O)N), 147.7 ($C_{Ar}NO_2$), 136.5 (C_{Ar}N), 133.8 (CH_2C_{Bn}), 133.6 (CH_{Ar}), 131.1 (CH_{Bn}), 130.4 (CH_{Ar}), 130.0 (C_{Ar}),

© 2023 Wiley-VHCA AG, Zurich, Switzerland

15222675, 2023, 10, Downloaded from https://onlinelibrary.wiley.com/doi/10.1002/hlca.202300133 by Tallin Technical University, Wiley Online Library on [09/11/2023]. See the Terms and Conditions (https://onlinelibrary.wiley.com/terms-and-conditions) on Wiley Online Library for rules of use; OA articles are governed by the applicable Creative Commons License

129.3 (CH_{Bn}), 128.7 (C_{Ar}), 128.0 (CH_{Ar}), 126.7 (CH_{Ar}), 125.5 (CH_{Ar}), 124.2 (C_{Ar}), 123.1 (CH_{Ar}), 117.3 (CH_{Bn}), 108.1 (CH_{Ar}), 77.2 (CH_2Ph).

5-(Benzyloxy)-2-nitrophenanthridin-6(5*H*)-one (**2j**). Compound **2j** was synthesized according to *GP2* and obtained as a yellowish solid in 46% yield. M.p. 149 °C. HR-EI-MS: 347.1019 ($[M+H]^+$; calc. 347.1026). ^{1}H-NMR (400 MHz, $CDCl_3$): 9.15 (d, J = 2.4, 1H), 8.61 (dd, J = 8.0, 1.4, 1H), 8.41–8.31 (m, 2H), 7.91 (ddd, J = 8.2, 7.3, 1.5, 1H), 7.81–7.69 (m, 2H), 7.65–7.56 (m, 2H), 7.48–7.34 (m, 3H), 5.34 (s, 2H). ^{13}C-NMR (101 MHz, $CDCl_3$): 157.6 (C(O)N), 148.3 ($C_{\mathbf{Ar}}NO_2$), 137.2 (C_{Ar}N), 133.4 (CH_2C_{Bn}), 131.5 (CH_{Ar}), 130.4 (CH_{Bn}), 130.3 (CH_{Ar}), 130.3 (CH_{Bn}), 129.8 (CH_{Ar}), 129.1 (CH_{Ar}),129.0 (C_{Ar}), 127.5 (CH_{Ar}), 124.4 (CH_{Ar}), 123.4 (C_{Ar}),123.2 (C_{Ar}), 117.6 (CH_{Bn}), 109.2 (CH_{Ar}), 78.1 (CH_2Ph).

5-(Benzyloxy)-7-hydroxy-3-nitrophenanthridin-6(5*H*)-one (**2k**). Compound **2k** was synthesized according to *GP2* and obtained as a yellowish solid in 66% yield. M.p. 157 °C. HR-EI-MS: 363.0975 ($[M+H]^+$; calc. 363.0975). ^{1}H-NMR (400 MHz, $CDCl_3$): 12.55 (s, 1H), 8.47 (d, J = 2.3, 1H), 8.33 (d, J = 8.9, 1H), 8.14 (dd, J = 8.9, 2.3, 1H), 7.81–7.70 (m, 2H), 7.65–7.57 (m, 2H), 7.47–7.36 (m, 3H), 7.20 (dd, J = 7.0, 2.2, 1H), 5.36 (s, 2H). ^{13}C-NMR (101 MHz, $CDCl_3$): 162.5 (C(O)N), 161.9 ($C_{\mathbf{Ar}}OH$), 148.3 ($C_{\mathbf{Ar}}NO_2$), 136.2 (C_{Ar}N), 135.5 (CH_2C_{Bn}), 133.0 (CH_{Ar}), 132.3 (CH_{Bn}), 130.4 (C_{Ar}), 130.0 (CH_{Bn}), 129.1 (CH_{Ar}), 125.0 (CH_{Ar}), 124.0 (C_{Ar}), 118.3 (CH_{Ar}), 117.9 (CH_{Ar}), 113.4 (C_{Ar}), 111.3 (CH_{Bn}), 109.5 (CH_{Ar}), 78.6 (CH_2Ph).

*General Procedure 3 (GP3). Synthesis of Amino Derivatives **3a** and **3b***

Preparation of NiB_2 Catalyst. To a solution of nickel acetate (1 mmol) in 50 mL of MeOH was added sodium borohydride (2 mmol) over a period of 30 min under vigorous stirring. The obtained mixture was further stirred for 30 min and left standing for 1 h to precipitate the produced catalyst. Thereafter, the dark residue was filtered off on filter paper and washed with an excess of MeOH to remove sodium hydroxide, the by-product of the borohydride oxidation. This catalyst could be stored in MeOH for up to 2 days without losing its catalytic activity.

5-(Benzyloxy)-6-oxo-5,6-dihydrophenanthridin-3-aminium Chloride (*Scheme 9*; **3a**).

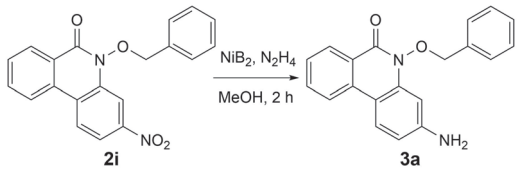

Scheme 9. Synthesis of 5-(benzyloxy)-6-oxo-5,6-dihydrophenanthridin-3-aminium chloride (**3a**).

To a solution of the corresponding nitro derivative of 5-(benzyloxy)-3-nitrophenanthridin-6(5*H*)-one (**2i**; 1.0 mmol) in 50 mL of methanol (MeOH) at r.t. was added the freshly prepared NiB_2 catalyst, followed by an excess of hydrazine. The reaction was heated to 50 °C for autocatalytic activation. The progress of reduction was monitored by thin layer chromatography, then the solution was filtered to remove the catalyst on Celite®. The resulting solution was concentrated *in vacuo* and the residue was washed with diluted hydrochloric acid. The obtained salt was insoluble in water and cleared of the impurities on the glass filter by 2–3 drops of CH_2Cl_2. A grey powder was obtained in 97% yield. M.p. 173 °C. HR-EI-MS: 317.1278 ($[M+H]^+$; calc. 317.1285). ^{1}H-NMR (400 MHz, DMSO-d_6): 10.13 (br. s, 2H), 8.44 (dd, J = 8.0, 1.4, 1H), 8.41–8.31 (m, 3H), 7.98–7.92 (m, 1H), 7.79–7.73 (m, 2H), 7.67–7.66 (m, 1H), 7.58 (dd, J = 8.9, 2.2, 1H), 7.49–7.44 (m, 3H), 5.26 (s, 2H). ^{13}C-NMR (101 MHz, DMSO-d_6): 156.2 (C(O)N), 134.6 (C_{Ar}N), 134.0 (CH_2C_{Bn}), 133.4 ($C_{Ar}NH_2$), 131.7 (CH_{Bn}), 129.9 (C_{Ar}), 129.2 (CH_{Ar}), 129.1 (CH_{Bn}), 129.1 (CH_{Ar}), 128.6 (C_{Ar}), 128.0 (CH_{Ar}), 126.1 (CH_{Ar}), 124.5 (CH_{Ar}), 122.5 (CH_{Ar}), 118.4 (C_{Ar}), 117.0 (CH_{Bn}), 114.2 (CH_{Ar}), 76.6 (CH_2Ph).

5-(Benzyloxy)-6-oxo-5,6-dihydrophenanthridin-2-aminium Chloride (**3b**). Compound **3b** was synthesized according to *GP3* and obtained as a grey powder in 98% yield. M.p. 164 °C. HR-EI-MS: 317.1281 ($[M+H]^+$; calc. 317.1285). ^{1}H-NMR (400 MHz, DMSO-d_6): 10.17 (br. s, 2H), 8.46–8.35 (m, 3H), 7.97 (ddd, J = 8.4, 7.2, 1.5, 1H), 7.80–7.73 (m, 2H), 7.69–7.64 (m, 2H), 7.59 (dd, J = 8.9, 2.2, 1H), 7.48–7.41 (m, 3H), 5.26 (s, 2H), 3.55 (s, 3H). ^{13}C-NMR (101 MHz, DMSO-d_6): 155.4 (C(O)N), 134.3 (C_{Ar}N), 132.7 (CH_2C_{Bn}), 132.6 ($C_{Ar}NH_2$), 129.7 (CH_{Bn}), 129.0 (C_{Ar}), 128.5 (CH_{Ar}), 127.9 (CH_{Bn}), 127.8 (CH_{Ar}), 127.2 (C_{Ar}), 126.08 (CH_{Ar}), 125.9 (CH_{Ar}), 122.3 (CH_{Ar}), 118.6 (CH_{Ar}), 117.8 (C_{Ar}), 113.6 (CH_{Bn}), 106.4 (CH_{Ar}), 76.2 (CH_2Ph).

© 2023 Wiley-VHCA AG, Zurich, Switzerland

15222675, 2023, 10, Downloaded from https://onlinelibrary.wiley.com/doi/10.1002/hlca.202300133 by Tallin Technical University, Wiley Online Library on [09/11/2023]. See the Terms and Conditions (https://onlinelibrary.wiley.com/terms-and-conditions) on Wiley Online Library for rules of use; OA articles are governed by the applicable Creative Commons License

General Procedure 4 (GP4). Synthesis of the Compounds **4a–4h**

5-Hydroxyphenanthridin-6(5H)-one (*Scheme 10*; **4a**).

A stirred solution of **2a** (0.5 mmol) in dry MeOH (10 mL) in an argon atmosphere was treated with a catalytic quantity of Pd/C at r.t., kept stirring overnight at ambient temperature and hydrogen was bubbled through the reaction mixture. The mixture was filtered through a plug of Celite® and concentrated *in vacuo* to give the desired product as a white powder in 84% yield. M.p. 257 °C. HR-EI-MS: 212.0703 ($[M+H]^+$; calc. 212.0706). ^{1}H-NMR (400 MHz, DMSO-d_6): 11.36 (s, 1H), 8.58 (d, J = 8.2, 1H), 8.51 (d, J = 8.0, 1H), 8.39 (d, J = 7.9, 1H), 7.88 (t, J = 7.0, 1H), 7.78 (d, J = 8.3, 1H), 7.70–7.63 (m, 2H), 7.38 (t, J = 7.6, 1H). ^{13}C-NMR (101 MHz, DMSO-d_6): 156.7 (*C*(O)N), 136.9 (C_{Ar}N), 132.5 (C_{Ar}), 132.3 (C_{Ar}), 130.1 (C_{Ar}), 128.2 (CH_{Ar}), 127.5 (CH_{Ar}), 125.4 (CH_{Ar}), 123.4 (CH_{Ar}), 122.8 (CH_{Ar}), 122.7 (CH_{Ar}), 117.4 (CH_{Ar}), 113.1 (CH_{Ar}).

5-Hydroxy-10-methoxyphenanthridin-6(5*H*)-one (**4b**). To a stirred solution of **2b** (0.5 mmol) in dry MeOH (10 mL) in an argon atmosphere was added a catalytic quantity of Pd/C at r.t. The solution was stirred overnight at ambient temperature and hydrogen was bubbled through the reaction mixture. The mixture was filtered through a plug of Celite® and concentrated *in vacuo* to give the desired product as a white powder in 84% yield. M.p. 262 °C. HR-EI-MS: 242.0807 ($[M+H]^+$; calc. 242.0812). ^{1}H-NMR (400 MHz, DMSO-d_6): 11.36 (s, 1H), 8.51 (d, J = 9.0, 1H), 8.45–8.39 (m, 1H), 7.83–7.72 (m, 2H), 7.58 (ddd, J = 8.4, 7.1, 1.3, 1H), 7.47 (dd, J = 8.9, 2.9, 1H), 7.39–7.31 (m, 1H), 3.96–3.89 (m, 3H). ^{13}C-NMR (101 MHz, DMSO-d_6): 159.2 (*C*(O)N), 156.4 ($C_{Ar}OCH_3$), 135.9 (C_{Ar}N), 128.9 (C_{Ar}), 126.8 (C_{Ar}), 125.7 (C_{Ar}), 124.7 (CH_{Ar}), 122.8 (CH_{Ar}), 121.4 (CH_{Ar}), 121.4 (CH_{Ar}), 117.4 (CH_{Ar}), 113.0 (CH_{Ar}), 108.6 (CH_{Ar}), 55.6 (OCH_3).

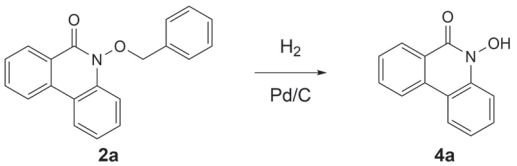

Scheme 10. Synthesis of 5-hydroxyphenanthridin-6(5*H*)-one (**4a**).

5-(Benzyloxy)-3-methoxyphenanthridin-6(5*H*)-one (**4c**). To a solution of **1a** (2.0 mmol) in 25 mL of glacial acetic acid at r.t. was added 1-iodo-4-methoxybenzene (3.5 mmol), followed by grey, powdery silver oxide (4 mmol) and orange palladium catalyst (5 mol-%). The resulting mixture was degassed and flushed with nitrogen three times. After being heated at 120 °C for 24 h, the resulting mixture was concentrated *in vacuo*. The resulting residue was filtered on a short pad with Celite® and CH_2Cl_2 as an eluent, followed by concentration by rotary evaporation. The crude product was purified by column chromatography using PE/AcOEt (4:1) as an eluent, and the product was obtained as white crystals in 84% yield. M.p. 147 °C. HR-EI-MS: 332.1276 ($[M+H]^+$; calc. 332.1281). ^{1}H-NMR (400 MHz, $CDCl_3$): 8.55 (dd, J = 8.0, 1.4, 1H), 8.16 (t, J = 9.0, 2H), 7.76 (ddd, J = 8.4, 7.2, 1.5, 1H), 7.67–7.61 (m, 2H), 7.55 (ddd, J = 8.1, 7.1, 1.1, 1H), 7.48–7.36 (m, 4H), 7.15 (d, J = 2.6, 1H), 6.90 (dd, J = 8.8, 2.6, 1H), 5.32 (s, 2H), 3.87 (s, 3H). ^{13}C-NMR (101 MHz, $CDCl_3$): 160.9 (*C*(O)N), 156.9 ($C_{Ar}OCH_3$), 137.6 (C_{Ar}N), 134.2 (CH_2C_{Bn}), 133.1 (C_{Ar}), 133.0 (C_{Ar}), 129.9 (C_{Ar}), 129.2 (CH_{Ar}), 128.6 (CH_{Bn}), 127.7 (CH_{Ar}),127.2 (CH_{Bn}), 125.4 (CH_{Ar}), 124.4 (CH_{Bn}), 122.3 (CH_{Ar}), 111.0 (CH_{Ar}), 110.9 (CH_{Ar}), 96.5 (CH_{Ar}), 76.6 (CH_2Ph), 55.4 (OCH_3).

5-Hydroxy-3-methoxyphenanthridin-6(5*H*)-one (**4d**). To a stirred solution of **4c** (0.5 mmol) in dry MeOH (10 mL) in an argon atmosphere, a catalytic quantity of Pd/C was added at r.t. The solution was stirred overnight at ambient temperature and hydrogen gas was bubbled through the reaction mixture. The mixture was filtered through a plug of Celite® and concentrated *in vacuo* to give desired product as a white powder in 89% yield. M.p. 156 °C. HR-EI-MS: 242.0803 ($[M+H]^+$; calc. 242.0812). ^{1}H-NMR (400 MHz, DMSO-d_6): 11.38 (s, 1H), 8.42 (dd, J = 14.9, 8.4, 2H), 8.33 (d, J = 7.8, 1H), 7.81 (t, J = 7.6, 1H), 7.59 (t, J = 7.5, 1H), 7.24 (d, J = 2.3, 1H), 7.00–6.93 (m, 1H), 3.89 (s, 3H). ^{13}C-NMR (101 MHz, DMSO-d_6): 160.8 (*C*(O)N), 157.0 ($C_{Ar}OCH_3$), 138.4 (C_{Ar}N), 132.5 (C_{Ar}), 132.4 (C_{Ar}), 127.4 (C_{Ar}), 127.0 (CH_{Ar}), 125.1 (CH_{Ar}), 124.0 (CH_{Ar}), 122.1 (CH_{Ar}), 110.7 (CH_{Ar}), 110.5 (CH_{Ar}), 96.7 (CH_{Ar}), 55.5 (OCH_3).

2-{[5-(benzyloxy)-6-oxo-5,6-dihydrophenanthridin-3-yl]amino}-*N*,*N*-dimethyl-2-oxoethan-1-aminium Chloride (*Scheme 11*; **4e**).

To a solution of **3a** (1 mmol) in 15 mL of dry CH_2Cl_2 was added triethylamine (2 mmol), followed by powdered *N*,*N*-dicyclohexylcarbodiimide (DCC, 2.0 mmol),

© 2023 Wiley-VHCA AG, Zurich, Switzerland

15222675, 2023, 10, Downloaded from https://onlinelibrary.wiley.com/doi/10.1002/hlca.202300133 by Tallin Technical University, Wiley Online Library on [09/11/2023]. See the Terms and Conditions (https://onlinelibrary.wiley.com/terms-and-conditions) on Wiley Online Library for rules of use; OA articles are governed by the applicable Creative Commons License

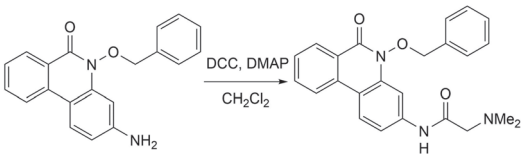

Scheme 11. Synthesis of 2-{[5-(benzyloxy)-6-oxo-5,6-dihydrophenanthridin-3-yl]amino}-*N*,*N*-dimethyl-2-oxoethan-1-aminium chloride (**4e**).

N,*N*-dimethylpyridin-4-amine (DMAP, 5 mol-%), and *N*,*N*-dimethylglycine (1.5 mmol). The mixture was stirring for 24 h at r.t., filtered through a plug of Celite® and concentrated *in vacuo*. The residue was washed with water (100 mL), brine (10 mL) and AcOEt (2×25 mL). The combined organic layer was separated and dried over anhydrous sodium sulfate. The solution was concentrated *in vacuo*. The residue was acidified with dilute aqueous hydrochloric acid to pH 2 and filtered on a glass filter, followed by flash column chromatography on silica gel with AcOEt and MeOH (10 : 1) as eluents to afford the corresponding product as a grey powdery salt in 77% yield. M.p. 183 °C. HR-EI-MS: 402.1803 ($[M+H]^+$; calc. 402.1812). ^{1}H-NMR (400 MHz, DMSO-d_6): 11.38 (s, 1H), 10.11 (s, 1H), 8.51 (dd, J = 8.7, 7.1, 2H), 8.39 (dd, J = 8.0, 1.4, 1H), 8.29 (d, J = 2.2, 1H), 7.89 (ddd, J = 8.4, 7.1, 1.5, 1H), 7.78–7.69 (m, 2H), 7.69–7.65 (m, 1H), 7.62 (dd, J = 8.8, 2.1, 1H), 7.53–7.41 (m, 3H), 5.23 (s, 2H), 4.24 (s, 2H), 2.91 (s, 6H). ^{13}C-NMR (101 MHz, DMSO-d_6): 169.1 (C(O)CH_2N(CH_3)$_2$), 156.7 (C(O)N), 140.7 (C_{Ar}NH), 136.4 (CH_2C_{Bn}), 133.9 (C_{Ar}N), 133.1 (C_{Ar}), 132.8 (C_{Ar}), 130.0 (C_{Ar}), 129.1 (CH_{Ar}), 128.5 (CH_{Ar}), 127.7 (CH_{Bn}), 127.6 (CH_{Ar}), 124.9 (CH_{Ar}), 124.5 (CH_{Ar}), 122.4 (CH_{Bn}), 114.8 (CH_{Ar}), 113.2 (CH_{Bn}), 102.3 (CH_{Ar}), 76.2 (CH_2Ph), 63.2 (C(O)CH_2N(CH_3)$_2$), 45.3 (N(CH_3)$_2$).

2-[(5-Hydroxy-6-oxo-5,6-dihydrophenanthridin-3-yl)amino]-*N*,*N*-dimethyl-2-oxoethan-1-aminium Chloride (**4f**). To a stirred solution of **4e** (0.5 mmol) in dry MeOH (10 mL) in an argon atmosphere was added a catalytic quantity of Pd/C at r.t. The solution was stirred overnight at ambient temperature and hydrogen gas was bubbled through the reaction mixture. The mixture was filtered through a plug of Celite® and concentrated *in vacuo* to give the desired product as a white powder in 89% yield. M.p. 271 °C. HR-EI-MS: 312.1343 ($[M+H]^+$; calc. 312.1343). ^{1}H-NMR (400 MHz, DMSO-d_6): 11.40 (s, 1H), 11.30 (s, 1H), 10.17 (s, 1H), 8.48 (dd, J = 8.6, 4.8, 2H), 8.35 (d, J = 7.9, 1H), 8.27–8.22 (m, 1H), 7.85 (t, J = 7.7, 1H), 7.68–7.58 (m, 2H), 4.18 (s, 2H), 2.88 (s, 6H). ^{13}C-NMR (101 MHz, DMSO-d_6): 163.9 (C(O)CH_2N(CH_3)$_2$), 157.0 (C(O)N), 139.7 (C_{Ar}NH), 137.6 (C_{Ar}N), 132.5 (C_{Ar}), 132.2 (C_{Ar}), 127.6 (C_{Ar}), 127.5 (CH_{Ar}), 124.7 (CH_{Ar}), 124.3 (CH_{Ar}), 122.3 (CH_{Ar}), 114.1 (CH_{Ar}), 113.4 (CH_{Ar}), 103.1 (CH_{Ar}), 58.3 (C(O)CH_2N(CH_3)$_2$), 43.4 (N(CH_3)$_2$).

2-{[5-(Benzyloxy)-6-oxo-5,6-dihydrophenanthridin-2-yl]amino}-*N*,*N*-dimethyl-2-oxoethan-1-aminium Chloride (**4g**). To a solution of **3b** (1 mmol) in 15 mL of dry CH_2Cl_2 was added triethylamine (2 mmol), followed by powdered DCC (2.0 mmol), DMAP (5 mol-%), and *N*,*N*-dimethylglycine (1.5 mmol). The mixture was stirred for 24 h at r.t., filtered through a plug of Celite® and concentrated *in vacuo*. The residue was washed with water (100 mL), brine (10 mL) and AcOEt (2×25 mL). The combined organic layers were dried over anhydrous sodium sulphate and concentrated *in vacuo*. The residue was acidified with dilute aqueous hydrochloric acid to pH 2 and filtered on a glass filter, followed by flash column chromatography on silica gel with AcOEt and MeOH (10 : 1) as eluents to afford the corresponding product as a grey powdery salt in 67% yield. M.p. 171 °C. HR-EI-MS: 402.1804 ($[M+H]^+$; calc. 402.1812). ^{1}H-NMR (400 MHz, DMSO-d_6): 11.57 (s, 1H), 10.32 (s, 1H), 8.83 (d, J = 2.2, 1H), 8.43 (dd, J = 8.0, 1.4, 1H), 8.28 (d, J = 8.2, 1H), 8.00–7.88 (m, 2H), 7.74 (t, J = 7.5, 1H), 7.71–7.62 (m, 4H), 7.50–7.38 (m, 4H), 5.26 (s, 2H), 4.26 (s, 2H), 2.92 (d, J = 2.6, 6H). ^{13}C-NMR (101 MHz, DMSO-d_6): 169.0 (C(O)CH_2N(CH_3)$_2$), 157.3 (C(O)N), 134.0 (C_{Ar}NH), 133.5 (CH_2C_{Bn}), 133.0 (C_{Ar}N), 132.8 (C_{Ar}), 132.6 (C_{Ar}), 129.9 (C_{Ar}), 129.2 (CH_{Ar}), 128.7 (CH_{Bn}), 128.5 (CH_{Ar}), 128.4 (CH_{Ar}), 126.7 (CH_{Ar}), 122.5 (CH_{Ar}), 121.5 (CH_{Bn}), 119.0 (CH_{Ar}), 113.7 (CH_{Bn}), 113.6 (CH_{Ar}), 77.23 (CH_2Ph), 63.7 (C(O)CH_2N(CH_3)$_2$), 46.1 (N(CH_3)$_2$).

2-[(5-Hydroxy-6-oxo-5,6-dihydrophenanthridin-2-yl)amino]-*N*,*N*-dimethyl-2-oxoethan-1-aminium Chloride (**4h**). To a stirred solution of **4g** (0.5 mmol) in dry MeOH (10 mL) in an argon atmosphere was added a catalytic quantity of Pd/C at r.t. The solution was stirred overnight at ambient temperature and hydrogen gas was bubbled through the reaction mixture. The mixture was filtered through a plug of Celite® and concentrated *in vacuo* to give the desired product as a white powder in 76% yield. M.p. 269 °C. HR-EI-MS: 312.1342 ($[M+H]^+$; calc. 312.1343). ^{1}H-NMR (400 MHz, $CDCl_3$): 11.38 (s, 1H), 9.28 (s, 1H), 8.63 (s, 1H), 8.52 (d, J = 8.0, 1H), 8.26 (d, J = 8.2, 1H), 7.74 (t, J = 7.7, 1H), 7.59–7.46 (m, 3H), 7.40 (d, J = 8.5, 2H), 3.16 (s, 2H), 2.43

© 2023 Wiley-VHCA AG, Zurich, Switzerland

15222675, 2023, 10, Downloaded from https://onlinelibrary.wiley.com/doi/10.1002/hlca.202300133 by Tallin Technical University, Wiley Online Library on [09/11/2023]. See the Terms and Conditions (https://onlinelibrary.wiley.com/terms-and-conditions) on Wiley Online Library for rules of use; OA articles are governed by the applicable Creative Commons License

(s, 6H). ^{13}C-NMR (101 MHz, $CDCl_3$): 168.9 (C(O)CH_2N-(CH_3)$_2$), 156.3 (C(O)N), 134.1 (C_{Ar}NH), 133.2 (C_{Ar}N), 132.3 (C_{Ar}), 131.8 (C_{Ar}), 128.2 (C_{Ar}), 127.5 (CH_{Ar}), 125.7 (CH_{Ar}), 122.3 (CH_{Ar}), 122.1 (CH_{Ar}), 117.4 (CH_{Ar}), 113.7 (CH_{Ar}), 113.4 (CH_{Ar}), 63.4 (C(O)CH_2N(CH_3)$_2$), 45.5 (N(CH_3)$_2$).

General Bioassay Procedures

Cell Cultures. Human embryonic kidney cells HEK 293, murine fibroblast NIH 3T3, human hepatoblastoma HepG2, human cervical cancer HeLa, human breast cancer MDA-MB-231 and human pancreatic cancer BxPC3 cell lines were obtained from the American Type Culture Collection. The cells were propagated in Dulbecco's modified Eagle's medium (DMEM) (Gibco), supplemented with 10% bovine calf serum (Gibco) and 5% penicillin/streptomycin. All cell lines were incubated at 37 °C in a humidified 5% CO_2 and 95% air atmosphere.

Cell Treatment Procedures. The cells were plated at a density of 2.5×10^5 cells/well (The Countess Automated Cell Counter, Invitrogen) in 96-well plates and incubated overnight. After 24 h of incubation, 100 μL of either fresh media or fresh media containing diluted agents (25 μM or 50 μM) was added into each well and incubated for a further 48 h. The experiments with addition of MeOH were used as a solvent control.

Cell Viability Measured by WST-1. The effects of agents on the viability of cells were determined using the cell viability assay WST-1 (Roche). WST-1 allows the colorimetric measurement of cell viability due to reduction of tetrazolium salts to water-soluble formazan by viable cells. The amount of formed formazan dye correlates with the number of viable cells. The measurements were completed 48 h after the cell treatments. Experiments with an addition of 5 μL of MeOH were used as a solvent control. Five microliters per well of the WST-1 reagent was added to 100 μL of the cell culture medium and incubated at 37 °C for 2 h, after which the absorbance was measured at 450 nm by using a TECAN GENios Pro Microplate Reader. Data is collected in *Table S6.*

PARP-1 Colorimetric Enzyme Assay. The PARP-1 enzymatic activity was measured following the manufacturer's instructions for the universal PARP colorimetric assay kit from R&D Systems, 4677-096-K. Briefly, increasing concentrations of compounds (0.01–100 μM) were added to histone-coated strip wells in a 96-well plate. Inhibitors were then pre-incubated for 10 min at r.t. with 0.5 U/well recombinant human PARP. Wells were then incubated for 1 h with PARP cocktail and then washed twice with phosphate buffered saline (PBS) containing 0.1% Triton X-100 and twice with PBS. Streptavidin-HRP was then added to each well and incubated for 1 h. Wells were again washed twice with PBS-0.1% Triton X-100 and twice with PBS. The colorimetric reaction was developed upon addition of TACS-Sapphire for 15 min, followed by reaction termination with 0.2 M HCl. Absorbance was measured on a TECAN GENios Pro Microplate Reader and enzyme inhibition curves were fit using non-linear regression dose-response inhibition equations from GraphPadPrism version 8.0.0 for Windows, GraphPad Software, San Diego, California USA, www.graphpad.com.

HDAC1 Colorimetric Enzyme Assay. HDAC1 enzymatic activity was measured following the manufacturer's instructions for the Fluorogenic HDAC1 assay kit from BPS Bioscience, #50061. All tested compounds were dissolved in dimethyl sulfoxide (DMSO) and then diluted in HDAC assay buffer to obtain various concentrations. The enzymatic reactions were performed in duplicate at 37 °C for 30 min. A mixture of 50 μL was used, comprising HDAC assay buffer, 5 μg of bovine serum albumin (BSA), HDAC substrate, human recombinant HDAC1 enzyme, and varying concentrations of the tested compounds. Subsequently, 50 μL of 2×HDAC Developer was introduced to each well, and the microplate was incubated for 15 min at r.t. Fluorescence was measured at an excitation of 350 nm and an emission of 440 nm using a TECAN GENios Pro Microplate Reader and enzyme inhibition curves were fit using non-linear regression dose-response inhibition equations from GraphPadPrism version 8.0.0 for Windows, GraphPad Software, San Diego, California USA, www.graphpad.com.

Statistical Analysis. Statistical analysis was performed using two-way Anova, together with Dunnett's multiple comparisons test. The graphs represent data from at least 3 independent experiments, all performed in triplicate, as the mean ± standard deviation. In the cell viability assay, data of solvent-treated was used as control. A statistical significance between non-malignant HEK 293 cells and other cell lines for each used compound was found, where $p < .05$ is represented as *, $p < .01$ as **, $p < .001$ as *** and $p < .0001$ as ****. Statistical analysis was performed with GraphPad Prism 9.

© 2023 Wiley-VHCA AG, Zurich, Switzerland

15222675, 2023, 10, Downloaded from https://onlinelibrary.wiley.com/doi/10.1002/hlca.202300133 by Tallin Technical University, Wiley Online Library on [09/11/2023]. See the Terms and Conditions (https://onlinelibrary.wiley.com/terms-and-conditions) on Wiley Online Library for rules of use; OA articles are governed by the applicable Creative Commons License

Acknowledgements

This work was supported by NATO SPS MYP grant G5565 (to D.B., Y.K.), Estonian Research Council grant COVSG5 (to D.B., O.B., Y.K.), and National Institutes of Health grants R01GM139297 and R01 NS117000 (to I.B., J.Y.L). The authors express their gratitude to all defenders of Ukraine that made finalizing this publication possible.

Data Availability Statement

The data that support the findings of this study are available in the supplementary material of this article.

Author Contribution Statement

Denys Bondar: conceptualization; methodology; investigation (synthesis and characterization of studied compounds), validation; data curation; visualization; writing – original draft preparation, reviewing and editing. *Olga Bragina*: methodology; investigation (cell viability, inhibition activity); formal analysis; data curation; visualization; writing – original draft preparation. *Ji Young Lee*: methodology; investigation (molecular dynamics simulations), data curation; visualization. *Ivan Semenyuta*: methodology; software; investigation (molecular docking); data curation; visualization; writing – reviewing and editing. *Ivar Järving*: investigation (mass-spectroscopy, HPLC analysis, purity control); data curation; writing – reviewing and editing. *Volodymyr Brovarets*: conceptualization; resources; writing – reviewing and editing. *Peter Wipf*: conceptualization, methodology; writing – reviewing and editing. *Ivet Bahar*: conceptualization; methodology; formal analysis; writing – reviewing and editing. *Yevgen Karpichev*: conceptualization, methodology; resources; funding acquisition; writing – original draft preparation; writing – reviewing and editing; project administration.

References

[1] P. Jagtap, C. Szabo, 'Poly(ADP-ribose) polymerase and the therapeutic effects of its inhibitors', *Nat. Rev. Drug Discovery* **2005**, *4*, 421–440.
[2] N. Li, Y. Wang, W. Deng, S. H. Lin, 'Poly (ADP-Ribose) Polymerases (PARPs) and PARP Inhibitor-Targeted Therapeutics', *Anti-Cancer Agents Med. Chem.* **2019**, *19*, 206–212.
[3] J. Mateo, C. J. Lord, V. Serra, A. Tutt, J. Balmaña, M. Castroviejo-Bermejo, C. Cruz, A. Oaknin, S. B. Kaye, J. S. de Bono, 'A decade of clinical development of PARP inhibitors in perspective', *Ann. Oncol.* **2019**, *30*, 1437–1447.
[4] K. M. Milam, J. E. Cleaver, 'Inhibitors of Poly(Adenosine Diphosphate-Ribose) Synthesis: Effect on Other Metabolic Processes', *Science* **1984**, *223*, 589–591.
[5] M. Banasik, H. Komura, M. Shimoyama, K. Ueda, 'Specific inhibitors of poly(ADP-ribose) synthetase and mono(ADP-ribosyl)transferase', *J. Biol. Chem.* **1992**, *267*, 1569–1575.
[6] D. Ferraris, R. P. Ficco, D. Dain, M. Ginski, S. Lautar, K. Lee-Wisdom, S. Liang, Q. Lin, M. X.-C. Lu, L. Morgan, B. Thomas, L. R. Williams, J. Zhang, Y. Zhou, V. J. Kalish, 'Design and synthesis of poly(ADP-ribose) polymerase-1 (PARP-1) inhibitors. part 4: Biological evaluation of imidazobenzodiazepines as potent PARP-1 inhibitors for treatment of ischemic injuries', *Bioorg. Med. Chem.* **2003**, *11*, 3695–3707.
[7] M. Cohen-Armon, 'The Modified Phenanthridine PJ34 Unveils an Exclusive Cell–Death Mechanism in Human Cancer Cells', *Cancers* **2020**, *12*, 1628.
[8] E. Wahlberg, T. Karlberg, E. Kouznetsova, N. Markova, A. Macchiarulo, A.-G. Thorsell, E. Pol, Å. Frostell, T. Ekblad, D. Öncü, B. Kull, G. M. Robertson, R. Pellicciari, H. Schüler, J. Weigelt, 'Family-wide chemical profiling and structural analysis of PARP and tankyrase inhibitors', *Nat. Biotechnol.* **2012**, *30*, 283–288.
[9] Y.-Q. Wang, P.-Y. Wang, Y.-T. Wang, G.-F. Yang, A. Zhang, Z.-H. Miao, 'An Update on Poly(ADP-ribose)polymerase-1 (PARP-1) Inhibitors: Opportunities and Challenges in Cancer Therapy', *J. Med. Chem.* **2016**, *59*, 9575–9598.
[10] H. E. Bryant, N. Schultz, H. D. Thomas, K. M. Parker, D. Flower, E. Lopez, S. Kyle, M. Meuth, N. J. Curtin, T. Helleday, 'Specific killing of BRCA2-deficient tumours with inhibitors of poly(ADP-ribose) polymerase', *Nature* **2005**, *434*, 913–917.
[11] H. Farmer, H. McCabe, C. J. Lord, A. H. J. Tutt, D. A. Johnson, T. B. Richardson, M. Santarosa, K. J. Dillon, I. Hickson, C. Knights, N. M. B. Martin, S. P. Jackson, G. C. M. Smith, A. Ashworth, 'Targeting the DNA repair defect in *BRCA* mutant cells as a therapeutic strategy', *Nature* **2005**, *434*, 917–921.
[12] C. Y. Chan, K. V. Tan, B. Cornelissen, *Clin. Cancer Res.* **2021**, *27*, 1585–1594.
[13] A. G. Patel, S. B. De Lorenzo, K. S. Flatten, G. G. Poirier, S. H. Kaufmann, 'Failure of Iniparib to Inhibit Poly(ADP-Ribose) Polymerase *In Vitro*', *Clin. Cancer Res.* **2012**, *18*, 1655–1662.
[14] G. Wurz, O. Hofer, H. Greger, 'Structure and Synthesis of Phenaglydon, a New Quinolone Derived Phenanthridine Alkaloid from *Glycosmis cyanocarpa*', *Nat. Prod. Lett.* **1993**, *3*, 177–182.
[15] D. Inbar-Rozensal, A. Castiel, L. Visochek, D. Castel, F. Dantzer, S. Izraeli, M. Cohen-Armon, 'A selective eradication of human nonhereditary breast cancer cells by phenanthridine-derived polyADP-ribose polymerase inhibitors', *Breast Cancer Res.* **2009**, *11*, R78.
[16] Y. Li, W. Lu, D. Chen, R. J. Boohaker, L. Zhai, I. Padmalayam, K. Wennerberg, B. Xu, W. Zhang, 'KIFC1 is a novel potential therapeutic target for breast cancer', *Cancer Biol. Ther.* **2015**, *16*, 1316–1322.
[17] M. Mann, S. Kumar, S. S. Chauhan, N. Bhatla, S. Kumar, S. Bakhshi, R. Gupta, A. Sharma, L. Kumar, 'PARP-1 inhibitor

 © 2023 Wiley-VHCA AG, Zurich, Switzerland

15222675, 2023, 10, Downloaded from https://onlinelibrary.wiley.com/doi/10.1002/hlca.202300133 by Tallin Technical University, Wiley Online Library on [09/11/2023]. See the Terms and Conditions (https://onlinelibrary.wiley.com/terms-and-conditions) on Wiley Online Library for rules of use; OA articles are governed by the applicable Creative Commons License

modulate β-catenin signaling to enhance cisplatin sensitivity in cancer cervix', *Oncotarget* **2019**, *10*, 4262–4275.
[18] B.-Y. Lian, M. Xiong, G.-B. Ji, E.-L. Zhang, Z.-Y. Zhang, K.-S. Dong, X.-P. Chen, Z.-Y. Huang, 'Synergistic suppressive effect of PARP-1 inhibitor PJ34 and HDAC inhibitor SAHA on proliferation of liver cancer cell', *J. Huazhong Univ. Sci. Technol.* **2015**, *35*, 535–540.
[19] G. Costantino, A. Macchiarulo, E. Camaioni, R. Pellicciari, 'Modeling of Poly(ADP-ribose)polymerase (PARP) Inhibitors. Docking of Ligands and Quantitative Structure–Activity Relationship Analysis', *J. Med. Chem.* **2001**, *44*, 3786–3794.
[20] Z. Rappoport, J. F. Liebman, 'The Chemistry of Hydroxylamines, Oximes, and Hydroxamic Acids', Wiley & Sons, Ltd., 2009.
[21] Y. S. Simanenko, T. M. Prokop'eva, A. F. Popov, C. A. Bunton, E. A. Karpichev, V. A. Savelova, K. K. Ghosh, 'O-nucleophilicity of hydroxamate ions in reactions with ethyl 4-nitrophenyl ethylphosphonate, diethyl 4-nitrophenyl phosphate, and 4-nitrophenyl 4-toluenesulfonate', *Russ. J. Org. Chem.* **2004**, *40*, 1337–1350.
[22] N. Singh, Y. Karpichev, R. Sharma, B. Gupta, A. K. Sahu, M. L. Satnami, K. K. Ghosh, 'From α-nucleophiles to functionalized aggregates: exploring the reactivity of hydroxamate ion towards esterolytic reactions in micelles', *Org. Biomol. Chem.* **2015**, *13*, 2827–2848.
[23] Z. Syed, K. Sonu, A. Dongre, G. Sharma, M. Sogani, 'A review on Hydroxamic Acids: Widespectrum Chemotherapeutic Agents', *Int. J. Biol. Biomed. Eng.* **2020**, *14*, 75–88.
[24] S. Bertrand, J.-J. Hélesbeux, G. Larcher, O. Duval, 'Hydroxamate, a Key Pharmacophore Exhibiting a Wide Range of Biological Activities', *Mini-Rev. Med. Chem.* **2013**, *13*, 1311–1326.
[25] D. Bondar, I. V. Kapitanov, L. Pulkrabkova, O. Soukup, D. Jun, F. D. Botelho, T. C. C. França, K. Kuča, Y. Karpichev, 'N-Substituted arylhydroxamic acids as acetylcholinesterase reactivators', *Chem.-Biol. Interact.* **2022**, *365*, 110078.
[26] B. Lou, K. Yang, 'Molecular Diversity of Hydroxamic Acids: Part II. Potential Therapeutic Applications', *Mini-Rev. Med. Chem.* **2003**, *3*, 609–620.
[27] A. Mai, 'Hydroxamic Acids: Biological Properties and Potential Uses as Therapeutic Agents', in 'Hydroxylamines, Oximes and Hydroxamic Acids', in 'PATAI'S Chemistry of Functional Groups', John Wiley & Sons, Ltd., 2010.
[28] J. Keth, T. Johann, H. Frey, 'Hydroxamic Acid: An Underrated Moiety? Marrying Bioinorganic Chemistry and Polymer Science', *Biomacromolecules* **2020**, *21*, 2546–2556.
[29] W. Liu, Y. Liang, X. Si, 'Hydroxamic acid hybrids as the potential anticancer agents: An Overview', *Eur. J. Med. Chem.* **2020**, *205*, 112679.
[30] Z. Yuan, S. Chen, Q. Sun, N. Wang, D. Li, S. Miao, C. Gao, Y. Chen, C. Tan, Y. Jiang, 'Olaparib hydroxamic acid derivatives as dual PARP and HDAC inhibitors for cancer therapy', *Bioorg. Med. Chem.* **2017**, *25*, 4100–4109.
[31] Z. Chi, Y. Bai, J. Li, K. Wang, Y. Xu, Y. Luan, 'Design, synthesis and antitumor activity study of PARP-1/HDAC dual targeting inhibitors', *Bioorg. Med. Chem. Lett.* **2022**, *71*, 128821.
[32] R. Rani, C. Granchi, 'Bioactive heterocycles containing endocyclic *N*-hydroxy groups', *Eur. J. Med. Chem.* **2015**, *97*, 505–524.
[33] A. Citarella, D. Moi, L. Pinzi, D. Bonanni, G. Rastelli, 'Hydroxamic Acid Derivatives: From Synthetic Strategies to Medicinal Chemistry Applications', *ACS Omega* **2021**, *6*, 21843–21849.
[34] L. Zhong, Y. Li, L. Xiong, W. Wang, M. Wu, T. Yuan, W. Yang, C. Tian, Z. Miao, T. Wang, S. Yang, 'Small molecules in targeted cancer therapy: advances, challenges, and future perspectives', *Signal Transduct. Target Ther.* **2021**, *6*, 201.
[35] S. E. Nasrabady, A. Kuzhandaivel, M. Mladinic, A. Nistri, 'Effects of 6(5H)-phenanthridinone, an Inhibitor of Poly-(ADP-ribose) Polymerase-1 Activity (PARP-1), on Locomotor Networks of the Rat Isolated Spinal Cord', *Cell. Mol. Neurobiol.* **2011**, *31*, 503–508.
[36] Y. Kuwata, M. Sonoda, S. Tanimori, 'Facile Synthesis of Phenanthridinone Alkaloids via Suzuki–Miyaura Cross-coupling', *J. Heterocycl. Chem.* **2017**, *54*, 1645–1651.
[37] V. Rajeshkumar, T.-H. Lee, S.-C. Chuang, 'Palladium-Catalyzed Oxidative Insertion of Carbon Monoxide to *N*-Sulfonyl-2-Aminobiaryls through C–H Bond Activation: Access to Bioactive Phenanthridinone Derivatives in One Pot', *Org. Lett.* **2013**, *15*, 1468–1471.
[38] S. L. Yedage, B. M. Bhanage, 'Palladium-Catalyzed Deaminative Phenanthridinone Synthesis from Aniline via C–H Bond Activation', *J. Org. Chem.* **2016**, *81*, 4103–4111.
[39] A.-G. Thorsell, T. Ekblad, T. Karlberg, M. Löw, A. Filipa Pinto, L. Trésaugues, M. Moche, M. S. Cohen, H. Schüler, 'Structural Basis for Potency and Promiscuity in Poly(ADP-ribose) Polymerase (PARP) and Tankyrase Inhibitors', *J. Med. Chem.* **2017**, *60*, 1262–1271.
[40] P. Gandeepan, T. Müller, D. Zell, G. Cera, S. Warratz, L. Ackermann, '3d Transition Metals for C–H Activation', *Chem. Rev.* **2019**, *119*, 2192–2452.
[41] P. Gandeepan, K. Parthasarathy, C.-H. Cheng, 'Synthesis of Phenanthrone Derivatives from *sec*- Alkyl Aryl Ketones and Aryl Halides via a Palladium-Catalyzed Dual C–H Bond Activation and Enolate Cyclization', *J. Am. Chem. Soc.* **2010**, *132*, 8569–8571.
[42] D. Sharma, L. de Falco, S. Padavattan, C. Rao, S. Geifman-Shochat, C.-F. Liu, C. A. Davey, 'PARP1 exhibits enhanced association and catalytic efficiency with γH2 A.X-nucleosome', *Nat. Commun.* **2019**, *10*, 5751.
[43] J. A. De Soto, R. Mullins, 'The use of PARP inhibitors as single agents and as chemosensitizers in sporadic pancreatic cancer', *J. Clin. Oncol.* **2011**, *29*, e13542.
[44] X. Mao, S. Du, Z. Yang, L. Zhang, X. Peng, N. Jiang, H. Zhou, 'Inhibitors of PARP-1 exert inhibitory effects on the biological characteristics of hepatocellular carcinoma cells in vitro', *Mol. Med.* **2017**, *16*, 208–214.
[45] Y. Li, Y. Wang, W. Zhang, X. Wang, L. Chen, S. Wang, 'BKM120 sensitizes BRCA-proficient triple negative breast cancer cells to olaparib through regulating FOXM1 and Exo1 expression', *Sci. Rep.* **2021**, *11*, 4774.
[46] M. Kuhtinskaja, O. Bragina, M. Kulp, M. Vaher, 'Anticancer Effect of the Iridoid Glycoside Fraction from *Dipsacus fullonum* L. Leaves', *Nat. Prod. Commun.* **2020**, *15*, 1–6.
[47] V. M. Kavsan, A. V. Iershov, O. V. Balynska, 'Immortalized cells and one oncogene in malignant transformation: old insights on new explanation', *BMC Cell Biol.* **2011**, *12*, 23.
[48] 'Human ARTD1 (PARP1) - Catalytic domain in complex with inhibitor PJ34', https://doi.org/10.2210/pdb4UXB/pdb.

© 2023 Wiley-VHCA AG, Zurich, Switzerland

15222675, 2023, 10, Downloaded from https://onlinelibrary.wiley.com/doi/10.1002/hlca.202300133 by Tallin Technical University, Wiley Online Library on [09/11/2023]. See the Terms and Conditions (https://onlinelibrary.wiley.com/terms-and-conditions) on Wiley Online Library for rules of use; OA articles are governed by the applicable Creative Commons License

[49] M. F. Sanner, 'Python: a programming language for software integration and development', *J. Mol. Graphics Modell.* **1999**, *17*, 57–61.
[50] ChemAxon, https://www.chemaxon.com, 2022.
[51] M. D. Hanwell, D. E. Curtis, D. C. Lonie, T. Vandermeersch, E. Zurek, G. R. Hutchison, 'Avogadro: an advanced semantic chemical editor, visualization, and analysis platform', *J. Cheminf.* **2012**, *4*, 17.
[52] T. A. Halgren, 'MMFF VI. MMFF94s option for energy minimization studies', *J. Comput. Chem.* **1999**, *20*, 720–729.
[53] O. Trott, A. J. Olson, 'AutoDock Vina: Improving the speed and accuracy of docking with a new scoring function, efficient optimization, and multithreading', *J. Comput. Chem.* **2010**, *31*, 455–461.
[54] 'Discovery Studio Visualizer', 2021, https://www.3ds.com.
[55] S. Kim, J. Lee, S. Jo, C. L. Brooks III, H. S. Lee, W. Im, 'CHARMM-GUI ligand reader and modeler for CHARMM force field generation of small molecules', *J. Comput. Chem.* **2017**, *38*, 1879–1886.
[56] L. Schrödinger, W. DeLano, 'PyMOL', retrieved from http://www.pymol.org/pymol, 2020.
[57] S. Jo, T. Kim, V. G. Iyer, W. Im, 'CHARMM-GUI: A web-based graphical user interface for CHARMM', *J. Comput. Chem.* **2008**, *29*, 1859–1865.
[58] J. C. Phillips, R. Braun, W. Wang, J. Gumbart, E. Tajkhorshid, E. Villa, C. Chipot, R. D. Skeel, L. Kalé, K. Schulten, 'Scalable Molecular Dynamics with NAMD', *J. Comput. Chem.* **2005**, *26*, 1781–1802.
[59] J. Huang, S. Rauscher, G. Nawrocki, T. Ran, M. Feig, B. L. de Groot, H. Grubmüller, A. D. MacKerell Jr., 'CHARMM36m: an improved force field for folded and intrinsically disordered proteins', *Nat. Methods* **2017**, *14*, 71–73.
[60] W. L. Jorgensen, J. Chandrasekhar, J. D. Madura, R. W. Impey, M. L. Klein, 'Comparison of simple potential functions for simulating liquid water', *J. Chem. Phys.* **1983**, *79*, 926–935.
[61] K. Vanommeslaeghe, A. D. MacKerell Jr., 'CHARMM additive and polarizable force fields for biophysics and computer-aided drug design', *Biochim. Biophys. Acta* **2015**, *1850*, 861–871.
[62] W. Humphrey, A. Dalke, K. Schulten, 'VMD: Visual Molecular Dynamics', *J. Mol. Graphics* **1996**, *14*, 33–38.
[63] T. Williams, C. Kelley, 'Gnuplot 4.5: An Interactive Plotting Program', Retrieved from http://gnuplot.info. 2011.
[64] Z. Kurkcuoglu, P. I. Koukos, N. Citro, M. E. Trellet, J. P. G. L. M. Rodrigues, I. S. Moreira, J. Roel-Touris, A. S. J. Melquiond, C. Geng, J. Schaarschmidt, L. C. Xue, A. Vangone, A. M. J. J. Bonvin, 'Performance of HADDOCK and a simple contact-based protein–ligand binding affinity predictor in the D3R Grand Challenge 2', *J. Comput.-Aided Mol. Des.* **2018**, *32*, 175–185.

Received August 2, 2023
Accepted September 9, 2023

© 2023 Wiley-VHCA AG, Zurich, Switzerland

15222675, 2023, 10, Downloaded from https://onlinelibrary.wiley.com/doi/10.1002/hlca.202300133 by Tallin Technical University, Wiley Online Library on [09/11/2023]. See the Terms and Conditions (https://onlinelibrary.wiley.com/terms-and-conditions) on Wiley Online Library for rules of use; OA articles are governed by the applicable Creative Commons License

Curriculum vitae

Personal data

Name:	Denys BONDAR
Date of birth:	08/XI/1987
Place of birth:	Kremenchuk, Ukraine
Citizenship:	Ukrainian

Contact data

E-mail:	denysbondar@icloud.com

Education

2018–2023	Tallinn University of Technology, School of Science, Chemistry and biotechnology, PhD
2009–2011	Taras Shevchenko National University of Kyiv, Department of Chemistry, Organic Synthesis, MSc (*cum laude*)
2005–2009	Taras Shevchenko National University of Kyiv, Department of Chemistry, Organic Chemistry, BSc (*cum laude*)
1995–2005	Kremenchuk Lyceum No. 25 “Humanitarian Collegium”

Language competence

Ukrainian	native
English	fluent
Russian	fluent

Professional employment

2011–2018	R&D scientist, JSC Ukrtatnafta

Honours and awards

2022	Dora Plus T1.2 long-term mobility scholarship (The Archimedes Foundation, Estonia)
2022	Dora Plus T1.1 short-term mobility scholarship (The Archimedes Foundation, Estonia)
2021	Dora Plus T1.1 short-term mobility scholarship (The Archimedes Foundation, Estonia)
2021	Letter of Appreciation (DAAD, Germany)
2020	Dora Plus T1.1 short-term mobility scholarship (The Archimedes Foundation, Estonia)
2019	CHAOS COST Action CA15106 Trainee scholarship (COST ACTION, EU)

Teaching expertise and supervision

2022	Green Chemistry Metrics, exercise tutorial (graduate course)
2021	Baltic Mobility for Research Internships, supervisor (undergraduate course)
2021	Green Chemistry Metrics, exercise tutorial (graduate course)
2020	Scientific project at Tallinna Kesklinna Vene Gümnaasium, supervisor

Elulookirjeldus

Isikuandmed

Nimi:	Denys BONDAR
Sünniaeg:	08/XI/1987
Sünnikoht:	Krementšuk, Ukraina
Kodakondsus:	Ukraina

Kontaktandmed

E-post:	denysbondar@icloud.com

Hariduskäik

2018–2023	Tallinna Tehnikaülikool, Teaduskond: Keemia ja Biotehnoloogia Instituut, doktorantuur
2009–2011	Taras Ševtšenko nimeline Kiievi Rahvusülikool, Keemia osakond, Orgaaniline Süntees, MSC (*cum laude*)
2005–2009	Taras Ševtšenko nimeline Kiievi Rahvusülikool, Keemia osakond, Orgaaniline Keemia, BSC (*cum laude*)
1995–2005	Krementšuki Lütseum nr 25 “Humanitaarne kolledž”

Keelteoskus

Ukraina keel	Emakeel
Inglise keel	Kõrgtase
Vene keel	Kõrgtase

Teenistuskäik

2011–2018	Uurimis- ja Arendusteadur, JSC Ukrtatnafta

Autasud ja tunnustused

2022	Dora Plus T1.2 pikaajaline liikuvusstipendium (Archimedes Fond, Eesti)
2022	Dora Plus T1.1 pikaajaline liikuvusstipendium (Archimedes Fond, Eesti)
2021	Dora Plus T1.1 pikaajaline liikuvusstipendium (Archimedes Fond, Eesti)
2021	Tänuavaldus (DAAD, Saksamaa)
2020	Dora Plus T1.1 lühiajaline liikuvusstipendium (Archimedes Fond, Eesti)
2019	CHAOS COST Action CA15106 praktikandistipendium (COST ACTION, EL)

Õpetamis- ja juhendamiskompetents

2022	Roheline keemia: mõõdikud, harjutustund (magistrikursus)
2021	Balti liikuvus teadusinternatuuride jaoks, juhendaja (bakalaureusekursus)
2021	Roheline keemia: mõõdikud, harjutustund (magistrikursus)
2020	Teadusprojekt Tallinna Kesklinna Vene Gümnaasiumis, juhendaja

ISSN 2585-6898 (publication)
ISBN 978-9916-80-089-8 (publication)